TOXICITY OF MICROPLASTICS, GRAPHENE QUANTUM DOTS AND MOLYBDENUM DISULFIDE TO THE FRESHWATER ORGANISM *DAPHNIA MAGNA*

UNIVERSITY OF BIRMINGHAM

by

HOSSEIN HAYAT DAVOUDI

A thesis submitted to the University of Birmingham for the degree of DOCTOR OF PHILOSOPHY

School of Geography, Earth and Environmental Science

College of Life and Environmental Sciences

University of Birmingham

February 2023

Abstract

Production and use of engineered nanomaterials (ENMs) in consumer products has significantly increased in the last decades due to their unique characteristics. This results in ENMs being released into the environment and interacting with living organisms. In parallel, the increase in plastic use worldwide leads to their breakdown into micro (MPs) and nano plastics (NPPs), further increasing environmental particle burdens. A key question addressed in this thesis is whether particles of very different characteristics affect aquatic organisms in a similar manner. Polystyrene (PS) is a popular representative of MPs/NPPs widely used in many applications. Graphene quantum dots (GQDs) and molybdenum disulfide (MoS_2) are recently emerged ENMs, used in a wide range of applications. *Daphnia magna* (*D. magna*) is an important freshwater environmental indicator for toxicity assessments. The toxicity of PS, GQDs and MoS_2 towards *D. magna* was assessed, considering factors controlling their physicochemical properties and toxicity, to address literature gaps. The toxicity of particles mainly depended on their size (smaller > larger), surface charge (+ve > -ve), ageing, chemical additives, and the composition of dispersant solutions. Applying environmentally relevant conditions greatly reduced the toxicity of the NMs relative to standardized test medium, suggesting the need for updating of regulatory test guidelines.

Acknowledgements

I would like to express my deepest appreciation to my primary supervisor Prof. Iseult Lynch for her invaluable help and support during my PhD journey as well as her patience.

Additionally, I would like to thank my Co-supervisor, Prof. Eugenia Valsami-Jones for always being there for me whenever I needed any kind of help or advice. I also cannot forget the support I received from all my lab colleagues, and it was great to know you all as colleagues and wonderful friends.

To my dear mother I always run out of words, I will never be able to thank you enough for everything you have done for me and for doing your best to fund my PhD studies despite all the challenges.

My dear wife, you have been the biggest supporter during this journey and without you, things would have been much harder, thank you very much I appreciate your patience, love and everything you have done for me to stay focused and complete my work.

Last but not least, I would like to thank all my family, especially my uncles and aunties, who have also participated in funding my studies, and, more importantly, their mental support was invaluable, and to those who passed away (uncle Tawfeeq, Uncle Saleh and my cousin Mohammed) you will never be forgotten and I will never forget all the help and love you provided before leaving this journey of life.

Table of Contents

List of Figures

List of Tables

1

Introduction

Nanotechnology is defined as the manipulation of matter on an atomic, molecular, and supramolecular scale for industrial purposes resulting in what is been referred to as nanomaterials (NMs) and nanoparticles (NPs). Due to their unique characteristics, NMs are being used in a wide range of applications such as medical, electronic and environmental applications. The significant rise in demand for NMs in recent years is due to their small size and large surface area to volume ratio, their superior performance over bulk equivalents and their adjustable biological, physical and chemical properties, allowing new levels of control at the molecular and atomic dimensions (Salem *et al.*, 2022). Although many research efforts have been and are still being conducted to evaluate their behaviour and impact on biological systems, there still remains a significant gap in understanding their effects on biological systems once they are released into the environment. The environmental fate and transportation of NMs are important factors in evaluating the applicability and safety of these materials. Thus, when assessing the biocompatibility/toxicity of NMs to evaluate their risk, the complexity of biological systems should be considered in experimental designs and various exposure scenarios designed in order to achieve environmentally relevant results. In this thesis, we aim to understand the interaction of various types of high-interest /high-value NMs with the important environmental indicator *Daphnia magna* (*D. magna*) for ecotoxicity assessment in freshwater systems.

1.1. *Daphnia* as A Model Organism and Its Role in Toxicology

The freshwater crustacean genus *Daphnia* has been a species of interest to environmentalists and experimental biologists for more than 150 years (Harris *et al.,* 2012). They fulfil a central role in establishing environmental regulations for governments and agencies around the globe (e.g., the Organization for Economic Cooperation and Development (OECD), and the Environmental Protection Agency (EPA)) (Hogstrand and Kille, 2008). Within the toxicological databases, *Daphnia* represents 8% of all experimental data for aquatic animals, and they are mainly used for assessing environmental quality and monitoring pollutants (Benson and Giulio, 2006). Early studies undertaken on *Daphnia* focused on their unusual mode of life (parthenogenetic reproduction except when under stress when males are produced to enable sexual reproduction and formation of resting eggs, enabling them to survive the unfavourable conditions), biogeography, toxicity classification and on their functional morphology (Hogstrand and Kille, 2008). Water flea is their common name given by (Swammerdam, 1758), years later Mueller in 1785 provided their scientific name; *Daphnia* (Shaw *et al.*, 2008). *D. magna* is the most used species for toxicity tests, followed by *Daphnia pulex* (Persoone *et al.*, 2009). Being one of the largest daphnids*; D. magna's* size played a major role in its widespread acceptance (Hogstrand and Kille, 2008). As a result of being filter-feeders, *D. magna* is an important indicator species for the environment and is especially sensitive to fine particles such as nanoparticles (Briffa *et al.*, 2018). According to some studies, *Daphnia* is more tolerant compared to other organisms, with *D. magna* being the most resistant species (Koivisto *et al.,* 1992; Shaw *et al.*, 2006). In the freshwater ecosystem, they fulfil a major role as daphnids consume the phytoplankton that is responsible for forming organic compounds from dissolved carbon dioxide, maintaining the aquatic ecosystem (Brett *et al.*, 2009).

The life cycle of these aquatic organisms is determined by environmental sex determination, parthenogenesis (clonal reproduction) and their ability to produce two different types of eggs, where one type can remain dormant for decades (Ebert, 2005). They are capable of both sexual and clonal reproduction, and due to clonal reproduction, their genetic background can remain constant, maintaining a permanent intact genotype (Hebert and Ward, 1972). The following characteristics are required for an organism to be considered as a suitable indicator species for use in aquatic biomonitoring: (i) it must be sensitive to a range of different stressors, (ii) have a short cycle of life but the lifecycle should be long enough to allow it to respond to rapid environmental changes, (iii) live in environments where toxins tend to accumulate such as sediments or low flowing water columns, (iv) be easy to identify by a non-specialist, (v) have high abundance, (vi) it should be an important component of the ecosystem, and (vii) be suitable for laboratory experimentation (Le *et al.*, 2016). *Daphnia* covers all the criteria of a suitable bioindicator to evaluate the effects of toxicants on aquatic systems and indicate environmental changes. In addition, individual daphnids are transparent, which makes it easy to visualize accumulated NPs, including agglomeration of particles in the gut, making it ideal for bioaccumulation studies (Tan *et al.*, 2016; Jensen *et al.*, 2017). Daphnids are fed controlled diets of algae and/or bacteria, and maintained in a simply defined medium (Shaw *et al.*, 2008). *Daphnia* inhabits significant aquatic environments around the globe, ranging from temporary ponds to permanent lakes, freshwater to hypersaline, eutrophic to oligotrophic, and they also extend into the high alpine lakes and UV-rich settings of coastal dune ponds (Shaw *et al.*, 2008).

1.1.2 The Biology, Characteristics and Feeding Behaviour of *Daphina*

Daphnia belongs to the crustaceans class Phyllopoda/Branchiopoda (Ebert, 2005, 2022). The males are smaller in size than females and have modified first legs and post-abdomen, and they can be distinguished from females by their larger antennules (Ebert, 2005). They use their flattened leaf-like legs to generate a water current to be filtered by the feeding apparatus (Ebert, 2005). The bodies of *Daphnia* are enclosed by the carapace, which is an uncalcified shell that is made of chitin (a polysaccharide) (Ebert, 2005). Water fleas have up to 10 appendage pairs which are (from back to front): 6 limbs on the trunk (5 in *Daphnia*), which form an apparatus for respiration and feeding, mandibles, maxillae, antennae and antennules. There is a pair of claws at the abdomen end. *Daphinds'* body lengths range from around 0.5 mm to 6 mm, depending on their age and species (Ebert, 2005). The filters of *Daphnia* function like sieves retaining the food-suspended particles when they are larger than the mesh size of the filters (Gophen and Geller, 1984). The sieving paradigm has been widely accepted in the past, and whether particles are collected by sieving or not has been a major point of discussion on the animal's feeding mechanism for decades (Hartmann and Kunkel, 1991). However, a recent study stated that sieving might not be their mechanism of feeding and water current/motion may be controlling their feeding behaviour as well as other complex factors (Gophen, 2022). It is the hypothesis of the 'leaky-sieve' that in the absence of modifying factors, *Daphnia* non-selectively feeds on all the particles that exceed the setular mesh size of limbs 4 and 3 (Burns, 1968; Boyd, 1976; Hartmann and Kunkel, 1991).

Diffusion and gravitational deposition, surface chemistry, actions of other limbs in the trunk and taste are other factors that could also intervene in the collection of small particles by *Daphnia* (Hartmann and Kunkel, 1991). It has been found from older studies that *Daphnia*

prefers small spherical diatoms over elongated greens, flagellates over coccales and smaller to larger plastic spheres or spherical algae (Julian Hartmann, 1985; Bern, 1990). However, the majority of studies that explain the biology and feeding behaviour of *Daphnia* are old. Most of the feeding or toxicity experiments in laboratories were done using either *Chlamydomonas* or *Scenedesmus* as the food source due to their ease of culturing and the *Daphnia* preference for green algae (Ebert, 2005). Even though in some large daphnids, particles up to 70 µm may be found in the gut, the particle size that they usually consume ranges from 1 - 50 µm in diameter (Ebert, 2005). Scientists previously developed a size-efficiency hypothesis assuming that the upper particle size limit to what a large cladoceran can ingest roughly accords with the body size of the zooplankton (Brooks and Dodson, 1965). Some studies on the filter's fine structure demonstrate that *Daphnia*'s filter mesh sizes differ with different species, age stages and populations (Gophen and Geller, 1984). *Daphnia* has been shown to have different abilities to filter bacteria (as smaller food particle)s, which can be explained by the known micromorphological characteristics of the animal's filtering systems (Gophen and Geller, 1984). The selectivity for particles varies with concentration, daphnid age and relative food proportions (Julian Hartmann, 1985).

One individual *Daphnia* is able to filter all the algae present in 4 mL/h from a lake, which gives them the ability to remove a significant portion of the algae/food typically present in the environment (Penalva *et al.*, 2007). By the rhythmical beating of the four morphologically complex thoracic legs, which are enclosed by the carapace and located in their ventral region, daphnids begin breathing and collecting food particles from the water column from the moment they are born (Penalva *et al.*, 2007). The particles are transferred by a special seta and collected by *Daphnia* while the current flows (Ebert, 2005). The tubular gut of *Daphnia* consists of three parts: (1) the esophagus, (2) the midgut and (3) the hindgut

(Ebert, 2005). In the midgut, two digestive ceca (a pouch in the intestine) can be seen (Figure 1.1), which are lined by an epithelium bearing microvilli (Ebert, 2005). The hindgut expels food by a peristaltic movement, and it also needs pressure from recently consumed food to drive out food particles (Ebert, 2005). In the posterior part of the midgut, the pH is between 6.6 and 7.2, while in the anterior part, the pH is between 6 and 6.8 (Ebert, 2005). The predominant food in *Daphnia's* diet controls their colour, as individuals feeding on bacteria will most likely have a pink or white colour, whereas those feeding on green algae would gain a yellow or green colour (Ebert, 2005). Starved daphnids are less strongly coloured than those that are fed well (Ebert, 2005).

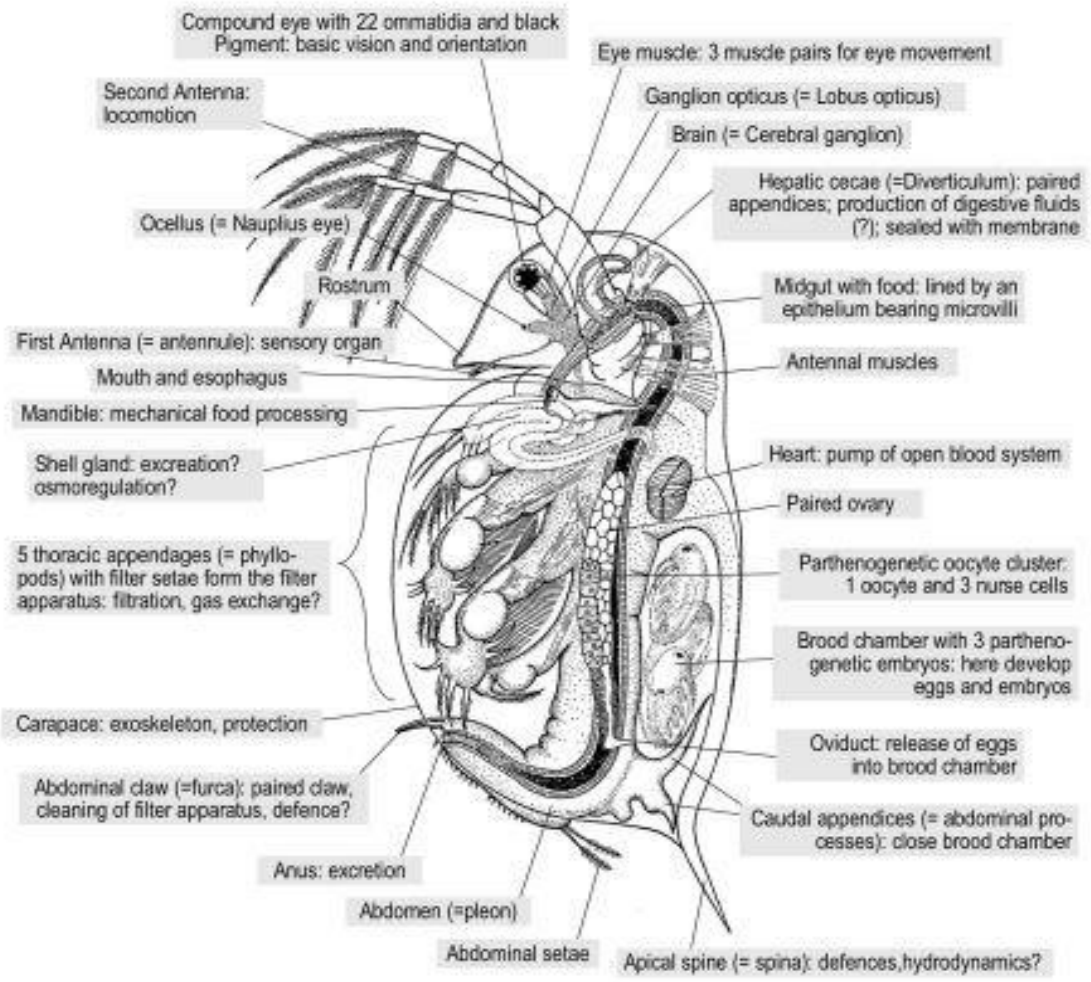

Figure 1.1. The functional anatomy of Daphnia (Ebert, 2005).

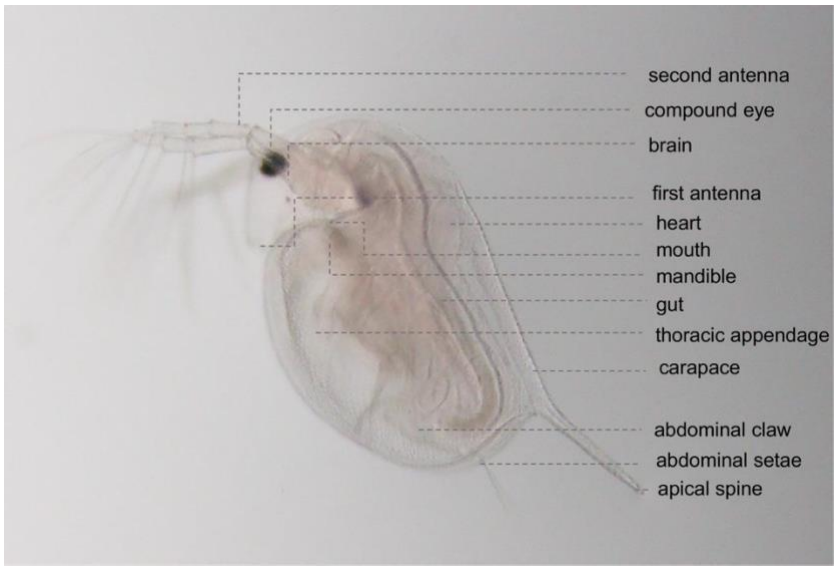

Figure 1.2. The basic anatomy of *D. magna* (Tkaczyk et al., 2021).

Having an open circulation of blood, the heart of *Daphnia* is located in the back of the organism, as well as the front of the brood chamber (Ebert, 2005). Daphnids heart rate is affected by temperature, beating up to 200 times per minute at 20 ˚C, and as the temperature drops down, the heartbeat slows (Ebert, 2005). Flowing through the body cavity, blood cells can be easily seen through their transparent body (Ebert, 2005). Oxygen transport is supported by the extracellular respiratory protein hemoglobin (Hb) (Ebert, 2005). The osmoregulatory problems experienced by freshwater organisms are present in *Daphnia*, i.e., few solutes and too much water (Ebert, 2005). With their chloride-absorbing glands, they can absorb ions (Ebert, 2005). The osmoregulation and excretion may be affected by the shell gland (Ebert, 2005). Located close to the eye and near the gut, the nervous system is distinguished by the cerebral ganglion. Embryos have two eyes that spot fuse during the last part of the development, whereas adult and juvenile *Daphnia* have one compound large eye which helps them to orient while swimming (Ebert, 2005). On the top of the cerebral ganglion and between the compound eye and the mouth lies a small structure called a naupliar eye which is their major visual organ (Ebert, 2005; Brandon, 2015). When food levels are low, daphnids will also stir up sediments or browse the bottom of the water body to use the resuspended particles as food (Horton *et al.*, 1979; Lampert, 1987; Gillis *et al.*, 2005). Therefore, they may ingest sediments and any contaminants associated with them, including metals, by scraping at the water interface sediment or sieving resuspended particles, even though they mainly feed on bacteria and algae (plankton) (Gillis *et al.*, 2005). There are no clear reports or evidence to demonstrate the amount of time needed to purge *Daphnia's* gut after feeding on contaminated sediments (Gillis *et al.*, 2005). Knowing that the time passage of the gut is inversely related to the food concentration, the residence time of food in *Daphnia's* gut may vary from 2 min up to 55

min (Gillis *et al.*, 2005). Studies of gut passage time were documented while the investigated organisms were feeding on glass beads, clay particles or suspended algae. Some studies suggested that starved individuals may indefinitely retain faeces in the mid-gut, knowing that as more algae are packed into the fore-gut and ingested; unassimilated algae will be excreted from the hind-gut (Gophen and Gold, 1981). The particles that resist digestion can also accumulate in the hindgut after all the other materials have been digested (Lampert, 1987). It has been determined that when animals were feeding on metal-contaminated algae, 3-6 hours were needed to clear the animal's gut, whereas for *Daphnia* exposed to uncontaminated algae just 15-30 min were enough for the animal to clear their gut, which means that exposure to and ingestion of metal contaminated sediment particles could lengthen the passage time in *D. magna's* gut (Gillis *et al.*, 2005; Barata *et al.*, 2002).

The English name *Daphnia* originates from the jumping-like behaviour that they exhibit. This behaviour, which is most likely developed as a strategy to avoid predators, is controlled by the beating of the antennae, which is used by *Daphnia* to direct themselves while swimming in the water (Ebert, 2005). A high density of the organisms causes sinking, while the fast downbeat produces a rapid upward movement (Ebert, 2005). Diel vertical migration, the synchronised movement of zooplankton and fish up and down in the water column over a daily cycle, is another behavioural trait of *Daphnia*, whereby in the night time they migrate towards the upper water levels and during the daytime and early morning, they migrate downward back to the lower levels of the water (Ebert, 2005).

1.1.3. Parameters Used in *D. magna* Toxicity Tests

Acute immobilization, lethality and reproduction tests, standardised by the OECD test guideline, are commonly used parameters to evaluate the toxicity of chemical compounds towards *D. magna*. The most commonly used end-point is the acute immobilisation test due to the simplicity and the short time (24-48 h) required to achieve relevant results (Tkaczyk *et al.*, 2021). Additionally, many parameters can be considered and monitored to achieve a more detailed analysis, such as biochemical analyses, swimming behaviour, molting, heart rate, ingestion rate, post-abdominal movement, feeding rate and thoracic limb activity (Tkaczyk *et al.*, 2021).

1.1.3.1 Acute Toxicity Tests

The most used toxicity test in ecological studies is Test No. 202 regulated by the OECD test guideline; as this test is determined by analyzing the concentration of a chemical that causes 50% *D. magna* neonates immobilisation (determined as no movement during 15 seconds of gentle agitation) after 24 and 48 h, where an effective concentration (EC_{50}) value is estimated (Tkaczyk *et al.*, 2021).

1.1.3.2. Reproductive Toxicity Tests

The OECD Reproduction Test No. 211, known as the chronic test (21 days), is another commonly used end-point to assess the toxicity of chemicals on *D. magna* delivering insights into the reproduction impacts of chemical compounds (Tkaczyk *et al.*, 2021). Compared to the acute immobilization tests, the chronic toxicity test provides details about reproduction parameters such as the size and number of broods per animal, the sex ratio of the offspring, production of offspring by a parent, the total number of living offspring, mortality of parents (longevity), reproductive rate, time to produce first broods, and

cumulative molts/embryo-toxicity (number of undeveloped antennules, aborted eggs, curved or inexistent shell spines, abnormal offspring) (Tkaczyk *et al.*, 2021).

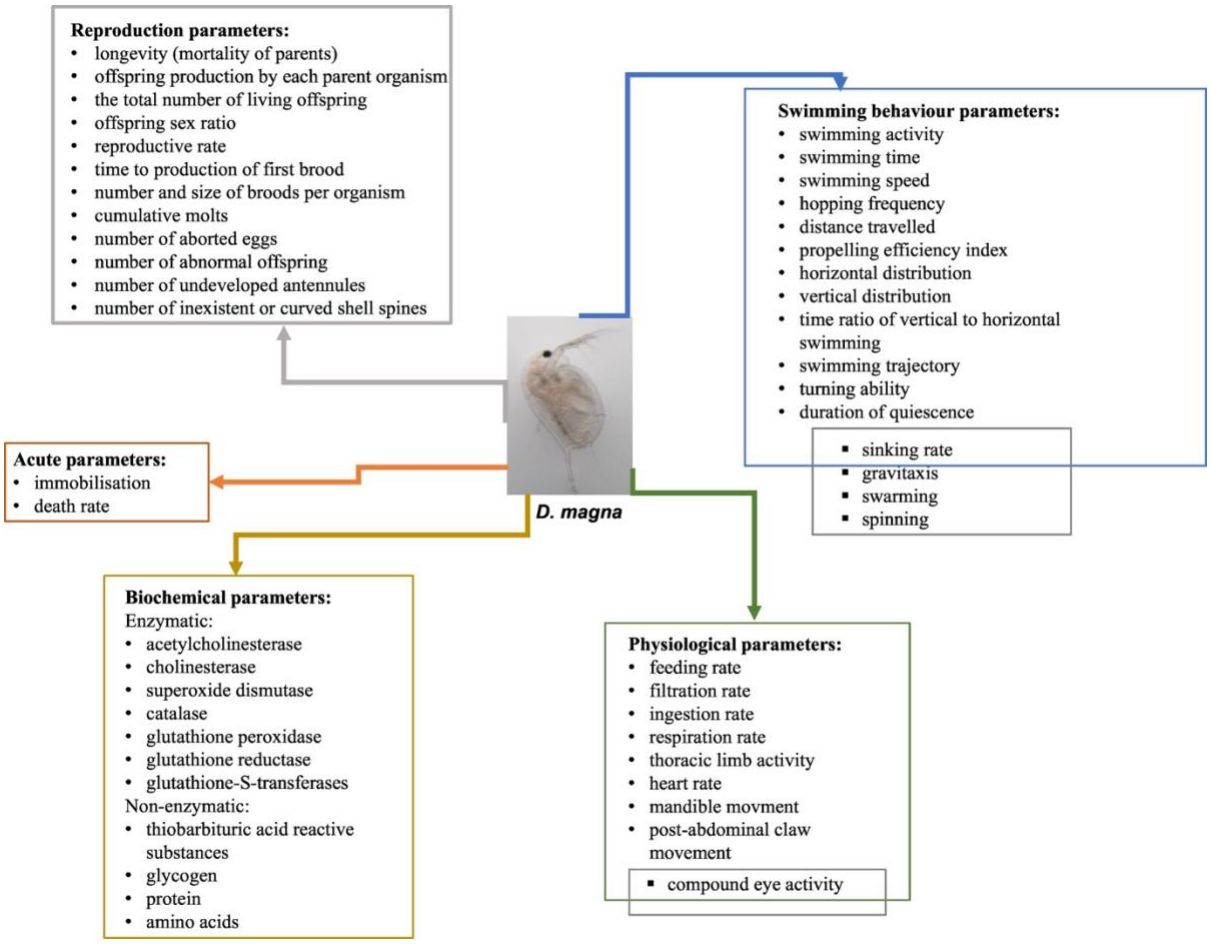

Figure 1.3. Parameters used in assessing the toxicity of chemicals towards D. magna (Tkaczyk et al., 2021).

1.1.3.2.1. Moulting

At different stages through their life cycle, *D. magna* undergoes the essential process of moulting, where they shed their carapace to enable further development and growth (Zou and Fingerman, 1997). Depending on the presently available food, they are known to shed their carapace 1 to 3 times within the first 96 hours of their life (Dabrunz *et al.*, 2011). The process of moulting is significantly affected by environmental conditions, such as temperature, and it frequency decreases with age, as neonates shed their exoskeleton more

frequently than when they are older (Porcella *et al.,* 1969; Work and Gophen, 2001). The absorbed toxins that have bound to the exoskeleton can be shed by *D. magna,* making the molting process a defensive mechanism (Rabus *et al.*, 2013). Numerous authors determined that nanomaterials can bind to biological surfaces, and thus it is very likely that NMs bind to the carapace of *D. magna* due to the large surface area of these particles, which gives them a sorption capacity (Baun *et al.*, 2008; *Handy et al.,* 2008). NMs that are adhered to the carapace increase the weight of *D. magna* neonates, causing a decrease in their movement and increasing the energy required to swim, as well as the required physical endurance (Dabrunz *et al.*, 2011). The previous author demonstrated that the entire layer of bound NMs was eradicated during the moulting process, allowing *D. magna* to be free from NMs when the moult ends, and noted that re-absorption of more NMs onto *D. magna* took place due to the presence of NMs in the suspension.

1.1.3.3. Biochemical Tests

Biochemical parameters are another pathway used to evaluate the bioavailability of chemicals. At the sub-cellular level, the metabolic equilibrium may be affected when organisms are exposed to chemical compounds (Tkaczyk *et al.*, 2021).

There are various biochemical parameters involved when assessing changes in complex metabolic biomarkers in *D. magna*, including enzymatic and non-enzymatic assessments.

1.1.3.3.1 Digestive Enzymes

The majority of available studies investigating the toxicity of chemicals on the activity of digestive enzymes of *D. magna* are outdated and more research is needed to fill the literature gaps, which encouraged us to attempt to assess their digestive enzyme activity, as being filter feeders leads to most toxicity effects in daphnids occurring via digestion. A

number of digestive enzymes are required for *Daphnia* to be able to digest food particles of different biochemical composition (Schwarzenberger and Fink, 2018). Hasler was the first author to describe the digestive enzymes of *Daphnia,* including amylase, lipase and proteinase activity (Hasler, 1935). Endogenous cellulase was later added to this list (Schoenberg *et al.,* 1984). The major digestive proteases of *D. magna* were characterized as trypsin and chymotrypsin (Von Elert *et al.*, 2004, 2012). One of the most challenging aspects of toxicological research is the evaluation of all the biomarker (sub-organismal) test endpoints due to the fact that the ecological relevance of each biomarker needs to be established for them to be useful as 'toxic stress early indicators (Moriarty, 1983). For detecting the influence of toxicant sublethal concentrations on the metabolism of tested organisms, enzyme activity responses have been used frequently (De Coen and Janssen, 1997). Most of these studies have focused on the intermediary pathways of enzymes because they are related directly to the energy balance of the studied organism, demonstrating homeostatic adjustments in the budget of energy as a result of the stress caused by the toxic substance (De Coen and Janssen, 1997). So far, *D. magna* has received little attention in terms of the function of its digestive enzyme system.

The exposure to toxic materials leads to an interaction between the target site and the chemical in the test animal, causing a chain reaction of subcellular level biochemical processes to restore the metabolic equilibrium, which may lead to significant effects at higher levels of the biological organization if not achieved (De Coen *et al.,* 2001). The assessment of the metabolic condition of an organism can never be based on measuring a single enzyme activity because of the high complexity of metabolic pathways (De Coen *et al.,* 2001). Carbohydrate metabolism is the central part of the organism's metabolic process, which provides important building blocks for the various anabolic pathways and fuels the

energy needed for synthetic reactions (De Coen *et al.,* 2001). In terms of the influence of toxic stress, little attention has been paid to the impacts on the carbohydrate metabolism of zooplankton animals (De Coen *et al.,* 2001). The long-term effects of these organisms can be easily studied because of their short life cycle and their small size, which is necessary for assessing the ecological relevance of the sub-organismal level criteria (De Coen *et al.,* 2001). It should be noted that this section was written at the beginning of this PhD work while still exploring and understanding the mechanism of *D. magna* digestive enzymes activity from early-stage studies, which requires a further update, and it was not updated due to the challenges and shift in this thesis aims and objectives.

1.2 Nanomaterials

NPs are a subset of NMs, as the British Standards Institution described NMs as having at least one dimension less than 100nm, and the ones having each of (all 3) of their dimensions between 1-100 nm are termed (NPs) by the same institution. NMs can be naturally occurring in nature, incidental (resulting from the byproduct of other reactions or anthropogenic activity), or engineered (manufactured) which are produced by industrial activities (Jeevanandam *et al.*, 2018). During synthesis, NMs are normally coated with stabilizers to control their size and limit their potential for agglomeration (Buesser and Pratsinis, 2012). Based on their chemical composition, NMs can be divided into 6 types: zero-valent metals, organic polymers, metal oxides, quantum dots (QDs), carbon-based NMs including graphene, as well as other NMs (Zhu *et al.*, 2022).

NMs are distinguished from other non-nanoscale materials by their unique physicochemical properties (Haase and Lynch, 2018). These properties are the reason why scientists are very concerned with understanding the fate and impact of NMs on the environment, as accessing

and obtaining data to understand the safety of these materials remains a big challenge (Haase and Lynch, 2018). Being small in size, NMs have a larger surface area per unit mass than larger (micron-sized) particles, which makes them more reactive because their large surface that can interact with different molecules and biological systems (Rosenkranz *et al.*, 2009). Studies showed that some nano-sized particles such as polystyrene beads, fullerene and carbon black, are capable of inducing the production of reactive oxygen species (ROS), free radicals, or both, which can lead to inflammation and oxidative stress leading to a number of diseases in humans and other species (Rosenkranz *et al.*, 2009). Many biological studies proved that NMs can be toxic to mammals, fish, bacteria, and algae (Zhu *et al.*, 2022). The toxicity of NMs mainly depends on the concentration and property of the particles, but they are also controlled by various physical, chemical and biological factors, which remain poorly understood in terms of their behaviour in different biological systems.

1.2.1. Transformation of NMs

(This section has been published in Frontiers in Toxicology as (Reilly et al., 2023)).
When NMs are released into the environment, they interact with many environmental components and go through various dynamic transformation processes which can change their physicochemical properties (Abbas *et al.*, 2020). These processes can be physical, chemical, biological and macromolecular, and they can significantly impact the toxicity, reactivity, fate and transport of NMs in both environmental and biological systems. Transformation processes such as adsorption of molecules/ions and macromolecules, aggregation, oxidation and reduction (redox) reactions, sulfidation and dissolution all occur easily in biological and environmental systems and can greatly affect the behaviour of NMs in many different ways (Lowry *et al.*, 2012). It is common that NMs are manufactured with a

stabilizer or an organic capping agent and the transformation of the produced NM can affect the capping agent, the core materials or both, and the properties of the initial NM, its coatings and surrounding biological and chemical environment can significantly impact the type, extent and rate of the possible transformation processes (Lowry *et al.*, 2012). The fate and toxicity of NMs can be greatly affected by the processes that take place during exposure. The physicochemical transformation of NMs under different environmental conditions is driven by several variables such as ionic strength, pH, stability, synthesis method, valency, capping agent, and cation type (Goswami *et al.*, 2017). To understand how NMs behave in ecosystems and to determine their toxicity and fate, we must first understand the mechanism of NMs transformation processes upon their release into and interaction with the surrounding environmental components (Figure 1.4).

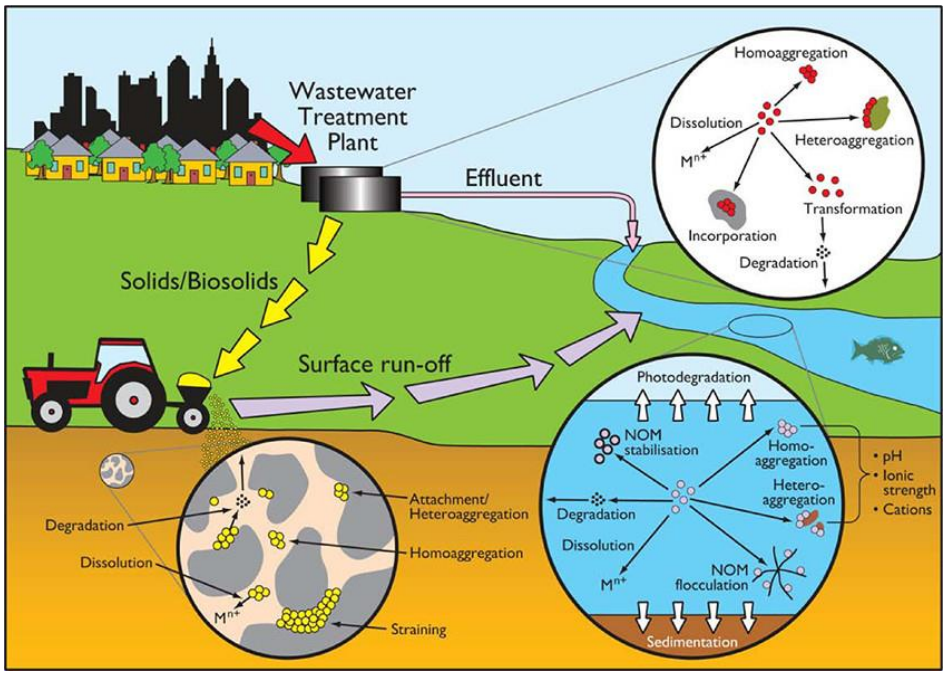

Figure 1.4. Transformation processes of NMs in the environment (Batley, Kirby and McLaughlin, 2013).

1.2.1.1. Chemical Transformations

When NMs enter the environment, they may interact with the organic or inorganic matter present as well as with the soil/sediments and water systems, and they undergo various chemical transformation processes such as dissolution, adsorption, oxidation-reduction (redox) reaction, complexation, degradation and photochemically induced reactions (Abbas *et al.*, 2020). These chemical transformations are important for understanding the behaviour, fate and toxic mechanism of the NMs. One of the main chemical transformation processes for many metal NMs is sulfidation, particularly when enhanced concentrations of sulfide are present, such as the ones found in sub-oxic or anoxic sediments or in some parts of wastewater treatment plants (Lead *et al.*, 2018). Sulfidation can affect the behaviour, toxicity and fate of NMs, as those reactions can change the solubility, particle size and surface charge of NMs. Both sulfide and oxygen are required for the reaction to occur, and it can either be an indirect slow surface reaction or a faster direct reaction (Lead *et al.*, 2018). Another major route for transformations of NMs in the environment are photochemically induced reactions such as photolysis, photo-oxidation and photo-catalysis. These are processes where sunlight plays an important role in the dissociation of NMs, causing the release of ROS and affecting the toxicity of NMs (Goswami *et al.*, 2017).

Dissolution is also considered a key chemical transformation process that is driven by the release of water-soluble molecules or ions from NMs. Engineered NMs can be classified into insoluble materials such as carbon nanotubes (CNTs), carbon black (CB), fullerenes and graphene, highly soluble materials such as (FeO, Ag, Cu/CuO, Zn/ZnO and QDs) and poorly soluble particles such as (CeO_2, TiO_2) (Abbas *et al.*, 2020). The equilibrium solubility

(amount of dissolved matter) and the kinetics of particle dissolution (rate of solubility) of NMs will affect their toxicity, behaviour and environmental fate (Hartmann *et al.*, 2014). Oxidation is an important step in the dissolution of metals, but generally, it is not an essential pathway for the transformation of most NMs, whereas transformations of metal oxides such as ceria and FeO are important for determining the fate and behaviour of NMs (Lead *et al.*, 2018).

Redox reactions are processes that involve the coupled oxidation-reduction in the environment, this process takes place when the transfer of electrons (gain or loss) occurs between the reacting chemical moieties (Abbas *et al.*, 2020). For inorganic substances, redox reactions are the basis for chemical transformation processes, which include dissolution, and these reactions are relevant to NMs that participate in the transfer of electrons (Hartmann *et al.*, 2014).

1.2.1.2. Physical Transformations

Agglomeration/aggregation and sedimentation/deposition are the main physical transformation processes that NMs go through once released into the environment (Abbas *et al.*, 2020). Aggregates are particle clusters held together by electrostatic interactions or chemical bonds, they cluster together due to the attractive forces between particles, and this can occur during use, production, storage or upon release of NMs into the environment (Hartmann *et al.*, 2014). Agglomeration is a term usually used for processes of weaker interactions than aggregation, although the terms are used somewhat interchangeably in the literature (Lead *et al.*, 2018). The aggregation process is considered to be irreversible, while agglomeration can be reversible as the particles are clustered together by weaker forces, and the direction of this process depends on the surrounding medium conditions

(Hartmann *et al.*, 2014). The effect of surface area to volume ratio on NMs reactivity is reduced by the aggregation and agglomeration processes, which will affect their toxicity, transport in porous media, reactivity, sedimentation and uptake by organisms (Lowry *et al.*, 2012). Two forms of aggregation (more correctly in this case agglomeration) may take place: heteroaggregation between a NM and a different particle in the environment or homoaggregation between the same type of NM. A review article indicated that although many studies showed that aggregation usually reduces the bioavailability of NMs, no evidence has proven that it can affect the bioavailability of ingested NMs, although a few studies showed that in some cases, aggregation can enhance bioaccumulation by increasing the ingestion rate or by making the particles more accessible (Lead *et al.,* 2018). The same review highlighted that at realistic environmental concentrations, homoaggregation was proven to be quantitatively unimportant, suggesting that heteroaggregation, for example with suspended clay particles, could be more important due to the higher concentrations of natural colloids. Particle size increases over time due to agglomeration, and this process leads to a reduction in NMs number concentration in water or soil suspensions, as a result of the deposition of agglomerated (larger) particles (Abbas *et al.*, 2020).

As larger particles tend to settle faster than smaller particles, sedimentation is significantly influenced by the agglomeration process, and the gravitational settling can be explained by Stoke's law, which indicates that larger aggregates and agglomerates will settle faster than dispersed particles (Hartmann *et al.*, 2014).

1.2.1.3. Biological Transformation

The major biologically mediated transformation processes that NMs undergo upon their release into natural environments are nano-bio and eco/bio-corona interactions,

biodegradation and interactions with macromolecules facilitating NMs formation (Abbas *et al.*, 2020). The process of biodegradation is driven by the ability of microorganisms to decompose organic substances. The interaction of NMs with microbes, extracellular polymeric substances and extracellular enzymes determines their relative significance and rate of the biodegradation processes.

Biodegradation of NMs core components and surface coatings is a possible transformation pathway of NMs depending on the surrounding environment, particularly for carbon-based NMs that include fullerenes and carbon nanotubes (CNTs) (Abbas *et al.*, 2020). The biodegradation of organic surface coating is relevant to all types of manufactured NMs. Biomodification is an additional process that can affect the fate and toxicity of NMs, which includes processes that are indirectly mediated by organisms as this process occur after NMs are taken up into the guts of organisms and potentially transferred further into the tissues.

1.2.1.4. Macromolecular Transformations

The diverse groups of organisms in natural environments produce and secrete a variety of molecules (e.g., proteins) alongside other biomolecules that are naturally present in the environment, such as natural organic matter (NOM) and polysaccharides. Biomolecules can be easily adsorbed to NMs present in ecosystems, and NMs that are taken up by biological organisms can be transformed upon their interaction with biomolecules, which may coat and transform their outer surfaces (Lowry *et al.*, 2012). The biomolecule layers forming around the surface of NMs are called the protein corona, which will be discussed in detail in section 1.2.2.2 of this chapter.

1.2.1.5. Bioaccumulation of NMs in Aquatic Biota

Uptake and bioavailability studies are significant for studying the behaviour of NMs in natural environments and for linking the biological effects to the environmental chemistry of NMs (Lead *et al.*, 2018). In addition to microorganisms, crustaceans such as *D. magna* are widely used in chemical safety studies as representative aquatic biota. They are involved in the degradation of nutrients and organic matter (nutrient cycling), working as shredders in natural ecosystems and acting as pivotal components of the food web (He *et al.*, 2014). Ingestion is the most likely route of NMs uptake by *D. magna* through active selection by the feeding apparatus, as well as uptake or passive diffusion alongside other larger materials (Rosenkranz *et al.*, 2009). Some studies showed that after feeding, ingested particles very rapidly appear in the gut of *Daphnia*, and it has been reported that their gut will fill within 30 min of exposure to food under optimal conditions (Rosenkranz *et al.*, 2009). After ingestion, food particles will be digested, and the nutrients will transport to large spherical storage cells through the digestive tract epithelial lining. The storage cells are dispersed along the digestive tract, and their largest concentration happens to be near the posterior curve of the digestive tract in the animals abdominal part.

Many studies have investigated the toxicity of NMs on different aquatic organisms, but little is known about the kinetics of their accumulation (Tan *et al.*, 2016). Available information and data about the interaction of manmade NMs and aquatic species are very limited. The environmental health effects of NMs are beginning to be addressed in laboratories at the organ and cellular level, but the degree of interaction of these particles with each organ and cell type is an area of research that needs more attention from the ecotoxicity community.

1.2.2. Micro and Nanoplastics

It has been demonstrated that microplastics are a worldwide threat to marine environments. They continuously break down and undergo fragmentation because of the chemical and physical forces they face from waves, wind and hydrolysis and UV degradation (Della Torre *et al.*, 2014). Therefore, microplastics, as well as nanoplastics, will continue increasing with time, and their global distribution will increase due to their abundance in seawater, even reaching remote areas (Della Torre *et al.*, 2014). Microplastics are widely released as pellets, powders and granules used in different applications in industry, such as personal care products and nanomedicine (Della Torre *et al.*, 2014). The fate and impact of nanoscale plastics is poorly investigated within fresh water ecosystems, although microplastics have been well investigated in terms of fate and marine environmental impact (Della Torre *et al.*, 2014). Due to their small size microplastics are likely to accumulate and be ingested by marine and freshwater organisms.

It has been reported that polystyrene (PS) nanoparticles were transferred in the food chain from algae to fish through zooplankton and the fish behaviour and fat metabolism were affected (Della Torre *et al.*, 2014). PS is one of the most used plastics around the world, being used in medical applications, food, insulation, compact disc cases, industrial packaging, disposal cutlery, toys and building materials (Della Torre *et al.*, 2014). It is the fourth most abundant plastic in oceans as nano- and micro-debris, and in estuarine habitats, it represents 24% of the identified microplastics (Della Torre *et al.*, 2014).

PS NPs are nanoscale particles with a core of PS and variable functional groups determining the particle's effective surface charge (Della Torre *et al.*, 2014). Plain PS NPs are the most common PS NPs, with carboxyl and amine functionalization also widely available (Della Torre *et al.*, 2014). PS NPs are available in various sizes and different surface

functionalizations, and they act as a model system for both microplastics and nanoplastics. They are also available in fluorescently labelled forms which makes them ideal for tracking and localization (Nasser and Lynch, 2016). Those features make them of interest for toxicity studies to answer unsolved environmental impact issues within aquatic species (Nasser and Lynch, 2016). After the first evidence that was recently published about their abundance and accumulation in terrestrial and freshwater environments, microplastics are now identified as a major and significant environmental pollutant (Tibbetts *et al.*, 2018). Studies show that every day 8 million metric tonnes of plastic find their way to the oceans (Tibbetts *et al.*, 2018). Microplastics can remain in the environment for hundreds to thousands of years, due to the fact that they are highly durable, and they have a variable potential for biogeochemical or physical breakdown (Tibbetts *et al.*, 2018). When microplastics are ingested, a fraction of the ingested particles can reach tissue or even the liver depending on their size, which can result in reduced growth, inflammation and lipid accumulation, mortality and immobilisation (Tibbetts *et al.*, 2018).

A significant increase in the abundance of microplastics has been noticed with the growth of NMs applications (Nasser and Lynch, 2016). They could be manufactured (less than 5 mm in size) or derived from the breakdown of large plastic debris, which over time become weathered and transform into sizes within the nanoscale (Nasser and Lynch, 2016).

1.2.2.1. A Review on *Daphnia magna* and Mixture Toxicity with Polymeric NPs

(this section was published in nano today as (Martinez *et al.*, 2022)).

This section was written to contribute to a study reviewing the literature of mixture toxicity studies of different types NMs combined with other materials towards *D. magna* and our

contribution involved reviewing the studies that investigated the joint toxic effects of nano plastics to *D. magna.*

Polymeric NMs are a large group of materials. They can be micelles, vesicles, star polymers, and inorganic-polymer hybrids of different shapes and sizes, different surface chemistry, surface charge, etc. Due to these numerous different types, a wide number of potential applications have been suggested, from environmental applications to nanomedicine. In this section, five studies were found addressing co-exposure of pollutants with polymeric NMs by searching the keywords *Daphnia magna*, mixture toxicity, joint toxicity and nanoplastics in the web of science.

A recent study quantitatively looked into the effects of the combined acute toxicity of nano-polystyrene (100 nm diameter) and polychlorinated biphenyls (PCBs) on *D. magna* based on analytical chemical speciation by measuring the sorption coefficients of PCBs to nano-polystyrene (PS NPs) (Lin *et al.*, 2019). Their findings showed that the toxicity of the combined chemicals depended on the relative concentrations of PCB and PS NPs. When PCB were obtained with a certain amount of PS, they were less toxic towards *D. magna* as the dissolved concentration of PCB was lowered and thus it was less bioavailable to the daphnids, while the toxicity was increased when using excessive amounts of PS, likely as a result of increased internal exposure due to internalization of PCB bound to NPs. In this study they applied a passive dosing method to analyse the sorption coefficients of 8 solid chemicals [PCB-1, 3, 9, 11, 18, 77, hexachlorobenzene (Hexa-CB) and pentachlorobenzene (Penta-CB)] with 100 nm PS particles and correlated the speciation results with the observed toxicity endpoints, identifying joint toxicity effect of PS and PCB-18 to *D. magna*. For the mixture toxicity experiment they monitored the lethality to *D. magna over* 48 h by exposing

the daphnids to a fixed concentration of PCB-18 (640 µg L^{-1}, i.e., the LC_{50} of PCB-18 alone) and varying the PS concentration from 0 to 75 mg L^{-1}. Their results showed that when *D. magna* were exposed to PS at concentrations lower than 1 mg L^{-1}, their lethality decreased as the concentration of PS increased. When the PS concentrations were higher than 1mgL^{-1}, the lethality of *D. magna* increased with the addition of PS particles. To interpret their results, the authors studied the sorption coefficient to understand the combined toxicity of PCB and 100 nm PS NPs, and the results indicated that combining PCB-18 with PS can reduce the free concentration of organic pollutants and thus the toxicity towards *D. magna* at low PS concentrations, while at higher PS NP concentrations the uptake of the NPs with associated PCB increases the availability (local internal concentration) of the PCB-18 and thus its toxicity).

Another study revealed for the first time the effects of combining two complex matrices (PS NPs and humid acid (HA)) on the bioaccumulation of polycyclic aromatic hydrocarbons (PAHs) by *D. magna* (Lin *et al.*, 2020). The aim of this study was to evaluate the joint effects of dissolved organic matter (DOM) and NMs on the bioaccumulation of typical PAHs (e.g., anthracene, phenanthrene, pyrene and others) by applying a modified matrix- inclusive biodynamic model with full quantification for determining the uptake pathways of PAH for various complex systems under environmentally realistic conditions and concentrations. For simulating the open water scenarios, where PAHs are present from various sources they utilized passive dosing vials, which allowed identification of the uptake pathways by enabling constant determination of the concentrations of freely dissolved PAHs during the entire experiment. Suspensions of four different matrices for PAH exposure were prepared using the (M7) artificial culture medium: the mixture of 100 mgL^{-1} HA and 1 mgL^{-1} PS; 100

mgL^{-1} HA; 1 mgL^{-1} PS, and a solution of M7 medium as a control. The results showed that the rate of PAH ingestion of the HA-PS or the HA matrix was faster than the PS matrix, which could be due to the variation in matrix mass added at the beginning of the study. The transfer of anthracene from the HA-PS, HA and PS matrices via the gut to lipids were analysed and the uptake kinetics of anthracene had the same magnitude for the different matrices. To indicate the net mass transfer kinetics along treatments, the ratio of forward and backward rate constants (k_1/k_2) were used as a lipid-matrix partition coefficient. Results showed that in the PS matrix, all PAHs had a $k_1/k_2 < 1$ and with the increase of the PAHs hydrophobicity the k_1/k_2 increased, indicating a "hindering effect" from PS on the PAHs intestinal uptake by *D. magna*, and for PAHs with lower hydrophobicity, the "hindering effect" was higher. In the HA-PS and HA matrixes, all PAHs had $k_1/k_2 > 1$ and with increasing PAH hydrophobicity the value of k_1/k_2 decreased, indicating that the HA-PS and HA matrices enhanced the mass transfer of PAHs from the matrices to lipids. While for the PAHs with low hydrophobicity, the facilitation of mass transfer was more significant. Furthermore, anthracene was utilized to study the transfer efficiency. At the beginning of treatments, the transfer efficiency was larger than zero, and at 1.2 h and 1.0 h the efficiency decreased to less than zero in the HA and PS suspensions, which indicated a "carrier effect" of the matrix, implying that there were net mass transfers from matrices to lipids. In contrast, the transfer efficiency slowly decreased over time becoming less than zero at 5.0 h in the HA-PS suspension, which indicates that the intestinal uptake reached equilibrium after a period of time turning the matrix transfer into a "cleaning" process when the transfer efficiency was less than zero. The role / contribution of different uptake pathways to equilibrium bioaccumulation for treatments that contain different types of matrices were evaluated. Results showed that dermal uptake is the major route for the bioaccumulation of

PAHs, while intestinal uptakes from singular or complex matrices at environmentally realistic concentrations are trivial. The effect of a complex matrix on PAHs bioaccumulation was evaluated by a lipid normalized bioaccumulation factor (BAFL). Evaluations indicated that the bioaccumulation of PAHs in *D. magna* was through dermal uptake from the solution that had no complex matrix (i.e., no PS particles or HA). With increasing hydrophobicity of PAH, the logBAFL values substantially increased in all suspensions. Compared with the control groups, PS decreased the BAFL for anthracene, phenanthrene, acenaphthene and fluorene. For the highly hydrophobic PAHs, no significant effects were observed. The BAFL (of anthracene, phenanthrene, acenaphthene and fluorene) had no significant variation in both HA-PS and HA matrixes, whereas for pyrene and fluoranthene, an increase of 1.22–3.61 times and 1.75–2.78 times were observed respectively. The total concentrations of PAHs, as well as the affinity of NMs for *D. magna,* were decreased with the addition of HA.

The effects of co-exposing PS NPs with phenanthrene (Phs) as a model PAH, as well as the bioaccumulation and environmental fate of ^{14}C-Phs within freshwater systems using *D. magna* as a model organism were studied (Ma *et al.*, 2016). The authors tested five different sizes of PS particles ranging from 50 nm to 10 µm. The effects of the PS particles on the bioaccumulation and transformation of Phs, which is mutagenic and carcinogenic, were determined using a radioactive tracer. Their findings revealed that the 50 nm PS NPs at 10 mg L^{-1} were toxic and caused significant physical damage to the thoracopods of *D. magna*, affecting their swimming and filter feeding behaviour by accumulating on the surface of the thoracopods. An additive effect was observed from the joint toxicity of 50 nm PS NPs and Phs when co-exposed to daphnids. For the bioaccumulation tests the authors performed a 14-day incubation experiment and showed that the presence of 10 µm MPs did not

significantly affect the transformation, dissipation, and bioaccumulation of Phs while the 50 nm NPs showed a significant effect, enhancing the bioaccumulation of Phs-derived residues in the body of *D. magna*. This could be due to the higher adsorption capacity of Phs on the 50 nm PS NPs compared tto the larger particles which have lower surface area at fixed mass. The findings of this experiment confirm the importance of assessing both chemical and physical impacts and quantifying the bioaccumulation of the individual components and the mixture in order to have a better understanding of the interaction of NPs with hydrophobic pollutants in the environment.

The role of dissolved organic matter (DOM) on the sorption of silver ions (Ag^+) onto 300 nm polyethylene (PE) and 600 and 300 nm polystyrene (PS) particles as models of nanoscale plastic debris (NPD) was investigated over 6 days (Abdolahpur Monikh *et al.*, 2020). *D. magna* was used as a model organism to determine how NPD affects the toxicity profile of Ag^+ in the absence and presence of DOM. Their findings demonstrated that under environmentally realistic conditions, the sorption of Ag^+ ions onto NPD is influenced by the size and chemical composition of the particles. Their study showed that when using a constant particle number concentration for all treatments, a higher quantity of Ag^+ absorbed to the 600 nm PS-NPD compared to the 300 nm PS-NPD and PE-NPD. However, in the presence of 300 nm PS and PE, the toxicity of Ag^+ to *D. magna* was higher that when the 600 nm PS was present, implying that larger particles of NPD can be potentially less toxic than smaller particles of NPD even if smaller particles absorb a lower number of contaminants per particle. PE NMs sorbed a lesser amount of Ag^+ compared to PS of the same size (300 nm). However, in the presence of PE-NPD, the toxicity of Ag^+ ions was higher in some cases, suggesting that the toxicity of NPD can be affected by the chemical

composition of thr particles. Their findings also showed that when DOM were present at concentrations from 1 mg L^{-1} to 50 mg L^{-1}, the sorption of Ag^{+} onto the 600 nm PS decreased, while the sorption of Ag^{+} onto the 300 PE and PS increased when mixed with DOM. This study suggested that the Trojan horse effects of NPD may be inhibited by the presence of DOM in natural aquatic ecosystems. This study demonstrated the importance of understanding the relationship between particle size, chemical composition and the role of DOM when evaluating the toxicity of NMs and determining the potential for a Trojan horse impact in model organisms.

1.2.2.2 Eco-corona and Their Impact on Micro- and Nano-scale Plastics Toxicity

(This section was published in an RSC book as a chapter (Reilly *et al.*, 2022)).

Once released into the environment, pristine MP will come into contact with living organisms and biological matter, undergoing transformation processes by interacting with environmental components which leads them to adsorb proteins and other biomolecules to form a complex layer on their surface called protein corona or eco-corona depending on the type of bound material (Treuel and Nienhaus, 2012; Fadare *et al.*, 2020). The eco-corona forms from interacting with the byproducts of living organisms' metabolic activities, such as the exoproteome, while the protein corona layer results from a focus on the NM interaction with endogenous proteins (Fadare *et al.*, 2020). The binding proteins provide NMs with a biological identity and can affect their uptake by cells and living organisms through recognition by endocytotic receptors (Chetwynd and Lynch, 2020). The protein-coated NMs interact specifically with biological systems rather than the non-specific membrane binding that occurs with bare NMs (which actually pull out a corona through damaging cellular

membranes), and can significantly influence the fate and toxicity of NMs (Lesniak *et al.*, 2012; Treuel and Nienhaus, 2012; Markiewicz *et al.*, 2018). The physicochemical properties and behaviour of NMs are strongly affected by their interactions with the environmental bio-matter (Fadare *et al.*, 2020). NM toxicity towards organisms can be enhanced or reduced by the presence of biomolecule (protein) coronas on their surface, as these proteins can change the distribution, adsorption, biotransformation and fate of NPs in natural environments as well as in individual organisms (Wheeler *et al.*, 2021). Transformation of NMs in biological media is a crucial issue in ecotoxicity studies, and understanding the process of corona formation is a complex task that should be carefully considered in experimental designs to better interpret and assess the biological impact of NMs.

Although many studies have assessed their impact on the environment, the biomolecular interactions of MPs/NPPs with aquatic organisms still require more attention to fill the large knowledge gap in the literature. The synthetic identity of NMs governs the extent of nano-bio interactions and along with the nature of the available biomolecules for binding, determines the composition and structure of the corona layer formed. Therefore, the curvature, topography and chemistry of the NMs surface are important factors to consider in protein corona interaction studies (Walkey and Chan, 2012). The characteristics and properties of NMs are significantly different from their macro-scale counterparts due to their high surface area to volume ratio, which leads to complexity when performing ecotoxicity studies. In addition to the physicochemical properties of NMs, such as size, surface charge and composition, there are other factors that play a major role in identifying the corona composition, including environmental such as pH, ionic strength, time and the relative biomolecules ratio to the surface area of NMs (Markiewicz *et al.*, 2018).

1.2.2.2.3 What are Eco-coronas- How, When and Why do They Form?

The adsorption of a protein corona to the surface of NMs in biological systems has been a major area of interest for researchers over the last decade (Chetwynd *et al.*, 2020). The macromolecular components of natural terrestrial and aquatic environments are poorly characterized compared to the complex physiological environments, such as lung surfactants, plasma and intestinal fluid, due to the vast investment in pharmaceuticals and human health. The composition of the formed protein corona in biological systems is significantly different from corona profiles in physiological fluids, which can affect the binding and affinity of biomolecules on surfaces of NMs (Markiewicz *et al.*, 2018). The exposure time of NPs to biological systems and their physical and chemical properties have been reported in many studies to affect their biodistribution as well as their pathophysiological and therapeutic effects (Tenzer *et al.*, 2013). The kinetics of protein adsorption is a time-dependent dynamic process, with proteins continuously adsorbing and desorbing from the NM surface based on abundance and affinity for the NMs surface (Walkey and Chan, 2012). The mechanism of adsorption is determined by how proteins migrate to the surface of NMs, either by travelling down a gradient of potential energy or by diffusion. Once proteins come close to the NM surface, adsorption will spontaneously occur if it is thermodynamically favourable (Walkey and Chan, 2012). The synergy of NMs and cells within living organisms is determined by the formulation of this corona layer on the surface of particles.

In addition to plastics and chemical contaminants in aquatic systems, natural organic matter (NOM) is also present, which are complex environmental macromolecules originating from decomposition processes or from organismal exudates with a great variation in their chemical and physical characteristics (Markiewicz *et al.*, 2018). Based on the origin of NOM, it is often categorized into two groups: (i) allochthonous: fulvic acids (FA), humic acids (HA) and humic substances originating from terrestrial environments, (ii) autochthonous: biopolymers secreted by living organisms (e.g., bacteria

and algae) and they are referred to as extracellular polymeric substances such as nucleic acids, proteins and polysaccharides (Markiewicz *et al.*, 2018). The protein corona layer includes proteins from NOM as well as proteins and polysaccharides secreted by living organisms. This layer of surface-bound biomolecules represents a major element of the ecological and biological identity of NMs due to their primary interactions with surrounding environmental components. The eco-corona can stabilize (e.g, stay dispersed) or destabilize NMs (e.g, agglomerate) and depending on the conditions of the surrounding systems they can change their affinity to biological surfaces (Markiewicz *et al.*, 2018). The structure and composition of protein corona can be characterized by the following parameters: (i) The affinity of proteins to NPs, which controls their adsorption and dissociation during their interactions with biosystems or during their translocation to new compartments. (ii) The density and thickness of the protein coronas, which dictates the overall size of the NMs. (iii) The orientation and arrangement of proteins in the corona, as this can determine the catalytic domains as well as the accessibility of prospective binding sites. (iv) The conformation of proteins in the corona, which may impact the activity of bound proteins and their interaction with macromolecules (such as cellular receptors). (v) The quantity and identity of proteins available to form the corona, which can help to identify the possible array of bio-interactions besides their individual binding strengths (Walkey and Chan, 2012).

A recent review summarized the scientific evolution of studying the formation of bimolecular coronas on the surface of NMs as follows: the term protein corona was used to describe biomolecules, proteins binding to surfaces of NMs, metabolites and lipids formed within organisms living at high protein content environments, whereas the environmental corona results from complex environmental matrices consisting of various sets of humic acids and natural organic matter (NOM) forming independently of living organisms (Wheeler *et al.*, 2021). Conversely, the term eco-corona is used to describe biomolecules resulting from a certain organism when exposed to NMs including

proteins that may result from metabolites, dissolved organic matter (DOM), and exopolymeric substances in addition to the environmental coronas.

Proteins that strongly interact with the NMs surface are termed the “hard corona” and the more abundant proteins that form the initial corona layer and the loosely bound and exchanging proteins are termed the “soft corona” (Payne, 2019). Distinguishing between soft and hard coronas and the adsorption of multiple layers of proteins onto NMs surface has been one of the most debatable issues in the literature. The predominant hypothesis describes the “soft corona” as an outer layer of weakly bound proteins rapidly exchanging, whereas the “hard corona” was described as an inner layer of proteins that are tightly bound (Hadjidemetriou and Kostarelos, 2017). The soft corona is believed to be formed on short time scales within seconds to minutes from interacting with biological systems, and over time on the order of hours, it will evolve into a hard corona (Treuel and Nienhaus, 2012). It has been suggested by some proposed models that soft corona proteins are associated with the proteins in the hard corona through weak protein-protein interactions, while the hard corona proteins directly interact with the surface of NMs (Hadjidemetriou and Kostarelos, 2017), although in reality there is a more complex interplay with proteins and metabolites in terms of interactions with the NMs in the complete corona (Chetwynd and Lynch, 2020).

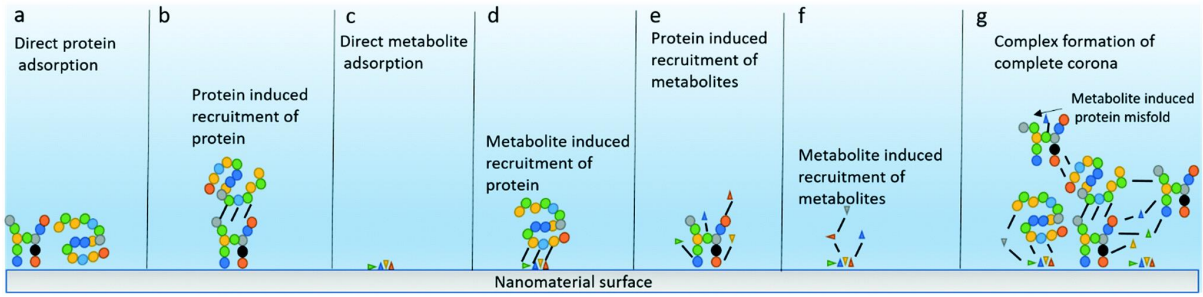

Figure 1.5. Illustration of the Mechanisms corona formation around NMs surfaces (Chetwynd and Lynch, 2020).

Mechanisms of protein corona formation are difficult to understand without enhancing our database and knowledge about the factors (e.g., NMs properties, protein exchange rate, experimental conditions) that govern its formation and composition within biological contexts. Evaluating the toxicity, fate and bioaccumulation of NMs in the environment can be improved by understanding the behaviour of adsorbed proteins (e.g., exchange rate) in new environments when NMs are transported through biological systems. Therefore, it is crucial to put more effort into understanding the and formation and kinetic evolution of coronas while studying and developing NMs for biomedical or biological applications.

1.2.3. Graphene Quantum Dots (GQDs)

The most abundant naturally occurring material, in the form of coal, is carbon. In the state of graphite, carbon has been classified into zero (0D), one (1D), two (2D), and three-dimension (3D) graphite, with 2D graphene being the strongest and thinnest ever known material, identified as a single layer NM peeled off multi-layer graphite due to the van der Waals force within the layers (Kumar *et al.*, 2020). Graphene and fullerene are recently discovered allotropes of carbon, attracting the attention of scientists from various disciplines across the globe. In 1985, the football shape fullerene, along with small needle-shaped carbon nanotubes (CNTs) were discovered for the first time in 1991 and were characterized, followed by the discovery of graphene shaped materials at the University of Manchester in 2004, which astonished scientists globally with their unique features making them the miracle of the 21st century (Al Jahdaly *et al.*, 2021). These discoveries led to the development of carbon quantum dots (CQDs) in 2004; then, in 2008, the youngest member of carbon-based NMs was born and named graphene quantum dots (GQDs), where bandgap effects and quantum confinement were revealed (Facure *et al.*, 2020).

The term carbon dots (CDs) is generally used to describe materials like carbon nanodots (CNDs), carbon quantum dots (CQDs), and carbonized polymer dots (CPDs and GQDs) (Kumar *et al.*, 2020). The classification of CDs is based on their carbon core structure, unique properties, and surface groups (Al Jahdaly *et al.*, 2021). In this thesis, our work focused on GQDs, evaluating the effect of surface functionalization and GQD ageing on the toxicity of these materials toward the model organism *D. magna*. GQDs unique properties are derived from both graphene and CDs. The unique properties of GQDs are what make them more desirable than inorganic CDs in many applications, e.g., in biomedical applications. GQD is considered better than graphene oxide or graphene due to various factors such as its small size and low toxicity (Zhao *et al.*, 2020). The ability to assemble and equip GQDs with functional groups at their edge is a unique feature, as this has the potential to alter photoluminescence and reduce non-radiative recombination to improve quantum yields, optical properties, biocompatibility, and electronic properties (Bacon *et al.,* 2014).

1.2.3.1. Structure, Characteristics, and Applications of GQDs

GQDs are derived from carbon-rich materials such as graphene oxide (GO), macromolecules such as polysaccharides, CNTs, carbon fibers, graphite or fullerene, and they are a subset of CQDs (Li *et al.*, 2019; Kumar *et al.*, 2020; Al Jahdaly *et al.*, 2021). They consist of single or multi-layers of graphene fragments with a transverse dimension of less than 100 nm and a height of less than ten graphene layers (Al Jahdaly *et al.*, 2021; Zhu *et al.*, 2022).

The characteristics of GQDs are what distinguish them from other carbon materials, such as their ability to adjust electrons, their quantum confinement behaviour, long-term opposition to photo-bleaching, vigorous chemical inertness, fluorescence activity, luminescence emission, excellent surface grafting than other carbon-based materials, high

surface area, *in vivo* and *in vitro* biocompatibility, corrosion resistance, high photo/pH stability and stability in aqueous solutions (Tabish *et al.*, 2018; Kumar *et al.*, 2020; Zhu *et al.*, 2022). Their solubility in organic solvents such as tetrahydrofuran (THF) ethanol, dimethylformamide (DMF), dimethyl sulfoxide (DMSO) and acetone is excellent, and the carboxyl and hydroxyl-containing moieties attached to their edges improve their dispersibility in water-based solvents (Kumar *et al.*, 2020). Depending on the method used to synthesise GQDs, they can be tuned by chemical methods empowering their hydrophilic nature.

The above-mentioned physical and chemical properties gave GQDs the quality to be useful in many medical applications such as the treatment of Alzheimer's and Parkinson's disease, delivery of drugs across the blood-brain barrier, bioimaging, biosensing, anti-diabetic and antibacterial substances, and tumour-targeted drug delivery (Henna and Pramod, 2020). They are also great candidates for designing devices in: i) novel catalyst systems for pollutant degradation; ii) adsorbent materials for the removal of contaminants; iii) and biosciences for detecting risk analytes such as heavy metals, food contaminants, antibiotics, and pesticides (Facure *et al.*, 2020).

1.2.3.2. Synthesis of GQDs

Normally there are two main approaches/methods applied to synthesise GQDs, following bottom-up or top-down strategies.

1.2.3.2.1. Top-down Method

The synthesis of GQDs by top-down methods means they are synthesised by cutting large graphite materials into small fragments. They can be prepared by chemical or physical means of cutting from materials such as graphite powder, graphene, graphene oxide, coal,

carbon fiber, or carbon nanotubes (Henna and Pramod, 2020). This strategy may involve different approaches such as hydrothermal cutting, solvothermal cutting, microwave-assisted, oxidative cleavage, electrothermal exfoliation, chemical vapour deposition / chemical oxidation, pulsed laser ablation, ultrasonic-assisted, or a combination of all the above-mentioned techniques (Henna and Pramod, 2020; Zhao *et al.*, 2020). GQDs are widely used due to the high product yield and availability of raw materials (Henna and Pramod, 2020). The top-down method is more cost-effective but still has disadvantages like the lack of morphological control and the harsh reaction conditions required. However, the main advantage of this approach is the resulting oxygen containing functional groups which enhance the functionalization and solubility of GQDs (Joshi *et al.*, 2016).

1.2.3.2.2. Bottom-up Method

This method is described by using small organic molecules as precursors for obtaining GQDs (Facure *et al.*, 2020). Typically, this approach involves molecular carbonization, electron beam irradiation techniques, and microwave methods. In general, small molecules such as sugars, citric acid, phenyl compounds, and amino acid are used as starting materials (Zhao *et al.*, 2020). Though this approach gives precise control on size, shape, and morphology, expensive precursors and complex synthesis steps are the main shortcomings associated with this approach (Joshi *et al.*, 2016). This method also results in GQDs that have a strong aggregation/agglomeration tendency which limits its applicability (Joshi *et al.*, 2016).

1.2.3.3. Surface Functionalization

The modification of GQDs surface is performed to adjust its electrical and optical characteristics, and usually, heteroatoms such as F, N, S, B, and Cl are used for doping (Al Jahdaly *et al.*, 2021). The different methods applied to manufacture graphene-based

materials result in products with different surface groups, such as hydroxyl-, carbonyl-, carboxyl-, and epoxy-groups, as well as different sizes and debris content such as O, H, and C (Kumar *et al.*, 2020). The functional groups generally contain oxygen, and the presence of oxygen assists GQDs in interacting with molecules, making them favourable for many applications such as catalysis and sensing (Facure *et al.*, 2020). The surface groups of GQDs are either attached on the edges or to the interlayer defects, which leads to the unique edge and quantum confinement effect (QCE) properties, noting that the QCE comes from both the size of GQDs as well as the conjugated π-domains isolated on the planes of graphene (Kumar *et al.*, 2020). Chemical functionalization can modify total dipole moment and energy band gap, which leads to the modification of GQDs properties (Al Jahdaly *et al.*, 2021). It has been demonstrated that the toxicity of GQDs is determined by their size, functional groups, and surface charge (Younis *et al.*, 2020). The surface chemistry, such as hydrophobicity and charge, is controlled by the surface functionalization of graphene-based materials, which can impact the environmental fate and behaviour of these NMs in biological systems (Guo *et al.*, 2021).

1.2.3.4. Toxicity/Biocompatibility of GQDs

Although GQDs are carbon materials with low assumed toxicity and have shown great potential in many applications, their toxicity in biological systems remains an area of concern. Despite the advantages and potential applications of GQDs, very little is known about their behaviour in the environment, and their interaction with living organisms needs more attention by studying the potential toxicity mechanisms of different GQDs forms and evaluating the different methods used in synthesizing them. The toxicity of GQDs has been studied in various organisms, cells, and tissues e.g., a cytotoxicity study on GQDs with

different functional groups (COOH, NH_2, and $N(CH_3)$) was performed using A549 cells and showed no cellular mortality up to concentrations of 200 µg/mL, revealing that different surface functionalization groups do not affect the biocompatibility of GQDs (Henna and Pramod, 2020). Compared to graphene oxide and colloidal semiconductors, GQDs were considered to be non-toxic in most publications. Here we highlight some of the key findings of related toxicity investigations performed by various research groups.

A recent study investigated the toxicity of GQDs and ZnO NMs individually and combined on dinoflagellate *Gymnodinium Sp.* (Zhu *et al.*, 2022). The response and growth of the marine algae exposed to 1, 10 and 20 mg/L GQDs and nano-ZnO were explored in f/2 medium. The growth of algal cells showed slight effects when exposed to nano-ZnO, while the *Gymnodinium's* growth inhibition increased upon increasing GQDs concentration, indicating a clear dose-response. The treatment with both materials induced ROS accumulation and triggered the intracellular defensive system. Compared to the single GQDs exposure, when combining GQDs and nano-ZnO, the inhibitory effects were decreased and showed an antagonist response. Due to the sedimentation and aggregation of NPs, the authors suggested that adding nano-ZnO can decrease the toxicity of GQDs. SEM images showed that NPs were adsorbed into the surface of cells causing cell shrinkage and leading to cell morphological changes (Zhu *et al.*, 2022).

Another study looked into the autophagy and cytotoxicity of three different kinds of GQDs, including hydroxylated hGQDs (HO-GQDs), carboxylated cGQDs (COOH-GQDs), and aminated aGQDs (NH_2-GQDs) using A549 lung cancer cell lines as a model (Xie *et al.*, 2019). The study concluded that aGQDs and cGQDs were non-cytotoxic within the tested concentration range, whilst hGQDs were the most toxic, causing significant cell death at a concentration of 100 µg/mL. The best biocompatibility was exhibited by cGQDs showing no

significant impact on autophagy and cell apoptosis, while hGQDs caused significant cell mortality while inducing low levels of autophagy. The aGQDs showed strong autophagy induction ability, although no significant cell viability loss was observed (Xie *et al.*, 2019). The biocompatibility of GQDs was evaluated by analyzing their impact on the embryonic development of zebrafish (Wang *et al.*, 2015). They investigated the *in vivo* toxicity and biodistribution by exposing embryonic zebrafish to a range of GQDs concentrations (0, 12.5, 25, 50, 100, and 200 μg/mL) for 4-96 h post-fertilization. The uptake of GQDs, larval behaviour, heart rate, spontaneous movement, hatch rate, malformation, and mortality were assessed. Their results showed that larval behaviour (visible light test) indicated that the speed and total swimming distance were decreased depending on the exposure dose. Embryos that were exposed to the higher concentrations (25, 50, 100, and 200 μg/mL) caused significant hyperactivity in the dark-light test, while exposure to a lower concentration (12.5 μg/mL) showed some hyperactivity. The intestine and heart were the main areas where GQDs fluorescence was detected. When exposed to GQDs at concentrations of 50, 100, and 200 μg/mL a significant decrease in spontaneous movement was observed. A variety of embryonic malformations were observed when exposed to high GQDs levels (200 μg/mL), including vitelline cyst, pericardial edema, and bent tail. The heart and hatch rates were decreased as the exposure concentrations increased, in parallel to an increase in mortality. Although this study concluded that GQDs are relatively non-toxic at low concentrations, the embryonic development progression is affected and disturbed at concentrations exceeding 50 μg/mL (Wang *et al.*, 2015).

In 2016 a comprehensive review of the toxicity of GQDs summarized the important existing tests in both *in vitro* and *in vivo* studies (Wang, Cole and Li, 2016). The authors discussed topics including the mechanism of uptake by cells and parameters that govern GQDs

toxicity, such as particle size, chemical doping, concentration, surface chemistry, ROS generation, and synthesis methods. Generally, studies on GQDs proved excellent biocompatibility and low *in vitro* and *in vivo* toxicity rates compared to their counterparts, including conventional semiconductor quantum dots, GO, and CNTs. However, there is a variation in GQDs toxicity reports for different kinds of GQDs and different assessment methods, with available evidence showing that certain cells can experience mortality with certain GQDs by generating intracellular ROS. The toxicity of GQDs is concentration dependent as studies with different cells and certain *in vivo* tests such as zebrafish embryos determined that GQDs toxicity increases with increasing GQD concentration. Some GQDs showed high cell viability at concentrations up to 0.5 μg/L and for many a concentration of 200 μg/L is considered a safe concentration cut-off. Different synthesis approaches also had different toxicity effects, whereby GQDs synthesised by top-down approaches were less biocompatible compared to the ones obtained by bottom-up methods. The size of GQDs was an important factor governing their toxic effects, as the small-sized GQDs (<10nm) showed lower toxicity compared to the larger-sized GQDs. In addition, a variety of toxic profiles were observed with different surface chemistry states where raw GQDs tend to be less biocompatible compared to GQDs doped with benign elements such as boron. Lastly, although the majority of studies showed low GQDs cytotoxicity, there was evidence showing that ROS was not completely excluded from GQDs, and to regulate their toxicity, polyethylene glycol (PEG) has been applied to reduce the generation of ROS, but more studies are needed (Wang, Cole and Li, 2016).

A 2016 publication briefly reviewed and summarized the toxicological effects of GQDs, wherein the authors concluded that many studies reported that GQDs are less toxic than GO which could be due to their smaller size causing less damage to the cell membrane (Joshi *et*

al., 2016). *In vitro* studies on animal cell lines concluded that the cytotoxicity of GQDs depends on the synthesis method and starting material, as GQDs synthesised from amino acids and GO are less toxic than those synthesised from carbon nanotubes (Joshi *et al.*, 2016).

The available data indicate that GQDs are less toxic than other graphene-based materials encouraging more developments in medical and biological fields. However, it is still very early to confirm that GQDs are nontoxic, as research is at its early stage with limited data available, and only little is known about how these materials behave in the environment. Although there have been graphene-based materials toxicity studies reported in the literature, based on our literature evaluation, we have not found any study investigating the effect of GQDs on *D. magna*, which is what encouraged us to investigate the effect of these materials on the studied model organism in this project.

1.2.4. Molybdenum Disulfide (MoS_2)

In addition to the previously discussed carbon-based NMs, researchers have recently focused on alternative 2D graphene-like materials to overcome the shortage of graphene and broaden its applications. While graphene and its composites showed success in a wide range of applications, it still has disadvantages and shortcomings such as zero band gap, intrinsic defects and low chemical reactivity (also called chemical inertness), which led scientists to search for better alternatives (Yadav *et al.*, 2019). 2D graphene-like Transition metal dichalcogenides (TMDs) have attracted the interests of scientists exploring many different materials applications, with Molybdenum disulfide (MoS_2) being one of the most stable and widely studied TMDs mainly due to it being a monolayer semiconductor with a direct band gap of 1.8 eV (Li and Zhu, 2015). The interest in TMDs comes from their

intriguing characteristics, such as excellent catalytic properties, biocompatibility, high transition charge-density-wave, and high conductivity (Yadav *et al.*, 2019). The recently emerging MoS_2 nanosheets stood out as an excellent alternative 2D material due to their unique electrical, biological, mechanical and physicochemical properties, which distinguish them from graphene-based nanocomposites, and leading to outstanding new developments and novel applications in biomedicine, energy storage, electronics, photocatalysis and wastewater remediation (Wang and Mi, 2017; Wang *et al.*, 2020; Ishag and Sun, 2021). The large bandgap of MoS_2, which changes from an indirect to a direct gap in thin structures, can solve many of the problems faced by the previously generation of graphene-based materials, which have zero bandgap. MoS_2 materials also have newer applications in many fields, such as oil/water separation and hydrogen generation, terahertz technology and hydrogen detection (Samy *et al.*, 2021). MoS_2 can be exfoliated from its bulk counterparts and is electrically and structurally similar to graphene. It can be synthesized with controlled morphologies such as nanotubes, radar-like particles, nanosheets, flower-like particles and quantum dots (Yadav *et al.*, 2019).

1.2.4.1. Structure, Properties and Synthesis of MoS_2

MoS_2 is an inorganic compound of the TDMs series composed of two atoms of sulfur and one atom of molybdenum. In its bulk form, it naturally exists as a black powder consisting of monolayers with weak van der Waals forces between neighbouring monolayers and strong S-Mo covalent bonds within each layer (Wang and Mi, 2017). The structure of MoS_2 varies from 0D (quantum dots and nanoplatelets), 1D (nanowires and nanotubes), 2D (nanosheets), or 3D (bulk) structures, and they exist in several shapes and layers (Samy *et al.*, 2021). Bulk MoS_2 exhibits an indirect bandgap of 1.2 eV, while exfoliated MoS_2 materials

have a direct band gap of 1.8 eV, leading to excellent photoluminescence and absorption properties (Yadav *et al.*, 2019). They can be metallic, superconducting or semiconducting materials as their properties and applications change from one dimension to another (Samy *et al.*, 2021). Exfoliated MoS_2 nanosheets generate electron-rich atoms, and they are negatively charged with a highly hydrophilic nature, which makes them water dispersible (Wang and Mi, 2017). The size of 0D MoS_2 quantum dots ranges from 2 to 10 nm; 1D MoS_2 nanowires have an approximate width of 0.6 nm and lengths of 14 to 30 nm, and 1D MoS_2 nanoplatelets are 12 to 30nm with a width of a one-unit cell, while the 2D MoS_2 nanoribbons have a thickness of 1 to 3 MoS_2 layers (Samy *et al.*, 2021).

MoS_2 can be synthesised by the previously discussed top-down and bottom-up methods. Other methods have also been applied to obtain MoS_2 nanosheets, nanotubes, thin films and quantum dots, including thermal anisotropy (sputtering), vapour-solid growth, electron-Fenton reaction, thermal decomposition, physical vapour decomposition, and wet chemistry approach (Yadav *et al.*, 2019). However, selecting the appropriate synthesis approach depends on the target application where the materials will be used, as each of the mentioned strategies has its own advantages and disadvantages.

1.2.4.2 MoS_2 for Heavy Metals Removal from Wastewater

Inorganic pollutants such as heavy metal ions (HMIs) (e.g., Ni, Cu, Cd, Zn, As, Cr, Pb, Hg and Ag) are released into waterbodies from industrial applications including agricultural use of pesticides and fertilizers, batteries, mining activities, paper production, refining and tanneries (Gusain *et al.*, 2019). Compared to organic pollutants, HMIs are highly toxic, non-degradable and very stable in water which can cause serious health problems as a result of their accumulation in living organisms (Feng *et al.*, 2022).

Even at low concentrations in the ppm range, these HMI contaminants can cause a hazard and be life-threatening to animals, humans, aquatic biota and other living organisms (Gusain *et al.*, 2019). Health effects associated with HMIs include kidney failure, cancer, nephritic syndrome, hepatitis, encephalopathy and anemia (Baby *et al.,* 2019).

Among these HMIs, cadmium (Cd) and copper (Cu) ions are vital contaminants, and they exist in water bodies as a result of industrial activities ranging from smelting operations, mining, fabric factories, electroplating, battery designs, smelting operations, and photovoltaic cells (Baby *et al.,* 2019; Luo *et al.*, 2019). Cd has been ranked by the Agency for toxic substances and Diseases Registry (ATSDR) as the seventh most toxic metal, as it can be carcinogenic to humans and damage the respiratory system, skeleton and kidney (Baby, Saifullah and Hussein, 2019). Cu has also been reported to cause lung cancer, nervous system complications, and kidney damage (Luo *et al.*, 2019).

Elimination and effective removal of HMIs from wastewater can be achieved by various methods such as electrochemical removal, ion exchange, chemical precipitation, adsorption, biosorption, membrane filtration, solvent extraction, floating, and reverse osmosis (Han *et al.*, 2022; Wang *et al.*, 2022). Adsorption is one of the most preferred methods for researchers to remove HMIs due to its technical maturity, effective cost, simplicity and recyclability (Wang *et al.*, 2022). Many sorbents such as polymers, graphene-based materials, activated carbon clay, biomass, nanocellulose, zeolites, and natural organic matter (especially humic acid) have been applied to treat water contaminated with toxic HMIs, but factors such as their active surface area, specific affinity to the target HMIs and the limitation of functional groups lower their selectivity and absorbance efficiency (Wang *et al.*, 2018, 2022; Baby *et al.,* 2019).

Due to their tunable band gap, more abundant availability (compared to graphene), low cost, high pollutant removal capacity and speed, excellent thermal and chemical stability, outstanding biocompatibility, large surface area and mechanical flexibility, 2D MoS_2 nanosheets have recently demonstrated superior performance in removing HMIs from wastewaters (Wang and Mi, 2017; Gusain *et al.*, 2019; Ishag and Sun, 2021; Han *et al.*, 2022). Compared to other materials, S-bearing sorbents such as MoS_2 have demonstrated strong HMIs binding affinity via Lewis soft acid - soft base interactions, which led to the preference of these materials over other sorbents (Luo *et al.*, 2019; Feng *et al.*, 2022). Moreover, the negatively charged MoS_2 surface from the edge position can enhance the adsorption capacity of the positively charged HMIs (Liu *et al.*, 2019). However, environmental factors such as the presence of NOM (e.g., humic acid), ionic strength and pH can affect the adsorption capacity and toxicity of MoS_2 materials, which requires further investigation and understanding (Wang and Mi, 2017). Thus, under extreme conditions such as high pH and temperature, MoS_2 can release extra ions, which is a disadvantage for environmental applications (Ishag and Sun, 2021).

1.2.4.3 Biocompatibility and Toxicity of MoS_2

Like all other NMs, once MoS_2 is released into the environment, it will interact with biological systems. The consequence of such interaction needs to be carefully considered by analyzing the fate, transport and toxic effects of MoS_2 particles. Due to their low solubility and the absence of dangling bonds in the sulfur atoms, MoS_2 is considered to be chemically stable against environmental stressors (Wang and Mi, 2017). Although there is variation in MoS_2 nanosheet toxicity results, which depends on the preparation method and assay

conditions, it is generally considered nontoxic at concentrations up to 100 ppm (100 mg/L) (Wang and Mi, 2017). MoS_2 nanosheets are able to quench reactive oxygen species (ROS), benefiting antioxidant applications such as conformal coating (a protective coating of thin polymeric film applied to printed circuit boards), which can reduce toxicity and ROS production (Wang *et al.*, 2018). However, MoS_2 in its bulk and exfoliated forms can be oxidized to molybdenum oxide (Mo_2O_3) under harsh conditions such as strong oxidation and high-temperature (Wang and Mi, 2017). Various organisms can ingest MoS_2 particles released into the environment through different routes; inhalation, direct ingestion, water filtration, and particle's surface contact, which can interact with different types of biomolecules and generate ROS leading to oxidative stress in the targeted cells (Arefi-Oskoui *et al.*, 2021). It has been reported that the cytotoxic impact of MoS_2 nanosheets increases with increasing degrees of exfoliation, which could be due to an increase in active edge sites and surface area (Khim Chng, Sofer and Pumera, 2014).

Recently, (Sethulekshmi *et al.*, 2022) systematically reviewed the literature on the toxicity of MoS_2 NMs, and it was clear that like all other NMs, MoS_2 nanocomposites can also be toxic to living organisms. However, it is currently difficult to conclude the risks and environmental health effects of MoS_2 NMs due to the limited number of toxicity studies available. Based on our search, only one study included the model organism *D. magna* which will be discussed below in line with other relatively few MoS_2 toxicity publications.

A study looked into the impact of exfoliated MoS_2 nanosheets on three human cell lines, including one normal epithelium keratinocyte (HaCaT), and two tumoral (U937 leukaemia and MCF5 breast cancer) cell lines (Kaur *et al.*, 2018). The study investigated the antibacterial behaviour of MoS_2 nanosheets towards two kinds of *Salmonella* (wild-type *S.typhimurium* and ATCC 14028). They observed induced cytotoxic effects in both tumour

cell lines and negligible cytotoxicity in the tested keratinocyte cell line. Scanning electron microscopy images revealed a bactericidal effect when *S. typhimurium* were treated with MoS_2 nanosheets, showing that the nanoflakes' sharp edges can damage or cut the bacterial membrane. Both Salmonellas and human cells demonstrated layer (number) and concentration-dependent modulation of cytotoxicity.

Furthermore, (Wu *et al.*, 2019) studied the effect of nano- and micro-sized MoS_2 on the microbiome and intestinal metabolome in mice by oral exposure. They introduced 15 and 150 mg/kg of nano and micro-MoS_2 materials to C57BL/6 mice *via* food premixes for 90 days. The Mo accumulation of both nano-MoS_2 and micro-MoS_2 was observed in mouse organs, especially in the large and small intestine. The micro-MoS_2 had lower bioavailability than nano-MoS_2, and the nano-sized materials caused higher intestinal inflammation than the micro-sized materials at constant exposure mass. The metabolic profiles of the intestinal microbiota and intestine were significantly changed when exposed to both sizes of MoS_2, and the nano-MoS_2 had a greater impact. Their findings conclude that the nano-MoS_2 changed the metabolic profiles of the intestine by changes in the direct toxicity and microbial community, while changes caused by micro-MoS_2 were only due to changes in the microbial community.

The ecotoxicological effects of bulk and 2D MoS_2 nanosheets have been recently assessed (Arefi-Oskoui *et al.*, 2021). The authors evaluated the aquatic acute toxicity of the studied materials using model organisms from four different taxonomic groups: *Spirodela polyrhiza* (freshwater duckweed), *Daphnia magna* (freshwater zooplankton), *Pseudokirchnerialla subcapitata* (freshwater microalgae), and *Vibrio fischeri* (marine photo bacterium).

The degree of toxicity of MoS_2 materials depended on the sensitivity/type of studied organism and the MoS_2 materials size/structural properties. All organisms were exposed to

a range of concentrations of both bulk MoS_2 catalysts and MoS_2 nanosheets (0.05-2.00 g/L). The authors found that *D. magna* was the most suitable organism for evaluating nanoparticle toxicity compared to the other tested organisms due to their high sensitivity throughout the study and ease of handling. Their results indicated that in all tested organisms, bulk MoS_2 was more toxic compared to its nanosheet form at constant mass concentration. In *D. magna,* which is the organism used in all bioassays in this thesis, the bulk MoS_2 had acute toxicity at low concentrations with an EC_{50} value of 0.073 g/L, while the nanosheets MoS_2 had no inhibitory effects. The effect of incubation time effect was negligible in *D. magna* acute tests as the degree of immobilization was similar after 24 h and 48 h. More comprehensive ecotoxicological studies are urgently needed to fill the knowledge gap and to keep pace with the increased production and disposal of MoS_2 NMs into biosystems.

1.2.5. Thesis Objectives and Guide to The Results Chapters

The general objective of this thesis is to evaluate the environmental behaviour of NMs in ecological systems, assess the level of risk associated with each material, and correlate this with the NMs characteristics that govern the level and significance of NM's toxicity toward the model organism *D. magna*.

After reviewing the literature on the interaction of different NMs with biological systems and highlighting key elements that control the toxicity mechanisms of NMs towards various living organisms, such as physicochemical properties, the presence of NOM, formation of protein eco-corona and experimental conditions, the central concept of this thesis was identified based on the research areas that lack clarity and require more/novel data to fill the knowledge gap by assessing the behaviour of various NMs in aquatic environments. The model organism *D. magna* was our choice in this thesis to evaluate the impact of the studied NMs mainly because of its vital role in the food chain, environmental significance and simplicity of handling, and its status as a regulatory test organism.

The tremendous increase in plastic production and use, including micro and nano-PS resulting from natural or manmade products, is now considered one of the most problematic environmental stressors on the planet. Therefore, we have chosen to evaluate their ecotoxicological impact. QGDs were selected due to their increased use in industrial, environmental and medical applications with a significant literature gap in evaluating their toxic behaviour, especially on *D. magna*. Similarly, MoS_2 composites are novel materials that gained much interest in recent years with increased production and disposal. Therefore, the lack of knowledge in understanding the toxic behaviour of these emerging high volume and multi-application materials strongly encouraged us to take part in filling the gap. Our generated data represents a novel contribution to the environmental science community.

Our thesis results are presented in three chapters. Each chapter includes different types of NMs and has its own objectives, as summarized below.

Chapter 3 Objectives

This chapter investigates the toxic impact of four different types of PS micro- and nanoscale plastics on *D. magna*. Many factors have been assessed in this regard, including the effect of surfactants/preservatives added to dispersions during manufacture, particle size, surface charge, the role of eco-corona and particle ageing, to evaluate the acute toxicity response.

Chapter 4 Objectives

In this chapter, we evaluate the interaction of three differently functionalized GQD types with *D. magna*. The goal is to understand the role and effect of particle ageing (during storage and in salt-only culture media), as well as the effect of different surface functionalization on the acute toxicity towards *D. magna*.

Chapter 5 Objectives

Here we investigate the effect of MoS_2 particle size by studying the interaction of Bulk and nano-MoS_2 with *D. magna*. We then assessed the mixture toxicity of three different MoS_2 sizes by combining them with two representative heavy metal ions (Cu^{2+} and Cd^{2+}). The mixture toxicity tests were also performed in the presence and absence of NOM (humic acid) to assess the role of binding, uptake and bioavailability of the MHIs to the daphnids on the observed toxicity.

References

Abbas, Q. *et al.* (2020) 'Transformation pathways and fate of engineered nanoparticles (ENPs) in distinct interactive environmental compartments: A review', *Environment International*, 138, p. 105646. Available at: https://doi.org/10.1016/j.envint.2020.105646.

Abdolahpur Monikh, F. *et al.* (2020) 'Metal sorption onto nanoscale plastic debris and trojan horse effects in Daphnia magna: Role of dissolved organic matter', *Water Research*, 186, p. 116410. Available at: https://doi.org/10.1016/j.watres.2020.116410.

Abdullahi, M. *et al.* (2022) 'Daphnia as a Sentinel Species for Environmental Health Protection: A Perspective on Biomonitoring and Bioremediation of Chemical Pollution', *Environmental Science & Technology*, 56(20), pp. 14237–14248. Available at: https://doi.org/10.1021/acs.est.2c01799.

Al Jahdaly, B.A. *et al.* (2021) 'Outstanding Graphene Quantum Dots from Carbon Source for Biomedical and Corrosion Inhibition Applications: A Review', *Sustainability*, 13(4), p. 2127. Available at: https://doi.org/10.3390/su13042127.

Arefi-Oskoui, S. *et al.* (2021) 'Toxicity evaluation of bulk and nanosheet MoS2 catalysts using battery bioassays', *Chemosphere*, 268, p. 128822. Available at: https://doi.org/10.1016/j.chemosphere.2020.128822.

Arienzo, M., Ferrara, L. and Trifuoggi, M. (2021) 'Research Progress in Transfer, Accumulation and Effects of Microplastics in the Oceans', *Journal of Marine Science and Engineering*, 9(4), p. 433. Available at: https://doi.org/10.3390/jmse9040433.

Baby, R., Saifullah, B. and Hussein, M.Z. (2019) 'Carbon Nanomaterials for the Treatment of Heavy Metal-Contaminated Water and Environmental Remediation', *Nanoscale Research Letters*, 14(1), p. 341. Available at: https://doi.org/10.1186/s11671-019-3167-8.

Bacon, M., Bradley, S.J. and Nann, T. (2014) 'Graphene Quantum Dots', *Particle & Particle Systems Characterization*, 31(4), pp. 415–428. Available at: https://doi.org/10.1002/ppsc.201300252.

Barata, C. *et al.* (2002) 'The relative importance of water and food as cadmium sources to Daphnia magna Straus', *Aquatic Toxicology*, 61(3), pp. 143–154. Available at: https://doi.org/10.1016/S0166-445X(02)00052-8.

Batley, G.E., Kirby, J.K. and McLaughlin, M.J. (2013) 'Fate and Risks of Nanomaterials in Aquatic and Terrestrial Environments', *Accounts of Chemical Research*, 46(3), pp. 854–862. Available at: https://doi.org/10.1021/ar2003368.

Baun, A. *et al.* (2008) 'Ecotoxicity of engineered nanoparticles to aquatic invertebrates: a brief review and recommendations for future toxicity testing', *Ecotoxicology (London, England)*, 17(5), pp. 387–395. Available at: https://doi.org/10.1007/s10646-008-0208-y.

Benson, W.H. and Giulio, R.T.D. (eds) (2006) *Genomic Approaches for Cross-Species Extrapolation in Toxicology*. Boca Raton: CRC Press. Available at: https://doi.org/10.1201/9781420043648.

Bern, L. (1990) 'Postcapture Particle Size Selection by Daphnia cucullata (Cladocera)', *Limnology and Oceanography*, 35(4), pp. 923–926.

Boyd, C.M. (1976) 'Selection of particle sizes by filter-feeding copepods: A plea for reason', *Limnology and Oceanography*, 21(1), pp. 175–180. Available at: https://doi.org/10.4319/lo.1976.21.1.0175.

Brandon, C. (2015) 'The Evolutionary Biology of Vision in *Daphnia*', *Theses and Dissertations* [Preprint]. Available at: https://scholarcommons.sc.edu/etd/3100.

Brendelberger, H. (1985) 'Filter mesh-size and retention efficiency for small particles: comparative studies with Cladocera', *Ergebnisse der Limnologie/Advances in Limnology*, 21, pp. 135–146.

Brett, M.T. *et al.* (2009) 'Phytoplankton, not allochthonous carbon, sustains herbivorous zooplankton production', *Proceedings of the National Academy of Sciences*, 106(50), pp. 21197–21201. Available at: https://doi.org/10.1073/pnas.0904129106.

Briffa, S.M. *et al.* (2018) 'Uptake and impacts of polyvinylpyrrolidone (PVP) capped metal oxide nanoparticles on Daphnia magna: role of core composition and acquired corona', *Environmental Science: Nano*, 5(7), pp. 1745–1756. Available at: https://doi.org/10.1039/C8EN00063H.

Brooks, J.L. and Dodson, S.I. (1965) 'Predation, Body Size, and Composition of Plankton', *Science*, 150(3692), pp. 28–35. Available at: https://doi.org/10.1126/science.150.3692.28.

Buesser, B. and Pratsinis, S.E. (2012) 'Design of Nanomaterial Synthesis by Aerosol Processes', *Annual Review of Chemical and Biomolecular Engineering*, 3(1), pp. 103–127. Available at: https://doi.org/10.1146/annurev-chembioeng-062011-080930.

Burns, C.W. (1968) 'The Relationship Between Body Size of Filter-Feeding Cladocera and the Maximum Size of Particle Ingested', *Limnology and Oceanography*, 13(4), pp. 675–678. Available at: https://doi.org/10.4319/lo.1968.13.4.0675.

Casarett, L.J. and Klaassen, C.D. (2001) *Casarett and Doull's toxicology: the basic science of poisons.* 6th. ed / editor, Curtis D. Klaassen. New York ; London: McGraw-Hill Medical Pub. Division.

Chetwynd, A.J. and Lynch, I. (2020) 'The rise of the nanomaterial metabolite corona, and emergence of the complete corona', *Environmental Science: Nano*, 7(4), pp. 1041–1060. Available at: https://doi.org/10.1039/C9EN00938H.

Clemente, Z. *et al.* (2014) 'Ecotoxicological Evaluation of Poly(ε-Caprolactone) Nanocapsules Containing Triazine Herbicides', *Journal of Nanoscience and Nanotechnology*, 14(7), pp. 4911–4917. Available at: https://doi.org/10.1166/jnn.2014.8681.

Dabrunz, A. *et al.* (2011) 'Biological Surface Coating and Molting Inhibition as Mechanisms of TiO2 Nanoparticle Toxicity in Daphnia magna', *PLOS ONE*, 6(5), p. e20112. Available at: https://doi.org/10.1371/journal.pone.0020112.

De Coen, W.M. and Janssen, C.R. (1997) 'The use of biomarkers in Daphnia magna toxicity testing II. Digestive enzyme activity in Daphnia magna exposed to sublethal concentrations of cadmium, chromium and mercury', *Chemosphere*, 35(5), pp. 1053–1067. Available at: https://doi.org/10.1016/S0045-6535(97)00172-0.

De Coen, W.M., Janssen, C.R. and Segner, H. (2001) 'The Use of Biomarkers in Daphnia magna Toxicity Testing V. In Vivo Alterations in the Carbohydrate Metabolism of Daphnia magna Exposed to Sublethal Concentrations of Mercury and Lindane', *Ecotoxicology and Environmental Safety*, 48(3), pp. 223–234. Available at: https://doi.org/10.1006/eesa.2000.2009.

Della Torre, C. *et al.* (2014) 'Accumulation and Embryotoxicity of Polystyrene Nanoparticles at Early Stage of Development of Sea Urchin Embryos Paracentrotus lividus', *Environmental Science & Technology*, 48(20), pp. 12302–12311. Available at: https://doi.org/10.1021/es502569w.

Ebert, D. (2005) *Ecology, Epidemiology, and Evolution of Parasitism in Daphnia*. National Center for Biotechnology Information (US).

Ebert, D. (2022) 'Daphnia as a versatile model system in ecology and evolution', *EvoDevo*, 13(1), p. 16. Available at: https://doi.org/10.1186/s13227-022-00199-0.

von Elert, E. *et al.* (2004) 'Protease activity in gut of Daphnia magna: evidence for trypsin and chymotrypsin enzymes', *Comparative Biochemistry and Physiology Part B: Biochemistry and Molecular Biology*, 137(3), pp. 287–296. Available at: https://doi.org/10.1016/j.cbpc.2003.11.008.

von Elert, E., Zitt, A. and Schwarzenberger, A. (2012) 'Inducible tolerance to dietary protease inhibitors in Daphnia magna', *Journal of Experimental Biology*, 215(12), pp. 2051–2059. Available at: https://doi.org/10.1242/jeb.068742.

Facure, M.H.M. *et al.* (2020) 'A review on graphene quantum dots and their nanocomposites: from laboratory synthesis towards agricultural and environmental applications', *Environmental Science: Nano*, 7(12), pp. 3710–3734. Available at: https://doi.org/10.1039/D0EN00787K.

Fadare, O.O. *et al.* (2020) 'Eco-Corona vs Protein Corona: Effects of Humic Substances on Corona Formation and Nanoplastic Particle Toxicity in Daphnia magna', *Environmental Science & Technology*, 54(13), pp. 8001–8009. Available at: https://doi.org/10.1021/acs.est.0c00615.

Feng, Y. *et al.* (2022) 'A novel polyurea nanofiltration membrane constructed by PEI/TA-MoS2 for efficient removal of heavy metal ions', *Separation and Purification Technology*, 300, p. 121785. Available at: https://doi.org/10.1016/j.seppur.2022.121785.

Gillis, P.L. *et al.* (2005) 'Daphnia need to be gut-cleared too: the effect of exposure to and ingestion of metal-contaminated sediment on the gut-clearance patterns of D. magna', *Aquatic Toxicology (Amsterdam, Netherlands)*, 71(2), pp. 143–154. Available at: https://doi.org/10.1016/j.aquatox.2004.10.016.

Gophen, M. (2022) 'Internal Water Flows and Particles Abstraction in Daphnia', *Open Journal of Ecology*, 12(11), pp. 742–755. Available at: https://doi.org/10.4236/oje.2022.1211043.

Gophen, M. and Geller, W. (1984) 'Filter mesh size and food particle uptake by Daphnia', *Oecologia*, 64(3), pp. 408–412. Available at: https://doi.org/10.1007/BF00379140.

Gophen, M. and Gold, B. (1981) 'The use of inorganic substances to stimulate gut evacuation in Daphnia magna', *Hydrobiologia*, 80(1), pp. 43–45. Available at: https://doi.org/10.1007/BF00130679.

Goswami, L. *et al.* (2017) 'Engineered nano particles: Nature, behaviour, and effect on the environment', *Journal of Environmental Management*, 196, pp. 297–315. Available at: https://doi.org/10.1016/j.jenvman.2017.01.011.

Grassi, G. *et al.* (2019) 'Proteomic profile of the hard corona of charged polystyrene nanoparticles exposed to sea urchin Paracentrotus lividus coelomic fluid highlights potential drivers of toxicity', *Environmental Science: Nano*, 6(10), pp. 2937–2947. Available at: https://doi.org/10.1039/C9EN00824A.

Guo, Z. *et al.* (2021) 'Surface Functionalization of Graphene-Based Materials: Biological Behaviour, Toxicology, and Safe-By-Design Aspects', *Advanced Biology*, 5(9), p. 2100637. Available at: https://doi.org/10.1002/adbi.202100637.

Gusain, R. *et al.* (2019) 'Efficient Removal of Pb(II) and Cd(II) from Industrial Mine Water by a Hierarchical MoS2/SH-MWCNT Nanocomposite', *ACS Omega*, 4(9), pp. 13922–13935. Available at: https://doi.org/10.1021/acsomega.9b01603.

Haase, A. and Lynch, I. (2018) 'Quality in nanosafety — Towards reliable nanomaterial safety assessment', *NanoImpact*, 11, pp. 67–68. Available at: https://doi.org/10.1016/j.impact.2018.02.005.

Hadjidemetriou, M. and Kostarelos, K. (2017) 'Evolution of the nanoparticle corona', *Nature Nanotechnology*, 12(4), pp. 288–290. Available at: https://doi.org/10.1038/nnano.2017.61.

Han, Q. *et al.* (2022) 'Tuning phase compositions of MoS 2 nanomaterials for enhanced heavy metal removal: performance and mechanism', *Physical Chemistry Chemical Physics*, 24(21), pp. 13305–13316. Available at: https://doi.org/10.1039/D2CP00705C.

Handy, R.D., Owen, R. and Valsami-Jones, E. (2008) 'The ecotoxicology of nanoparticles and nanomaterials: current status, knowledge gaps, challenges, and future needs', *Ecotoxicology (London, England)*, 17(5), pp. 315–325. Available at: https://doi.org/10.1007/s10646-008-0206-0.

Harris, K.D.M., Bartlett, N.J. and Lloyd, V.K. (2012) 'Daphnia as an Emerging Epigenetic Model Organism', *Genetics Research International*. Edited by J. Brisson, 2012, pp. 1–8. Available at: https://doi.org/10.1155/2012/147892.

Hartmann, H.J. and Kunkel, D.D. (1991) 'Mechanisms of food selection in Daphnia', *Hydrobiologia*, 225(1), pp. 129–154. Available at: https://doi.org/10.1007/BF00028392.

Hartmann, N.I.B. *et al.* (2014) *Environmental fate and behaviour of nanomaterials: New knowledge on important transfomation processes*, *Environmental fate and behaviour of nanomaterials*. Report. Copenhagen K: Danish Environmental Protection Agency, pp. 29–59.

HASLER, A.D. (1935) 'The Physiology of Digestion of Plankton crustacea, I. Some Digestive Enzymes of Daphnia', *The Biological bulletin (Lancaster)*, 68(2), pp. 207–214. Available at: https://doi.org/10.2307/1537264.

He, X. *et al.* (2014) 'Using a holistic approach to assess the impact of engineered nanomaterials inducing toxicity in aquatic systems', *Journal of Food and Drug Analysis*, 22(1), pp. 128–146. Available at: https://doi.org/10.1016/j.jfda.2014.01.011.

Hebert, P.D.N. and Ward, R.D. (1972) 'Inheritance during Parthenogenesis in DAPHNIA MAGNA', *Genetics*, 71(4), pp. 639–642.

Henna, T.K. and Pramod, K. (2020) 'Graphene quantum dots redefine nanobiomedicine', *Materials Science and Engineering: C*, 110, p. 110651. Available at: https://doi.org/10.1016/j.msec.2020.110651.

Hogstrand, C. and Kille, P. (2008) *Comparative toxicogenomics edited by Christer Hogstrand and Peter Kille.* 1st ed. Amsterdam ; Boston: Elsevier (Advances in experimental biology).

Horton, P.A. *et al.* (1979) 'Browsing and grazing by cladoceran filter feeders', *Canadian Journal of Zoology*, 57(1), pp. 206–212. Available at: https://doi.org/10.1139/z79-019.

Ishag, A. and Sun, Y. (2021) 'Recent Advances in Two-Dimensional MoS2 Nanosheets for Environmental Application', *Industrial & Engineering Chemistry Research*, 60(22), pp. 8007–8026. Available at: https://doi.org/10.1021/acs.iecr.1c01311.

Jeevanandam, J. *et al.* (2018) 'Review on nanoparticles and nanostructured materials: history, sources, toxicity and regulations', *Beilstein Journal of Nanotechnology*, 9, pp. 1050–1074. Available at: https://doi.org/10.3762/bjnano.9.98.

Jensen, L.H.S. *et al.* (2017) 'Not all that glitters is gold-Electron microscopy study on uptake of gold nanoparticles in Daphnia magna and related artifacts', *Environmental Toxicology and Chemistry*, 36(6), pp. 1503–1509. Available at: https://doi.org/10.1002/etc.3697.

Joshi, P.N. *et al.* (2016) *Graphene Quantum Dots - From Emergence to Nanotheranostic Applications*, *Smart Drug Delivery System*. IntechOpen. Available at: https://doi.org/10.5772/61932.

Julian Hartmann, H. (1985) 'Feeding of Daphnia pulicaria and Diaptomus ashlandi on mixtures of unicellular and filamentous algae', *SIL Proceedings, 1922-2010*, 22(5), pp. 3178–3183. Available at: https://doi.org/10.1080/03680770.1983.11897853.

Junaid, M. and Wang, J. (2021) 'Interaction of nanoplastics with extracellular polymeric substances (EPS) in the aquatic environment: A special reference to eco-corona formation and associated impacts', *Water Research*, 201, p. 117319. Available at: https://doi.org/10.1016/j.watres.2021.117319.

Kaur, J. *et al.* (2018) 'Biological interactions of biocompatible and water-dispersed MoS2 nanosheets with bacteria and human cells', *Scientific Reports*, 8(1), p. 16386. Available at: https://doi.org/10.1038/s41598-018-34679-y.

Khim Chng, E.L., Sofer, Z. and Pumera, M. (2014) 'MoS 2 exhibits stronger toxicity with increased exfoliation', *Nanoscale*, 6(23), pp. 14412–14418. Available at: https://doi.org/10.1039/C4NR04907A.

Koivisto, S., Ketola, M. and Walls, M. (1992) 'Comparison of five cladoceran species in short- and long-term copper exposure', *Hydrobiologia*, 248(2), pp. 125–136. Available at: https://doi.org/10.1007/BF00006080.

Kumar, Y.R. *et al.* (2020) 'Graphene quantum dot based materials for sensing, bio-imaging and energy storage applications: a review', *RSC Advances*, 10(40), pp. 23861–23898. Available at: https://doi.org/10.1039/D0RA03938A.

Lam, S.J. *et al.* (2018) 'Antimicrobial polymeric nanoparticles', *Progress in Polymer Science*, 76, pp. 40–64. Available at: https://doi.org/10.1016/j.progpolymsci.2017.07.007.

Lampert, W. (1987) 'Laboratory studies on zooplankton-cyanobacteria interactions', *New Zealand Journal of Marine and Freshwater Research*, 21(3), pp. 483–490. Available at: https://doi.org/10.1080/00288330.1987.9516244.

Le, Q.-A.V. *et al.* (2016) 'Daphnia in water quality biomonitoring - "omic" approaches', *Toxicology and Environmental Health Sciences*, 8(1), pp. 1–6. Available at: https://doi.org/10.1007/s13530-016-0255-3.

Lead, J.R. *et al.* (2018) 'Nanomaterials in the environment: Behaviour, fate, bioavailability, and effects—An updated review', *Environmental Toxicology and Chemistry*, 37(8), pp. 2029–2063. Available at: https://doi.org/10.1002/etc.4147.

Lesniak, A. *et al.* (2012) 'Effects of the Presence or Absence of a Protein Corona on Silica Nanoparticle Uptake and Impact on Cells', *ACS Nano*, 6(7), pp. 5845–5857. Available at: https://doi.org/10.1021/nn300223w.

Li, M. *et al.* (2019) 'Review of Carbon and Graphene Quantum Dots for Sensing', *ACS Sensors*, 4(7), pp. 1732–1748. Available at: https://doi.org/10.1021/acssensors.9b00514.

Li, X. and Zhu, H. (2015) 'Two-dimensional MoS2: Properties, preparation, and applications', *Journal of Materiomics*, 1(1), pp. 33–44. Available at: https://doi.org/10.1016/j.jmat.2015.03.003.

Lin, W. *et al.* (2019) 'Quantification of the combined toxic effect of polychlorinated biphenyls and nano-sized polystyrene on Daphnia magna', *Journal of Hazardous Materials*, 364, pp. 531–536. Available at: https://doi.org/10.1016/j.jhazmat.2018.10.056.

Lin, W. *et al.* (2020) 'Joint effect of nanoplastics and humic acid on the uptake of PAHs for Daphnia magna: A model study', *Journal of Hazardous Materials*, 391, p. 122195. Available at: https://doi.org/10.1016/j.jhazmat.2020.122195.

Liu, C. *et al.* (2019) 'Simultaneous removal of Hg2+, Pb2+ and Cd2+ from aqueous solutions on multifunctional MoS2', *Journal of Molecular Liquids*, 296, p. 111987. Available at: https://doi.org/10.1016/j.molliq.2019.111987.

Lovern, S.B., Owen, H.A. and Klaper, R. (2008) 'Electron microscopy of gold nanoparticle intake in the gut of Daphnia magna', *Nanotoxicology*, 2(1), pp. 43–48. Available at: https://doi.org/10.1080/17435390801935960.

Lowry, G.V. *et al.* (2012) 'Transformations of Nanomaterials in the Environment', *Environmental Science & Technology*, 46(13), pp. 6893–6899. Available at: https://doi.org/10.1021/es300839e.

Luo, J. *et al.* (2019) 'Phase-Mediated Heavy Metal Adsorption from Aqueous Solutions Using Two-Dimensional Layered MoS2', *ACS Applied Materials & Interfaces*, 11(42), pp. 38789–38797. Available at: https://doi.org/10.1021/acsami.9b14019.

Ma, Y. *et al.* (2016) 'Effects of nanoplastics and microplastics on toxicity, bioaccumulation, and environmental fate of phenanthrene in fresh water', *Environmental Pollution*, 219, pp. 166–173. Available at: https://doi.org/10.1016/j.envpol.2016.10.061.

Markiewicz, M. *et al.* (2018) 'Changing environments and biomolecule coronas: consequences and challenges for the design of environmentally acceptable engineered nanoparticles', *Green Chemistry*, 20(18), pp. 4133–4168. Available at: https://doi.org/10.1039/C8GC01171K.

Martinez, D.S.T. *et al.* (2022) 'Daphnia magna and mixture toxicity with nanomaterials – Current status and perspectives in data-driven risk prediction', *Nano Today*, 43, p. 101430. Available at: https://doi.org/10.1016/j.nantod.2022.101430.

Moriarty, F. (1983) *Ecotoxicology: the study of pollutants in ecosystems*. London: Academic.

Nasser, F., Constantinou, J. and Lynch, I. (2019) 'Nanomaterials in the environment acquire an "eco-corona" impacting their toxicity to Daphnia magna —a call for updating toxicity testing policies', *Proteomics* [Preprint], (1800412). Available at: https://doi.org/10.1002/pmic.201800412.

Nasser, F. and Lynch, I. (2016) 'Secreted protein eco-corona mediates uptake and impacts of polystyrene nanoparticles on Daphnia magna', *Journal of Proteomics*, 137, pp. 45–51. Available at: https://doi.org/10.1016/j.jprot.2015.09.005.

OECD (2004) *Test No. 202: Daphnia sp. Acute Immobilisation Test*. Paris: Organisation for Economic Co-operation and Development. Available at: https://www.oecd-ilibrary.org/environment/test-no-202-daphnia-sp-acute-immobilisation-test_9789264069947-en (Accessed: 9 August 2022).

Payne, C.K. (2019) 'A protein corona primer for physical chemists', *The Journal of Chemical Physics*, 151(13), p. 130901. Available at: https://doi.org/10.1063/1.5120178.

Penalva, C. *et al.* (2007) 'Studying Daphnia feeding behaviour as a black box: A novel electrochemical approach', *Hydrobiologia*, 594, pp. 153–163. Available at: https://doi.org/10.1007/s10750-007-9080-7.

Persoone, G. *et al.* (2009) 'Review on the acute Daphnia magna toxicity test – Evaluation of the sensitivity and the precision of assays performed with organisms from laboratory cultures or hatched from dormant eggs', *Knowledge and Management of Aquatic Ecosystems*, (393), p. 01. Available at: https://doi.org/10.1051/kmae/2009012.

Porcella, D.B., Rixford, C.E. and Slater, J.V. (1969) 'Molting and Calcification in Daphnia magna', *Physiological Zoology*, 42(2), pp. 148–159. Available at: https://doi.org/10.1086/physzool.42.2.30158469.

Rabus, M. *et al.* (2013) 'Uncovering Ultrastructural Defences in Daphnia magna – An Interdisciplinary Approach to Assess the Predator-Induced Fortification of the Carapace', *PLOS ONE*, 8(6), p. e67856. Available at: https://doi.org/10.1371/journal.pone.0067856.

Reilly, K. *et al.* (2023) 'Daphnia as a model organism to probe biological responses to nanomaterials—from individual to population effects via adverse outcome pathways', *Frontiers in Toxicology*, 5. doi:10.3389/ftox.2023.1178482.

Reilly, K. *et al.* (2022) 'Chapter 6. The Composition of the Eco-corona Acquired by Micro- and Nanoscale Plastics Impacts on their Ecotoxicity and Interactions with Co-pollutants', in, pp. 132–155. Available at: https://doi.org/10.1039/9781839166570-00132.

Rosenkranz, P. *et al.* (2009) 'A comparison of nanoparticle and fine particle uptake by Daphnia magna', *Environmental Toxicology and Chemistry*, 28(10), pp. 2142–2149. Available at: https://doi.org/10.1897/08-559.1.

Salem, S. *et al.* (2022) 'A Comprehensive Review of Nanomaterials: Types, Synthesis, Characterization, and Applications', *Biointerface Research in Applied Chemistry*, 13(1), p. 41. Available at: https://doi.org/10.33263/BRIAC131.041.

Samy, O. *et al.* (2021) 'A Review on MoS2 Properties, Synthesis, Sensing Applications and Challenges', *Crystals*, 11, p. 355. Available at: https://doi.org/10.3390/cryst11040355.

Schoenberg, S.A., Maccubbin, A.E. and Hodson, R.E. (1984) 'Cellulose digestion by freshwater microcrustacea1', *Limnology and Oceanography*, 29(5), pp. 1132–1136. Available at: https://doi.org/10.4319/lo.1984.29.5.1132.

Schwarzenberger, A. and Fink, P. (2018) 'Gene expression and activity of digestive enzymes of Daphnia pulex in response to food quality differences', *Comparative Biochemistry and Physiology Part B: Biochemistry and Molecular Biology*, 218, pp. 23–29. Available at: https://doi.org/10.1016/j.cbpb.2018.01.009.

Sethulekshmi, A.S. *et al.* (2022) 'MoS2 based nanomaterials: Advanced antibacterial agents for future', *Journal of Controlled Release*, 348, pp. 158–185. Available at: https://doi.org/10.1016/j.jconrel.2022.05.047.

Shaw, J. *et al.* (2008) 'Daphnia as an emerging model for toxicological genomics', *Advances in Experimental Biology*, 2, pp. 165–328. Available at: https://doi.org/10.1016/S1872-2423(08)00005-7.

Shaw, J.R. *et al.* (2006) 'Comparative toxicity of cadmium, zinc, and mixtures of cadmium and zinc to daphnids', *Environmental Toxicology and Chemistry*, 25(1), pp. 182–189. Available at: https://doi.org/10.1897/05-243r.1.

Swammerdam, J. (1758) *The book of nature; or, the history of insects: reduced to distinct classes, confirmed by particular instances, displayed in the anatomical analysis of many species, and illustrated with copper-plates ...* London : Printed for C. G. Seyffert. Available at: http://archive.org/details/b30448542 (Accessed: 9 August 2022).

Tabish, T.A. *et al.* (2018) 'Biocompatibility and toxicity of graphene quantum dots for potential application in photodynamic therapy', *Nanomedicine*, 13(15), pp. 1923–1937. Available at: https://doi.org/10.2217/nnm-2018-0018.

Tan, L.-Y. *et al.* (2016) 'TiO2 Nanoparticle Uptake by the Water Flea Daphnia magna via Different Routes is Calcium-Dependent', *Environmental Science and Technology*, 50(14), pp. 7799–7807. Available at: https://doi.org/10.1021/acs.est.6b01645.

Tibbetts, J. *et al.* (2018) 'Abundance, Distribution, and Drivers of Microplastic Contamination in Urban River Environments', *Water*, 10(11), p. 1597. Available at: https://doi.org/10.3390/w10111597.

Tkaczyk, A. *et al.* (2021) 'Daphnia magna model in the toxicity assessment of pharmaceuticals: A review', *Science of The Total Environment*, 763, p. 143038. Available at: https://doi.org/10.1016/j.scitotenv.2020.143038.

Treuel, L. and Nienhaus, G.U. (2012) 'Toward a molecular understanding of nanoparticle–protein interactions', *Biophysical Reviews*, 4(2), pp. 137–147. Available at: https://doi.org/10.1007/s12551-012-0072-0.

Tyagi, V. *et al.* (2009) 'Evaluation of Daphnia Magna as an Indicator of Toxicity and Treatment Efficacy of Municipal Sewage Treatment Plant', *Journal of Applied Sciences and*

Environmental Management (ISSN: 1119-8362) Vol 11 Num 1, 11. Available at: https://doi.org/10.4314/jasem.v11i1.46835.

Walkey, C.D. and Chan, W.C.W. (2012) 'Understanding and controlling the interaction of nanomaterials with proteins in a physiological environment', *Chemical Society Reviews*, 41(7), pp. 2780–2799. Available at: https://doi.org/10.1039/c1cs15233e.

Wang, S., Cole, I.S. and Li, Q. (2016) 'The toxicity of graphene quantum dots', *RSC Advances*, 6(92), pp. 89867–89878. Available at: https://doi.org/10.1039/C6RA16516H.

Wang, Y. *et al.* (2022) 'Alkynyl functionalized MoS2 mesoporous materials with superb adsorptivity for heavy metal ions', *Journal of Hazardous Materials*, 424, p. 127579. Available at: https://doi.org/10.1016/j.jhazmat.2021.127579.

Wang, Z. *et al.* (2018) 'Removal and Recovery of Heavy Metal Ions by Two-dimensional MoS2 Nanosheets: Performance and Mechanisms', *Environmental Science & Technology*, 52(17), pp. 9741–9748. Available at: https://doi.org/10.1021/acs.est.8b01705.

Wang, Z. *et al.* (2020) 'Highly effective remediation of Pb(II) and Hg(II) contaminated wastewater and soil by flower-like magnetic MoS2 nanohybrid', *Science of The Total Environment*, 699, p. 134341. Available at: https://doi.org/10.1016/j.scitotenv.2019.134341.

Wang, Z. and Mi, B. (2017) 'Environmental Applications of 2D Molybdenum Disulfide (MoS2) Nanosheets', *Environmental Science & Technology*, 51(15), pp. 8229–8244. Available at: https://doi.org/10.1021/acs.est.7b01466.

Wang, Z.G. *et al.* (2015) 'Toxicity of Graphene Quantum Dots in Zebrafish Embryo', *Biomedical and environmental sciences: BES*, 28(5), pp. 341–351. Available at: https://doi.org/10.3967/bes2015.048.

Work, K. and Gophen, M. (2001) 'Factors which affect the abundance of an invasive cladoceran, Daphnia Lumholtzi, in US reservoirs', *Freshwater Biology*, 42, pp. 1–10. Available at: https://doi.org/10.1046/j.1365-2427.1999.00449.x.

Wu, B. *et al.* (2019) 'Differential influence of molybdenum disulfide at the nanometer and micron scales in the intestinal metabolome and microbiome of mice', *Environmental Science: Nano*, 6(5), pp. 1594–1606. Available at: https://doi.org/10.1039/C8EN01019F.

Xie, Y. *et al.* (2019) 'Cytotoxicity and autophagy induction by graphene quantum dots with different functional groups', *Journal of Environmental Sciences*, 77, pp. 198–209. Available at: https://doi.org/10.1016/j.jes.2018.07.014.

Yadav, V. *et al.* (2019) '2D MoS2-Based Nanomaterials for Therapeutic, Bioimaging, and Biosensing Applications', *Small*, 15(1), p. 1803706. Available at: https://doi.org/10.1002/smll.201803706.

Younis, M.R. *et al.* (2020) 'Recent Advances on Graphene Quantum Dots for Bioimaging Applications', *Frontiers in Chemistry*, 8. Available at:

https://www.frontiersin.org/articles/10.3389/fchem.2020.00424 (Accessed: 10 August 2022).

Zhao, C. *et al.* (2020) 'Synthesis of graphene quantum dots and their applications in drug delivery', *Journal of Nanobiotechnology*, 18(1), p. 142. Available at: https://doi.org/10.1186/s12951-020-00698-z.

Zhu, X. *et al.* (2022) 'Alone and combined toxicity of ZnO nanoparticles and graphene quantum dots on microalgae Gymnodinium', *Environmental Science and Pollution Research*, 29(31), pp. 47310–47322. Available at: https://doi.org/10.1007/s11356-022-19267-y.

Zou, E. and Fingerman, M. (1997) 'Effects of Estrogenic Xenobiotics on Molting of the Water Flea,Daphnia magna', *Ecotoxicology and Environmental Safety*, 38(3), pp. 281–285. Available at: https://doi.org/10.1006/eesa.1997.1589.

2

Methodology

2.1 Characterization of NMs by Dynamic Light Scattering

2.1.1 Size

Since cohesive light sources such as commercial lasers came into use in the 1970s, dynamic light scattering (DLS) has been widely utilized to measure small particles and macromolecules in dilute suspension, and in recent years DLS has become one of the most used techniques to characterize NMs (Xu, 2008).

DLS, also known as Quasi-Elastic Light Scattering or Photon Correlation, is a technique typically used to determine the size and size distribution of particles in the sub-micrometer range. The size measurement obtained by DLS is the hydrodynamic diameter, which is described as the size of a hypothetical hard sphere diffusing in the same manner as the measured particle diffuses ('DLS in 30 Minutes - Q&A - Materials Talks', 2017; *Dynamic Light Scattering (DLS) | Common Terms Defined | Malvern Panalytical*, 2017). Measurement of the size of non-spherical particles results in an apparent size of the dynamic solvated/hydrated particle based on the mean size of it tumbling in solution, and as such is typically somewhere between the longest and shortest dimensions.

The so-called Brownian motion means that particles move randomly due to bombardment by the surrounding solvent molecules. Due to this Brownian motion of particles in suspension, DLS measures the fluctuations of light intensity over time, allowing the determination of the diffusion coefficient (*D*), which is related to the hydrodynamic radius

(R_h) of particles according to the Stokes-Einstein equation (equation 2.1) (Carvalho *et al.*, 2018).

$D = k_bT / 6\pi \eta R_h$ (Equation 2.1)

where K_b is represented by the Boltzmann constant (1.38064852 x 10^{-23} J/K), T represents the absolute temperature (0 K), and η is the medium viscosity.

According to this equation, the hydrodynamic diameter of particles is inversely proportional to the diffusion coefficient (D), meaning that larger particles show a smaller diffusion coefficient compared to smaller particles (Nickel *et al.*, 2014). This results in larger particles moving more slowly than smaller particles. When correlating the intensity of scattered light over time, the scattered intensities are similar at the beginning; then, due to differences in the particles movements, the similarity will be lost over time (Figure 2.1) (Carvalho *et al.*, 2018).

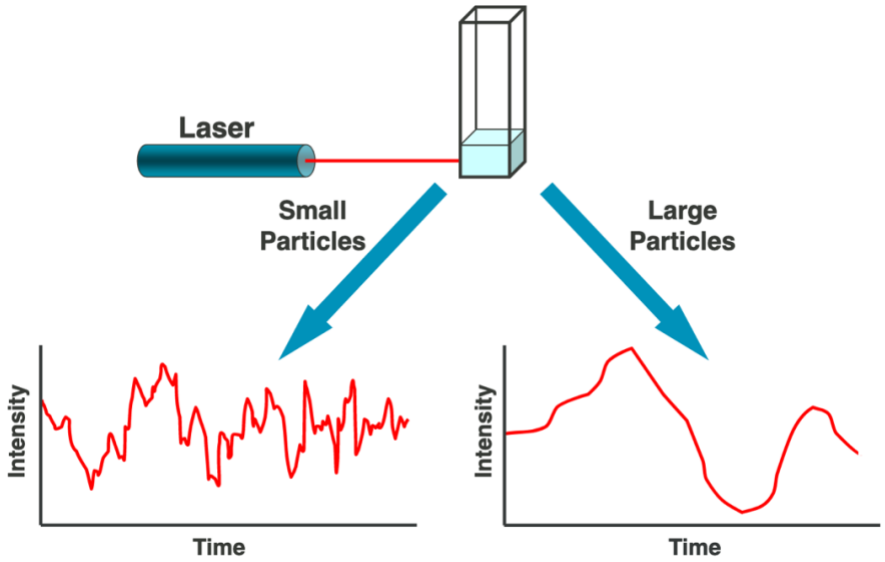

Figure 2.1. An illustration of the Brownian motion and fluctuations in light intensity related to particle size (Sagar, 2017).

DLS size measurements reported in this thesis were carried out using a Malvern Zetasizer and low-volume polystyrene cuvettes. Using the line highlighted by the manufacturer on the

polystyrene cuvettes as a volume reference, around 1 cm of each sample was pipetted into the cuvette and placed into the instrument sample holder. A standard operating procedure (SOP) was applied for each NM type by choosing the relative absorption value and refractive index (RI) of the NM and diluent. Each sample was measured at least three times with 12 runs per measurement to obtain the mean size (Z-average diameter), and where possible, triplicate samples were prepared and measured. However, due to the shortage of materials, suppliers not being able to deliver orders during the covid pandemic and the high number of experimental scenarios and samples required for our work, we were unable to use more than one sample in many DLS measurements, but the number of measurements for each sample was kept at n=3 minimum. Before starting the measurements, samples were equilibrated for 2 minutes at room temperature (~20 °C).

2.1.2 Zeta Potential

Zeta potential (ZP) is a measure of the charge at the surface of a particle, and is often used as a proxy for particle electrostatic stability due to repulsion between particles of like charge. ZP is determined by measuring the magnitude of the charge attraction between particles (*Zeta Potential | Malvern Panalytical*, 2022). Any particle in suspension will exhibit a ZP around each particle, there is an electrical double layer resulting from the particles' surface net charge, which affects the distribution of ions in the surrounding region (Malvern, 2015). This will increase the concentration of ions that have an opposite charge to that of the particle close to the surface (Figure 2.2). The solution layer surrounding the particle is composed of two parts: an outer region and an inner region. The inner region is where the ions are bound strongly, and it is referred to as the Stern layer, while the outer region is where the ions are less firmly bound, and it is known as the diffuse layer. The outer

region contains a hypothetical boundary known as the slipping plane, where particles and ions form a stable entity. Any movement of a particle is caused by the ions within this plane boundary, and the ions that are beyond the boundary will not move with the particle and instead remain with the surrounding dispersant. The ZP is the potential identified at this boundary/slipping plane (Figure 2.2). The stability of an electrostatically stabilized particle can be indicated by measuring the magnitude of the ZP. Particles with large positive or negative zeta potential (more positive than +30 or more negative than -30 mV) are considered to be stable with no tendency to agglomerate, whilst particles with low zeta potential values are less stable and have no force to prevent agglomeration due to changes in pH or ionic strength, unless supplemented with other means of stabilization such as steric stabilization through polymer or protein binding to the surface, for example.

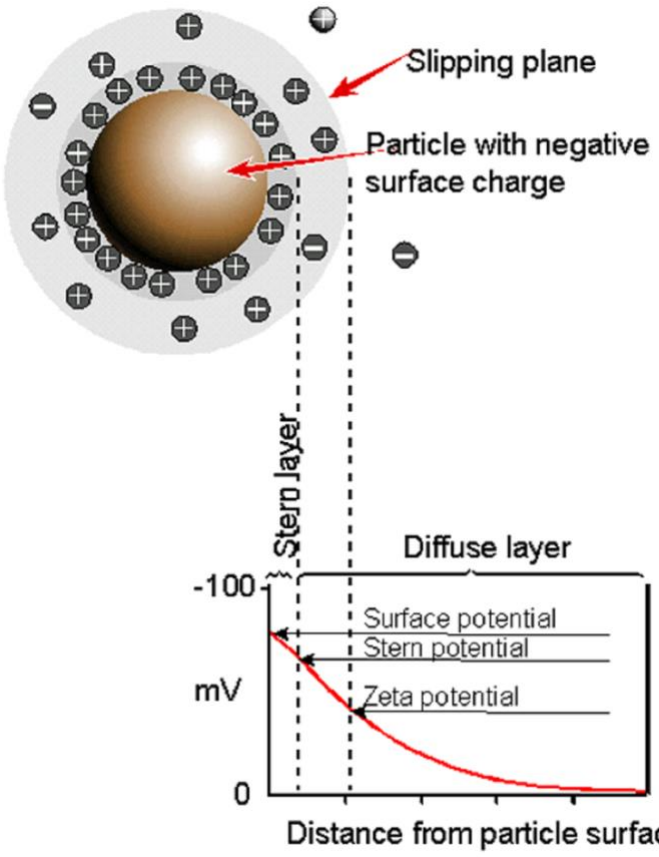

Figure 2.2. Zeta potential schematic illustration (ZetaPotential-Introduction-in-30min-Malvern.pdf - TECHNICAL NOTE Zeta potential - An introduction in 30 minutes ZETA POTENTIAL Introduction Zeta | Course Hero, no date, p. 201).

The zeta potential can be measured in colloidal dispersions by applying a voltage across a pair of electrodes at two ends of the cell containing the dispersion of particles (Kaszuba *et al.*, 2010). The charged particles are then attracted to the electrode with an opposite charge and as their electrophoretic mobility, their viscosity is then determined and expressed in unit field strength (Kaszuba *et al.*, 2010). The particle's electrophoretic mobility can be determined by light scattering, which measures small frequency shifts in light that is scattered from the movement of particles in within an applied particle field (Kaszuba *et al.*, 2010). This is then used to calculate the zeta potential by applying the Henry equation below (equation 2.2).

$$UE = \frac{2\varepsilon z f(\mathrm{ka})}{3\eta} \qquad \text{(Equation 2.2)}$$

Where UE is the electrophoretic mobility, ε is the dispersant dielectric constant, z is the zeta potential, F(ka) is the Henry function, and ŋ is the viscosity.

For ZP sample analyses, around 0.9 mL of each sample was incubated in a capillary cell using a syringe to avoid bubble formation and the cell was then closed by caps and inserted into the DLS sample holder and measured for ZP by the chosen SOP. Each measurement had at least 12 runs and was repeated at least three times in all ZP measurements presented in this thesis.

2.2 Biological Culturing

2.2.1 D. magna Culturing in High-Hardness Combo Medium

All *Daphnia* experiments were conducted using *D. magna* cultures in high-hardness combo (HH combo) medium which was made using ultra-pure water (UPW) with 18.2 M Ω cm^{-1} maximum resistance. The HH combo medium is commonly used to maintain *Daphnia*

cultures, and it represents a hard water standard that matches the hardness of water found in the freshwater environment but without natural organic matter (Ellis *et al.,* 2020).

The reagents used to prepare the HH Combo culture medium are analytical grade commercially available chemicals purchased from Sigma-Aldrich. The details of preparing the HH combo medium are shown in Tables 2.1, 2.2 and 2.3 (Baer and Goulden, 1998).

Table 2.1. Animate solution components. The stock solution is prepared and then the required aliquot (4 mL) is added to the HH Combo medium as described below.

Components of the Animate (stored at -20 ºC)		
Compound	**Chemical formula**	**Stock (g/100 mL)**
Potassium iodide	KI	0.33
Sodium bromide	NaBr	1.6
Strontium chloride Hexahydrate	$SrCl_2 \cdot 6H_2O$	15
Rubidium chloride	RbCl	7
Lithium chloride	LiCl	31

The animate solution was prepared by adding 1 mL of each of the five compound stocks shown in Table 3.3 to 500 mL of UPW. The final volume was then brought up to 1 L, and the solution was transferred into a glass bottle and stored in the fridge to be used for HH combo medium preparation.

Table 2.2. Vitamin components required for HH Combo medium. The stock solution is prepared as described here and then a 2mL aliquot is added to the HH Combo solution as described.

Stoch solutions of vitamin		
Compound	**Original stock**	**Working stock**
B_{12}	10 mg into 89 mL H_2O	Aliquoted into 1.5 mL Eppendorf tubes and frozen at -20 ºC
Biotin (d-biotin)	10 mg into 96 mL H_2O	Aliquoted into 1.5 mL Eppendorf tubes and frozen at -20 ºC

For preparing the vitamins (VIM) stocks, one aliquot of B_{12} and biotin was taken out from the freezer and left to thaw at room temperature. 30 mL of UPW, 10 mg of thiamine HCL, 0.5 mL of B_{12} and 0.5 mL of biotin were then added to a 50 mL volumetric flask. The final volume was then adjusted to 50 mL with UPW, and the solution was moved into a glass bottle covered with foil and stored in the fridge for one week maximum.

Table 2.3. HH Combo components, which are then supplemented with vitamins (VIM, prepared as described in Table 2.2) and aminate (prepared as described in Table 2.1).

	Components of HH combo		
Number	**Compound**	**Chemical formula**	**Stock (g L^{-1})**
1	Sodium bicarbonate	$NaHCO_3$	63
2	Potassium chloride	KCl	5.96
3	Boric acid	H_3BO_3	24
4	Sodium metasilicate nonahydrate	$Na_2SiO_3 \cdot 9H_2O$	28.42
5	Sodium nitrate	$NaNO_3$	17
6	Potassium phosphate dibasic	K_2HPO_4	1.742
7	Magnesium sulphate heptahydrate	$MgSO_4 \cdot 7H_2O$	113.5
8	Calcium chloride, dihydrate	$CaCl_2 \cdot 2H_2O$	110.28

The HH combo medium was prepared by adding 8 mL of sodium bicarbonate (compound #1 in Table 2.3) and 4 mL of each of the rest of the compounds in Table 3 (#2-8) to 3.5 mL of UPW in a 4L glass beaker. 200 µL of 40 µg/mL sodium selenite (Na_2SeO_3) was then added, and the final volume was adjusted to 4L by adding UPW. The solution was then left to aerate for one day to achieve the required level of oxygen. The pH was then adjusted to be between 7.6-7.8 by using 1 M HCL. After adjusting the pH, 2 mL of the vitamin solution (VIM) (Table 2.2) and 4 mL of animate (Table 2.3) were added before using the medium for culturing daphnids.

D. magna cultures of Bham2 strain were maintained in the HH combo medium under a controlled temperature environment (20 °C) with a 16:8 h light:dark cycle. The medium was refreshed at least twice a week to maintain healthy cultures. *Chlorella vulgaris* (*C. vulgaris)* algae was used to feed the daphnids daily (0.5 mg carbon for daphnids less than 5 days old and 0.75 mg carbon for daphnids older than 5 days). Cultures were discarded every 6 weeks, and new cultures were started using 1-day-old neonates from the 3rd brood of a previous culture. For experimental analyses, neonates of third broods and beyond were used in all tests.

2.2.2 Acute Immobilisation Test (OECD 202) to Assess NM Toxicity to *D. magna*

To establish the baseline toxicity and determine the EC values (initial effect concentrations) of the pristine PS nano/micro-materials, acute immobilization toxicity tests (OECD 202) were conducted on *D. magna* neonates (1-2 days old) in HH combo medium. The baseline toxicity was then used to compare the toxic effects of the pristine and treated NMs according to each treatment scenarios presented in the specific results chapters (see below also). We recognize that EC concentrations can be much higher than environmental concentrations. However, we used these concentrations as they are the basis of regulatory assessment of chemicals including nanomaterials, and allow for comparison across materials and exposure conditions to allow relative comparisons of materials by understanding their behaviour and impact on biological receptors.

Determination of EC_{50} values (half maximum effect) was conducted according to the OECD 202 guideline by exposing ten *D. magna* neonates in triplicate to a range of concentrations (0.01 mg/L - 1000 mg/L) for each of the NMs being tested, diluted in HH Combo medium

with a final volume of 5 mL per sample replicate. All exposures were performed without feeding. The number of immobilized animals, defined as animals which do not move for 15 seconds following gentle agitation, was recorded after 48 h. The exposure was repeated three times, and average values were recorded as mean ± standard deviation (SD). The EC_{50} values were then calculated by plotting the log concentrations of particles against the % of animal survival using the software Graphpad Prism 9.

2..2.3 Conditioning of HH Combo Medium with Proteins Secreted by *D. magna*

As filter feeders, daphnids filter the surrounding water through their gut, which results in release of proteins into the gut fluid which is then secreted back into the surrounding medium. Thus, even when experiments start with freshly prepared salt-only medium, it very quickly acquires a biomolecule component as a result of this filtering activity. These secreted proteins can then interact with any NMs present in the medium, resulting in the formation of an eco-corona, as described in Chapter 1.

Depending on the amount of medium needed for a specific exposure experiment, the optimal ratio of 2 *D. magna* neonates per one mL of fresh HH combo was used to condition the medium with secreted proteins. Neonates are then carefully removed after 48 h of exposure using a Pasteur pipette. The resulting conditioned medium can then be used according to each experimental plan, for dispersion of NMs and to explore the impact of different daphnia-stressors on the secreted proteins.

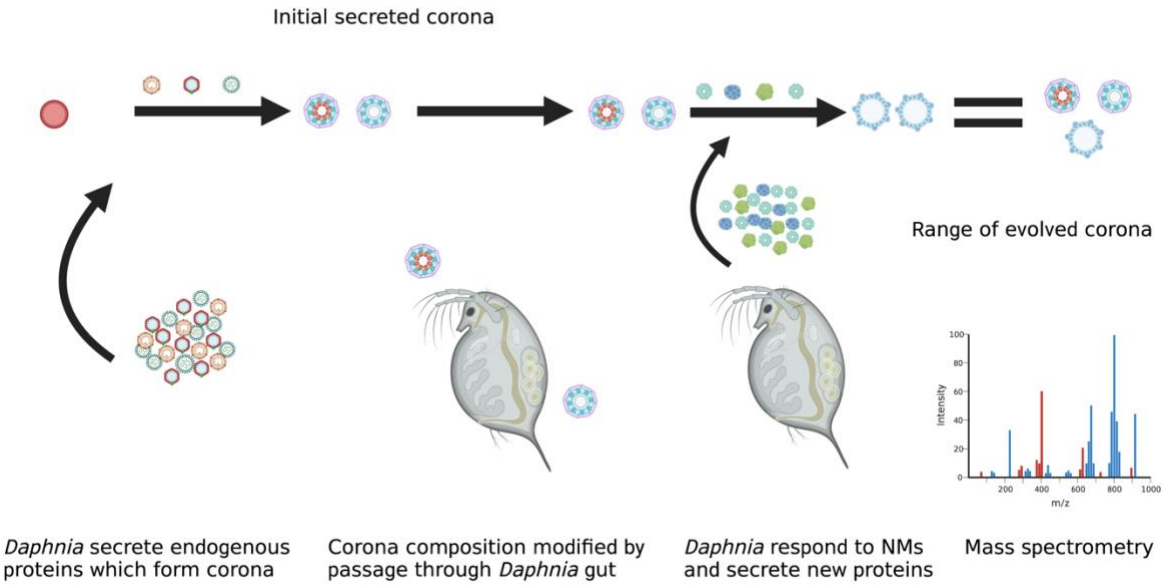

Figure 2.3. Schematic illustration of the conditioning of medium by daphnids as filter feeders, and the consequences of the secreted proteins for the NMs corona composition and evolution. Information contained in the NM corona can be utilized to provide mechanistic insights into how the daphnids respond to the presence of the NMs by secreting proteins related to uptake, repair and damage. (Replicated from (Ellis and Lynch, 2020)).

2.3 Analytical Measurements

2.3.1.1 Protein Quantification by The BCA Assay

The bicinchoninic acid assay (BCA) is a commonly used method for quantifying protein concentrations. The colour formation observed in the BCA assay is the result of two chemical reactions: under alkaline medium conditions, the first reaction involves the reduction of copper (Cu) ions from Cu^{+2} to Cu^{+} by the proteins through the Buret reaction, at a rate proportional to the amount of proteins present (Brady and Macnaughtan, 2015; Hussain *et al.,* 2019). The second reaction gives a characteristic purple colour, by forming a complex between two molecules of BCA and Cu^{+} (Brady and Macnaughtan, 2015; Hussain *et al.,* 2019). An absorbance spectrophotometer is then used to measure the intensity at 562 nm. Typically, a calibration curve of protein mass concentration vs absorbance at 562 nm is plotted by using a standard solution of bovine serum albumin (BSA). The protein

concentrations of unknown samples are then determined by assuming that the analysed proteins behave in the same way as the BSA standard. However, the results of this assay are not always accurate, and they can lead to under or over-estimation when quantifying proteins due to interference from various agents, such as lipids (Hussain *et al.,* 2019).

In this thesis, we have used the Pierce Rapid Gold BCA Protein Assay Kit, purchased from Thermo Fisher Scientific, for protein quantification. This is an optimized, fast, detergent-compatible, two-component, highly precise assay for the determination of total protein concentration. The Rapid Gold BCA assay uses the same copper-chelating technology as described above, but produces an orange-gold coloured reaction product instead of purple with less time required (5 minutes), measured at 480 nm and incubated at room temperature, compared to the standard BCA assay which requires 30 minutes incubation at 37 °C. Eliminating of the exposure of samples to elevated temperatures further improved the method, and it is much faster to perform, while providing comparable accuracy. However, in very few cases we have used the standard BCA kit or Bradford assay to compare results with our main kit and which will be discussed in the results of chapter 3 of this thesis.

For analyzing protein samples, a series of known protein concentration dilutions were prepared using the provided 2 mg/mL BSA to generate a standard curve, and they were analysed alongside the unknown samples in a 96-well transparent plate (Greiner). The standard curve was then used to determine the concentration of each unknown sample. The BSA standards were prepared according to the manufacturer's instruction manual using Table 4 below as a guide (*Pierce™ Rapid Gold BCA Protein Assay Kit*, no date).

Table 2.4. BSA standards dilution scheme (PierceTM Rapid Gold BCA Protein Assay Kit, no date).

Vial	Dilutent volume (µL)	Source and volume of BSA	Final concentration of BSA (µg/mL)
A	0	300 µL from stock	2000
B	62.5	187.5 µL from stock	1500
C	100	100 µL from stock	1000
D	100	100 µL from vial B	750
E	100	100 µL from vial C	500
F	100	100 µL from vial E	250
G	100	100 µL from vial F	125
H	160	40 µL from vial G	25
I	200	0	0

The content of one BSA standard ampule was diluted into clean vials using HH combo as the diluent for the known and unknown samples for every test. 200 µL of working reagent (WR) is required for each sample in the microplate plate. The WR for each test was prepared according to the number of tested samples by following the equation below to determine the required amount:

Total amount of required WR = (number of standards + number of unknowns) x (number of replicates) x volume of working reagent per sample (200 µL) (*Equation 2.3*).

The WR reagent was prepared by mixing 50 parts of the provided reagent A (proprietary copper chelator) with one part of reagent B (cupric sulfate) [50:1, reagent A:B]. Once the standards and the WR were ready, 20 µL of each unknown and standard sample were pipetted into a microplate in triplicate (3 wells for each sample, as shown schematically in Figure 2.4). 200 µL of WR was then added to each well, and samples were mixed by using a plate shaker for 30 seconds. The plate was incubated for 5 minutes at room temperature

then the absorbance was measured at or near 480 nm on a plate reader (Tecan). The average 480 nm absorbance measurement of the blank standard was subtracted from the measurement of all other unknown and standard (BSA) samples. A standard curve was then created by plotting the average blank corrected measurements for each BSA standard vs its concentration in µg/mL to identify the protein concentration of the unknown samples. Below is an example of a Rapid Gold BCA assay which was conducted on a HH combo medium conditioning experiment.

Table 2.5. The initial Adsorption values measured by the plate reader at 480 nm in replicates.

	Initial Absorbance Measurements						
Concentration of BSA (µg/mL)	**Blank**	**25**	**125**	**250**	**500**	**750**	**1000**
Absorbance of BSA standards	0.779	0.9256	1.0593	1.288	1.662	1.9343	2.1927
	0.7974	0.9403	1.1021	1.3053	1.6324	1.9445	2.3127
	0.7941	0.9647	1.1044	1.3236	1.6816	1.9473	2.3434
Unknown sample absorbance	**Sample 1**	**Sample 2**	**Sample 3**	**Sample 4**			
	0.9268	0.956	0.9321	0.9592			
	0.9262	0.9413	0.9327	0.9466			
	0.947	0.9465	0.9427	0.9492			

Table 2.6. The Adsorption values after subtracting the average blank absorbance values measured by the plate reader at 480 nm in replicates.

	Corrected Adsorption Measurements						
Concentration of BSA (µg/mL)	**Blank**	**25**	**125**	**250**	**500**	**750**	**1000**
Absorbance of BSA standards	-0.01117	0.135433	0.269133	0.497833	0.871833	1.144133	1.402533
	0.007233	0.150133	0.311933	0.515133	0.842233	1.154333	1.522533
	0.003933	0.174533	0.314233	0.533433	0.891433	1.157133	1.553233
Unknown samples absorbance	**Sample 1**	**Sample 2**	**Sample 3**	**Sample 4**			
	0.136633	0.165833	0.141933	0.169033			
	0.136033	0.151133	0.142533	0.156433			
	0.156833	0.156333	0.152533	0.159033			

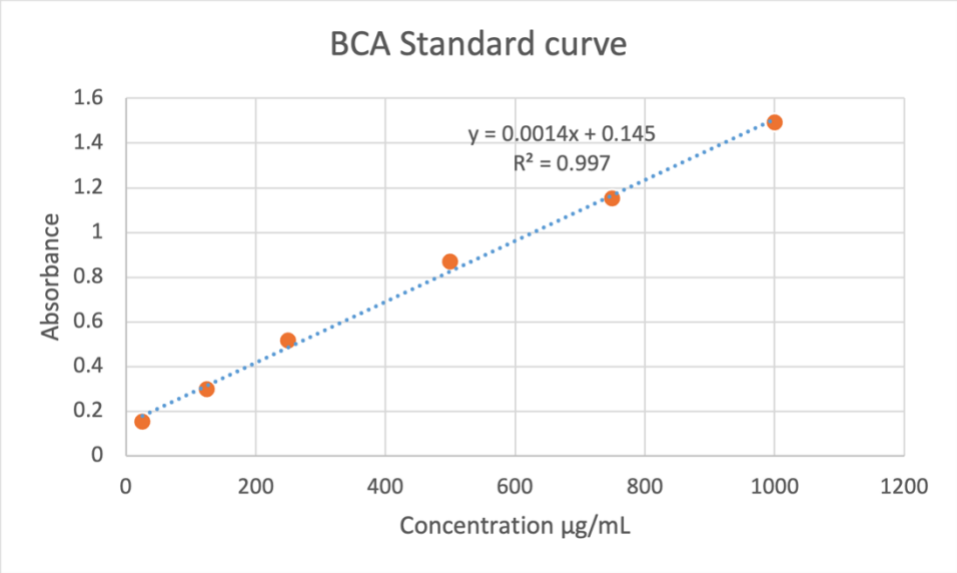

Figure 2.4. The standards obtained by plotting the corrected absorbance values against the known BSA standard concentrations in µg/mL. Slope = 0.0014 and y-intercept = 0.145.

The protein concentrations of unknown samples were determined by subtracting the y-intercept value from the absorbance value of the unknown sample and then dividing the subtracted value by the slope (Table 2.7).

Table 2.7. Measured Protein concentrations of unknown samples (the minus values indicate no proteins were detected).

	Protein Concentrations of the Unknown Samples (µg/mL)			
	Sample 1	**Sample 2**	**Sample 3**	**Sample 4**
Replicate 1	-5.9	14.9	-2.2	17.2
Replicate 2	-6.4	4.4	-1.8	8.2
Replicate 3	8.45	8.1	5.4	10.0
Average	**-1.28**	**9.1**	**0.47**	**11.8**

2.3.2 Particle Uptake/Accumulation Determined by Inductively Coupled Plasma Mass Spectrometry

Inductively Coupled Plasma Mass Spectrometry (ICP-MS) is an analytical technique widely used to determine trace amounts of elements extracted from or in complex samples. It can measure up to 80 elements from the periodic table, as shown in figure 2.5 below. The

significance of using this technique comes from the instrument detection limits, which can be at or below part per trillion (ppt) which corresponds to nanogram L^{-1} concentrations. The ability to measure multiple elements simultaneously in a single analysis is another significant advantage of the ICP-MS technique.

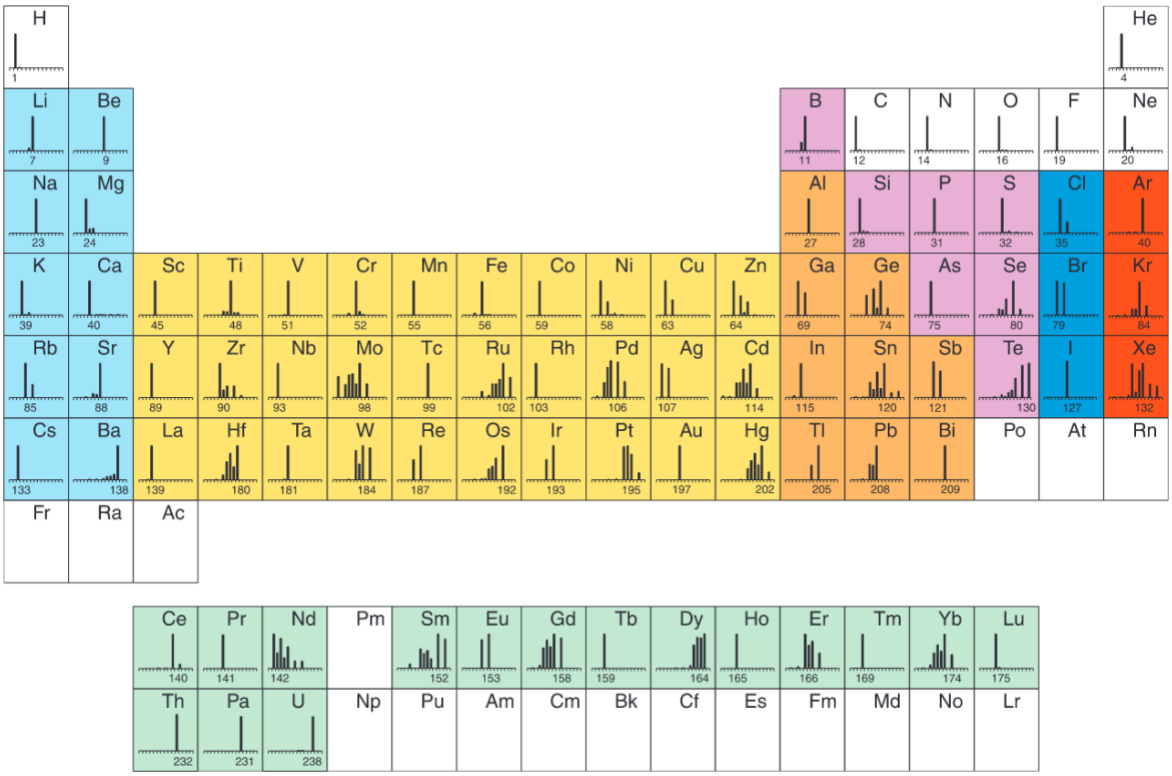

Figure 2.5. Elements that can be detected by ICP-MS (Perkin Elmer, 2011). Note that these can be measured to different levels of accuracy and with different limits of detection, which is also influenced by the sample complexity and the presence of potential interferences.

The ICP-MS instrument works by using an inert argon gas as a source of plasma to provoke the ionization state of elements, which decomposes samples into their constituent elements, and those elements are then transformed into ions that can be detected (Al-Hakkani, 2019; *Inductively Coupled Plasma Mass Spectrometry (ICP-MS) Information - UK*, no date).

An ICP-MS system is generally composed of the following parts (Figure 2.6):

- The sample introduction system (spray chamber and nebulizer)
- The radiofrequency (RF) coil and ICP torch
- A vacuum interface (ion source)
- A reaction/collision cell (collimator)
- Ion optics such as focusing lenses
- A mass spectrometer filter
- A data-controlling system with a detector.

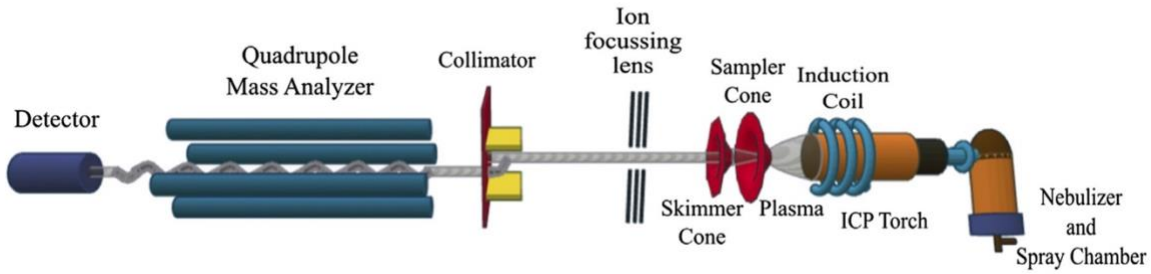

Figure 2.6. A schematic diagram of the basic features of an ICP-MS instrument (Nageswaran, Choudhary and Jagannathan, 2017).

When samples are analysed by the instrument, they first get nebulized (converted into an aerosol) in the sample introduction system, generating a fine aerosol which is then transferred to the argon plasma (Wilschefski and Baxter, 2019). The high-temperature plasma dissociates the molecules and dries out the aerosol, which eliminates an electron from the sample which then forms single-charged ions ('The 30-Minute Guide to ICP-MS', no date, p. 30). The ions are then directed into the mass spectrometer (MS) which acts as a filter. While ions enter and exit this filter, the MS only allows one mass-to-charge ratio to pass through it at any given time. When ions exit the MS, they strike the first electron multiplier dynode (detector). A cascade of electrons is then released due to the ions'

impact, and those electrons get amplified until they reach a pulse that can be measured. Finally, the concentration of elements can be detected by a software that compares the intensities of standards (calibration curve) with the intensities of the measured pulses ('The 30-Minute Guide to ICP-MS', no date). More details of the sample preparations are presented below in the Chapter 5 specific protocols, where ICP-MS is utilized to quantify the accumulation of metal-based NMs by *D. magna*.

2.3.3 Particle Uptake / Accumulation Determined by Fluorescence

Luminescence in solid systems is when an external source of energy excites the electronic states of solids, and the energy of the excitation is then released as light (Shionoya, 1998). When the excitation energy derives from a short wavelength light, such as ultraviolet light, the phenomenon is described as photoluminescence (Shionoya, 1998). Fluorescence is a physical process based on photoluminescence in which light is emitted after being absorbed by a substance (*Fluorescence Intensity Measurements | BMG LABTECH*, 2022). The fluorescence intensity is the magnitude of the emission, which indicates the amount of emitted light (photons) depending on the exited fluorophore concentration. Fluorophores are fluorescent molecules that absorb light (energy) which creates the fluorescence process. The absorbed light increases the energy level of electrons. This state of excitation is unstable, which causes the excited electrons to fall back to their ground state, leading to the emission of light (Figure 2.7) (*Fluorescence Intensity Measurements | BMG LABTECH*, 2022).

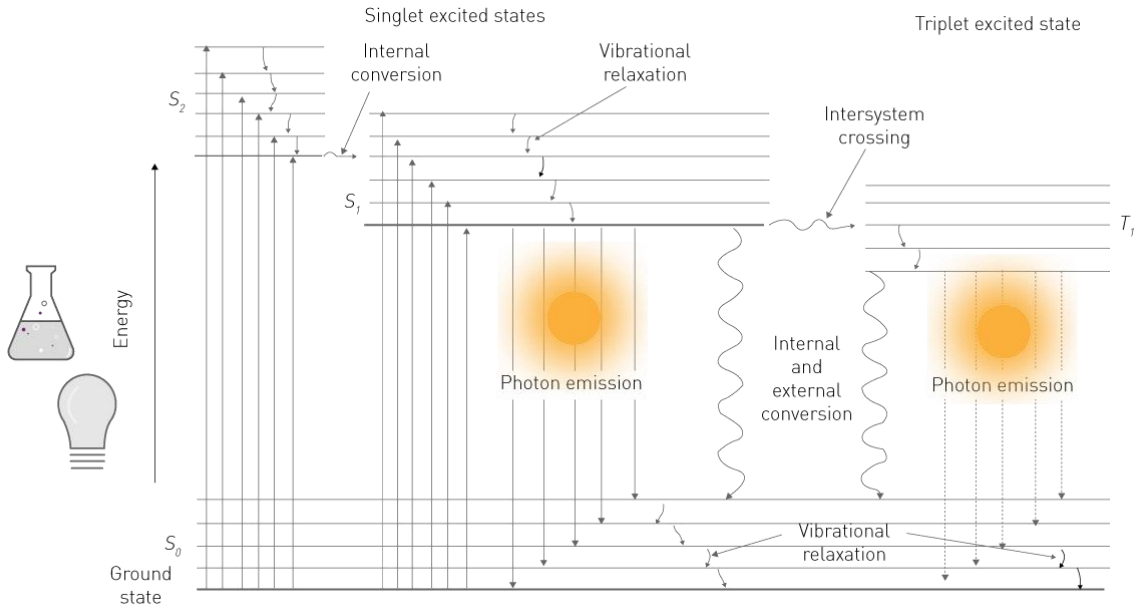

Figure 2.7. Illustration of the process involved in light absorbance and emission as fluorescence, presented as a modified Jablonski diagram. S2: An energy source results in the excitation of the molecules. S0: The ground state to which the electrons return with the emission of light from fallen-back electrons, which generates the fluorescence signal (Fluorescence Intensity Measurements | BMG LABTECH, 2022).

A small amount of the absorbed light is transformed into heat and movement, which causes the energy that is produced by the fallen-back electrons to be less than the energy required for electron excitation. The light used in the excitation has a lower wavelength than the emitted light. This is because the radiation of a short wave is more energetic than the radiation of a longer wave (*Fluorescence Intensity Measurements | BMG LABTECH*, 2022). The interval measured between the peaks of emission and excitation is known as the Stokes shift (Figure 2.8).

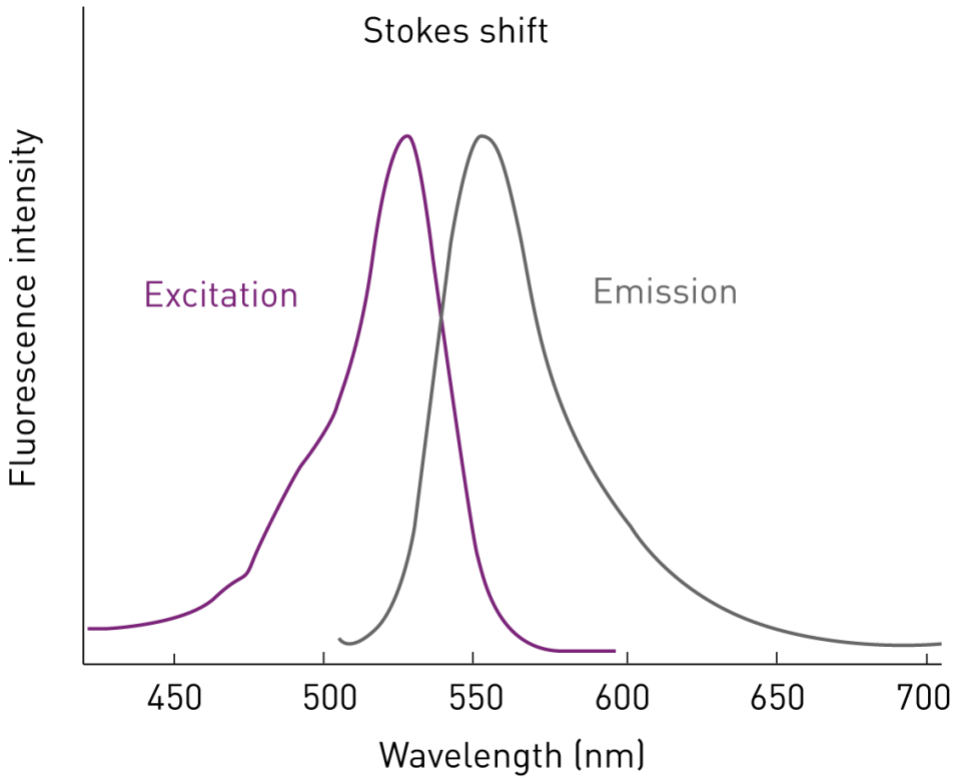

Figure 2.8. The wavelength difference between emission and excitation peaks representing the Stokes shift (Fluorescence Intensity Measurements | BMG LABTECH, 2022).

Due to the described characteristics of the emitted/excited lights, fluorescence intensity is now widely used in analytical studies to determine, localize, and quantify the concentration of fluorescent materials. Fluorescence can be measured using an instrument called a plate reader, which uses a source of light (typically a tungsten-halogen lamp), filters to select excitation and emission wavelengths, and a detector. The system converts the light signal (photons) generated by a fluorescent sample placed in a microplate into an electric signal that can be measured by the instrument to quantify materials of interest.

For fluorescence intensity analysis, black flat-bottom 96-well microplates were used (Nunclon and Greiner) with a maximum load of 300 µL. To avoid light interference with fluorescent samples, microplates were covered with foil before being analysed by the plate reader. The excitation and emission wavelengths were selected using the software and

filters supplied by the manufacturer (Tecan), and fluorescence was measured by the instrument according to the protocol of each experiment, which is detailed in the individual Chapter methodology sections below. Fluorescence was used in Chapter 3 to quantify the fluorescently labelled NMs and to explore the possibility for quantification of NMs uptake by daphnids.

2.3.4 Protein Analysis by Gel Electrophoresis

Gel electrophoresis is a laboratory technique used for separating macromolecules such as proteins based on their molecular size (Mesapogu, Jillepalli and Arora, 2013). When placing charged molecules in an electrical field, they move based on their net charge through small pores in a gel toward either the negative or positive pole of the system (Mesapogu, Jillepalli and Arora, 2013). The gel is formed using polyacrylamide, which has *N, N*-methylene bisacrylamide comonomers to cross-link the polymer chains. The polymerization of the gel is initiated by a radical source (ammonium persulfate) and catalyzed by Tetramethylethylenediamine (TEMED) (Mesapogu *et al.,* 2013).

The lengths of macromolecules are inversely related to their migration speed, as smaller molecules migrate faster than larger molecules within the gel pores (*gel electrophoresis | Learn Science at Scitable*, 2014). Proteins can have either a net positive or net negative charge (Mesapogu *et al.,* 2013). However, most small proteins normally have a positive charge causing them to move towards the negative pole, which is opposite to how the system works. To overcome this issue, proteins need to be first mixed with sodium dodecyl sulphate (SDS), which is an anionic detergent that denatures proteins and coats them with a negative charge (Mesapogu *et al.,* 2013; *gel electrophoresis | Learn Science at Scitable*, 2014). Molecules can then be separated and migrate toward the gel's positive pole based

on their molecular weights. When protein molecules are separated, bands will form which can be stained to support visualisation, allowing for the detection of different molecular sizes. More details of sample preparation and experimental design is discussed in the chapter 3 specific protocol.

2.4 Chapter-specific Materials and Methods

2.4.1 Chapter 3 Protocols

2.4.1.1 Selected NMs

Polystyrene is the most nano-sized plastic used in ecotoxicological studies (Kelpsiene *et al.*, 2022). PS 100 nm and 50 nm PS-NMs non-fluorescent polybead carboxylate-modified microspheres suspended in distilled water with a minimum amount of sulfate-based surfactants were purchased from Polyscience, Inc., USA. These particles have been widely used for protein binding and ecotoxicological studies. 50 nm and 2 µm fluorescent blue amine-modified PS latex beads (Excitation/Emission, λ_{ex} ~360 nm; λ_{em} ~420 nm) suspended in distilled water with 0.25% sodium azide were purchased from Sigma Aldrich, Gillingham UK.

2.4.1.2 Toxicity Range Finding Study

To establish the baseline toxicity and determine the EC values (initial effect concentrations) of the pristine PS nano/micro-materials, acute immobilization toxicity tests (OECD 202) were conducted on *D. magna* neonates (1-2 days old) in HH combo medium.

Determination of EC_{50} values (half maximum effect) was conducted according to the OECD 202 guideline by exposing ten *D. magna* neonates in triplicates to a range of concentrations (0.01 mg/L - 1000 mg/L) for each of the four different types of PS micro/NMs, diluted in HH

Combo medium with a final volume of 5 mL per sample replicate. All exposures were performed without feeding. The number of immobilized animals was recorded after 48 h. The exposure was repeated three times, and average values were recorded. The EC_{50} values were then calculated by plotting the log concentrations of particles against the % of animal survival using the software Graphpad Prism 9.

2.4.1.3 Characterization of NMs

To assess the characteristics of NMs before and after each treatment in this chapter, the hydrodynamic size and surface charge of the materials were measured in deionized water, fresh and conditioned HH combo using the Malvern Instruments nano zetasizer. Sample measurements were conducted in triplicate to increase reliability. The z-average size, the polydispersity index (PDI) and the zeta potential (ZP) were monitored and recorded for each sample treatment.

2.4.1.4 Impact of Surfactants and Preservatives on *D. magna* EC_{50}

Two different methods were applied to evaluate the impact of surfactants and preservatives that are included in the as-purchased PS NM dispersions on the acute toxicity of four different types of PS NMs dispersions (details of the surfactants and preservatives are given in section 2.4.1.2). The first method to wash the NMs and remove the dispersants and/or preservatives was conducted by dialysis, and the second method was performed by centrifugation and re-dispersion of the NMs in a fresh medium.

2.4.1.4.1 Washing of Particles by Dialysis

To wash the suspended particles from chemical surfactants, preservatives or other additives, Visking dialysis tubes with a molecular weight cut-off (MWCO) of 12-14000 daltons, a wall thickness of 0.03mm, and a diameter of 19mm were used. Working stock

solutions of each studied material were prepared (500 mg/L for the 50 nm PS-NH_2 and 1000 mg/L for all the other PS particles) in HH combo medium with a final volume of 20 mL. To prevent any leakage, the Viskin tubes were folded at their ends and clipped with dialysis tubing closures purchased from Sigma Aldrich. Samples were pipetted into the dialysis tubes and dialyzed for 5 days against DI water. In the first 12 h, the DI water was changed every 6 hours, and for the remaining days, it was changed once every 24 h. Samples from the surrounding DI water were also collected each day for fluorescence analysis. After the dialysis process, the dialyzed suspensions were analysed alongside non-dialyzed suspensions by measuring their fluorescence intensity to assess if there was any loss of particles, or leeching of dye from the particles, during the process by using the Tecan plate reader and a 96-well flat bottom microplate.

2.4.1.4.2 Washing of Particles by Centrifugation

Stock solutions of all PS NMs were prepared with the same concentrations used in the dialysis protocol. Samples were placed in 50 mL centrifuge tubes and were centrifuged for 1 h at 9,300 RPM and 20 °C. The supernatants were collected, and the pellets were resuspended in HH combo medium (final volume 20 mL) and sonicated with a sonic bath for 15 minutes. All solutions were then analysed for fluorescent intensity.

The acute toxicity of all the samples that were collected from the dialysis and the centrifugation protocols were assessed on *D. magna,* and the stability of NMs in each sample was assessed by DLS for the determination of size and zeta potential.

All subsequent experiments on the PS NMs were conducted using the particles washed by dialysis.

2.4.1.5 Impact of Ageing on NMs Stability and *D. magna* EC_{50}

50 nm and 2µm amine-modified latex beads PS-NMs were selected for this study. Ageing of both NMs (unwashed) was achieved by preparing stock solutions of 500 mg/L in HH combo medium and storing them for 2 years. Stock solutions were sealed, covered with foil, and kept refrigerated at 4 °C during the process. The acute toxicity of the aged NMs was then evaluated at 48 h according to the OECD 202 test guideline, and their stability was assessed by measuring their size and zeta potential using the zetasizer from Malvern Instruments.

2.4.1.6.1 Protein Concentration Range-finding Study

Two experiments were conducted in this study. The first was to determine the protein concentrations that can be released by *D. magna* into HH combo medium as part of their normal water filtering activity. The second experiment was to determine the concentration of proteins that can be acquired by homogenizing whole *D. magna* tissues. All samples were analysed for total protein concentrations in triplicate by applying the previously discussed BCA protocol (Section 2.3.1).

To determine the protein concentration that can be released by *D. magna* to condition fresh HH combo medium, a series of tests have been conducted by incubating various numbers of neonates in the culture medium under a variety of scenarios as follows:

(i) Incubation of 5, 10, 15, 20 and 25 neonates (1-2 days old) in 5 mL HH combo for 6 h. This test was applied to two groups of animals using neonates that had been fed prior to the exposure in one group and neonates that had not been fed prior to the exposure in another group.

(ii) Incubation of 5 or 10 *D. magna juveniles (5 days old)* in 5 mL HH combo for 6 h, 24 h and 48 h. The test was conducted on two groups of animals (fed and not fed 24 h before the test).

(iii) *D. magna* neonates (< 48 hours old) were introduced to a chemical stressor ($CdCl_2$). A 48 h acute toxicity range-finding test was first performed on the chosen heavy metal ion (HMI) using triplicates of 10 neonates for each concentration in HH combo medium (final volume 5 mL). Ten $CdCl_2$ exposure concentrations were selected, with the highest concentration causing 100% mortality and the lowest causing 0% mortality (0.1, 0.15, 0.25, 0.35, 0.45, 0.7, 0.9, 1.4, 2.5, 4 mg/L). Neonates were exposed to the selected concentration in triplicate for 48 h, and the surrounding water samples were collected for BCA protein concentration measurements.

2.4.1.6.2 Extraction of Total Proteins from whole *D. magna* Tissue Homogenate

The selected number of animals for each test was homogenised by using an agate mortar and pestle (Standard form, O.D. 25 mm) purchased from Sigma Aldrich. *D. magna* whole tissues were placed in the agate mortar incubated either in 0.1M Tris or 0.01M PBS buffer and were gently ground for 15-20 minutes using the agate pestle. Once all tissues were homogenised with the buffer, samples were carefully pipetted into a 1.5 mL Eppendorf tube and centrifuged at 14,000 RPM at 4 °C for 10 minutes. The supernatants were then collected to be analysed for total protein content.

To determine the protein concentrations that can be measured after homogenizing total *D. magna* tissue, the following tests were performed:

(i) A total of 5, 10, 15, 20, and 25 *D. magna* (5 days old) per sample were homogenised in 0.1 M Tris buffer (0.5 mL).

(ii) A total of 100, 200, 300, 400, and 500 *D. magna* neonates (< 48 h old) per sample were homogenised in 0.1 M Tris buffer (0.5 mL).

(iii) A total of 50 *D. magna* neonates per sample were homogenised in 0.5 mL of both 0.1 M Tris buffer and 0.01 M PBS buffer to compare the buffer effects on protein recovery.

2.4.1.7 The Effect of Conditioning HH Combo Medium on NMs Stability and *D. magna* EC_{50}

The effect of proteins secreted by daphnids to condition HH combo medium on the stability and toxicity of the four types of PS NMs were assessed. A stock solution of conditioned HH combo medium was prepared following the method described in section 2.3.1.2. The stability of NMs in the conditioned HH Combo was assessed by measuring their size and zeta potential using a zetasizer (ZS) nano from Malvern instruments. The same protocol previously conducted to determine the EC_{50} of the NMs was repeated using the dialyzed particles in HH Combo versus conditioned HH Combo medium. Each exposure particle solution (15 mL/concentration) was incubated in a conditioned HH combo medium for 2 h before the exposure. Less than 48 h old *D. magna* neonates were then exposed to the selected range of concentrations for each PS type, and the immobilization response was recorded to determine the EC_{50} at 48 h.

2.4.1.8 Assessment of NMs Accumulation and The Role of Corona Evolution During NM Passage Through *D. magna* Gut

The goal of this study is to explore the role of corona evolution during NMs passage through the *D. magna* gut and how this affects the accumulation and response of subsequently unexposed neonates to the NMs, by indicating whether the NMs that have exposed or passed through the gut and released by daphnids would be taken up by other Daphnids or not, as well as whether these NMs are more or less toxic to the Daphnids exposed to the gut-transformed NMs.

The 50 nm and 2 µm fluorescent PS-NH_2 NMs previously washed by dialysis were selected for this study. A minimum effect (100 mg/L dialyzed 2µm PS-NH_2, which had 0% neonate's immobilization) and (10 mg/L of dialyzed 50 nm PS-NH_2 which had around 20% neonate's immobilization) 48 h was chosen for the exposures.

This study involves two rounds of exposure (Figure 2.9). In the first round, 10 *D. magna* neonates (< 48 h old) of third broods or above were exposed to both PS NMs in three replicates. Each replicate was introduced to the selected concentrations in HH combo medium with a final volume of 50 mL in a 100 mL glass beaker. After 48 h of exposure, animals were collected and rinsed three times to clear any particles attached to their carapace by placing them in clean beakers filled with 50 mL fresh HH combo medium with 30 seconds of gentle shaking. After the rinsing process, each *D. magna* replicate was left to swim in 10 mL fresh medium for 3 h to allow some time for the deputation of ingested NMs. Organisms were then collected and analysed for the total accumulation of NMs within the whole animal's tissue by fluorescence, as described briefly below. This was done by incubating each replicate of neonates with 200 µL fresh medium into a single well of a flat bottom 96-well plate. The HH combo solutions used in the depuration process were also

analysed for total fluorescent intensity. All samples were assessed using the fluorescence function of the Tecan plate reader. The 10 mL HH combo medium used in each treatment for depurating NMs was collected to be exposed to a new set of *Daphnia* in the second round of the study, and those animals were then assessed for fluorescence uptake.

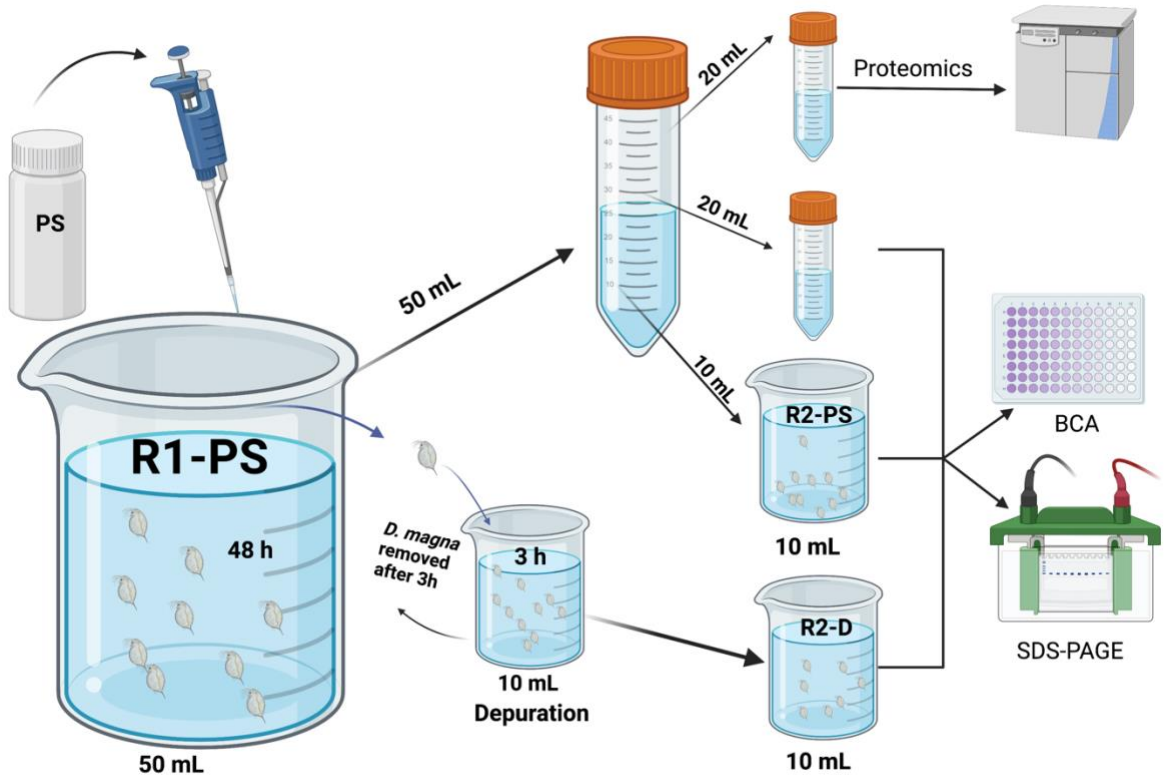

Figure 2.9. Illustrations demonstrating the experimental design of the PS eco-corona formation after passage through D. magna gut.

Water samples from the first round of exposures (minus the daphnids, which were removed to fresh medium for depuration) were collected to be used in the second round of exposure, as well as for BCA total protein quantification and eco-corona isolation for PAGE and proteomic assessments (details in the next section). Each 50 mL sample was split into three portions, 20 mL for PAGE and BCA, 20 mL for proteomics, and 10 mL to be exposed to a new set of *D. magna* neonates (these solutions are a mixture of NMs that had been excreted by daphnids as well as those that had not been internalized but had acquired a corona from

the conditioning proteins). In the second round of the study, a new set of neonate replicates were exposed to the previously recovered NM solutions for another 48 h, noting that this round involved 10 mL exposure volume for each sample compared to 50 mL in the first round. Samples were then collected and assessed for accumulation and protein analysis by applying the same methods conducted in the first round.

2.4.1.8.1 Hard Corona Isolation and Protein Identifications

The hard corona refers to the layer of proteins that are sufficiently strongly bound to the NMs that they can be easily recovered and isolated for quantification and identification. The collected water samples were assessed to identify the protein coronas that formed around the NMs during the 48 h exposures. For the SDS-PAGE analysis, protein complexes were isolated by applying the protocol described by (Bergese and Hamad-Schifferli, 2013). Briefly, the 20 mL samples of NMs were incubated in 50 mL centrifuge tubes. To remove any unbound proteins and contaminants, each sample was subjected to three replicates of washing and centrifugation steps. In each step, samples were centrifuged for 20 minutes at 5,200 *g* at 4 °C; the supernatant was removed, leaving only the pellet of NMs, which contain the bound protein coronas, and 10 mL of phosphate buffered saline (PBS) was added. After the last washing step, the pellets were incubated in 50 µL lysis PBS buffer. Each sample was then separated into two microtubes. One aliquot was used for BCA protein concentration measurements, and the other was incubated in 4x loading buffer for 5 minutes at 95 °C to denature the proteins and then transferred into a 12.5% sodium dodecyl sulphate-polyacrylamide gel for separation. Samples were then run through the SDS-PAGE system (applying 180 V and 110 mA) as detailed below, and their formed bands were analysed. Three replicates were evaluated by sample and gel run included a color pre-stained protein standard

(cod P7712S, New England BioLabs). After electrophoresis, separated proteins were stained with silver nitrate and a GelDoc imaging system was then used to capture the resulted bands.

Table 2.8. Components of the SDS-PAGE gel

Reagents	**12 % Separating Gel (20mL)**	**5.1 % Stacking Gel (10 ml)**
ddH_2O	6.6 mL	6.85 mL
SDS 10%	200 µL	100 µL
1.5 M Tris pH 8.8	5 mL	1.24 mL
(Bis-)Acrylamid 30%	8 mL	1.711 mL
TEMED	17 µL	10 µL
APS (10%)	200 µL	100 µL

For proteomic analysis by mass spectrometry, the second 20 mL of collected exposure samples were also subjected to three replicates of washing and centrifugation steps for 20 minutes at 5,200g at 4 °C, but ultra-pure water was used instead of PBS and the samples were then stored at -20 °C. However, due to some limitations, we were unable to perform this assessment yet but samples are stored at – 20 °C and it is planned to analyse them.

2.4.2 Chapter 4 Protocols

2.4.2.1 NMs Selected for The Study

Carboxylated graphene quantum dots (COOH-GQDs) dispersed in DI water (1 mg/mL) with a size < 10 nm synthesised by the bottom-up method, hydroxylated GQDs (OH-GQDs) dispersed in a mixture of DI water and ethylene glycol (1 mg/mL) with a size < 6 nm synthesised by the hydrothermal method, and Aminated GQDs (NH_2-GQDs) dispersed in DI water (1 mg/mL) with a size < 5 nm synthesised via the hydrothermal method were all purchased from ACS MATERIALS, and used as received.

2.4.2.2 The Role of Surface Functionalization and Medium Conditioning on The Toxicity of GQDs

The acute toxicity of all three selected NMs was assessed by preparing stock solutions of 100 mg/L and exposing *D. magna* neonates to a range of concentration between (10 mg/L and 100 mg/L) for each NM type for 48 h. All exposures were conducted in triplicate following the previously discussed OECD 202 test guideline. The same exposures were repeated using a conditioned HH combo medium. The conditioned medium was prepared by incubating *D. magna* neonates in the culture medium for 48 h (2 neonates per mL), and the stock solutions were incubated in the conditioned HH combo for 2 h before the exposures. Note: All the NMs used in this experiment were sealed and stored at 4 °C in their original containers for one year before the study was conducted.

2.4.2.3 The Impact of Ageing (storage) and Medium Conditioning on The Toxicity of GQDs

This experiment was conducted on three batches from each of the aminated, carboxylated and hydroxylated GQDs. The first batch was stored for one year, the second batch for two years and the third batch for three years. All batches were kept in their original pristine

state (opened) in the containers from the manufacturer and refrigerated at 4 °C during the ageing process. The acute toxicity of the NMs was then assessed by applying the OECD 202 protocol in both fresh and conditioned HH combo medium.

2.4.2.4 The Impact of The Ageing of GQDs in Culture Medium

The pristine NMs used to prepare stock solutions in this study were already stored (aged) for two years at 4 °C before starting the experiment. Stock solutions of (300 mg/L) in fresh HH combo were prepared for each NM type in 50 mL falcon tubes, sealed, protected from light, and refrigerated at 4 °C. The acute toxicity at 48 h and stability of NMs were assessed after 3 months and 6 months of incubation in HH combo medium by applying the same previously mentioned protocols (OECD 202 and DLS).

2.4.2.5 Accumulation of GQDs in *D. magna*

This study was conducted on the three types of GQDs using the 2 years aged (during storage) pristine GQDs, which were freshly dispersed versus after 6 months of ageing in fresh HH combo medium. Three replicates of 10 *D. magna* neonates (< 48 hours) were exposed to a concentration of GQDs that had no or minimum toxic effect. For the pristine NMs, 10, 40 and 80 mg/L were selected for OH-GQDs, COOH-GQDs andNH_2-GQDs, respectively. For the NMs aged for 6 months in HH combo medium, 60, 80 and 100 mg/L were chosen for the COOH-GQDs, OH-GQDs and NH_2-GQDs, respectively. After 48 h of exposure, each replicate of neonates was washed by moving them into 50 mL of fresh HH combo medium with gentle shaking for 30 seconds, repeated three times. Neonates were then transferred into 10 mL of fresh HH combo and left to depurate NMs for 3 h. Fluorescence measurements were then taken for all *D. magna* whole body replicates (each

replicate in 300 µL fresh HH per well in a 96-well plate). The fluorescence intensity of all the exposure and depuration solutions were also measured.

2.4.2.6 Protein Concentrations Released by *D. magna* Exposed to GQDs

The GQDs used in this study were from two batches of particles, one aged in HH combo medium for 6 months and the other group non-aged (pristine). Three replicates of 10 *D. magna* neonates were exposed to a series of concentrations (20, 40, 60, 80, and 100 mg/L) for each NM type and batch. After 48 h, the exposure medium solutions were collected and measured for their total protein content using the Pierce Rapid Gold BCA Protein Assay Kit from ThermoFisher Scientific (Section 2.3.1).

2.4.3 Chapter 5 Protocols

2.4.3.1 NMs Synthesis and Characteristics

The selected NMs for this chapter were purchased from ACS MATERIALS (Table 2.9).

Table 2.9. Types of MoS_2 purchased from ACS MATERIALS.

Material	Appearance	Diameter	Thickness
Bulk (B-MoS_2)	Black powder		
Monolayer MoS_2 (L-MoS_2)	Black powder	0.2-5 µm	~ 1 nm
Nanosize Monolayer MoS_2 (S-MoS_2)	Black powder	20-500 nm	~ 1 nm

The B-MoS_2 was synthesised by exfoliation, the L-MoS_2 and S-MoS_2 were synthesised via Lithium-based Intercalation as described by the supplier.

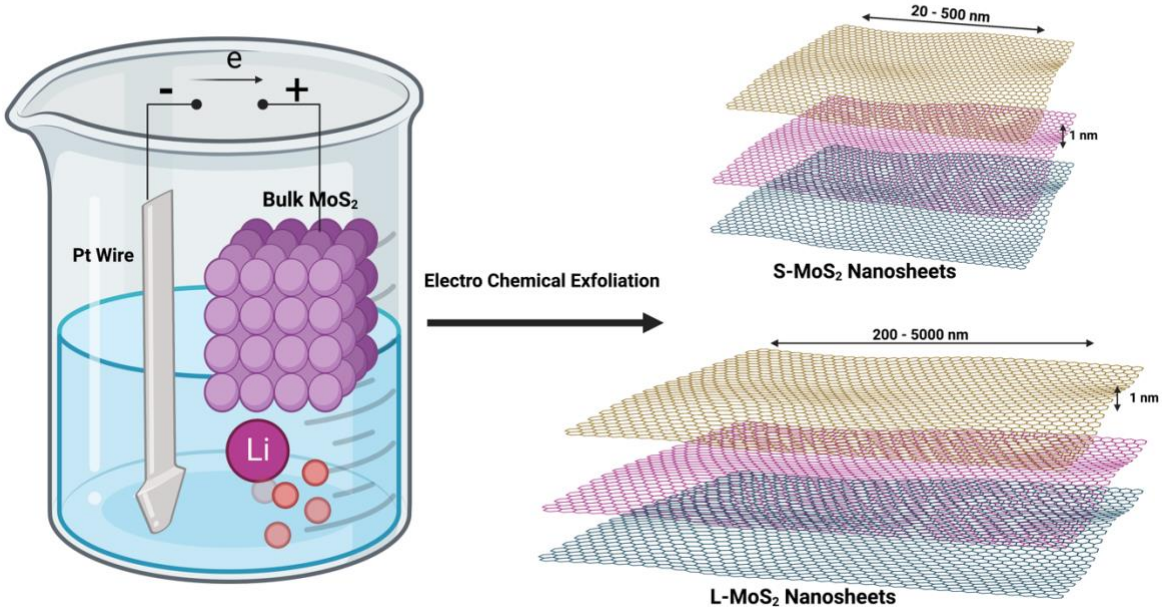

Figure 2.10. Illustration of MoS_2 NMs synthesis method (Lithium-based Intercalation).

2.4.3.2 Characterization of The MoS_2 NMs

The zeta potential, size and average PDI were measured by DLS in DI water, fresh and conditioned HH combo. The conditioned HH combo medium was prepared according to section 2.3.1.2 of this thesis.

2.4.3.3 Toxicity Assessment of The MoS_2 NMs

The 48 h acute toxicity of the three selected MoS_2 materials toward *D. magna* was investigated according to the OECD 202 guideline in both fresh and conditioned HH combo medium. Working stock solutions of 5 mg/mL were prepared for each MoS_2 type. 10 *D. magna* neonates were exposed to a range of MoS_2 concentrations (10-1000 mg/L) in triplicate, and the number of immobilized daphnids was recorded. The EC_{50} was determined for the three types of MoS_2 by plotting the results in a dose-response curve.

2.4.3.3 Toxicity of Heavy Metal Ions (HMI) in Combination With MoS_2 and Humic Acid

As discussed in the introduction of this thesis, NMs are never the only pollutant that humans and the environment are exposed to, and as a consequence of their reactive surfaces, NMs are very likely to interact with other pollutants present in the environment, leading to the potential for mixture toxicity. Additionally, MoS_2 materials are being used in pollutant adsorption studies and it has been reported that they can efficiently remove HMIs as discussed in chapter 1 of this thesis and it would be interesting to assess this in correlation with their toxicity. Copper (II) chloride dehydrate ($CuCl_2.\ 2H_2O$), and Cadmium nitrate tetrahydrate [$Cd(NO_3).4H_2O$] were purchased from Sigma Aldrich, and used as received. Suwanne River Humid Acid (HA) Standard III was purchased from the International Humic Substances Society, USA. The 48 h acute toxicity of Cd^{+2} and Cu^{+2}, as representative heavy metal ions (HMIs) that would likely be co-exposed with MoS_2 particles in the

environment, were individually determined by exposing *D. magna* neonates to a range of concentrations of the chemicals (0.001 to 1.5 mg/L) following the previously mentioned OECD 202 guideline.

To determine whether MoS_2 and HA can attenuate the toxicity of either of the representative HMIs and to evaluate the magnitude of any toxicity reduction, a series of exposures were introduced based on the previously performed toxicity range-finding studies. Two constant concentrations that had no toxic effect were chosen for the three types of MoS_2 (10 and 100 mg/L). The selected concentrations of MoS_2 particles were mixed with the HMIs individually at a range of concentrations; Cd^{+2} (0.001, 0.05, 0.1, 0.5, 1 and 1.5 mg/L) and Cu^{+2} (0.01, 0.05, 0.1, 0.5 and 1 mg/L) in HH combo medium. 15 mL of solution was prepared for each MoS_2-HMI mixture to be enough for three (10 *D. magna*) replicates. The toxicity of all mixtures was evaluated by recording the number of immobilized neonates after 48 h of exposure. All tests were performed in the presence and absence of 20 mg/L HA added to the medium (both unconditioned and *Daphnia* conditioned medium). The data were then used to calculate the EC_{50} of each treatment represented in a dose-response curve. The stability of the NMs was monitored by DLS in all mixture solutions during the study.

2.4.3.4 MoS_2 HMIs Adsorption Study Using ICP-MS

In a batch adsorption experiment, two fixed concentrations (10 and 100 mg/L) of each of the three types of MoS_2 were incubated with four different concentrations of either Cd^{+2} or Cu^{+2} (0.05, 0.1, 0.5, and 1 mg/L) in fresh HH combo medium (pH = 7.7) using 50 mL falcon tubes in triplicate (Table 2.10). All mixture solutions were placed in a rack and incubated on a laboratory bench without shaking at room temperature (20 °C) for 3 and 24 h (Figure 2.11).

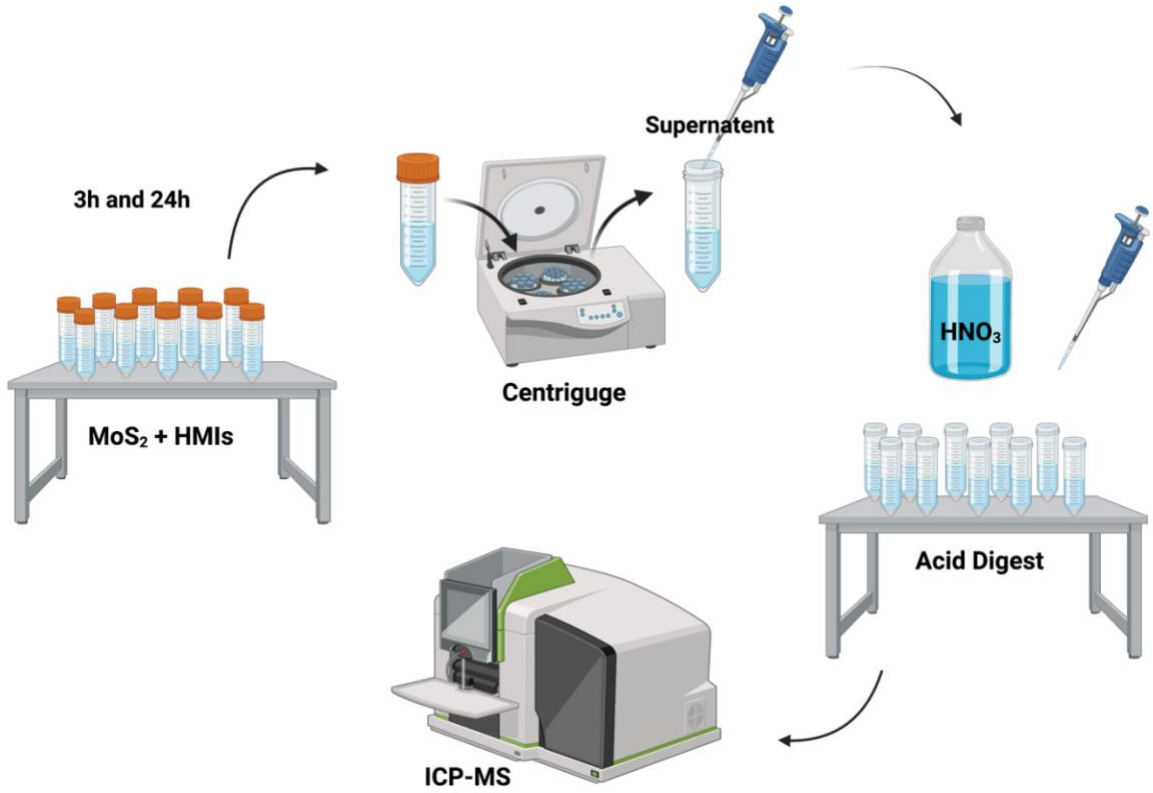

Figure 2.11. Illustration of the MoS_2 and HMIs batch adsorption study

Table 2.10. Summary of MoS_2 and HMIs mixture solutions (same mixtures were applied for B, L and S MoS_2).

#	MoS_2 & HMIs Mixture Solutions
1	10 mg/L MoS_2 + 0.05 mg/L $Cd(NO_3)$
2	10 mg/L MoS_2 + 0.1 mg/L $Cd(NO_3)$
3	10 mg/L MoS_2 + 0.5 mg/L $Cd(NO_3)$
4	10 mg/L MoS_2 + 1 mg/L Cd (NO_3)
5	100 mg/L MoS_2 + 0.05 mg/L $Cd(NO_3)$
6	100 mg/L MoS_2 + 0.1 mg/L $Cd(NO_3)$
7	100 mg/L MoS_2 + 0.5 mg/L $Cd(NO_3)$
8	100 mg/L MoS_2 + 1 mg/L Cd (NO_3)
9	10 mg/L MoS_2 + 0.05 mg/L $CuCl_2$
10	10 mg/L MoS_2 + 0.1 mg/L $CuCl_2$
11	10 mg/L MoS_2 + 0.5 mg/L $CuCl_2$
12	10 mg/L MoS_2 + 1 mg/L $CuCl_2$
13	100 mg/L MoS_2 + 0.05 mg/L $CuCl_2$
14	100 mg/L MoS_2 + 0.1 mg/L $CuCl_2$
15	100 mg/L MoS_2 + 0.5 mg/L $CuCl_2$
16	100 mg/L MoS_2 + 1 mg/L $CuCl_2$

Samples were collected after 3 h and 24 h, centrifuged at 14,000 RPM for 20 minutes at 20 °C to pellet the particles and any HMI bound to them, and supernatants containing the unbound HMI were collected carefully and digested with 2% nitric acid (3 mL of sample + 2 mL of 2% nitric acid) before being analysed by ICP-MS.

To prepare calibration curves and quantify the chemicals of interest by ICP-MS as described in section 2.3.2, standards of Cd-111, Mo-98 and Cu-63 were purchased from Sigma Aldrich. The calibration curves (Figure 2.12) were generated by diluting the standards to solutions of 10 ppb, 50 ppb, 125 ppb, 250 ppb 500 ppb and 1000 ppb with 2% nitric acid.

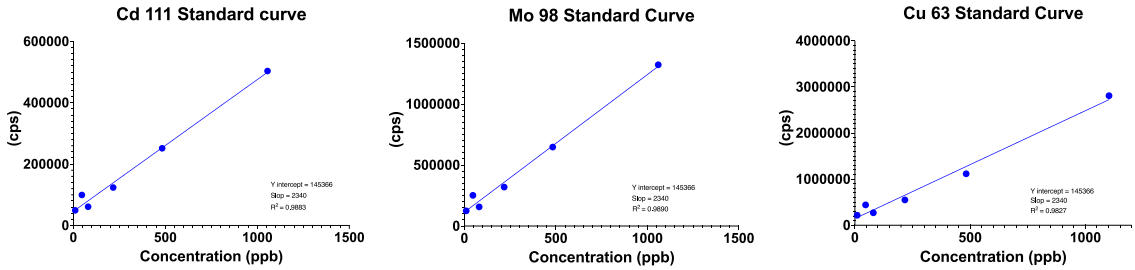

Figure 2.12. Calibrations of the HMIs of interest (Cd and Cu) and for the NMs (Mo) as determined by ICP-MS.

The supernatant samples were then analysed by ICP-MS, and the concentrations of sample triplicates were measured in comparison with the standards. The average results were used to calculate the adsorption % and adsorption capacity (Qe) of each treatment by applying equations 2.4 and 2.5.

$$\text{Adsorption (\%)} = ((C_0-C_e)/C_0)x\ 100\%$$

Equation 2.4.

where C_0 is the initial concentration, and C_e is the ion concentration measured by ICP-MS after incubation. In the case of Mo, this was to check if there was any dissolution of the particles during the incubation experiments, as the majority of the MoS_2 particles should have been removed as the particle pellet when the supernatant was separated.

$$Qe = ((C_0-C_e) \times V) / W$$

Qe is the adsorption capacity in mg/mg, C_0 is the initial concentration of HMI and C_e is the concentration of HMIs at the end of the adsorption assay in mg/L, V is the solution volume in L, and W is the adsorbent mass in g.

2.4.3.5 Accumulation of HMIs when Combined with MoS_2 within *D. magna* whole Tissue

This was a preliminary study to gain insight into the accumulation behaviour of the studied materials and the data will be used to build up the experimental design for a more detailed bioaccumulation experiment which we plan to conduct very soon for publication. 10 *D. Magna* neonates in triplicate were exposed to a mixture of MoS_2 and HMIs solutions in HH Combo medium at selected concentrations based on the observed acute toxicity results, which had a minimum toxic effect on neonates (Table 2.11). To explore the role of humic acid, the uptake of the HMIs in the presence of humic acid rather than the MoS_2 particles was also explored.

Table 2.11. Mixture solutions exposed to D. magna in HH Combo medium.

Number	**Concentrations/treatments Exposed to *D. magna***
1	Cd (1 mg/L) + HA (20 mg/L)
2	Cd (0.5 mg/L) + HA (20 mg/L)
3	Cu (1 mg/L) + HA (20mg/L)
4	Cu (0.5 mg/L) + HA (20 mg/L)
5	B-MoS_2 (100 mg/L) + Cd (0.1 mg/L)
6	B-MoS_2 (100 mg/L) + Cu (0.1 mg/L)
7	L-MoS_2 (100 mg/L) + Cd (0.05 mg/L)
8	L-MoS_2 (100 mg/L) + Cu (0.5 mg/L)
9	S-MoS_2 (100 mg/L) + Cd (0.5 mg/L)
10	S-MoS_2 (100 mg/L) + Cu (1 mg/L)
11	Cd (0.01 mg/L)
12	Cu (0.05 mg/L)
13	Controls (HH combo)

After 48 h of exposure, neonates were transferred into fresh HH combo medium and left to depurate the chemicals for 3 h. The solutions used in the exposures, as well as the solutions used in the depuration process, were collected and prepared for ICP-MS analyses following the same protocol applied in the batch adsorption experiment.

To prepare *D. magna* for ICP-MS analyses in order to assess the uptake of the MoS_2 materials and the associated HMIs, the 10 whole tissue neonates per replicate were incubated in 0.714 mL pure nitric acid in 15 mL falcon tubes for 48 h to digest the tissue. After the incubation time, no tissue was observed by the naked eye, and samples were diluted with DI water until the concentration of nitric acid reached 5%. Samples were then left in a hot water bath (80 °C) for 3 h before being analysed by ICP-MS by following the previously described mass spectrometry method.

References

Ellis, L.-J. and Lynch, I. (2020) 'Mechanistic insights into toxicity pathways induced by nanomaterials in Daphnia magna from analysis of the composition of the acquired protein corona', *Environmental Science: Nano*, 7(11), pp. 3343–3359. Available at: https://doi.org/10.1039/D0EN00625D.

Al-Hakkani, M.F. (2019) 'Guideline of inductively coupled plasma mass spectrometry "ICP–MS": fundamentals, practices, determination of the limits, quality control, and method validation parameters', *SN Applied Sciences*, 1(7), p. 791. Available at: https://doi.org/10.1007/s42452-019-0825-5.

Baer, K.N. and Goulden, C.E. (1998) 'Evaluation of a High-Hardness COMBO Medium and Frozen Algae forDaphnia magna', *Ecotoxicology and Environmental Safety*, 39(3), pp. 201–206. Available at: https://doi.org/10.1006/eesa.1997.1627.

Bergese, P. and Hamad-Schifferli, K. (eds) (2013) *Nanomaterial Interfaces in Biology: Methods and Protocols*. Totowa, NJ: Humana Press (Methods in Molecular Biology). Available at: https://doi.org/10.1007/978-1-62703-462-3.

Brady, P.N. and Macnaughtan, M.A. (2015) 'Evaluation of Colorimetric Assays for Analyzing Reductively Methylated Proteins: Biases and Mechanistic Insights', *Analytical biochemistry*, 491, pp. 43–51. Available at: https://doi.org/10.1016/j.ab.2015.08.027.

Carvalho, P.M. *et al.* (2018) 'Application of Light Scattering Techniques to Nanoparticle Characterization and Development', *Frontiers in Chemistry*, 6. Available at: https://www.frontiersin.org/articles/10.3389/fchem.2018.00237 (Accessed: 28 October 2022).

'DLS in 30 Minutes - Q&A - Materials Talks' (2017), 11 July. Available at: https://www.materials-talks.com/dls-in-30-minutes-qa/ (Accessed: 28 October 2022).

Dynamic Light Scattering (DLS) | Common Terms Defined | Malvern Panalytical (2017). Available at: https://www.malvernpanalytical.com/en/learn/knowledge-center/whitepapers/wp111214dlstermsdefined (Accessed: 28 October 2022).

Ellis, L.-Jayne.A., Kissane, S. and Lynch, I. (2020) 'Maternal Responses and Adaptive Changes to Environmental Stress via Chronic Nanomaterial Exposure: Differences in Inter and Transgenerational Interclonal Broods of Daphnia magna', *International Journal of Molecular Sciences*, 22(1), p. 15. Available at: https://doi.org/10.3390/ijms22010015.

Fluorescence Intensity Measurements | BMG LABTECH (2022). Available at: https://www.bmglabtech.com/en/fluorescence-intensity/ (Accessed: 14 November 2022).

gel electrophoresis | Learn Science at Scitable (2014). Available at: https://www.nature.com/scitable/definition/gel-electrophoresis-286/ (Accessed: 15 November 2022).

Hussain, M.T., Forbes, N. and Perrie, Y. (2019) 'Comparative Analysis of Protein Quantification Methods for the Rapid Determination of Protein Loading in Liposomal Formulations', *Pharmaceutics*, 11(1), p. 39. Available at: https://doi.org/10.3390/pharmaceutics11010039.

Inductively Coupled Plasma Mass Spectrometry (ICP-MS) Information - UK (no date). Available at: https://www.thermofisher.com/uk/en/home/industrial/spectroscopy-elemental-isotope-analysis/spectroscopy-elemental-isotope-analysis-learning-center/trace-elemental-analysis-tea-information/inductively-coupled-plasma-mass-spectrometry-icp-ms-information.html (Accessed: 13 November 2022).

Kaszuba, M. *et al.* (2010) 'High-concentration zeta potential measurements using light-scattering techniques', *Philosophical transactions. Series A, Mathematical, physical, and engineering sciences*, 368(1927), pp. 4439–4451. Available at: https://doi.org/10.1098/rsta.2010.0175.

Kelpsiene, E. *et al.* (2022) 'Review of ecotoxicological studies of widely used polystyrene nanoparticles', *Environmental Science: Processes & Impacts*, 24(1), pp. 8–16. Available at: https://doi.org/10.1039/D1EM00375E.

Mesapogu, S., Jillepalli, C.M. and Arora, Dilip K. (2013) 'Agarose Gel Electrophoresis and Polyacrylamide Gel Electrophoresis: Methods and Principles', in Dilip Kumar Arora, S. Das, and M. Sukumar (eds) *Analyzing Microbes: Manual of Molecular Biology Techniques*. Berlin, Heidelberg: Springer (Springer Protocols Handbooks), pp. 73–91. Available at: https://doi.org/10.1007/978-3-642-34410-7_5.

Nageswaran, G., Choudhary, Y.S. and Jagannathan, S. (2017) 'Inductively Coupled Plasma Mass Spectrometry', in *Spectroscopic Methods for Nanomaterials Characterization*. Elsevier, pp. 163–194. Available at: https://doi.org/10.1016/B978-0-323-46140-5.00008-X.

Nickel, C. *et al.* (2014) 'Dynamic light-scattering measurement comparability of nanomaterial suspensions', *Journal of Nanoparticle Research*, 16(2), p. 2260. Available at: https://doi.org/10.1007/s11051-014-2260-2.

Perkin Elmer (2011) 'The 30-Minute Guide to ICP-MS', *Perkin Elmer*, p. 8.

Pierce™ Rapid Gold BCA Protein Assay Kit (no date). Available at: https://www.thermofisher.com/order/catalog/product/A53225 (Accessed: 12 November 2022).

Sagar, C. (2017) 'Technical Support Manager', p. 37.

Shionoya, S. (1998) 'Photoluminescence', in D.R. Vij (ed.) *Luminescence of Solids*. Boston, MA: Springer US, pp. 95–133. Available at: https://doi.org/10.1007/978-1-4615-5361-8_3.

'The 30-Minute Guide to ICP-MS' (no date), p. 8.

Wilschefski, S.C. and Baxter, M.R. (2019) 'Inductively Coupled Plasma Mass Spectrometry: Introduction to Analytical Aspects', *The Clinical Biochemist Reviews*, 40(3), pp. 115–133. Available at: https://doi.org/10.33176/AACB-19-00024.

Xu, R. (2008) 'Progress in nanoparticles characterization: Sizing and zeta potential measurement', *Particuology*, 6(2), pp. 112–115. Available at: https://doi.org/10.1016/j.partic.2007.12.002.

Zeta Potential | Malvern Panalytical (2022). Available at: https://www.malvernpanalytical.com/en/products/measurement-type/zeta-potential (Accessed: 10 November 2022).

ZetaPotential-Introduction-in-30min-Malvern.pdf - TECHNICAL NOTE Zeta potential - An introduction in 30 minutes ZETA POTENTIAL Introduction Zeta | Course Hero (no date). Available at: https://www.coursehero.com/file/64183217/ZetaPotential-Introduction-in-30min-Malvernpdf/ (Accessed: 29 October 2022).

3

The Role of Chemical Surfactants and *D. magna* Secreted Proteins on the Toxicity of Polystyrene Micro/Nanoplastics

3.1 Introduction

Plastic production has significantly increased over the last decades due to its excellent properties (durability/resistance, lightness and strength) as well as the low production cost (Miloloža *et al.*, 2021). It has been reported that in 1950 ~ 1.5 million tons (MT) of plastic were produced, increasing to ~ 187 MT in 2000, ~ 265 MT in 2010 and up to 360 MT in 2018, with 60-80% of these produced materials being mis-managed at their end of life and resulting in anthropogenic litter in the environment (Miloloža *et al.*, 2021). Once these materials are released into the environment, they can break down into microplastics (MPs, 0.1 µm - 5mm) and nanoplastics (NPPs, < 0.1 µm) due to different processes, such as microbial degradation, photo-oxidation and mechanical forces (Banerjee and Shelver, 2021). The breakdown of plastics into MPs leads to changes in their physical and chemical characteristics, thereby affecting their bioavailability and fate in the ecosystem (Barreto *et al.*, 2020). It is very likely that MPs are present in aquatic environments and being consumed by living organisms, impacting their health and affecting animals that are vital in the food chain, such as *D. magna*. The toxicity of MPs towards biota has gained large attention in recent years, considering the MPs themselves, their associated additives, and the potential for MPs to transport other pollutants. However, the uncertainty in understanding their fate and level of interaction with freshwater animals remains an area that needs to be considered, as many studies reported the negative effects of MPs on marine organisms, but studies investigating their toxicological impact on freshwater organisms are rare,

particularly in terms of applying environmental relevance conditions (Li *et al.,* 2023). Realistic environmental conditions involve the interaction of NMs with biomolecules secreted by living organisms in aquatic environments, which can passivate the surface and reduce non-specific binding and membrane damage (Nasser and Lynch, 2019; Nienhaus *et al.*, 2022). Many studies fail to consider the specifics of their test MPs also, with most commercially available MPs dispersions including stabilizing surfactants (e.g., sodium dodecyl sulfate, SDS) and preservatives (e.g., sodium azide) which themselves can be toxic and thus need to be washed and removed from commercially produced MP materials when performing toxicity tests to avoid confounding effects (Pikuda *et al.*, 2019). Indeed, SDS is also widely used to remove bound proteins from particle surfaces and, as such, can also interfere with the composition of any eco-corona formed on the particles (Cruz de Carvalho *et al.*, 2022). Therefore, it is important to evaluate the ecotoxicological impact of MPs/NPPs while applying as many environmentally relevant conditions as possible and considering the presence of additive chemicals associated with the MPs.

The aims of this chapter were to:

1) Explore the toxicity of polystyrene particles with different sizes and surface functionalization groups (shown in Table 3.1) towards *D. magna*.
2) Evaluate the impact of chemical surfactants on the toxicity of commercial PS MPs/NPPs by washing the particles with two different methods (dialysis and centrifugation) and determine the difference between the two washing methods.
3) Assess the impact of pristine particle ageing [NH_2-PS (2 µm and 50 nm)] in HH combo medium on the stability and acute toxicity to *D. magna*.
4) Investigate the range of proteins that are secreted by *D. magna* to condition HH combo medium as a function of age and number of animals and the effect of this on

the acute toxicity of NMs. Additionally, assessing the concentration of proteins that can be extracted from the animal whole tissue homogenate to compare with the secreted proteins.

5) Understanding the role of corona formation around PS MPs/NPPs after interacting with proteins secreted by *D. magna* in the toxicity behaviour of PS.

Table 3.1. The types of PS materials studied in this chapter with the chemical additives as described by the supplier.

Surface modification	Size	Chemical additives
NH_2-PS latex beads	2 µm	(< 0.25 % Sodium azide).
NH_2-PS latex beads	50 nm	(< 0.25 % Sodium azide).
COOH-PS polybeads	100 nm	sulfate-based surfactant
COOH-PS polybeads	50 nm	sulfate-based surfactant

3.2 Results and Discussion

3.2.1 Impact of Chemical Additives on The Characteristics and Toxicity of Commercial NNPs/MPs Towards *D. magna*

MPs are found in water bodies and wastewater, in mixtures with other substances present in the environment, such as other particles and chemicals including surfactants (Guerranti *et al.*, 2021). Surfactants are commonly used as dispersants or to purify engineered nanomaterials (ENMs), and they may affect the mobility, and dispersion stability of the NMs, thereby altering also the potential toxic effects of the materials (Oleszczuk *et al.,* 2015). The toxicity of NMs towards aquatic species may be directly linked with surfactants and can also impact other substances due to the formation of micelles (aggregated surfactant lipids) which can influence the sorption and desorption of pollutants from the surfaces of MPs (Guerranti *et al.*, 2021). The ecotoxicity of complex and mixed NMs can

differ from a single substance, even if the compounds are present at low concentrations, as discussed in detail in chapter one of this thesis (Guerranti *et al.*, 2021; Martinez *et al.*, 2022). Thus, the toxicity of MPs could be influenced by antagonist/synergic interaction due to the presence of surfactants (Guerranti *et al.*, 2021).

The aim of this experiment is to investigate the toxicity of commercial PS MPs and NPPs in the presence and absence of sodium azide (preservative) and sulfate-based surfactants (anionic dispersants) by evaluating two removal/washing methods (dialysis and centrifugation).

To wash the suspended particles from chemical surfactants and other additives, two methods were applied. The first approach is dialysis, and the second is centrifugation, as described in Chapter 2 of this thesis. The fluorescence intensity, hydrodynamic size (HD) and zeta potential (ZP) of all particles were measured before and after the washing processes (Tables 3.2 - 3.5 and Figures 3.1 and 3.2). The measurements were performed on the supernatants and resuspended pellets in the groups washed by centrifugation. Although the COOH-PS NPPs are not fluorescently labelled, they still showed some level of fluorescence compared to the control HH combo and DI water samples due to the presence of particles in the solution, which allowed for the comparison.

The initial mean size of the pristine particles (in fresh HH combo) was confirmed to be 1599 **±** 306.5 nm, 31 **±** 0.71 nm, 54.4 **±** 1.352 nm, and 36.28 **±** 0.095 nm for the 2 µm NH_2-PS, 50 nm NH_2-PS, 100 nm COOH-PS, and 50 nm COOH-PS, respectively. Those obtained size values (Tables 3.2 – 3.5) were then used to compare subsequent results in order to evaluate any changes in particle physicochemical characteristics as a result of the washing steps. In all tested samples, the hydrodynamic size measured by DLS was smaller than what was reported by the supplier. However, it is worth mentioning that in a previous test that was

performed to assess the stability of both NH_2-PS particles over time, the size of the pristine particles was very close to the supplier-reported size, and they remained well dispersed in HH combo medium up to months of dispersion. We did not present those results here because the tested samples were from a different batch with a different lot number, but this confirms the importance of characterizing newly purchased particles even if they are the same type from the same supplier, as there was a considerable size difference in our DLS measurement observations between the two batches. All subsequent results in this chapter are from the same batch as characterized here, and we refer to the particles by their nominal (manufacturer stated) size.

Table 3.2 Characteristics of the 2 µm NH_2-PS particles used herein determined immediately upon dispersion in HH combo medium (pristine) and following washing by dialysis and centrifugation where both the supernatant and particle pellet were characterized. PDI – Polydispersity Index. SD – standard deviation. ZP – zeta potential.

2 µm NH_2-PS						
	Z-average (nm)	**SD ±**	**PDI**	**SD ±**	**ZP (mV)**	**SD ±**
Pristine	1599	306.5	0.542	0.469	-20.9	0.755
Dialyzed	1250	214.3	0.541	0.422	-16.6	0.85
Supernatant	522.7	117.3	0.816	0.113	-7.3	0.932
Pellets	1510	81.75	0.367	0.549	-13	1.22

Table 3.3. Characteristics of the 50 nm NH_2-PS particles used herein determined immediately upon dispersion in HH combo medium (pristine) and following washing by dialysis and centrifugation where both the supernatant and particle pellet were characterized. PDI – Polydispersity Index. SD – standard deviation. ZP – zeta potential.

50 nm NH_2-PS						
	Z-average (nm)	**SD ±**	**PDI**	**SD ±**	**ZP (mV)**	**SD ±**
Pristine	31	0.7108	0.184	0.019	25.5	2.72
Dialyzed	31.13	0.8041	0.194	0.019	13.2	0.0577
Supernatant	41.92	0.1909	0.142	0.008	23.8	0.379
Pellets	823.6	26.39	0.75	0.024	26	0.404

Table 3.4. Characteristics of the 100 nm COOH-PS particles used herein determined immediately upon dispersion in HH combo medium (pristine) and following washing by dialysis and centrifugation where both the supernatant and particle pellet were characterized. PDI – Polydispersity Index. SD – standard deviation. ZP – zeta potential.

100 nm COOH-PS						
	Z-average (nm)	**SD ±**	**PDI**	**SD ±**	**ZP (mV)**	**SD ±**
Pristine	54.42	1.352	0.025	0.014	-24	0.6
Dialyzed	54.57	1.485	0.036	0.023	-23.6	0.529
Supernatant	55.2	2.225	0.043	0.02	-27.9	0.379
Pellets	60.06	1.916	0.134	0.022	-24	0.153

Table 3.5. Characteristics of the 50 nm COOH-PS particles used herein determined immediately upon dispersion in HH combo medium (pristine) and following washing by dialysis and centrifugation where both the supernatant and particle pellet were characterized. PDI – Polydispersity Index. SD – standard deviation. ZP – zeta potential.

50 nm COOH-PS						
	Z-average (nm)	**SD ±**	**PDI**	**SD ±**	**ZP (mV)**	**SD ±**
Pristine	36.28	0.09539	0.113	0.035	-25.4	1
Dialyzed	34.45	0.3955	0.095	0.009	-22.2	0.252
Supernatant	108	4.498	0.47	0.024	-24.8	0.404
Pellets	199.3	33.11	0.458	0.065	-16.5	2.08

After washing the particles by dialysis, the 2 μm NH_2-PS showed a reduction in the hydrodynamic size from 1599 **±** 306.5 nm to 1250 **±** 214.3 nm, which may indicate that the surfactants drive bridging across MPs particles and this was effected by the dialysis process. The other three nanosized PS particles remained almost the same size following dialysis (Tables 3.2 - 3.5), indicating good size stability over the time of the dialysis process and following removal of the dispersant surfactant, which suggests that the charges on the particles provide sufficient electrostatic stabilisation. The 2 μm NH_2-PS washed by centrifugation also showed a reduction in size, which was observed both for particles remaining in the supernatant and those resuspended from the pellet samples. All the other PS NPPs tested showed an increase in size, indicating that agglomeration has occurred as a result of the centrifugation washing stapes. The overall hydrodynamic size observations

indicated better stability of the PS particles washed by dialysis than those washed by centrifugation.

Fluorescence intensity measurements of all solutions were conducted to assess any loss of particles/labels during the process, and no significant changes were observed in any washed by dialysis (Figure 3.1). However, there was a slight loss of fluorescence which we believe might not be due to the dialysis, as our previous observations showed a similar minor loss of fluorescence after 5 days of preparing stock solutions, even when the samples were protected from light exposure. Samples of the surrounding DI water from the dialysis experiments of all particles were also collected each day, analysed for fluorescence, and compared to a non-exposed sample of DI water which did not show any considerable difference in fluorescence intensities, thus ruling out direct loss of fluorescence moieties from the particles. Our findings are consistent with published data, which showed that the fluorescence intensity of PS nanoplastics was similar before and after dialysis, indicating that there was very limited loss of the tested NPPs during dialysis (Pikuda *et al.*, 2019).

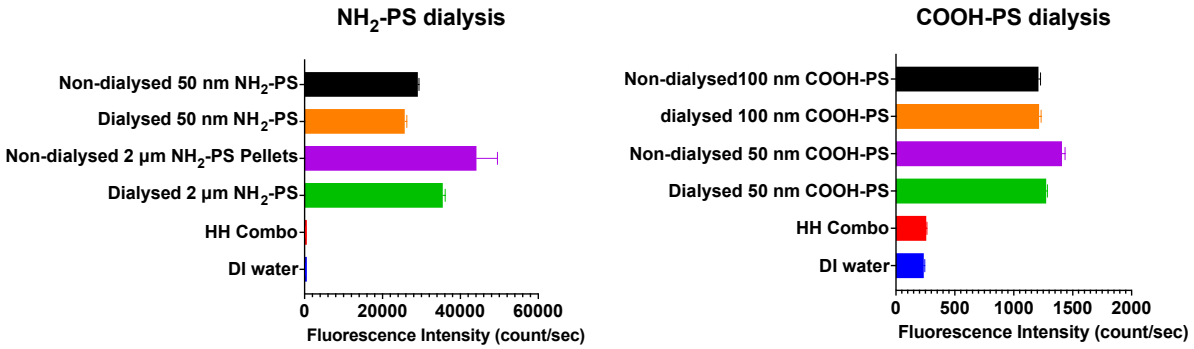

Figure 3.1. Fluorescence intensities of NH_2-PS and COOH-PS MPs/NNPs before and after dialysis (dispersed in HH combo), along with medium controls.

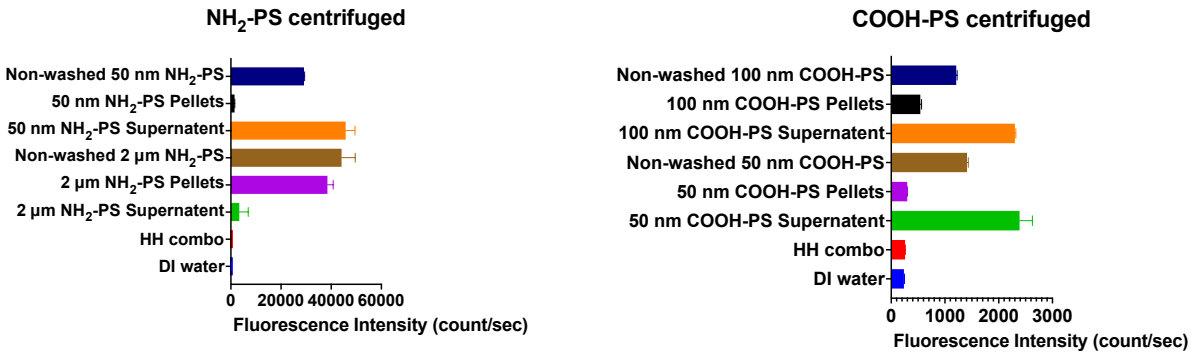

Figure 3.2. Fluorescence intensities of PS MPs/NNPs before and after washing by centrifugation. Particles were dispersed in HH combo medium.

On the other hand, samples that had been washed by centrifugation showed a variation in the fluorescent intensity results (Figure 3.2). The fluorescence intensity magnitude of the 50 nm NH_2-PS followed the order; supernatant > non-washed NPPs > pellets indicating that the largest amount of the fluorescence ended up in the supernatant – this could either mean that the particles did not pellet out effectively or that the label was released from the particles; in the case of the 2 µm NH_2-PS samples the order of the fluorescence intensity was non-washed MPs > pellets > supernatant, indicating that in this case the particles sediment well into the pellet and that very little or no fluorescent label is released from the particles. Both sizes of COOH-PS NPPs followed the order of supernatants > pellets > non-washed NPPs indicating a strong release of fluorescence labels from the COOH-PS NNPs. The centrifugal washing method results indicate some complexity in the removal process, which could lead to inconsistency and variation in subsequent experiments if the particles are not re-characterized fully following the centrifugation, also including a determination of particle number and fluorescence intensity per concentration of particles. Overall, the fluorescence intensities of the particles washed by dialysis showed better reliability compared to the centrifugally-washed particles in terms of maintaining fluorescence and surface properties after the washing process.

3.2.1 The Effect of Particles Washing on The Toxicity of PS MPs/NPPs Towards *D. magna*

In a toxicity range-finding study, we first determined the half-maximum effective concentration (EC_{50}) for each of the studied PS materials after 48 h of exposure of daphnids according to the OECD 202 acute toxicity test guidelines. The EC_{50} values obtained were 5.376 mg/L (2 µm NH_2-PS), 3.207 mg/L (50 nm NH_2-PS), 344.9 mg/L (100 nm COOH-PS, and 91.83 mg/L (50 nm COOH-PS), with higher values indicating lower toxicity, since the organisms are tolerant of the exposure to higher concentrations. When comparing the acute toxicity results, the 50 nm NH_2-PS was the most toxic towards neonates, followed by the 2 µm NH_2-PS, 50 nm COOH-PS and 100 nm COOH-PS, respectively. The amine-modified PS latex beads particles clearly showed higher toxicity than the carboxylated NPPs, as expected, given the known toxicity of cationic particles as a result of their strong interactions with anionic membranes, for example (Sharifi *et al.*, 2012; Huk *et al.*, 2015). In terms of particle size, smaller PS particles were more toxic than their larger size counterparts in both surface functionalizing groups, again as expected, as at a constant particle mass, the number of particles and their reactive surface area increases dramatically as particle size decreases such that there are many more particles present in the organisms (Huk *et al.*, 2014). After washing the particles from preservatives and dispersants by both methods, the acute toxicity of all solutions was assessed and compared with the initial pristine PS MPs/NPPs toxicity results (Figures 3.3 and 3.4).

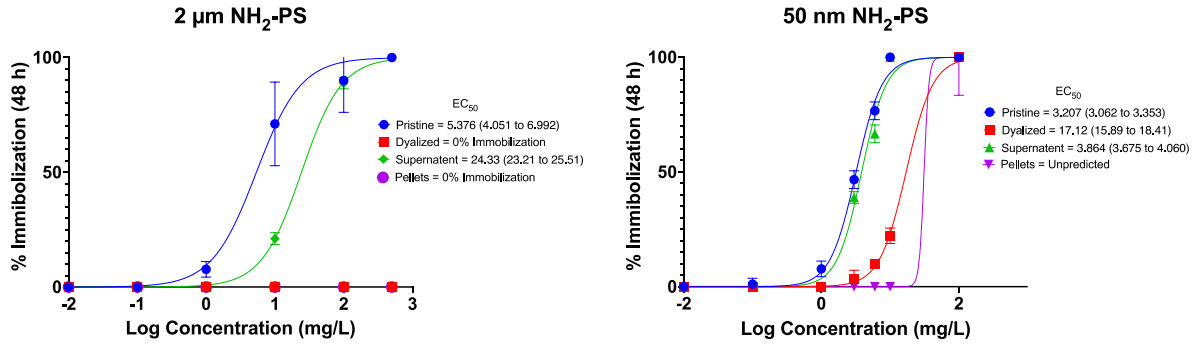

Figure 3.3. Comparison of the acute toxicity of positively charged NH_2-PS MPs and NNPs before and after washing to remove potential confounding factors such as preservatives and dispersants. Interestingly, the supernatant from the centrifugal washing followed the same curve as the pristine particles, and was nearly as toxic, while the washed particles, either by dialysis or centrifugation, were non-toxic at the concentrations tested (up to 500 mg/L 2µm-PS) and (10 mg/L 50nm-PS).

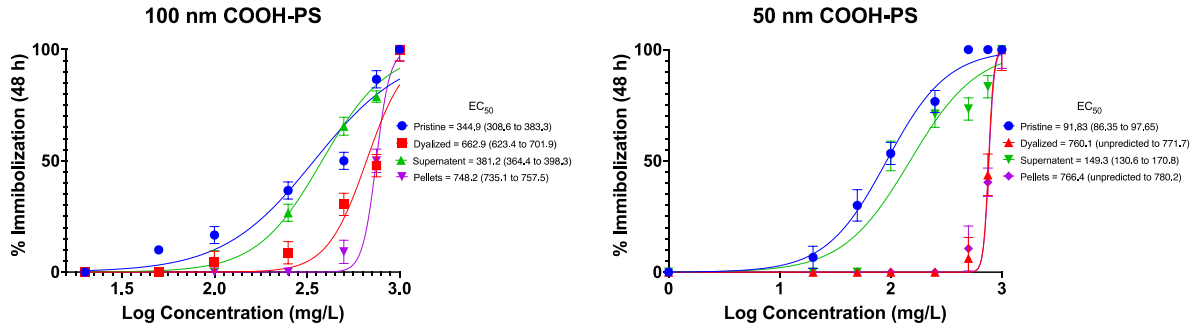

Figure 3.4. Comparison of the acute toxicity of negatively charged COOH-PS NNPs before and after washing to remove potential confounding factors such as preservatives and dispersants. Here, the supernatant from the centrifugal washing followed the same curve as the pristine particles, and was nearly as toxic, while the washed particles, either by dialysis or centrifugation were less-toxic (up to 1000 mg/L) as evidenced by the shift of the curves to the right (i.e., towards higher EC_{50} values).

The acute toxicity of all MPs/NPPs was greatly reduced after washing the particles by both methods, indicating that most of the toxicity effects associated with the pristine PS MPs/NNPs were actually derived from the chemicals (preservatives and/or surfactants) present in the particle dispersions. Those results are also consistent with a study that investigated the effect of sodium azide used as a preservative on the acute toxicities of dialyzed and pristine NPPs on *D. magna*, revealing that the acute toxicity of particles was mainly associated with the sodium azide and not the particles themselves (Pikuda *et al.*, 2019). The scale of reduction varied between particle types (Figures 3.3 and 3.4), with the 2 µm NH_2-PS having the most significant reduction observation reaching 0% immobilization at the highest tested concentration in both the dialyzed and re-dispersed particle pellets

(centrifuged) dispersions. The reduction in acute toxicity of the dialyzed samples was greater than the reduction obtained by centrifugation of the particles and re-dispersion of the particle pellets for all particle types except the 50 nm COOH-PS group, where the reduction was relatively similar for the dialyzed and pellet dispersions and indeed the overall reduction in toxicity here was also the lowest. Analysis of all samples collected from the centrifugal-washing method showed that the supernatant solutions had a much higher toxicity effect compared to the re-dispersed pellet dispersions, which may indicate that most surfactant and preservative remained in the sample supernatant. Overall, the obtained acute toxicity results from most particle types indicated that a better toxicity reduction performance was achieved by the dialysis than the centrifugal washing method.

3.3 The Effect of Particle Ageing on The Toxicity of NH_2-NPPs

It is well-known that the reactive surfaces of nanomaterials makes them highly dynamic and prone to change and evolution even during storage, especially in dispersions (Ellis *et al.,* 2020). To evaluate the ageing impact of NH_2-PS (50 nm and 2 µm) in HH combo medium on stability of particles and their toxicity towards *D. magna*, stock solutions of both particle sizes were incubated in the culture medium and stored in the fridge for around two years before being analysed for acute toxicity and DLS measurements. The hydrodynamic size of 2µm NH_2-PS decreased from 1599 **±** 306.5 nm to 1285 **±** 187.6 nm after the ageing process, while some agglomeration behaviour was observed in the 50 nm aged sample, with the hydrodynamic size increasing from 31 **±** 0.71 nm to 46.18 **±** 2.42 nm over two years of incubation in the culture medium (Tables 3.6 and 3.7). Although, our ageing test in the HH combo medium showed some difference in the physical properties between the tested particles before and after ageing as measured by DLS, the magnitude of change may be

much larger under other experimental conditions (e.g., light exposure), impacting the fate and toxicity of NPPs. For example, the ageing of NPPs by O_3 or UV exposure drastically increased the mobility of nano-sized PS particles in saturated loamy sand, mainly resulting from the surface oxidation of the NPPs which increased the hydrophilicity and negative surface charge of the materials, thus increasing their repulsion from naturally occurring clay particles and enhancing their transport through the soil column (Liu *et al.*, 2019; Zhang *et al.*, 2022).

Table 3.6. DLS characterization of the pristine 2 µm NH_2-PS and following ageing in HH Combo medium for 2 years.

Aged and Pristine 2 µm NH_2-PS						
	Z-average (nm)	**SD ±**	**PDI**	**SD ±**	**ZP (mV)**	**SD ±**
Pristine	1599	306.5	0.542	0.469	-20.9	0.755
Aged	1285	187.6	0.505	0.43	-3.55	0.0557

Table 3.7. DLS characterization of the pristine 50 nm NH_2-PS and following ageing in HH Combo medium for 2 years.

Aged and Pristine 50 nm NH_2-PS						
	Z-average (nm)	**SD ±**	**PDI**	**SD ±**	**ZP (mV)**	**SD ±**
Pristine	31	0.7108	0.184	0.019	25.5	2.72
Aged	46.18	2.428	0.306	0.007	23.8	1.04

Ageing can alter the toxicity of NPPs depending on the incubation conditions. It has been reported that the toxicity of NPPs aged by incubating the particles with polymeric substances secreted by freshwater algae into freshwater medium significantly decreased the acute toxicity of NPPs towards microalga *Scenedesmus obliquus,* by coating the particles and reducing their reactivity (Giri and Mukherjee, 2021). In our toxicity results (Figure 3.5) the acute toxicity of both sizes was decreased by ageing the particles in HH combo medium with the EC_{50} value increasing from 5.37 mg/L to 9.2 mg/L for the 2µm NH_2-PS NPs and from 3.2 mg/L to 4.2 mg/L for the 50 nm NH_2-PS NPs. The decrease in the toxicity was higher for the larger (2 µm) than for the smaller size (50 nm) aminated PS particles.

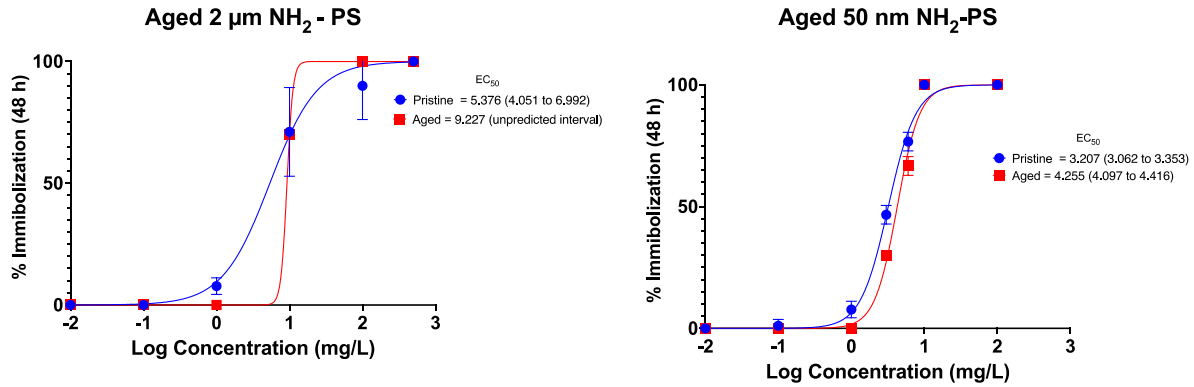

Figure 3.5. Acute toxicity of aged 2 µm and 50 nm PS-NH_2 NPs as dispersed (pristine) and after 2 years of ageing in HH Combo medium.

3.4 Assessment of Protein Secretion by Daphnids and Impact of Secreted Proteins on MP and NNP Stability & Toxicity of The Particles

3.4.1 Protein Secretion

Some of the key studies that documented the interaction of NMs with biomolecules naturally present in the environment or secreted by living organisms, and the consequent eco-corona formation on NMs surfaces, were discussed in Chapter 1 of this thesis, and it has been well documented that proteins present in the surroundings can significantly affect the properties and toxicity of NMs by forming an eco-corona layer. Due to the filter-feeding characteristic of the environmental indicator species *D. magna*, they could be especially susceptible to NMs as discussed in chapter one of this thesis. As the water passes through the daphnid guts, it collects secretions, including enzymes, gut microbial secretions and proteins secreted as part of the normal growth and functioning, as explored in detail in (Nasser *et al.,* 2019). The impact of corona formation on the characteristics and toxicity of NMs is an important factor that needs special attention in ecotoxicological studies. A study by (Nasser and Lynch, 2016) investigated the interaction of NPPs with biomolecules secreted by *D. magna* and the impact of this on the NPP uptake and toxicity towards the model organism. Their results demonstrated for the first time that proteins secreted by *D.*

magna to condition HH combo medium over 6 h formed an eco-corona layer around NPPs and increased their uptake and toxicity towards daphnia neonates (Nasser and Lynch, 2016). Studies in this section of the thesis focus on quantifying the concentrations of proteins that can be secreted by *D. magna* and the impact of this on the properties and toxicity of COOH and NH_2 PS MPs/NPPs by modifying the method (applying more scenarios) described by Nasser and Lynch (2016) to condition HH combo medium with biomolecules secreted by the model organism. The original paper indicated that the concentration of proteins secreted by 10 *D. magna* neonates to condition 5 mL HH combo medium over 6 h was 435 µg/mL, quantified via a Pierce BCA assay protein kit (Nasser and Lynch, 2016). The conditioning tests were conducted on neonates that had not been fed to ensure that the acquired proteins were only released by *D. magna* rather than also containing algal derived biomolecules.

An initial experiment was performed to condition 5 mL of HH combo medium with 5, 10, 15, 20 and 25 *D. magna* neonates (1 – 2 days old) for 6 h in order to assess if the concentration of proteins secreted scaled with the number of neonates present, which we would expect. In order to identify if feeding can affect the protein secretion rate, the tests were conducted on two groups, one that had been fed before the test and the other group were not fed. The concentration of proteins in our experiments, as quantified by the Pierce Rapid Gold BCA kit was much lower than the 435 µg/mL reported by (Nasser and Lynch, 2016), and no proteins were identified in many samples. The tests were repeated using the same assay kit that the author used (Pierce BCA) to determine any significant changes in the observations between the two assay kits, and the concentration of proteins was still low in all tested solutions. However, there were some proteins identified in some samples, as shown in Table 3.8 but in

low concentrations. Many samples had minus values after subtracting the blank from the unknown tested samples and calculating the concentrations using calibration curves.

Table 3.8. Protein concentrations secreted by D. magna neonates into 5 mL HH combo in µg/mL.

Number of neonates	**5**		**10**		**15**		**20**		**25**	
	Proteins	**Pierce BCA**								
	µg/ml	**SD±**	**µg/ml**	**SD±**	**µg/ml**	**SD±**	**µg/ml**	**SD±**	**µg/ml**	**SD±**
Non-fed	**-1.05**	4.286	**-2.5**	1.828	**2.63**	4.578	**-0.83**	1.258	**28.8**	50.05
Fed	**-1.58**	2.382	**-1.58**	1.722	**-2.4**	1.468	**0.88**	0.7920	**1.13**	1.958
		Pierce Rapid gold BCA								
Non-fed	**-73.28**	3.447	**-21.42**	2.517	**-7**	6.313	**-7.69**	1.500	**-8.07**	4.429
Fed	**-1.30**	8.457	**9.11**	5.324	**0.47**	4.253	**11.78**	4.752	**-631.59**	2.098

Due to the low observed protein concentrations, more tests were conducted to determine if more proteins could be achieved by conditioning the culture medium for a longer time, up to 72 h, but again very low or no proteins were detected by the BCA assay in all samples. In another test where larger animals were tested for secretion, between 50 to 70 *D. magna* juveniles (5 days old) were incubated in 5 mL HH combo medium for 48 h (Figure 3.6), no proteins were found using the Pierce Rapid Gold assay, and the calculated protein concentration was - 0.25 µg/mL. We were not able to pinpoint an exact reason for this difference given that the same strain of Bham daphnids were used in both studies, but we note that the period during which the current data was generated was one during which there were continual problems in the Daphnia culture facility, including bacterial & fungal infections in the algal cultures, problems with the air filters in the lab and more.

Figure 3.6. Photo showing the conditioning of medium by daphnids filtering – D. magna incubated in 5 mL HH combo medium.

Our findings are relatively consistent with the results of a recent study that tested the medium conditioning protocol by incubating 500 *D. magna* neonates (< 24 h) in 1.0 L of reconstituted water for 72 h, which was able to achieve 0.02 µg/mL of proteins using the Bradford assay (Martinez *et al.*, 2020). Furthermore, a different assay kit (Bradford QuantiPro BCA) was used to measure the concentration of proteins secreted by 5 or 10 *D. magna* juveniles (5 days old) in 5 mL HH combo medium for 6 h, 24 h and 48 h. The experiment was conducted on a group of animals that had not been fed (24 h before the test) and a group that had been fed in the 24 hours before the test. The highest observed protein concentration was 10.2 and 6.1 µg/mL in the non-fed and fed groups, respectively (Figure 3.7). The lower protein amount determined in the fed group could be the result of reduced filtering activity as a result of being full, and thus a reduced secretion activity.

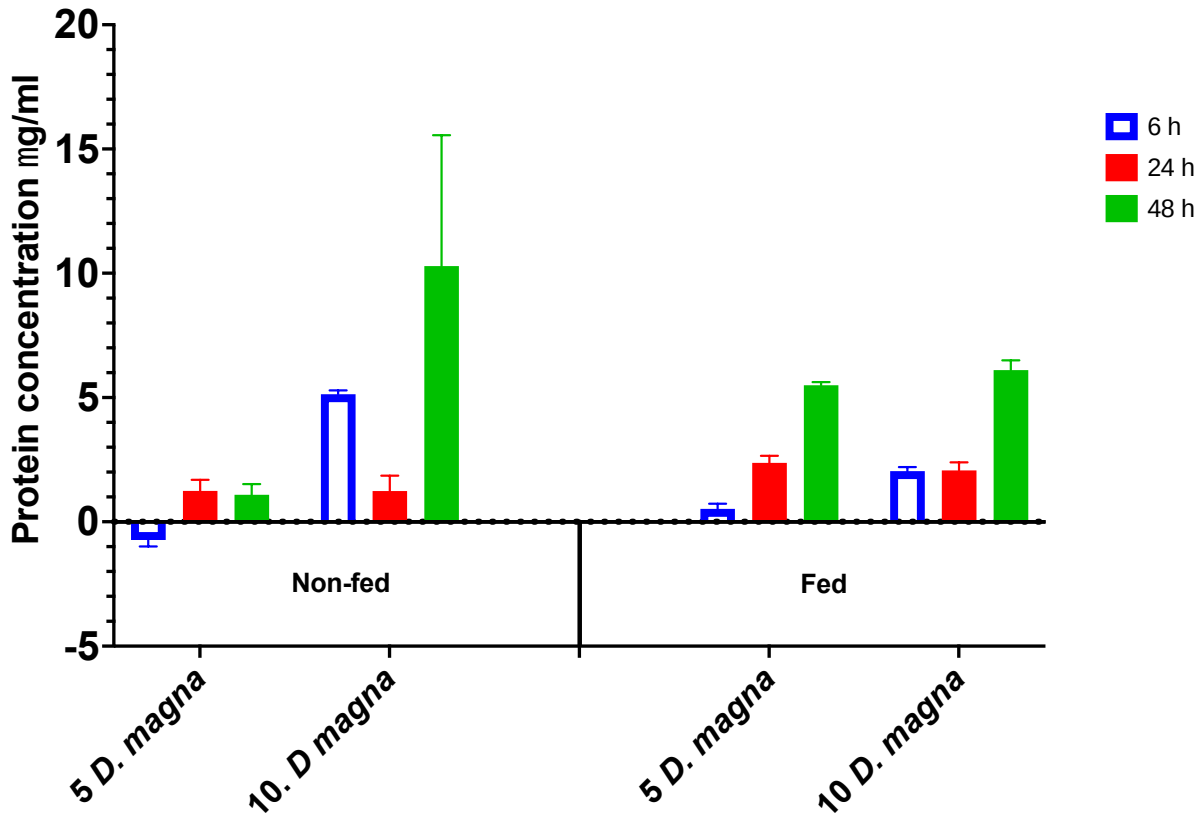

Figure 3.7. Protein concentrations secreted by D. magna juveniles into 5 mL HH combo in µg/mL – secreted protein amounts increased with increasing conditioning time, and were higher in the unfed organisms than in the fed groups, likely as a result of reduced filtering activity when the daphnids were fed.

The same assay kit (QuantiPro BCA) was used to quantify the protein secretion activity of 10 *D. magna* neonates exposed to a range of a chemical stressor (Cd) concentrations (0.1 - 4 mg/L) in 5 mL HH combo medium for 48 h. It has previously been shown that under stress, such as following exposure to TiO_2 or Ag NMs, daphnids secrete a lot of proteins into the medium, which are then bound into the eco-corona on the NMs surface – either as the NMs pass through the daphnia gut or following release of the proteins from the gut back into the medium (Ellis et al., 2020). The highest measured secreted protein concentration was 2.5 µg/mL observed for the animals exposed to 2.1 mg/L of the heavy metal, as shown in Figure 3.8, with a slight decrease at higher Cd concentrations (up to 4 mg/L). The highest Cd concentration tested resulted in the mortality of animals at the beginning of the tests, which could be the reason for the lower secretion at higher Cd concentrations, as the dead animals were no longer filtering.

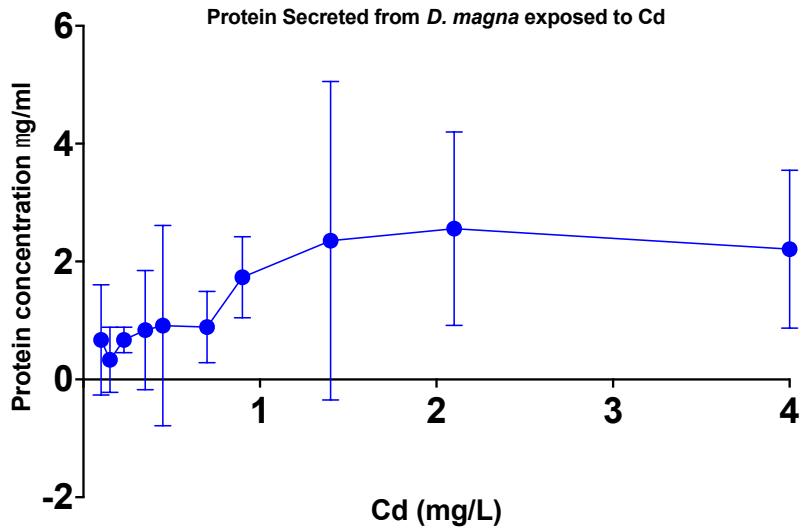

Figure 3.8. Concentrations of proteins secreted by D. magna exposed to Cd in 5 mL HH combo medium (µg/mL) over 48 h.

3.4.2 The Effect of Conditioned HH Combo Medium on The Stability and Toxicity of MPs/NPPs

Although the medium conditioning results (Figure 3.7) showed low concentrations of proteins were secreted by *D. magna* into the medium, the effect of these low protein contents on different types of NMs, which have different binding affinity/physicochemical properties, was evaluated. Therefore, the interaction of the proteins present in the conditioned medium with NMs was evaluated for all NMs types studied in this chapter. In all subsequent experiments in this chapter involving a conditioned medium test, a medium that had been conditioned with 2 *D. magna* neonates per mL for 48 h was used.

To assess the effect of the conditioned medium on the properties of the selected particles in this case the ones that had been dialyzed as described above to remove dispersants and preservatives, all particles were incubated in the conditioned HH Combo medium (or equivalent unconditioned medium for comparison) for 3 h before any characterization, and then the hydrodynamic size and ZP were measured by DLS in fresh and conditioned HH combo medium, and also compared with the previous measurements of pristine PS in DI water (Tables 3.9 – 3.12).

Table 3.9. DLS Characterization of the hydrodynamic size, polydispersity index (PDI) and Zeta potential (ZP) of 2 µm NH_2-PS dispersed in HH Combo medium, HH Combo medium conditioned by 2 daphnids/mL for 48 hours, and comparison to the same particles dispersed in DI water.

2 µm NH_2-PS						
Medium	**Z-average (nm)**	**SD ±**	**PDI**	**SD ±**	**ZP (mV)**	**SD ±**
Fresh HH Combo	1250	214.3	0.541	0.422	-16.6	0.85
Conditioned HH Combo	1120	116.1	0.489	0.436	-10.5	0.666
DI water	1261	236.3	0.251	0.098	-7.81	0.265

Table 3.10. DLS Characterization of size, PDI and ZP of 50 nm NH_2-PS dispersed in HH Combo medium, HH Combo medium conditioned by 2 daphnids/mL for 48 hours, and comparison to the same particles dispersed in DI water.

50 nm NH_2-PS						
Medium	**Z-average (nm)**	**SD ±**	**PDI**	**SD ±**	**ZP (mV)**	**SD ±**
Fresh HH Combo	31.13	0.8041	0.194	0.019	13.2	0.0577
Conditioned HH Combo	131.9	1.893	0.484	0.028	17.9	0.0577
DI water	29.57	1.119	0.129	0.015	29.8	0.862

Table 3.11. DLS Characterization of size, PDI and ZP of 50 nm COOH-PS dispersed in HH Combo medium, HH Combo medium conditioned by 2 daphnids/mL for 48 hours, and comparison to the same particles dispersed in DI water.

50 nm COOH-PS						
Medium	**Z-average (nm)**	**SD ±**	**PDI**	**SD ±**	**ZP (mV)**	**SD ±**
Fresh HH Combo	34.45	0.3955	0.095	0.009	-22.2	0.252
Conditioned HH Combo	34.11	0.7007	0.107	0.012	-20.8	0.473
DI water	28.83	0.3371	0.051	0.015	-54.8	1.11

Table 3.12. DLS Characterization of size, PDI and ZP of 100 nm COOH-PS dispersed in HH Combo medium, HH Combo medium conditioned by 2 daphnids/mL for 48 hours, and comparison to the same particles dispersed in DI water.

100 nm COOH-PS						
Medium	**Z-average (nm)**	**SD ±**	**PDI**	**SD ±**	**ZP (mV)**	**SD ±**
Fresh HH Combo	54.57	1.485	0.036	0.023	-23.6	0.529
Conditioned HH Combo	59.3	0.9134	0.125	0.012	-22.6	0.451
DI water	56.53	56.53	0.014	0.007	-46.3	1.42

After incubating the particles in the conditioned medium for 3 h, the hydrodynamic size of the positively charged 50 nm NH_2-PS increased from 31.13 to 131.9 nm, and the ZP from 13.2 to 17.9 mV. The size increase could be due to slight agglomeration of the particles or to

the formation of an eco-corona layer. There was also some change observed in the size and surface charge of the 2 negatively charged PS particles, but the degree of change was lower than for the positively charged particles (Tables 3.9 – 3.12).

The acute toxicity of all particles after 3 h of incubation in the conditioned HH combo medium was assessed using the OECD 202 daphnia immobilization assay, which measures the effective concentration at which 50% of the organisms are immobilized (unmoving) after 48 h, and compared to particles incubated for 3h in the fresh HH combo medium. Acute toxicity results are presented for the four tested particles in the two medium conditions (fresh versus conditioned) (Figures 3.9 and 3.10).

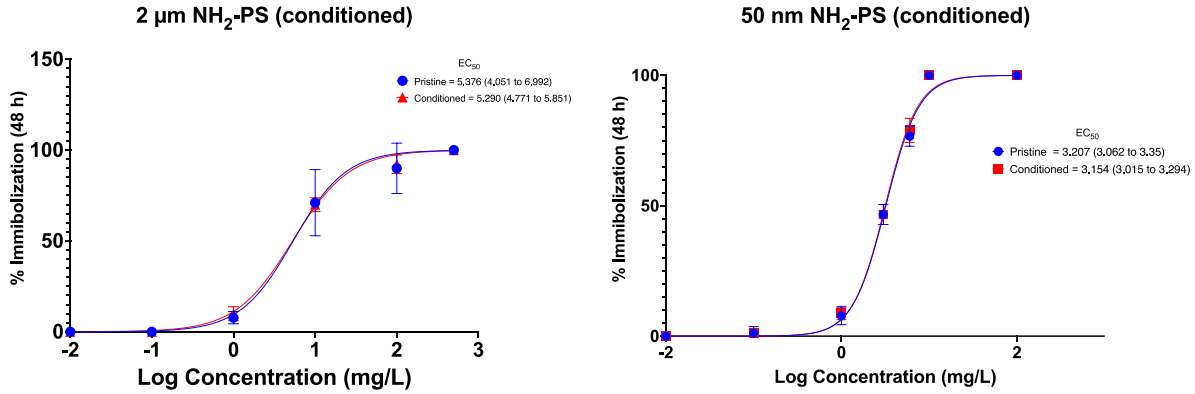

Figure 3.9. Acute toxicity assessment using the OECD 202 immobilisation assay of NH_2-PS particles dispersed in fresh or conditioned HH combo determined after 48 hours of exposure based on the numbers of organisms swimming after 15 seconds of gentle agitation.

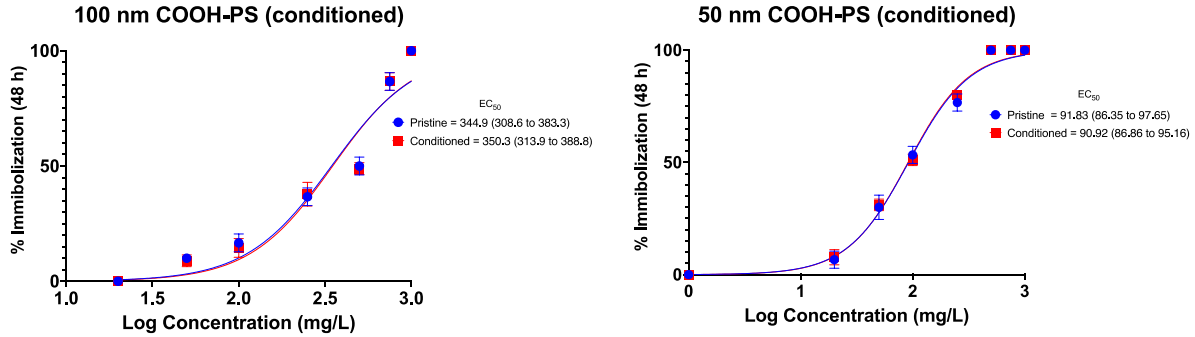

Figure 3.10. Acute toxicity assessment using the OECD 202 immobilisation assay of COOH-PS particles dispersed in fresh or conditioned HH combo determined after 48 hours of exposure based on the numbers of organisms swimming after 15 seconds of gentle agitation.

No significant change was observed in the 48 h acute toxicity results as a result of medium conditioning. However, the EC_{50} of the 100 nm COOH-PS slightly increased, indicating a decrease in toxicity, while the toxicity slightly increased for the other three PS types (Figures 3.9 and 3.10). Higher amounts of proteins or incubating the particles in the conditioned medium for longer times may have a larger impact than that observed here. However, we note that the particles are generally low in toxicity and that the conditioning does not greatly affect their toxicity in this case.

3.4.2 Assessment of MPs/NPPs Accumulation by *Daphnia* and The Role of Corona Evolution During MP/NPPs Passage Through *D. magna* Gut

The impact of the eco-corona on NMs toxicity to daphnids has been reported in several papers, showing increased toxicity in some cases (e.g., Nasser and Lynch, 2015), decreased toxicity in others (e.g., Briffa et al., 2018) for example by slowing the dissolution rate of particles. A recent study assessed the protein coronas formed around TiO_2 and Ag NMs during chronic exposure to daphnids, taking water samples after 7 days of NM incubation with the daphnids, and thus analysing NMs that had either not been taken up at all or had been excreted by the *Daphnia* back into the medium (Ellis et al., 2020). Thus, the coronas analysed were a combination of secreted coronas and coronas acquired during passage through the *Daphnia* guts. This work was inspired by a previous study to further explore the role of the secreted corona, and gut-acquired corona on NMs uptake by and toxicity towards *D. magna*, a two-step exposure experiment was designed to explore the impact of corona-aged NMs on *D. magna* (Ellis and Lynch, 2020).

The protocol detailing the steps of this experiment is described in Chapter 2of this thesis, and the illustration of the experiment design is demonstrated again here for the reader to easily follow up (Figure 3.11).

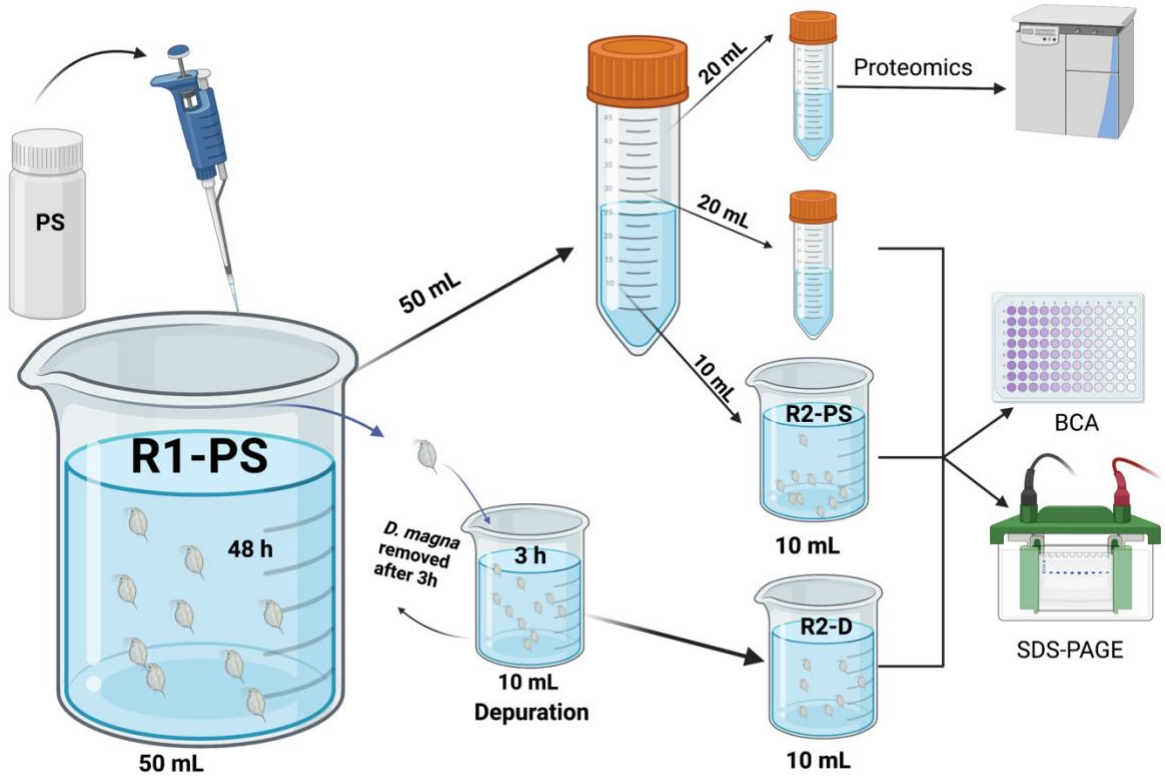

Figure 3.11. Illustrations of the experimental steps of the PS eco-corona formation after passage through D. magna gut.

Briefly, two rounds of exposures were introduced to 3 replicates of 10 *D. magna* neonates exposed to concentrations that had a low or no immobilization effect on animals (100 mg/L dialyzed 2µm PS-NH_2, which had 0% neonates immobilisation) and (10 mg/L of dialyzed 50 nm PS-NH_2 which had around 20% neonates immobilisation) determined from the experiments (Figure 3.3), each exposed to one of the two aminated PS fluorescent particles. In the first exposure round, animals were exposed to the selected particles (R1-PS) for 48 h. The animals were washed and transferred to a fresh medium to depurate the particles. In the second round, a new group of neonates were exposed to the previously exposed NMs

dispersions, which contained a mixture of particles that had not been taken up by the previously exposed daphnids but that had been conditioned by the presence of daphnids, and particles that had been taken up, passed through the gut and released by animals (R2-PS). The second round of exposure also involved exposing a group of fresh neonates to the depuration solution, which only contained particles that were recovered from *D. magna* guts (R2-D). Assuming that an eco-corona has formed around the particles during the tests, all exposure solutions were collected and passed through the hard corona isolation steps (Section 2.4.1.8), then tested for total proteins and SDS-PAGE analyses. In parallel, the fluorescent intensity of all solutions and animal tissue was measured by the Tecan plate reader, as a measure of the particle concentration.

Although our previous observations showed low *D. magna* protein secretion even after being exposed to a chemical stressor (Cd), the different experimental conditions may lead to changes in observations, and we conducted this study to gain insights into the interaction of the secreted protein with NMs and the effect of this on the model organism.

Results showed that the protein concentrations secreted by *D. magna* measured after going through the hard-corona isolation steps in some tested solutions, were higher than our previous secretion observations, even in the control group, which contained one animal per mL medium. This could be due to the proteins being concentrated at the bottom of solutions while being centrifuged. Our results are comparable with previous findings, which followed the same corona isolation protocol (Ellis and Lynch, 2020). Their results showed that the protein concentrations secreted by *D. magna* exposed to different types of TiO_2 and Ag NMs in 250 mL for 7 days were between (37 and 75 µg/mL) measured by BCA after the protein isolation steps (Ellis and Lynch, 2020). In this experiment, our incubation time was 48 h compared to the 7 days in the mentioned study, and the volume of our exposure solution

(50 mL and 10 mL) is lower than the 250 mL solution applied in the previously referenced study, indicating that more proteins may be observed for longer incubation times.

Table 3. 13. Protein concentration acquired in the adsorbed coronas of PS-NH_2 particles during first exposure to D. magna neonates (R1-PS), during second exposure to a new set of D. magna neonates (R2-PS), following depuration after R1-PS into clean medium (R2-D). Two controls solutions were analysed, control-1 (10 neonates/no NMs) that were treated the same way to concentrate the secreted proteins for determination of secreted amounts. Control-2 (fresh HH combo/no animals).

Protein Concentration Secreted by *D. magna* neonates (µg/mL)										
Exposure Solution	**R1-PS (50 mL)**	**SD±**	**R2-PS (10 mL)**	**SD±**	**Depurated (R2-D) (10 mL)**	**SD±**	**Control1 (non-exposed daphnids)**	**SD±**	**Control2 (fresh HH, no daphnids))**	**SD±**
50 nm PS-NH_2	**-27.67**	15.05	**8.467**	12.36	**-29.60**	29.01	**25.23**	10.36	**-7.667**	4.636
2 µm PS-NH_2	**-6.167**	6.696	**27.30**	38.14	**-16.70**	4.356				

Proteins were detected in the 10 mL (R2-PS) solutions while no proteins were detected in the 50 mL (R1-PS) solutions. Daphnids exposed to the 2 µm NH_2-PS secreted more proteins than those exposed to the 50 nm NH_2 in the R2-PS solutions, although the 50 nm PS-NH_2 was more toxic according to the acute toxicity results. This could be explained by the difference in particle mass concentrations, as a higher number of particles was present in the 2 µm PS-NH_2 solutions (100 mg/L) than the more toxic 50 nm PS-NH_2 (10 mg/L), potentially leading to more uptake and accumulation. The higher protein concentration in the R2-PS solutions than in the R1-PS solutions is consistent with a second round of daphnids secreting into the medium and conditioning it. However, it should be considered that the volume of solutions in the R2-PS groups was 10 mL compared to the 50 mL in the R1-PS solutions leading to more concentrated proteins per sample volume. No proteins were detected in the depuration dispersions exposed to new neonates (R2-D). Since the proteins detected previously were mainly associated with particle coronas, the number of particles, in this case, is also lower. The protein concentration secreted in the 2 µm NH_2 solutions was higher than those secreted by the control *D. magna* group, which was expected due to the

presence of particles which could cause the animals to secret proteins under stressful conditions, and the reactive surface of the particles, which has also been shown to “pull” proteins from cell membranes. It has been shown that under serum-free conditions NMs acquire a corona by damaging membranes and pulling out cytosolic proteins into their corona (Lesniak *et al.*, 2012). However, the same effect was not observed in the 50 nm PS-NH_2 group, with fewer detected proteins in the particle’s solution than in the controls (Table 3.13). This may be related to the fact that the smaller particles pass through the *Daphnia* gut more easily than the larger ones and thus are less “sensed” by the daphnids, whose normal food size is more on the order of 1 micron, such as algal particles.

It may be complex to judge and interpret the protein secretion results between all groups in this test due to the volume and concentration differences, but it was confirmed that proteins exist in tested solutions, which may have formed a corona layer around the NMs and caused the animals to release protein types due to the particle exposures that are different from those released by the control groups. Further tests were applied to confirm the presence of proteins on the NMs surface using SDS-PAGE analyses. The results showed that bands have formed in many solutions containing particles, which indicates the presence of proteins on the surface of PS NPPs and MPs (Figure 3.12). Bands were also observed in the control groups, which contain proteins that animals have secreted as part of their normal filtering activities, without interaction with the studied materials.

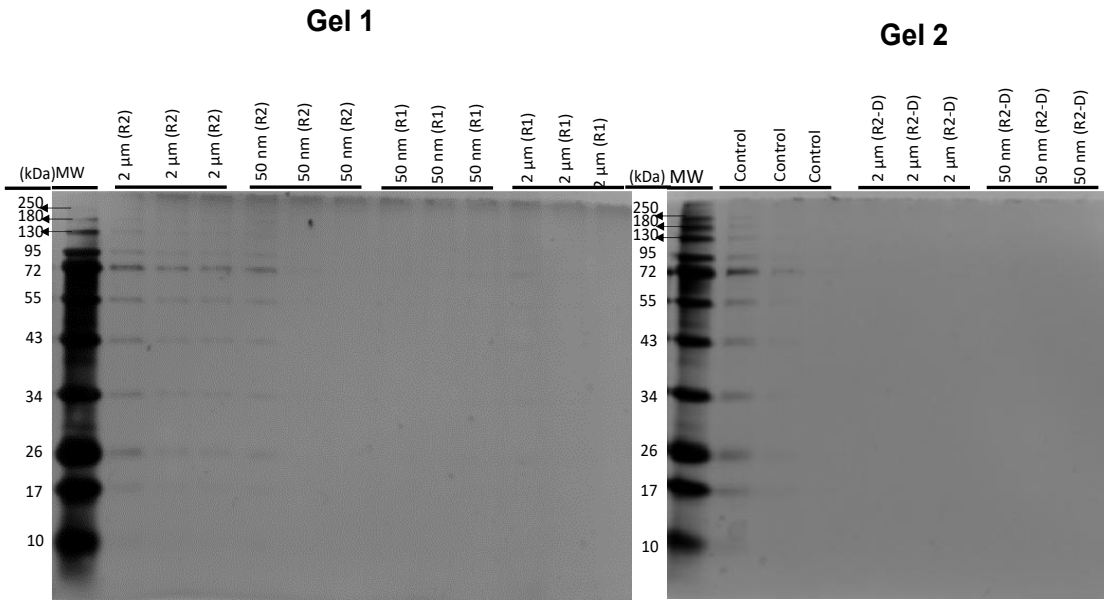

Figure 3.12. SDS-PAGE assay with Coomassie blue staining of the gels. We note that the intensity of the protein ladder was high, and thus if repeating would use lower concentrations here. We can clearly see that the R2 exposures had higher protein amounts associated, as expected, compared to the R1 exposures and the depurated samples, where the NM concentrations were low and, thus, the associated corona protein concentrations were not detected. A good amount of proteins are associated with the controls of conditioning HH combo in the absence of particles.

More bands were observed in the second-round solutions (R2-PS) than in the R1-PS. No visible bands were observed in the solutions used to depurate particles for 3 h. The strongest formed band was at a molecular size of around 72 kDa in all solutions where bands were observed, including the controls. Most observed bands were in the region of 20-130 kDa. The observations showed that the proteins present in the particle/exposure solutions have the same molecular weight as those observed in the control group since all the bands were parallel to each other (Figure 3.12). This indicates that the presence of the studied particles did not cause *D. magna* to secrete protein types that are different from those secreted by the control group in this particular experiment, which is consistent with the low toxicity of the particles generally, and the low concentration of the particles used. Due to the lab closures during the pandemic, it was not possible to explore this further, or to repeat the gels, as there is a slight concern that the similarity of bands across the samples

may be related to some carry over from the intense bands in the protein ladder, which are also at very similar positions.

3.4.2.1 Accumulation of MPs/NNPs in *D. magna*

The fluorescence intensity within *D. magna* whole body was assessed to identify the amount of particles that had accumulated or depurated from the animal's body during the exposures. In order to assess the reliability of this method to quantify the fluorescence of the particles in the animals' transparent tissue, the measurements were repeated four times without moving the 96-well plate from the instrument (Figure 3.13). The water samples remained relatively consistent during the repeated measurements, suggesting that we might be able to use this as a mean to estimate the concentration of particles in solution, but of course the impact of corona formation on binding would need to be assessed also. However, the samples that contained *D. magna* tissue showed a significant change in the fluorescence intensity between measurements, although they were repeated within approximately one minute of each other. This might be related to the fact that the pH of the *Daphnia* gut various considerably along its length, which can influence the fluorescence signal. Additionally, in some tests, even the control Daphnids were more (auto)fluorescent than those exposed to fluorescent materials or the fluorescent particles themselves. We found that this method is totally unreliable in assessing the uptake of particles within the tested animal tissue. Therefore, it would be inappropriate to interpret those results as they could be very far from the actual uptake based on our observations.

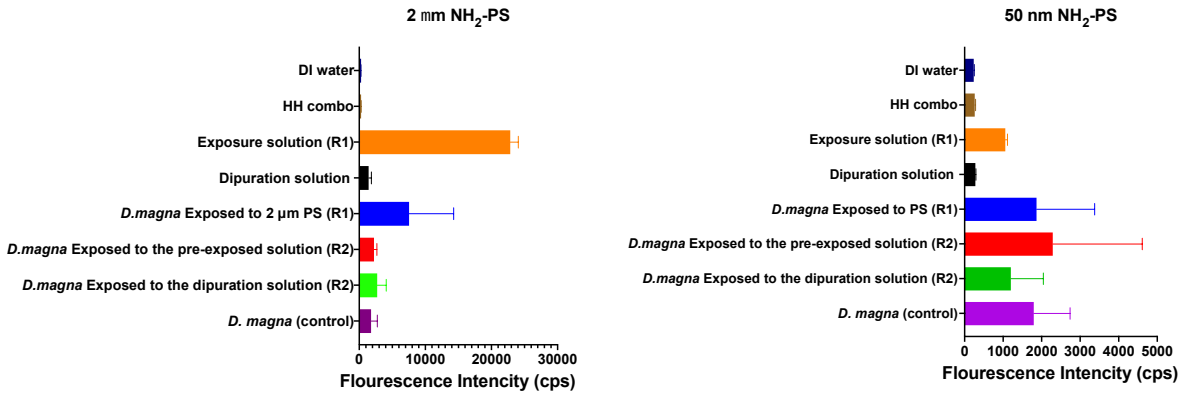

Figure 3.13. Fluorescent intensity of samples (solutions and daphnid tissues) measured from exposure, re-exposure and depuration studies described above. The measurements are based on 4 scans made at 1 minute intervals, and the SD is very large, especially in the daphnia tissues, making this method for semi-quantification of particle uptake of limited value.

3.4.3 Protein Extraction from *D. magna* Tissue Homogenate

One of the main objectives of this thesis in its original form (i.e., pre-pandemic and the resulting lab closures and required adjustments to the experimental plans as a result – see also Covid disruption statement) was to assess the digestive enzyme activities of *D. magna* after being exposed to NMs to explore the impact of NM accumulation in the gut on overall gut health and gut function. This required the homogenization of specific tissue (e.g., *Daphnia* gut) or whole animal tissue in a chosen buffer. Since enzymes are part of the total proteins present in animal tissue, it is important to determine the total protein concentration of the tissue when purifying an enzyme of interest, as the purity of an enzyme depends on removing unwanted proteins in order to assess the relationship between the total protein and the enzyme activity (Scopes, 2002). In this section, the quantity of proteins that can be acquired by homogenizing whole *D. magna* tissue was assessed. It is also useful to compare the concentration of total tissue proteins with the secreted proteins previously observed. All subsequent protein concentration analyses in this chapter were analysed by the Pierce Rapid Gold kit.

Groups containing 5, 10, 15, 20 and 25 *D. magna* juveniles (5 days old) were homogenised in 0.5 mL Tris buffer in parallel to groups containing 100, 200, 300, 400, and 500 *D. magna*

neonates (< 48 hours) whole tissue homogenate in 0.5 mL of the same buffer. The total protein concentration of all samples is presented in (Figure 3.14).

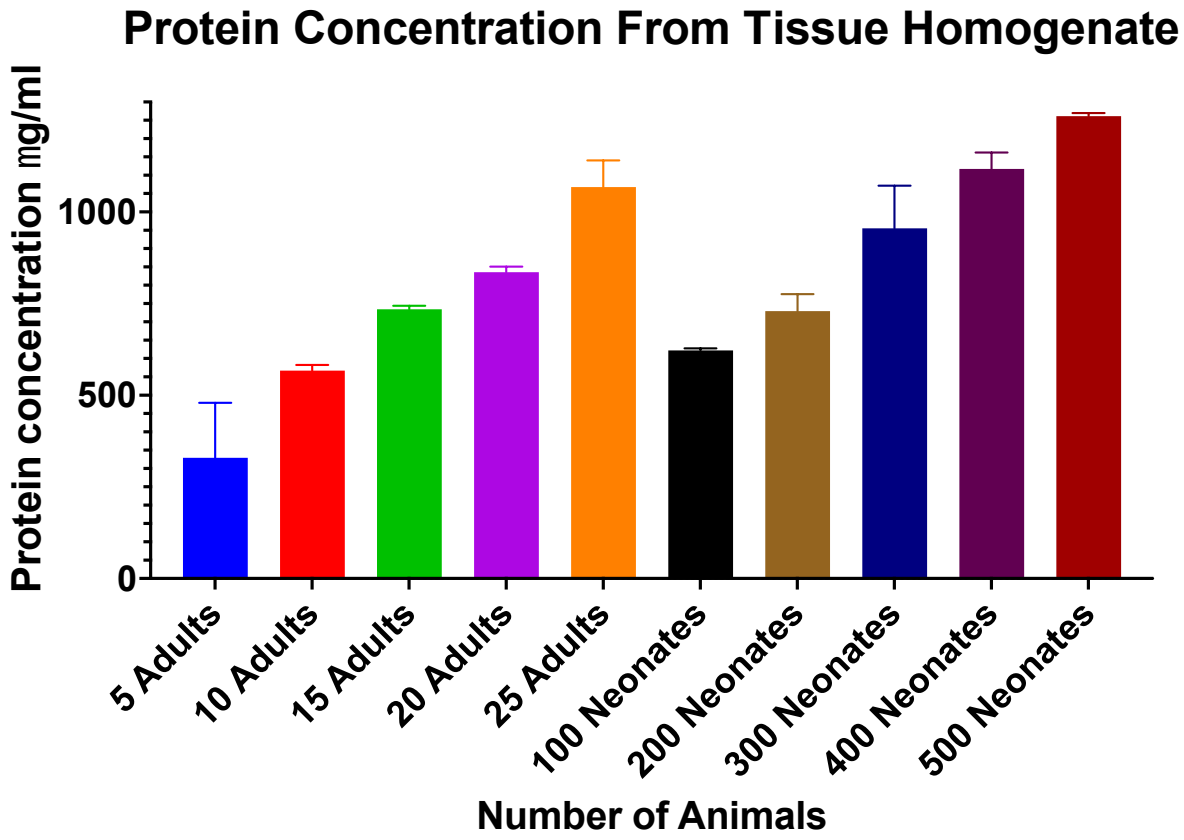

Figure 3.14. Protein Concentration determined using the BCA assay as extracted from homogenised D. magna tissue from juvenile (5 days old) and neonate (<48 hours old) daphnids, in µg/mL. Extracts are based on 3 replicates and presented as mean ± SD.

As expected, the concentration of proteins increased with increasing the number of organisms included in the tissue homogenates. The highest concentration observed in the juvenile tested group was 1068 µg/mL for 25 animals, equating to about 42.7 µg/mL per daphnid, and 1261 µg/mL from 500 animals in the neonate group equating to 2.5 µg/mL per animal.

Interference of experimental reagents with proteins, particularly enzymes, can be problematic in enzymatic assays, especially by strong buffers (Scopes, 2002). Therefore, if more than one buffer type is available, it is better to choose a buffer that can achieve more

proteins in the analyses if possible. In this regard, a comparison of the protein quantity extracted from tissue homogenate of 50 *D. magna* neonates in PBS and Tris buffers was performed. The total measured proteins were 196.3 µg/mL in Tris and 239.3 µg/mL in PBS, indicating a slight detection increase in the PBS compared to the Tris buffer (Figure 3.15). The PBS buffer also had a lower standard deviation between replicates (Figure 3.15).

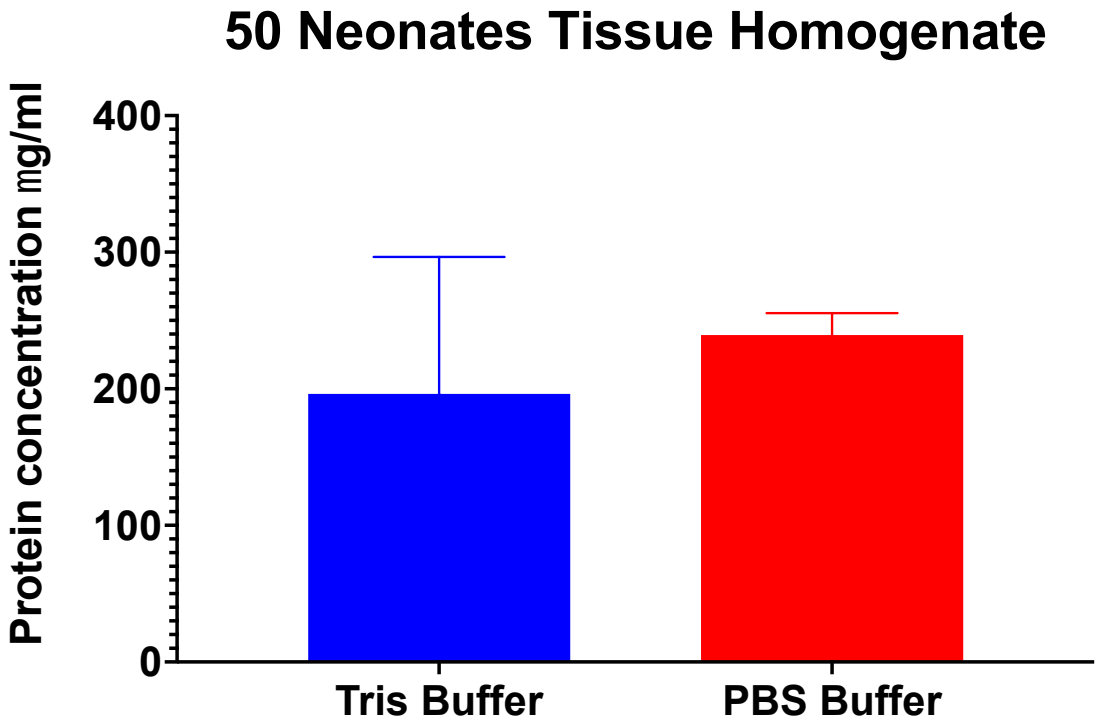

Figure 3.15. Comparison of the protein concentration extracted from homogenised tissue of 50 D. magna neonates into PBS and Tris buffer (µg/mL). Extracts are based on 3 replicates and presented as mean ± SD.

When comparing the tissue homogenate results with the findings of the previously discussed medium conditioning study reporting 435 µg/mL proteins secreted by *D. magna* neonates in a 5 mL culture medium, the equivalent of around 10 *D. magna* adults whole tissue homogenate (567 µg/mL) or 100 neonates (622 µg/mL), concentrated in 0.5 mL

buffer are needed to achieve a close concentration of proteins to the reported value. However, although our observations were significantly different from the reported results, laboratory conditions and experimental designs can lead to variations in results between researchers, and the medium conditioning method has not been explored enough in the literature, thus, more studies are needed to evaluate this method. We believe our findings provide more knowledge and proved that different experimental conditions, including the presence of NMs could lead to more secreted protein being detected by the BCA assay than the previous results, as previously demonstrated in this chapter. After studying the extraction of proteins from *D. magna* whole tissue, we attempted to assess the digestive enzyme activity of animals exposed to NMs by separating the animal's gut from the whole tissue but encountered some issues. Due to the complexity of enzymatic activity assays and our lack of experience in working with enzymes, we purchased three digestive enzyme activity kits (amylase, trypsin protease) from Sigma Aldrich. In the supplier website description, it was clearly stated that a single kit is enough for 100 tests (*Amylase Activity Assay Kit sufficient for 100 colorimetric tests | Sigma-Aldrich*, no date). However, this description was inaccurate, and when the kits arrived, they were enough for only two tests, and each test could take 80 samples in a 96-well plate. This was not enough for the planned number of experiments. Another issue encountered when reading the protocol provided with the kits is the amount of animal tissue required to perform the tests. For example, 100 mg of tissue is required to prepare an amylase activity sample which is equivalent to around 600 *D. magna* adults or 10,000 neonates, and that is impossible to achieve with our work. Therefore, we tried to perform a more traditional trypsin activity assay and purchased the required reagents, which took around 6 months to arrive. Once arrived, it took us another few months of trials before we were able to optimize an assay on a control group of

daphnids, which will need more optimization after daphnids are exposed to NMs. Enzymatic assays require consideration of several factors in order to optimize an assay, such as the concentration and type of enzyme, the concentration and type of substrate, the choice and composition of the buffer, and the technology of an assay (Onyeogaziri and Papaneophytou, 2019). It has been documented that the optimization of an enzyme in a traditional (one-factor-at-a-time) approach by experienced researchers can take 4 or more months to develop (Onyeogaziri and Papaneophytou, 2019). It was possible to receive training and carry on with the work, but with the covid-19 pandemic/laboratory-closure training was not completed, the large number of animals required to prepare samples, the time needed to culture and manually separate/homogenate tissues, and assay optimization, we decided not to proceed with this experiment considering the time we have left to finish the work of this thesis.

3.5 Conclusion

Most of the toxic effects of MPs/NPPs were derived from chemical additives, and dialysis was found to be a more reliable method to wash MPs than centrifugation. After washing the particles by dialysis, no immobilization was observed up to the highest tested concentration (500 mg/L) for the 2 µm NH_2-PS which had an EC_{50} of 5.376 mg/L before washing, and the EC_{50} value was increased from 3.207 to 17.12 mg/L (50 nm NH_2-PS), from 344.9 to 662.9 mg/L (100 nm COOH-PS) and from 91.83 to 760.1 mg/L (50 nm COOH-PS). The toxicity was also affected by the surface functionalization of particles, and it was confirmed that the positively charged materials (NH_2-PS) had a greater toxic impact on *D. magna* than the negatively charged particles (COOH-PS) even after washing the particles from chemical additives.

The size of PS particles had a great impact on the toxicity of particles, with the smaller sizes being more toxic than the larger PS particles at constant mass exposure. This may have resulted from the difference in the number of particles as well as the differences (after *D. magna* ingestion) in the particle's potential to infiltrate between their gut microvilli, as previous studies indicated that once particles are located in the gaps between the microvilli the peristaltic pressure causes them to stay there causing daphnids to feel full and filter less, interference with enzyme secretion, cell damage, which will subsequently lead to impaired swimming, impaired growth, increased predation and decreased reproduction.

Ageing of the pristine PS-NH_2 particles for two years, which have not been washed, in HH combo medium (protected from light and stored at 4 C°) caused changes in the physicochemical properties of particles and altered their toxicity towards *D. magna*. The HD was slightly decreased (from 1599 ± 306.5 to 1285 ± 187.6 nm) after the ageing of the 2 µm PS-NH_2, while the HD was increased (from 31 ± 0.71 to 46.18 ± 2.42 nm) after two years for the 50 nm PS-NH_2. The EC_{50} concentrations of the same particles were increased after ageing, from 5.37 to 9.2 mg/L (2µm PS-NH_2) and from 3.2 to 4.2 mg/L (50 nm PS-NH_2), indicating reduced toxicity after ageing in the culture medium. The protein concentration analyses indicated that *D. magna* secreted amount of proteins under the tested conditions compared to reports in the literature. Although we have not identified the reason for this, it could be related to infection/pollution in the *Daphnia* facility, which affected all lab users in terms of reproducing some results, as others also noted reductions in the number of offspring and other deviations from earlier periods – note that while beyond the scope of this thesis, these findings have resulted in our group implementing stricter quality control and monitoring of the health of our running cultures, and continuous monitoring of the numbers of offspring per adult daphnid, as well as routine testing of the amount of secreted proteins by 3rd broods as new running or test cultures are established, which is an excellent outcome from a particularly frustrating period of the PhD work. Despite the low amount of

detected proteins to condition the culture medium, it still affected the physicochemical properties of PS MPs/NNPs as well as a slight change in the acute toxicity of particles.

Passage of NH_2-PS through the animal's gut formed an eco-corona layer around their surfaces and the higher mass concentrated particles caused more secretion of proteins, which could subsequently lead to more uptake and bioaccumulation. We found the fluorescent intensity measurement protocol of PS MPs in live *D. magna* may lake reproducibility and needs further investigation.

The results of this chapter provided important information about the impact of many factors that can control the toxicity of PS MPs and showed that the standardized OECD 202 guidelines may significantly overestimate the toxic impact of NMs if realistic environmental conditions are not considered (e.g., ageing of particles, removing additives) and based on this work it is recommended that researchers and regulators should take more consideration of such factors.

References

A. Ellis, L.-J. and Lynch, I. (2020) 'Mechanistic insights into toxicity pathways induced by nanomaterials in Daphnia magna from analysis of the composition of the acquired protein corona', *Environmental Science: Nano*, 7(11), pp. 3343–3359. Available at: https://doi.org/10.1039/D0EN00625D.

A. Ellis, L.-J., Valsami-Jones, E. and Lynch, I. (2020) 'Exposure medium and particle ageing moderate the toxicological effects of nanomaterials to Daphnia magna over multiple generations: a case for standard test review?', *Environmental Science: Nano*, 7(4), pp. 1136–1149. Available at: https://doi.org/10.1039/D0EN00049C.

Amylase Activity Assay Kit sufficient for 100 colorimetric tests | Sigma-Aldrich (no date). Available at: http://www.sigmaaldrich.com/ (Accessed: 17 January 2023).

Banerjee, A. and Shelver, W.L. (2021) 'Micro- and nanoplastic induced cellular toxicity in mammals: A review', *Science of The Total Environment*, 755, p. 142518. Available at: https://doi.org/10.1016/j.scitotenv.2020.142518.

Barreto, A. *et al.* (2020) 'How Can Nanoplastics Affect the Survival, Reproduction, and Behaviour of the Soil Model Enchytraeus crypticus?', *Applied Sciences*, 10(21), p. 7674. Available at: https://doi.org/10.3390/app10217674.

Cruz de Carvalho, R. *et al.* (2022) 'Ecotoxicological Effects of the Anionic Surfactant Sodium Dodecyl Sulfate (SDS) in Two Marine Primary Producers: Phaeodactylum tricornutum and Ulva lactuca', *Toxics*, 10(12), p. 780. Available at: https://doi.org/10.3390/toxics10120780.

Giri, S. and Mukherjee, A. (2021) 'Ageing with algal EPS reduces the toxic effects of polystyrene nanoplastics in freshwater microalgae Scenedesmus obliquus', *Journal of Environmental Chemical Engineering*, 9(5), p. 105978. Available at: https://doi.org/10.1016/j.jece.2021.105978.

Guerranti, C. *et al.* (2021) *Action of Surfactants in Driving Ecotoxicity of Microplastic-Nano Metal Oxides Mixtures: A Case Study on Daphnia magna under Different Nutritional Conditions*, *Surfactants and Detergents - Updates and New Insights*. IntechOpen. Available at: https://doi.org/10.5772/intechopen.99487.

Huk, A. *et al.* (2014) 'Is the toxic potential of nanosilver dependent on its size?', *Particle and Fibre Toxicology*, 11(1), p. 65. Available at: https://doi.org/10.1186/s12989-014-0065-1.

Huk, A. *et al.* (2015) 'Impact of nanosilver on various DNA lesions and HPRT gene mutations – effects of charge and surface coating', *Particle and Fibre Toxicology*, 12, p. 25. Available at: https://doi.org/10.1186/s12989-015-0100-x.

Lesniak, A. *et al.* (2012) 'Effects of the Presence or Absence of a Protein Corona on Silica Nanoparticle Uptake and Impact on Cells', *ACS Nano*, 6(7), pp. 5845–5857. Available at: https://doi.org/10.1021/nn300223w.

Li, X. *et al.* (2023) 'From marine to freshwater environment: A review of the ecotoxicological effects of microplastics', *Ecotoxicology and Environmental Safety*, 251, p. 114564. Available at: https://doi.org/10.1016/j.ecoenv.2023.114564.

Liu, J. *et al.* (2019) 'Aging Significantly Affects Mobility and Contaminant-Mobilizing Ability of Nanoplastics in Saturated Loamy Sand', *Environmental Science & Technology*, 53(10), pp. 5805–5815. Available at: https://doi.org/10.1021/acs.est.9b00787.

Martinez, D.S.T. *et al.* (2020) 'Effect of the Albumin Corona on the Toxicity of Combined Graphene Oxide and Cadmium to Daphnia magna and Integration of the Datasets into the NanoCommons Knowledge Base', *Nanomaterials*, 10(10), p. 1936. Available at: https://doi.org/10.3390/nano10101936.

Martinez, D.S.T. *et al.* (2022) 'Daphnia magna and mixture toxicity with nanomaterials – Current status and perspectives in data-driven risk prediction', *Nano Today*, 43, p. 101430. Available at: https://doi.org/10.1016/j.nantod.2022.101430.

Miloloža, M. *et al.* (2021) 'Ecotoxicological Assessment of Microplastics in Freshwater Sources—A Review', *Water*, 13(1), p. 56. Available at: https://doi.org/10.3390/w13010056.

Nasser, F., Constantinou, J. and Lynch, I. (2019) 'Nanomaterials in the environment acquire an "eco-corona" impacting their toxicity to Daphnia magna —a call for updating toxicity testing policies', *Proteomics* [Preprint], (1800412). Available at: https://doi.org/10.1002/pmic.201800412.

Nasser, F. and Lynch, I. (2016) 'Secreted protein eco-corona mediates uptake and impacts of polystyrene nanoparticles on Daphnia magna', *Journal of Proteomics*, 137, pp. 45–51. Available at: https://doi.org/10.1016/j.jprot.2015.09.005.

Nasser, F. and Lynch, I. (2019) 'Updating traditional regulatory tests for use with novel materials: Nanomaterial toxicity testing with Daphnia magna', *Safety Science*, 118, pp. 497–504. Available at: https://doi.org/10.1016/j.ssci.2019.05.045.

Nienhaus, K. *et al.* (2022) 'Protein adsorption onto nanomaterials engineered for theranostic applications', *Nanotechnology*, 33(26), p. 262001. Available at: https://doi.org/10.1088/1361-6528/ac5e6c.

Oleszczuk, P., Jośko, I. and Skwarek, E. (2015) 'Surfactants decrease the toxicity of ZnO, TiO2 and Ni nanoparticles to Daphnia magna', *Ecotoxicology (London, England)*, 24(9), pp. 1923–1932. Available at: https://doi.org/10.1007/s10646-015-1529-2.

Onyeogaziri, F.C. and Papaneophytou, C. (2019) 'A General Guide for the Optimization of Enzyme Assay Conditions Using the Design of Experiments Approach', *SLAS Discovery*, 24(5), pp. 587–596. Available at: https://doi.org/10.1177/2472555219830084.

Pikuda, O. *et al.* (2019) 'Toxicity Assessments of Micro- and Nanoplastics Can Be Confounded by Preservatives in Commercial Formulations', *Environmental Science & Technology Letters*, 6(1), pp. 21–25. Available at: https://doi.org/10.1021/acs.estlett.8b00614.

Scopes, R.K. (2002) ‘Enzyme Activity and Assays’, in John Wiley & Sons, Ltd (ed.) *eLS*. 1st edn. Wiley. Available at: https://doi.org/10.1038/npg.els.0000712.

Sharifi, S. *et al.* (2012) ‘Toxicity of nanomaterials’, *Chemical Society reviews*, 41(6), pp. 2323–2343. Available at: https://doi.org/10.1039/c1cs15188f.

Zhang, Y. *et al.* (2022) ‘Aging significantly increases the interaction between polystyrene nanoplastic and minerals’, *Water Research*, 219, p. 118544. Available at: https://doi.org/10.1016/j.watres.2022.118544.

4

Toxicity of Graphene Quantum Dots: Role of Surface Functionalization and Aging

4.1 Introduction

Quantum dots are semiconducting nanomaterials with unique electronic and optical properties, having a typical size of less than 20 nm (Perini *et al.*, 2020). Graphene quantum dots (GQDs) can be described as graphene nanosheets with properties deriving from both quantum dots and graphene (Zhou *et al.*, 2017). Since they were first produced in 2008, GQDs have attracted the interest of many researchers due to their excellent properties, such as high biocompatibility and photostability (Zhou *et al.*, 2017). Their small size (< 20 nm) allows them to cross biological barriers, such as the blood-brain barrier, giving them a strong ability to selectively transport substances that circulate in the blood towards cerebral compartments, which favours their use as a potential treatment for brain tumours (Perini *et al.*, 2020). It has been reported that GQDs can be taken up by endocytosis cells without causing cytotoxic effects, which makes them great candidates for biomedical applications, including therapeutics, biosensors, imaging and drug delivery (Zhou *et al.*, 2017). There have, however, also been reports of cytotoxic effects caused by GQDs, which were discussed in Chapter 1 of this thesis.

Due to their benzene-like structures, pristine carbon-based NMs are hydrophobic, leading to aqueous instability and restricting their use in biomedical applications (Chong *et al.*, 2014). Surface functionalizing of NMs with hydrophilic polymers is a popular way of stabilizing carbon-based NMs (Chong *et al.*, 2014). Another popular strategy to enhance their aqueous stability and dispersability is making ultra-small carbon NMs (e.g., GQDs) so that their Brownian motion can provide enough energy to prevent aggregation, making them less

hydrophobic due to the oxygen-rich surface functional groups at their edges (Chong *et al.*, 2014). The potential toxicity and cellular uptake of NMs can be affected by modifying their surface chemistry, and different surface functional groups may alter the physicochemical properties of NMs by changing the binding affinity, surface adsorption and aggregation behaviour of the particles (Kinaret *et al.*, 2021).

Despite the promised applications of GQDs, their potential toxic impacts and mechanism of uptake and clearance have not been explored enough. The biosafety of GQDs should be critically evaluated before they are practically applied, especially the risk of surface modification, as it is the first point of contact between NMs and surrounding environments. Based on our literature review, most toxicity studies on GQDs involved cell cytotoxicity with very limited information about their interaction with aquatic organisms such as *D. magna* available in the literature. Thus, this study can provide valuable insights into the potential for aquatic toxicity of GQDs and add knowledge to what has already been reported in the literature regarding their interaction with living systems.

Three types of GQDs with different chemical surface functionalization groups were investigated (Table 4.1). Negatively charged carboxylated GQDs (C-GQDs), neutral hydroxylated GQDs (H-GQDs) and positively charged aminated GQDs (A-GQDs). The acute toxicity of the three selected NMs towards *D. magna* was assessed by investigating, and the role of particle ageing in their pristine condition (i.e., during storage of the as-received stock solutions) as well as during incubation in HH combo culture medium during storage at 4 °C in the absence of light was investigated.

Table 4.1. Summary of the properties of the functionalized GQDs used in this chapter and their as-received dispersions.

Surface Modification	Particle Size	Synthesis methods	Dispersion solution
Carboxylated	< 10 nm	Bottom-up	DI water
Hydroxylated	< 6nm	Hydrothermal	DI water and ethylene glycol
Aminated	< 5 nm	Hydrothermal	DI water

The Aims and Objectives of Chapter 4 were to:

1. Determine the overall acute toxicity of GQDs towards the model freshwater organism *D. magna.*

2. Evaluate the role of surface functionalization on the acute toxicity of GQDs.

3. Determine the impact of HH combo medium conditioned by *D. magna* on the stability and toxicity of GQDs.

4. Investigate the role of particle ageing on the physicochemical properties and toxicity of GQDs.

5. Assess whether the amount of protein secreted by *D. magna* exposed to GQDs serves as a stress/toxic response mechanism.

4.2 Toxicity of GQDs Aged in Their Pristine State

In this experiment, the acute toxicity of the three selected GQDs types towards *D. magna* was assessed over two years while stored in their pristine state refrigerated at 4 °C. It should be noted that before starting this experiment, the particles were purchased and had been stored (opened) at 4 °C for around one year, meaning that the whole ageing process actually took place over three years. However, since we have not tested these particles once purchased and to avoid confusion, we will refer to the pristine one-year-aged particles as the (non-aged) and the toxicity of particles aged during the subsequent 2 years of storage will be compared to those non-aged particles. The tested concentration range for the 48 h acute toxicity tests chosen for this study (10 to 100 mg/L) was based on the OECD 202 test

guidelines, which recommended that 100 mg/L is the highest concentration representing environmentally relevant conditions for testing chemicals. Although the OECD guidelines were not designed for testing of NMs, we found this concentration range to be efficient for this study to compare the toxic effects before and after ageing, and also, many GQDs published toxicity studies were conducted approximately in this concentration range. Analyses of the immobilization behaviour of *D. magna* exposed to the non-aged NMs indicated that the C-GQDs were the most toxic out of the three investigated NMs, with an EC_{50} value of 79.39 mg/L, followed by the H-GQDs with an EC_{50} value of 92.65 mg/L. In the A-GQDs group, no immobilization (0%) of *D. magna* neonates was observed in the exposure solutions up to the highest tested concentration (100 mg/L), indicating that the amine-modified group were the least toxic of the three studied NMs in this experiment, at constant mass concentration. Other studies also found that aminated graphene or GQDs have lower toxicity than carboxylated and hydroxylated ones (Hu *et al.*, 2019; Guo *et al.*, 2020; Xie *et al.*, 2020).

Although in our literature search, we have not found a relevant study conducted on the model organism *D. magna* to compare our results to, there are a number of studies that evaluated the cytotoxicity of GQDs with different surface chemistry, and our results are relatively comparable with available data. For example, It has been reported that the toxicity of GQDs towards lung carcinoma A549 cells depended on their surface chemistry and hydroxylated and carboxylated GQDs showed much higher cell uptake amounts compared to the amine-modified GQDs (Xie *et al.*, 2019). However, their results indicated that H-GQDs were the most toxic compared to the C-GQDs and A-GQDs groups, as significant cell death was induced by the hydroxylated particles at the concentration of 100 mg/L, but in our study, the carboxylate group were the most toxic towards *D. magna*.

After one year of ageing of the pristine particles (i.e., the stock solutions) in the fridge, the EC_{50} value of the C-GQDs decreased from 79.39 to 44.53 mg/L, indicating a high increase in toxicity towards *D. magna*. The same behaviour was observed for the H-GQDs with an EC_{50} value decreasing from 92.65 to 59.24 mg/L. In contrast, the A-GQDs remained non-toxic in terms of immobilisation of *D. magna* after one year of storage.

After 1.5 and 2 years of storage, the acute toxicity has slightly increased further for both (C/-GQDs and H-GQDs), but with a much lower degree of change compared to the that arising during the first year of storage (4.1 and 4.2). While no immobilization effect of *D. magna* neonates was recorded in the A-GQDs group after 1.5 years of storage and only around 1 % of immobilization was observed at the highest tested concentration (100 mg/L) after 2 years of storage, indicating that these materials were also stable against transformations during storage in the as-supplied dispersions.

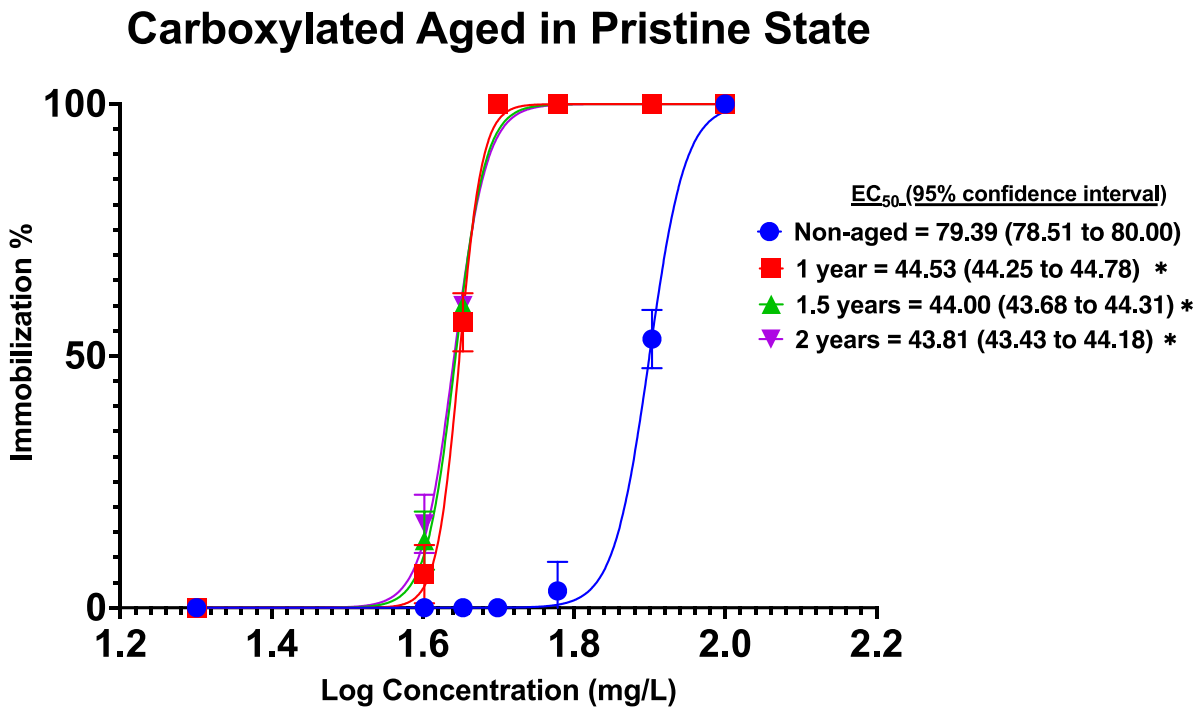

Figure 4.1. Plot of % immobilization of D. magna neonates versus log of the exposure concentration (mg/L) of C-GQDs comparing the just-opened bottle (non-aged) C-GQDs versus after ageing of the as-received dispersion for 1 year, 18 months and 2 years All solutions were prepared by dispersing the particles in HH Combo medium and were tested immediately using neonates < 48 hours old, with 3 replicates (n=3). Data are presented as mean ± S.D.

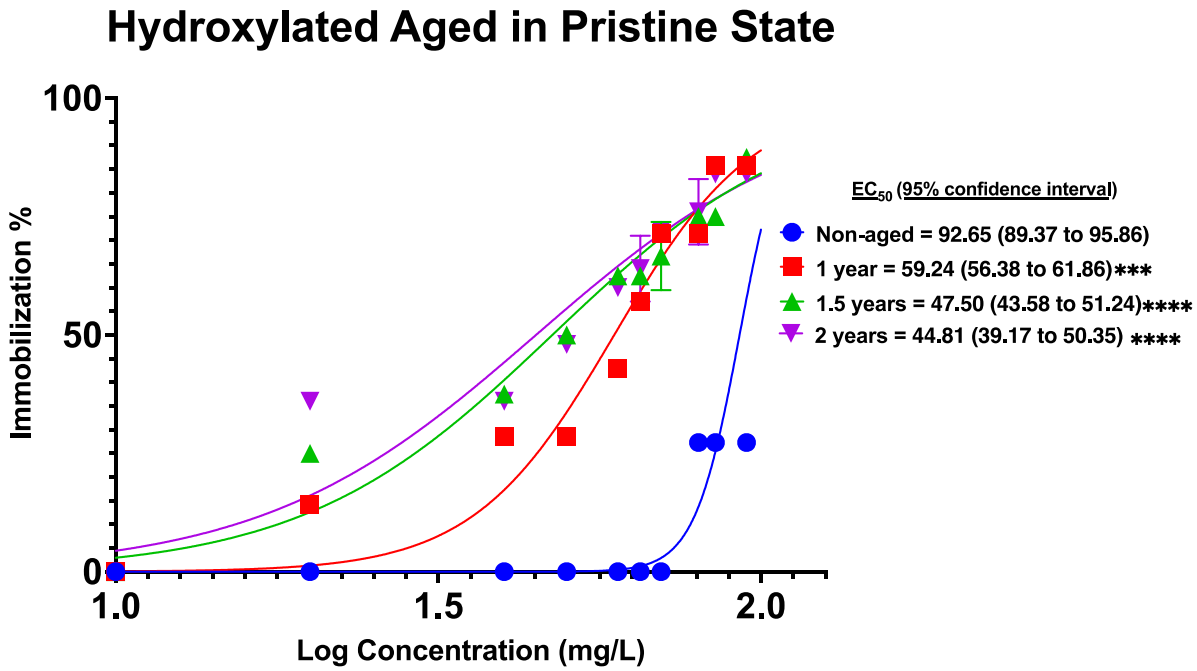

Figure 4.2. Plot of % immobilization of D. magna neonates versus log of the exposure concentration (mg/L) of H-GQDs comparing the just-opened bottle (non-aged) H-GQDs versus after ageing of the as-received dispersion for 1 year, 18 months and 2 years. All solutions were prepared by dispersing the particles in HH Combo medium and were tested immediately using neonates < 48 hours old, with 3 replicates (n=3). Data are presented as mean ± S.D.

The high increase in toxicity with time during storage may have resulted from transformation processes leading to particle degradation in water. It has been reported that quantum dots can be degraded by multiple molecular interactions with water and oxygen, thermal heating and UV light exposure (Moon *et al.*, 2019). Water and oxygen can chemically and physically adsorb onto the surface of QDs, which can trigger the oxidation of the core atoms and change their properties (Moon *et al.*, 2019; Nikazar *et al.*, 2020). The surface functionalization of GQDs may play an essential role in the stability and toxicity behaviour of GQDs. A study that investigated the photostability and reactive oxygen species (ROS) generation ability of GQDs with different surface modifications found that the oxygen-containing groups were primarily responsible for ROS generation, and the photostability of GQDs can be improved, and ROS production can be reduced by removing these oxygen-functional groups from the surface of particles (Zhou *et al.*, 2017). This would also explain the higher toxicity of the oxygen-containing C-GQDs and H-GQDs relative to the A-GQDs which do not contain any oxygen groups.

4.3 The Impact of *D. magna* Secreted Proteins on the Properties and Toxicity of GQDs

When NMs enter the aquatic environment, they will most likely go through transformation processes (e.g., photochemical, physical, biological) due to the interaction of the particles with materials present in the surrounding environment (e.g., biomolecules, NOM, other chemicals, light). Therefore, the toxicity of NMs may be increased or decreased compared to the pristine NMs. Proteins secreted by living organisms are one source of biomolecules existing in aquatic environments, and the interaction of these biomolecules with NMs can change the identity of particles and alter their environmental fate by forming an eco-corona layer around the surface of NMs. In Chapter 3 of this thesis, we explored the role of *D.*

magna protein secretion to condition HH combo medium and concluded that the protein concentration that can be acquired by this method was relatively low (below 5 µg/mL) in our studies and did not significantly affect the toxicity of polystyrene NMs. However, different NMs have different physical and chemical properties and depending on their unique properties and binding affinity, their identity might be affected by any amount of existing biomolecules.

Here, we investigated the effect of conditioning HH combo medium (2 neonates per mL for 48 h) on the 48 h acute toxicity of GQDs with different surface functionalization groups. The particles were incubated in the conditioned medium for 3 h before any exposure took place. The tests were conducted on the same particles that had been used in the previous study, which had 2-year aged EC_{50} values of 44.53 mg/L and 59.24 mg/L for the C-GQDs and H-GQDs, respectively, while 0% immobilization was observed in the amine-modified group.

Although DLS analyses do not represent the actual size of non-spherical NMs such as GQDs, this approach was conducted to qualitatively monitor changes between tested groups. The polydispersity index and surface charge measurement obtained by DLS can give an estimation of the stability of NMs in the tested solutions. The DLS measurements were conducted on particles from each GQDs surface modified group in DI water, fresh HH combo medium, and particles that had been incubated in conditioned HH combo medium for 3 h prior DLS measurements.

Table 4.2. Physicochemical characterization of the carboxyl functionalized GQDs (C-GQDs) in fresh HH Combo medium, daphnia conditioned HH Combo medium versus DI water.

C-GQDs						
Medium	**Z-average (nm)**	**SD ±**	**PDI**	**SD ±**	**ZP (mV)**	**SD ±**
Fresh HH	1097	144.2	0.984	0.027	-8.16	0.377
Conditioned HH	1409	480	1	0	-9.15	1.83
DI water	78.1	110.5	0.151	0.214	1.16	1.03

Table 4.3. Physicochemical characterization of the hydroxyl functionalized GQDs (H-GQDs) in fresh HH Combo medium, daphnia conditioned HH Combo medium versus DI water.

H-GQDs						
Medium	**Z-average (nm)**	**SD ±**	**PDI**	**SD ±**	**ZP (mV)**	**SD ±**
Fresh HH	794.2	141.1	0.756	0.204	-18	1.07
Conditioned HH	669.3	87.94	0.903	0.087	-15.6	1.4
DI water	3928	6422	0.504	0.442	0.159	1.03

Table 4.4. Physicochemical characterization of the amine functionalized GQDs (A-GQDs) in fresh HH Combo medium, daphnia conditioned HH Combo medium versus DI water.

A-GQDs						
Medium	**Z-average (nm)**	**SD ±**	**PDI**	**SD ±**	**ZP (mV)**	**SD ±**
Fresh HH	873.1	67.48	0.728	0.039	-19.8	0.503
Conditioned HH	876.8	243.6	0.918	0.143	-21.9	2.63
DI water	509.2	617.4	0.389	0.535	-9.48	5.17

The hydrodynamic size measurements indicated that agglomeration may have occurred once all studied particles were incubated in fresh HH combo medium (as compared to the size in DI water) (Tables 4.2-4.4). However, given the sheet-like shape of the GQDs, these results are not the actual sizes of the particles but rather an average size of the particles tumbling in solution, and as such we focus on the PDI and ZP measurements to compare the stabilities of the particles. The PDI values in all tested groups showed that GQDs had a narrower PDI in DI water than in HH combo medium, which could be due to the interaction of particles with cation species present in the culture medium introducing some agglomeration as a result of charge neutralizing and screening of the electric double layer between the particles resulting in closer contact. The most toxic GQDs (carboxylated)

showed the highest PDI intensity value, which is in accordance with the finding of a study that investigated the characteristics and toxicity of non-functionalized, carboxylated and aminated GQDs to U87 cells (Zhou *et al.*, 2017). The authors found that the C-GQDs had the highest PDI value as measured by DLS and that the A-GQDs were the least toxic and did not affect cell membrane permeability or viability.

Surface charge is an essential factor controlling the toxicity of NMs and can influence the agglomeration behaviour of NMs as well as the adsorption of biomolecules and ions, which can change an animal or cellular response towards NMs (Sharifi *et al.*, 2012). It is generally believed that anionic surfaces are normally less toxic than cationic surfaces, as positively charged surfaces are more likely to cause hemolysis and platelet (cells circulating in the blood) aggregation, whilst neutral surfaces are believed to be the most biocompatible (Sharifi *et al.*, 2012).

ZP was negatively increased (become more negative) for all particles incubated in fresh HH combo compared to DI water, indicating that GQDs steric stability was improved when interacting with cations and anions present in the HH combo medium. The carboxylate and hydroxylate groups were positively charged in DI water; however, the values were relatively close to 0 mV (neutral), and the charge was changed to negative in the fresh and conditioned HH combo media. The surface of the amine-modified GQDs was negatively charged in all tested solutions.

After incubating the three types of GQDs in a conditioned HH combo medium for 3 h, the PDI value increased in all tested groups compared to the unconditioned HH combo medium showing a broader distribution of particles sizes in the conditioned medium. This effect could be due to the interaction of GQDs with the secreted proteins. The ZP measurements of all tested groups were relatively close in the fresh and conditioned HH combo medium, as

demonstrated in Tables 4.2 – 4.4, showing a slight decrease from - 18 ± 1.07 mV in the fresh HH combo to -15.6 ± 1.4 mV in the conditioned HH combo for the hydroxylated particles. An increasingly negative ZP, from - 8.16 ± 0.37 mV to - 9.15 ± 1.83 mV and from - 19.8 ± 0.5 mV to - 21.9 ± 2.6 mV was determined for the hydroxylated and aminated groups, respectively, as shown in Tables 4.3 and 4.4. The changes in physicochemical properties of particles between the fresh and conditioned HH combo medium may indicate that an eco-corona layer has formed around their surfaces. However, if a corona layer has formed, we might expect a change in the toxicity behaviour of the particles, although in this case, since the ZPs didn't change much the toxicity may also be similar. To assess the effect of medium conditioning by proteins secreted from *D. magna* neonates on the toxicity of GQDs, a 48 h acute toxicity test was conducted on all three GQDs groups, and indeed no considerable change was observed between the fresh and conditioned solutions, indicating that the medium conditioning step did not affect the toxicity of GQDs towards *D. magna* neonates. However, the amount of proteins was low in the conditioned medium (< 5 μg/mL) and may not have been enough to completely cover the surface of GQDs or to affect their toxicity in this study, but we do expect that the different GQDs would result in different responses by daphnia and secretion of proteins into the medium that reflect the repair pathways induced by the presence of the GQDs.

4.4 The Impact of Ageing in HH Combo Medium on The Properties and Toxicity of GQDs

In this study, stock solutions from the GQDs that were aged in their pristine state for one year in the previous study were chosen and prepared in HH combo medium. Those particles have already shown a high increase in toxicity after one year of ageing in the pristine state compared to the non-aged particles for both the C-GQDs and H-GQDs. This test was

performed to compare the toxicity behaviour of GQDs aged in their pristine state with particles aged in HH combo culture medium. Here, we will refer to the particles chosen to prepare stock solutions as non-aged particles. Acute toxicity tests (48h) were conducted on the non-aged, 3 months aged and 6 months aged GQDs in HH combo medium. The hydrodynamic size and zeta potential were measured by DLS for all tested groups (4.5 to 4.7).

Table 4.5. Physicochemical characterization of the carboxyl functionalized GQDs (C-GQDs) that had been aged for 3 and 6 months in HH Combo medium.

C-GQDs Aged in HH Combo						
Ageing time	**Z-average (nm)**	**SD ±**	**PDI**	**SD ±**	**ZP (mV)**	**SD ±**
Non-aged	1097	144.2	0.984	0.027	-8.16	0.377
3 months	1106	47.52	1	0	0.522	0.645
6 months	433.7	31.8	0.634	0.09	-16.7	0.7

Table 4.6. Physicochemical characterization of the hydroxyl functionalized GQDs (H-GQDs) that had been aged for 3 and 6 months in HH Combo medium.

H-GQDs Aged in HH Combo						
Ageing time	**Z-average (nm)**	**SD ±**	**PDI**	**SD ±**	**ZP (mV)**	**SD ±**
Non-aged	794.2	141.1	0.756	0.204	-18	1.07
3 months	540.7	22.28	0.304	0.075	-5.36	0.212
6 months	554.3	27.74	0.314	0.107	-5.38	0.356

Table 4.7. Physicochemical characterization of the anime functionalized GQDs (A-GQDs) that had been aged for 3 and 6 months in HH Combo medium.

A-GQDs Aged in HH Combo						
Ageing time	**Z-average (nm)**	**SD ±**	**PDI**	**SD ±**	**ZP (mV)**	**SD ±**
Non-aged	873.1	67.48	0.728	0.039	-19.8	0.503
3 months	494.6	5.916	0.407	0.017	-8.39	1.41
6 months	416.8	14.35	0.375	0.006	-10.7	0.862

From the obtained DLS hydrodynamic size measurements, it was clear that the size decreased with increasing the time of particle incubation in HH combo for all tested groups, as shown in Tables 4.5-4.7. However, in the C-GQDs group, the change of size was relatively

small during the first 3 months of incubation (from 1097 ± 144 nm to 1106 nm ± 47), while after 6 months, the size decreased dramatically from 1097 ± 144 nm to 433.7 ± 31.8 nm. During the first three months of C-GQDs incubation, the polydispersity index (PDI) value slightly increased from 0.984 ± 0.02 to 1 ± 0, indicating a widening of the particle size distribution, while the same value decreased to 0.634 ± 0.06 after 6 months of incubation in HH combo medium, showing better stability after 6 months of incubation in the culture medium. In contrast, the ZP value of the same group (C-GQDs) changed from -8.16 ± 0.377 mV to 0.522 ± 0.64 mV, also indicating a decrease in electrostatic stability and a change in the surface charge of particles (from negative to positive) during the first 3 months of incubation. After 6 months of incubating the same particles in HH combo medium, the ZP potential value negatively increased to -16.7 ± 0.7 mV, demonstrating higher electrostatic stability than during the first 3 months of incubation.

For the other two GQDs groups (hydroxylated and aminated), a decrease in the PDI was observed, and most of the change was observed during the first 3 months of incubation, showing better polydispersity for the aged particles compared to the non-aged ones (Tables 4.6 and 4.7). Whilst the surface charge remained negative over the ageing time for the hydroxylated and aminated GQDs, the overall ZP measurements for both groups indicated lower electrostatic stability after the ageing process than for the non-aged particles. A general interpretation of DLS measurement results may indicate complexity in the behaviour of GQDs, but the PDI and surface charge stabilisation of the C-GQDs in HH combo medium was lower than that of the H-GQDs and A-GQDs, noting that this lower stability of the carboxylated particles correlated also with them being the most toxic towards *D. magna* based on the previous 48 h acute toxicity observations.

4.4.1 Toxicity of GQDs Aged in HH Combo Medium

It is known that medium composition can impact the toxicity and physicochemical properties of NMs, and in addition to the pristine (highly reactive) state of particles, ecotoxicological studies should consider the transformation of NMs when incubated in environmentally representative mediums for longer times (aged) to reflect realistic exposure scenarios in risk assessments (Ellis et al., 2020). Only a few studies have explored the impact of ageing on the toxicity and physicochemical properties of NMs, including the previously cited study, and there is a large literature gap in understanding the impact of ageing on the physicochemical properties and toxicity of NMs, especially on newly emerging materials such as GQDs. Assessing the effects of pristine NMs being released into the environment is also essential, which is why this study was conducted to compare the ageing of pristine particles in the as-supplied dispersion versus following dilution in HH combo medium. Long-term ageing in a purely salt-based medium (HH combo) has been reported to passivate the surface chemistry of NMs, leading to a significant reduction in the toxicity towards Daphnia compared to pristine NMs (Ellis et al., 2020). In the 48 h acute toxicity experiments reported above, where all three types of GQDs were aged in their pristine state, the toxicity of particles towards *D. magna* neonates increased with particle ageing time (Figures 4.1 and 4.2). Here, an opposite reaction was observed when the particles were incubated and aged in HH combo medium. The EC_{50} value of the C-GQDs increased from 44.53 mg/L in the non-aged group to 81.91 mg/L and 82.84 mg/L after 3 and 6 months of incubation in the culture medium, respectively, showing a sizable decrease in toxicity in the medium-aged groups. A similar effect was noted in the hydroxylated particles group, where the EC_{50} value increased from 59.24 mg/L (non-aged) to 89.77 mg/L and 95 mg/L after 3

months and 6 months of incubation, respectively. No immobilization of *D. magna* neonates was recorded in all the A-GQDs tested solutions, and as such the data are not plotted.

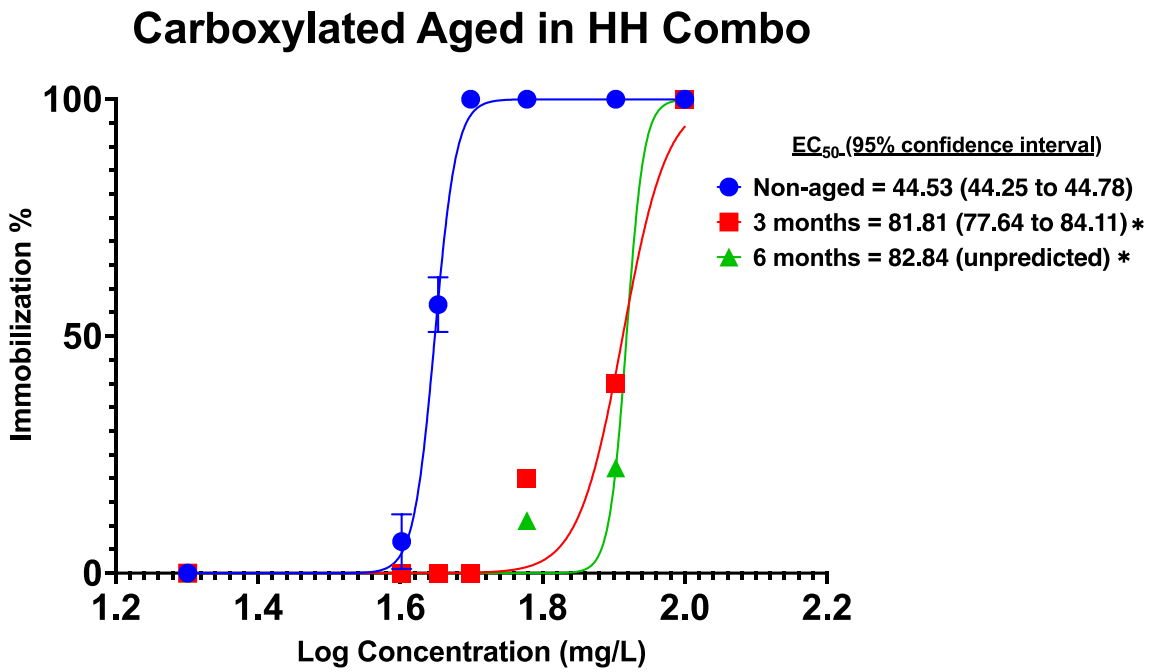

Figure 4.3. Plot of % immobilization of D. magna neonates versus log of the exposure concentration (mg/L) of G-GQDs aged for 3 and 6 months compared to the non-aged C-GQDs prepared by dispersing the particles in HH Combo medium and testing immediately using neonates < 48 hours old, with 3 replicates (n=3). Data are presented as mean ± S.D.

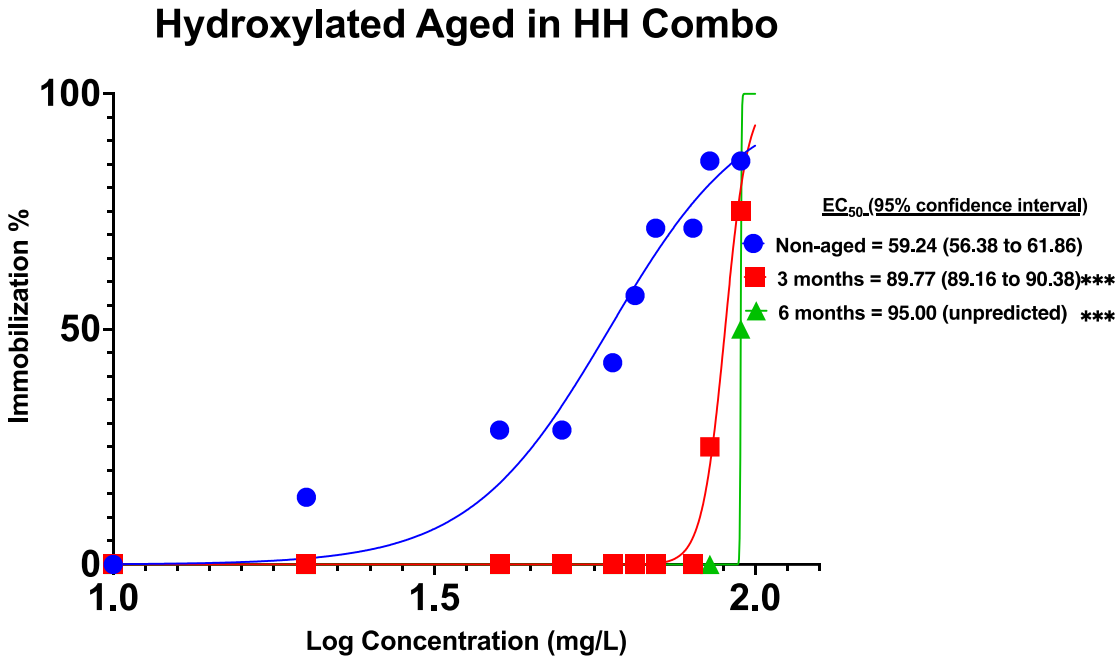

Figure 4.4. Plot of % immobilization of D. magna neonates versus log of the exposure concentration (mg/L) of H-GQDs aged for 3 and 6 months compared to the non-aged H-GQDs prepared by dispersing the particles in HH Combo medium and testing immediately using neonates < 48 hours old, with 3 replicates (n=3). Data are presented as mean ± S.D.

The decrease in toxicity of the aged GQDs in HH combo was surprisingly high, and the mechanism of reduction could be related to the transformation of NMs through interacting with the medium salts. These results are consistent with the findings of (Ellis et al., 2020), which investigated the ageing effects of Ag and TiO_2 NMs in HH combo medium and NOM-containing water (class V) and demonstrated that the toxicity, *D. magna* uptake and internalized concentrations of NMs were always lower in the aged exposures than the pristine NMs (Ellis et al., 2020). The authors suggested that the toxicity reduction of the aged NMs was mainly related to the ionic strength of media and transformations to less reactive surfaces through interactions with the salts present in the HH combo medium, or in that particular case with NOM present in the class V water (Ellis et al., 2020).

4.4.2 The Effect of GQDs Toxicity on Protein Secretion *by D. magna*

To further understand the toxic effects of GQDs with different surface functional groups, we exposed *D. magna* neonates to a range of concentrations (20, 40, 60, 80, and 100 mg/L) of each NM type for 48 h. The exposures were conducted using two groups of particles, one aged in HH combo medium for 6 months and the other group non-aged (pristine), although of course as noted above the ageing process also occurred in the stock solutions during storage in the fridge. Here again, the non-aged particles were more toxic than the aged particles according to the previous acute toxicity results. Samples from each exposure solution were collected and analysed for total protein content using the Pierce Rapid Gold BCA kit. Protein secretion is known to be related to stress and toxic responses by living organisms depending on the amount/type of secreted proteins obtained from chemical exposures.

Results obtained from the BCA analyses showed that *D. magna* neonates did not secret any proteins after being exposed to the aminated GQD particles, which were non-toxic to the tested animals according to our previous observations (Figure 4.5).

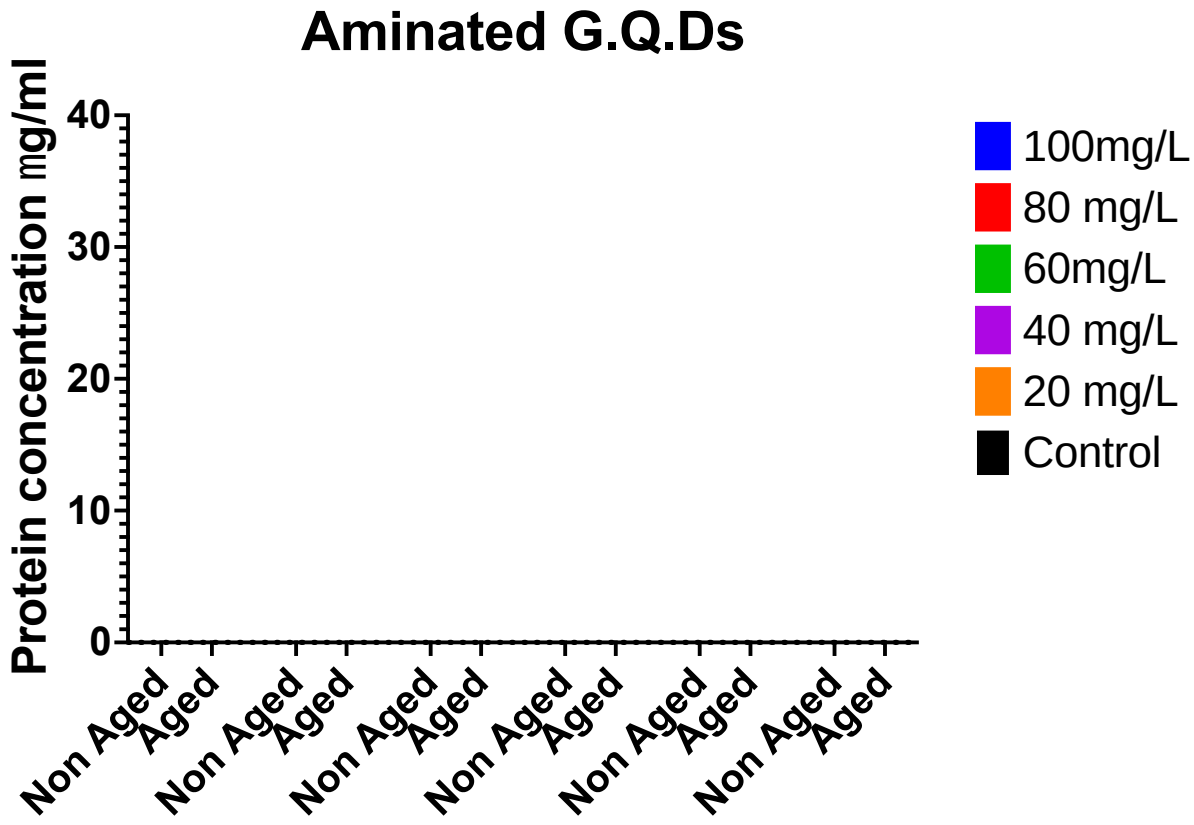

Figure 4.5. Confirmation of the limited response of D. magna to the presence of the A-GQDs as also evidenced by the lack of protein secretion by the daphnids in response to the presence of the A-GQDs as determined after 48 hours of exposure.

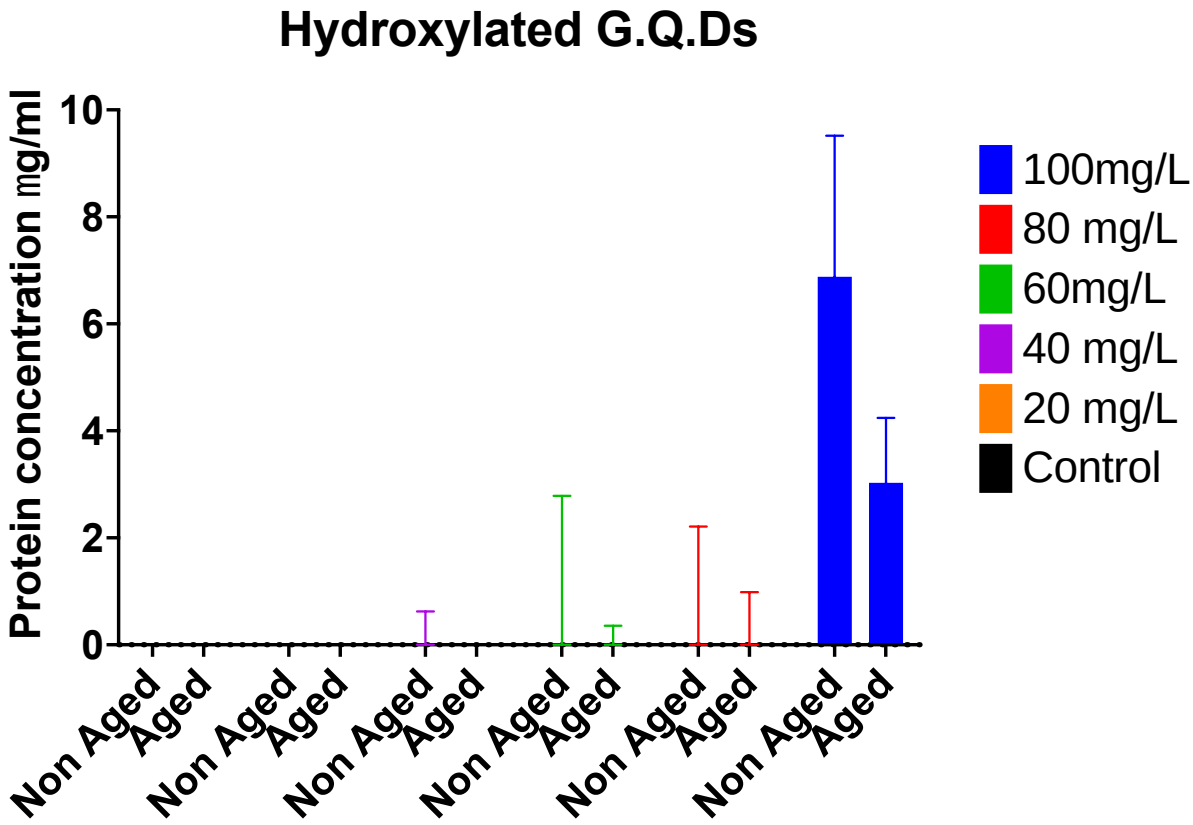

Figure 4.6. Protein secretion by D. magna to the presence of increasing concentrations of non-aged and aged H-GQDs, determined after 48 hours of exposure.

In contrast, daphnids exposed to the hydroxylated GQDs have secreted proteins into the tested solutions (Figure 4.6) with the highest concentration of proteins (8.6 µg/mL) found in the non-aged groups with an H-GQDs concentration of 100 mg/L.

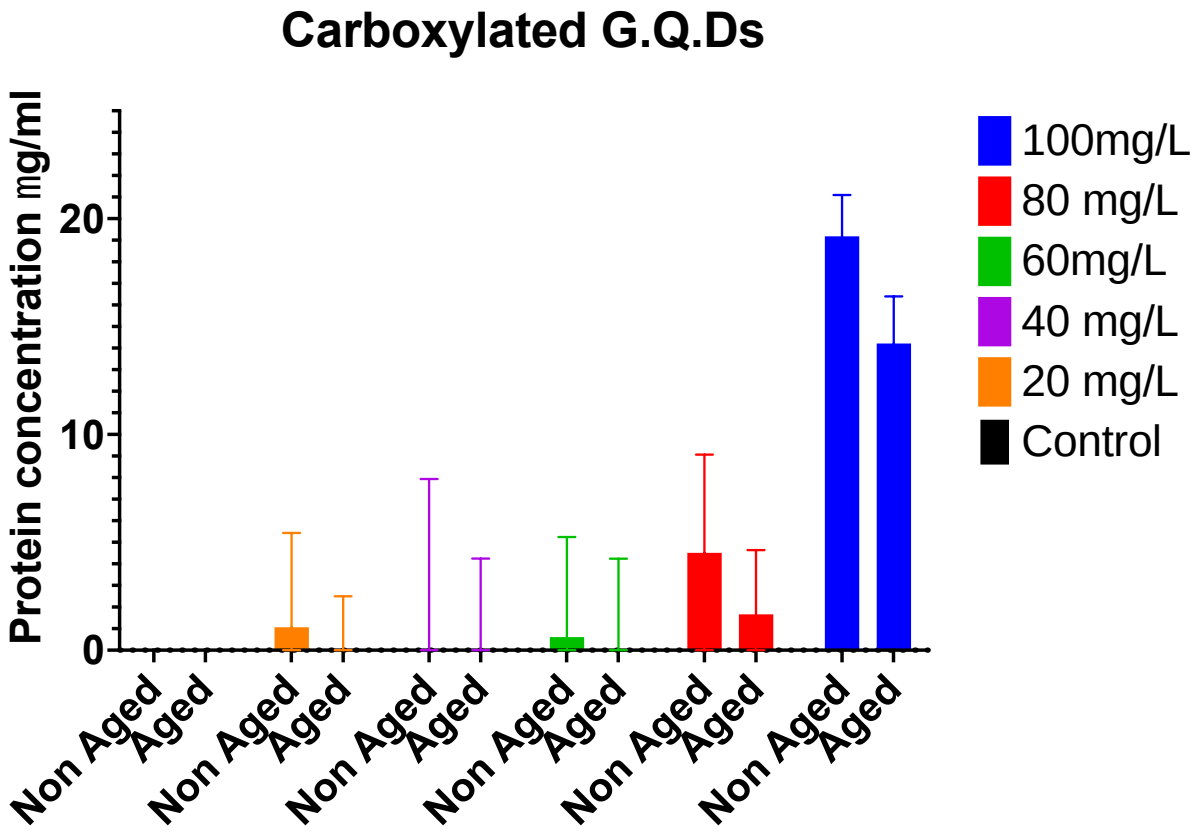

Figure 4.7. Protein secretion by D. magna to the presence of increasing concentrations of non-aged and aged C-GQDs, determined after 48 hours of exposure.

In the case of daphnids exposed to the carboxylated GQDs, which were the most toxic to *D. magna* neonates, more proteins were identified in most of the tested solutions, with the highest concentration (21.3 µg/mL) observed in the non-aged groups containing 100 mg/L of the C-GQDs. In every tested solution where proteins were detected by the BCA test, daphnids that were exposed to the non-aged particles (more toxic) secreted more proteins than those exposed to the particles aged in HH combo medium for 6 months. The overall protein secretion results showed that the more toxic the particles were to daphnids, the more proteins that were being secreted by the tested animals (Figures 4.5 to 4.7). This is consistent with previous findings from our group, which found that the proteins secreted by daphnids in response to NMs could be utilized to shed light on how the daphnids were responding to the presence of the particles, and into the mechanism(s) of toxicity induced

by the particles (Ellis and Lynch, 2020). One of the objectives of this study was to characterize the proteins found in the exposure solution based on their molecular weight using the SDS-PAGE method, but this goal was not achieved due to insufficient remaining time to finish the project. We note that the data will be included in the resulting publication. In chapter 3 of this thesis, we attempted to evaluate the amount of uptake of PS NMs by *D. magna* using the fluorescent function of the Tecan plate reader, but we found this method to be unreliable for animal uptake analysis. Here, we tried once more to observe if this method may give better results with a different type of fluorescent particles (GQDs), but the results still did not indicate reliability, as the control groups of animals were more fluorescent than animals that were exposed to the fluorescent particles themselves in some tested samples, which may be the result of residual autofluorescence from algae consumed by the daphnids before the exposure studies were performed. Therefore, we have not presented those results here, and we believe that uptake studies that use this method may be able to achieve good results depending on the type of animal, type of particles and the condition of the experiment, but it is recommended to consider another alternative (e.g., Mass Spectrometry) to achieve more reliable analyses.

Although all GQDs selected in this experiment indicated low overall acute toxicity towards *D. magna*, especially the aminated GQDs, which were nontoxic in all tested solutions, the carboxylated and hydroxylated groups caused high immobilization at higher exposure concentrations (> 40 mg/L). The C-GQDs were the most toxic to *D. magna* and caused the animals to secret more proteins than the aminated and hydroxylated NMs. The toxic effects depended on the surface chemistry of GQDs, and the mechanism of toxicity was not widely investigated in this experiment, but the results can give insights into the overall biosafety, effects of surface chemistry and the role of ageing on the toxicity of GQDs. However, the

mechanism of GQDs toxicity and the difference in toxicity between the three surface functional groups could be related to many factors that have been reported for carbon-based NMs in the literature. For example, a review article which approached a theoretical investigation using molecular dynamic simulations on GQDs reported that high GQDs concentrations caused the particles to aggregate in water but disaggregate once crossing the cell membrane interior, which can induce changes in the fluidity and structural properties of the lipid bilayer, impacting cell signal transduction (Nikazar *et al.*, 2020). Moreover, the same study reported that smaller sized GQDs were not large enough to damage the lipid membrane and concluded that the cytotoxic effects of GQDs were size-dependent and smaller particles may be a more appropriate option for biomedical applications (Nikazar *et al.*, 2020). Another study explored the effect of two functional groups (carboxylated and hydroxylated) on the genotoxicity of single-walled carbon nanotubes (SWCNT) and concluded that the carboxylated particles induced a greater toxic impact than the hydroxylated particles and indicated that DNA damage and oxidative stress were the primary toxic mechanism for SWCNT functionalized with carboxylation and hydroxylation (Jiang *et al.*, 2020). Although the toxicogenomics assay results of the same study indicated that the carboxylated particles induced greater overall toxicity, protein damage, genotoxicity and chemical stress compared to the hydroxylated SWCNT, both surface functionalization groups had comparable/similar oxidative stress levels (Jiang *et al.*, 2020).

4.5 Conclusion

The environmental indicator *D. magna* is an important model organism to assess the toxicity of NMs due to their filter-feeding behaviour and their essential role in the food chain. Employing the model organism to assess the toxic behaviour of GQDs in this chapter provided valuable information to evaluate the environmental risks of the investigated NMs supporting the evaluation of their suitability for various applications. The obtained results, which address the objectives of this study, can be summarized as follows:

1. The overall toxicity of GQDs in this study can be classified as relatively low compared to other NMs released into the environment but can still be highly toxic in concentrations below 100 mg/L, depending on the type of surface chemistry and exposure scenario.
2. The aminated GQDs were the most biocompatible compared to the carboxylated and hydroxylated GQDs.
3. Conditioning HH combo medium with proteins secreted by *D. magna* neonates for 3 h changed the physicochemical properties of the particles to some degree but did not affect the acute toxicity of the GQDs towards daphnids. Increasing the incubation time of particles in the conditioned medium may increase the change in the observed physicochemical properties, thus affecting the toxicity of GQDs.
4. Ageing of particles either during storage in the as-received dispersion, or in HH Combo medium, led to the transformation of GQDs NMs and changes in toxicity behaviour compared to pristine particles.
5. The toxicity of GQDs depends not only on a single factor but also on a combination of factors, including surface chemistry, ageing and composition of dispersant solution.

6. The toxicity of GQDs can be related to the quantity of proteins secreted by *D. magna*, as the higher the toxic effects, the more proteins were observed.

The obtained data indicate the role of surface functionalization and ageing in changing the physicochemical properties of GQDs and that reporting of particle "age", including purchase date, initial vial opening date, and assumed age at the time of the experiment, is essential in order to increase the comparability between studies, as particles of different shelf-age have quite different toxicity. Similarly, the increased toxicity that resulted from ageing during storage was largely reversed by further ageing the GQDs in HH Combo medium, and thus suggests that older particles in the environment may be less toxic than when initially released. Whether this applies to other materials and to other organisms, which might have different exposures, uptakes and interactions compared to *D. magna*, remains to be explored. Moreover, ecotoxicity studies on pristine NMs can be greatly overestimated, and employing environmentally realistic scenarios can dramatically change the toxicity observations between pristine and treated NMs. Therefore, it is necessary to employ efforts in understanding the mechanism of toxic effects when regulating environmental risk assessments, which needs consideration and comparison between medium composition, surface chemistry, ageing and transformation of NMs.

References

A. Ellis, L.-J., Valsami-Jones, E. and Lynch, I. (2020) 'Exposure medium and particle ageing moderate the toxicological effects of nanomaterials to Daphnia magna over multiple generations: a case for standard test review?', *Environmental Science: Nano*, 7(4), pp. 1136–1149. Available at: https://doi.org/10.1039/D0EN00049C.

Chong, Y. *et al.* (2014) 'The in vitro and in vivo toxicity of graphene quantum dots', *Biomaterials*, 35(19), pp. 5041–5048. Available at: https://doi.org/10.1016/j.biomaterials.2014.03.021.

Jiang, T. *et al.* (2020) 'Toxicity of Single-Walled Carbon Nanotubes (SWCNTs): Effect of Lengths, Functional Groups and Electronic Structures Revealed by a Quantitative Toxicogenomics Assay', *Environmental science. Nano*, 7(5), pp. 1348–1364. Available at: https://doi.org/10.1039/d0en00230e.

Kinaret, P.A.S. *et al.* (2021) 'Toxicogenomic Profiling of 28 Nanomaterials in Mouse Airways', *Advanced Science*, 8(10), p. 2004588. Available at: https://doi.org/10.1002/advs.202004588.

Moon, H. *et al.* (2019) 'Stability of Quantum Dots, Quantum Dot Films, and Quantum Dot Light-Emitting Diodes for Display Applications', *Advanced Materials*, 31, p. 1804294. Available at: https://doi.org/10.1002/adma.201804294.

Nikazar, S. *et al.* (2020) 'Revisiting the cytotoxicity of quantum dots: an in-depth overview', *Biophysical Reviews*, 12(3), pp. 703–718. Available at: https://doi.org/10.1007/s12551-020-00653-0.

Perini, G. *et al.* (2020) 'Graphene Quantum Dots' Surface Chemistry Modulates the Sensitivity of Glioblastoma Cells to Chemotherapeutics', *International Journal of Molecular Sciences*, 21(17), p. 6301. Available at: https://doi.org/10.3390/ijms21176301.

Sharifi, S. *et al.* (2012) 'Toxicity of nanomaterials', *Chemical Society reviews*, 41(6), pp. 2323–2343. Available at: https://doi.org/10.1039/c1cs15188f.

Xie, Y. *et al.* (2019) 'Cytotoxicity and autophagy induction by graphene quantum dots with different functional groups', *Journal of Environmental Sciences*, 77, pp. 198–209. Available at: https://doi.org/10.1016/j.jes.2018.07.014.

Zhou, Y. *et al.* (2017) 'How functional groups influence the ROS generation and cytotoxicity of graphene quantum dots', *Chemical Communications*, 53(76), pp. 10588–10591. Available at: https://doi.org/10.1039/C7CC04831A.

5

The Role of Molybdenum Disulfide (MoS_2) Materials in Mitigating the Toxicity of Heavy Metal Ions Towards *D. magna*

5.1 Introduction

Sulfur-containing materials have a high affinity to heavy metal ions (HMIs) through Lewis soft acid -soft base interactions, and as such have been widely studied and used as superior HMIs adsorbents (Wang *et al.*, 2020). Due to their sulfur-rich surface, the newly emerged mono-layered MoS_2 NMs, which are part of the family of two-dimensional (2D) transition metal dichalcogenides (TMDs) materials - one-layer-thick materials that undergo a quantum confinement effect that leads to a tunable band structure, high electron mobility, superconductivity, photoconductivity, and photothermal effects , have demonstrated excellent adsorption ability to remove HMIs from environmental systems (Gusain *et al.*, 2019; Sinha, Huang and Zhao, 2019; Li *et al.*, 2022).

Although MoS_2 NMs studies promise high metal ion adsorption performance, there is still a literature gap in understanding the effect of their physicochemical properties (e.g., redox potential, surface area, surface charge, size) on the removal efficiency of HMIs (Wang *et al.*, 2020). In addition, the potential impact of MoS_2 on the toxicity of HMIs to aquatic animals remains largely unknown as there is considerable literature uncertainty around mixture effects, especially mixtures containing nanomaterials (Martinez *et al.*, 2020, 2022) that needs attention in order to understand the diversity and complexity of the interaction of MoS_2 NMs with model organisms and biomolecules *in vivo* and ensure the safe application of these emerging materials.

Based on the identified knowledge gaps, our study aims to investigate the removal performance of the three different types of MoS_2 materials shown in Table 5.1, dispersed in HH combo medium to evaluate the effect of materials' properties on the removal efficiency of Cd^{+2} and Cu^{+2}. We also assessed the joint toxicity effects of the selected HMIs on the model organism *D. magna* in the presence and absence of MoS_2 and humic acid as an alternative binding source that is present in the environment and is well-known to act as a sink for pollutants altering their bioavailability and toxicity (Klučáková and Pavlíková, 2017; Wang *et al.,* 2020). This is the first study that provides insight into the heavy metal adsorption behaviour of MoS_2 NMs and the potential for ameliorating HMI toxicity through sorption to MoS_2 NMs, by exploring the mixture toxicity toward the model organism *D. magna*.

Table 5.1. Types of MoS_2 particles, as described by the supplier.

Material	Appearance	Diameter	Thickness	Synthesis method
Bulk (B-MoS_2)	Black powder	1.5 µm	Multi-layered	Exfoliation
Monolayer (L-MoS_2)	Black powder	0.2-5 µm	~ 1 nm	Lithium-based Intercalation
Nanosize Monolayer (S-MoS_2)	Black powder	20-500 nm	~ 1 nm	Lithium-based Intercalation

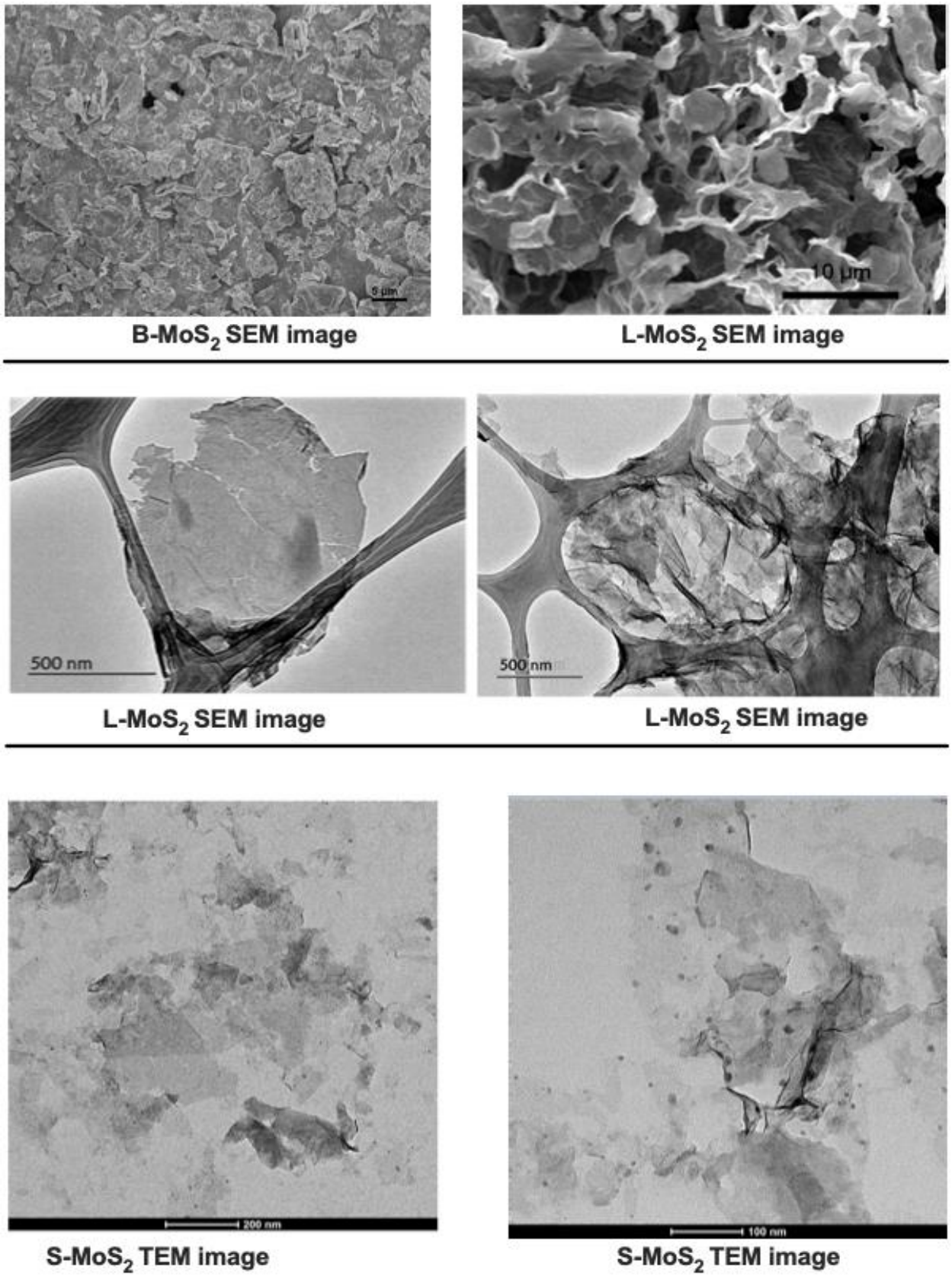

Figure 5.1. Characterization of MoS_2 provided by the supplier (MoS_2 ACS MATERIALS, no date).

5.2 Characterization

Evaluating the physico-chemical properties of NM, including their stability under the conditions of exposure, is an essential step in nanotoxicity assessments. Since *D. magna* are cultured in HH combo medium, it is important to monitor any transformation of the MoS_2 NMs in the culture medium, which can be driven by the medium components and the exposure conditions such as pH and ionic strength, therefore, influencing the fate and ecotoxicity mechanism of the NMs.

The effect of different media on the stability of the three studied MoS_2, was assessed by measuring the Z-average diameter (hydrodynamic size) and the surface charge (zeta potential) of particles in DI water, fresh HH combo and conditioned HH combo medium that had been filtered by daphnid neonates for 48 hours as described in Chapter 2. The analyses were carried out using dynamic light scattering (DLS). Samples were prepared as described in chapter 2 of this thesis (methodology) to obtain the hydrodynamic diameter (HD), polydispersity index (PDI) and zeta potential (ZP). Although DLS measurements are not capable of distinguishing van der Waals bonds (agglomeration) from strong chemical bonds (aggregation) events, and the actual size of non-spherical particles such as MoS_2 is not accurately represented by the hydrodynamic diameter (HD) values that result from DLS measurements, DLS can still be an interesting qualitative approach to evaluate changes in the physicochemical properties of non-spherical NMs, such as whether a protein corona is formed (Martinez *et al.*, 2020). The PDI can give an overall estimation of NMs stability over the timescale of the exposure to daphnids, as changes in polydispersity are correlated with agglomeration. TEM, SEM or AFM are better alternatives to observe the size and shape of non-spherical NMs, but due to time limitations, we were not able to perform these tests (TEM images will be included for the resulting publication).

The obtained PDI values (Figure 5.2) indicated that the bulk and both of the nano-sized MoS_2 showed much higher stability in DI water than in either of the fresh or conditioned HH combo media. Once the particles were incubated in the fresh culture medium, agglomeration and wider size distribution were observed in all particles. The agglomeration behaviour most likely resulted from the interaction of the NMs with the cationic species present in the culture medium, which can affect the repulsive and attractive energy between particles (Martinez *et al.*, 2020). The PDI values also indicated that the stability of all three particle types was increased in the conditioned HH combo medium compared to the fresh culture medium dispersions (Figure 5.2). The improvement in polydispersity was observed despite the low concentration of proteins found in the conditioned medium (as reported in Chapter 3), indicating that the conditioning step did change the characteristics of the particles and that a corona layer may have formed. The magnitude of this change in stability could increase further if more proteins were present.

The stability increase observed in the conditioned HH Combo medium is most likely related to the biomolecules that were secreted by *D. magna* and adsorbed onto the surface of NMs. This can promote steric repulsion forces between the particles, affecting the effectiveness of the compression of layers caused by the cations present in the culture medium (Martinez *et al.*, 2020). However, if a protein corona layer is formed, an increase in the HD value may be expected, due to the thickness of the layer of coated proteins and the potential for agglomeration by protein-protein interactions (Martinez *et al.*, 2020). This behaviour was only observed in the case of the S-MoS_2 NMs with the HD value increasing from 874.7 **±** 235.1 nm to 1006 **±** 541.4 nm in fresh and conditioned HH combo medium, respectively, indicating that the smaller-size MoS_2 NMs have a strong ability to bind proteins compared to the larger MoS_2 particles, which is consistent with their higher surface to volume ratio. In

fact, the average HD for both the B-MoS_2 and the L-MoS_2 was decreased in the conditioned medium compared to the fresh culture medium (Figure 5.2).

In colloidal systems, the ZP depends on the ionic strength of a solution at a given pH value and as the salt content increase in the solution, the ZP should decrease due to the compression of the electric double layer. The ZP values obtained in DI water were -34 **±** 0.404 mV (B-MoS_2), -42.2 **±** 1.27 mV (L-MoS_2) and -31.3 **±** 0.812 mV (S-MoS_2), indicating good electrostatic stability as al ZPs > **±** 30 mV. Those values were decreased to -17.2 **±** 1.05 mV (B-MoS_2), -16 **±** 0.723 mV (L-MoS_2) and -18 **±** 1.02 mV (S-MoS_2) in fresh HH combo medium, indicating a decrease in the electrostatic stability due to counterion interactions reducing the overall repulsion between particles. If a protein corona layer is formed, it can prevent the molecules of NMs to come into contact with each other, and due to the fact that many proteins are themselves slightly negatively charged or zwitterionic, the ZP of protein-coated NMs can be low / close to 0 but the steric stabilization prevents too much agglomeration (Martinez *et al.*, 2020). When the MoS_2 NMs were incubated in the conditioned culture medium, the ZP decreased further for all the studied particles compared to the ZP in the fresh medium; -15.4 **±** 1.080 mV (B-MoS_2), -12.6 **±** 0.557 mV (L-MoS_2) and -16.9 **±** 1.330 mV (S-MoS_2). Furthermore, the ZP of the MoS_2 materials was measured in combination with HMIs and HA, as these mixtures were applied in the adsorption and toxicity studies, and the surface charge of all mixture solutions (Figure 5.3). The ZP was either almost the same or slightly decreased negatively when HMIs were added compared to the solutions that had only bare MoS_2 materials in most cases for the B-MoS_2 and L-MoS_2. However, in the S-MoS_2 group, the ZP negatively increased when Cu^{+2} or Cd^{+2} were added to S-MoS_2 in the fresh HH combo medium compared to the solution that had bare S-MoS_2 (Figure 5.3).

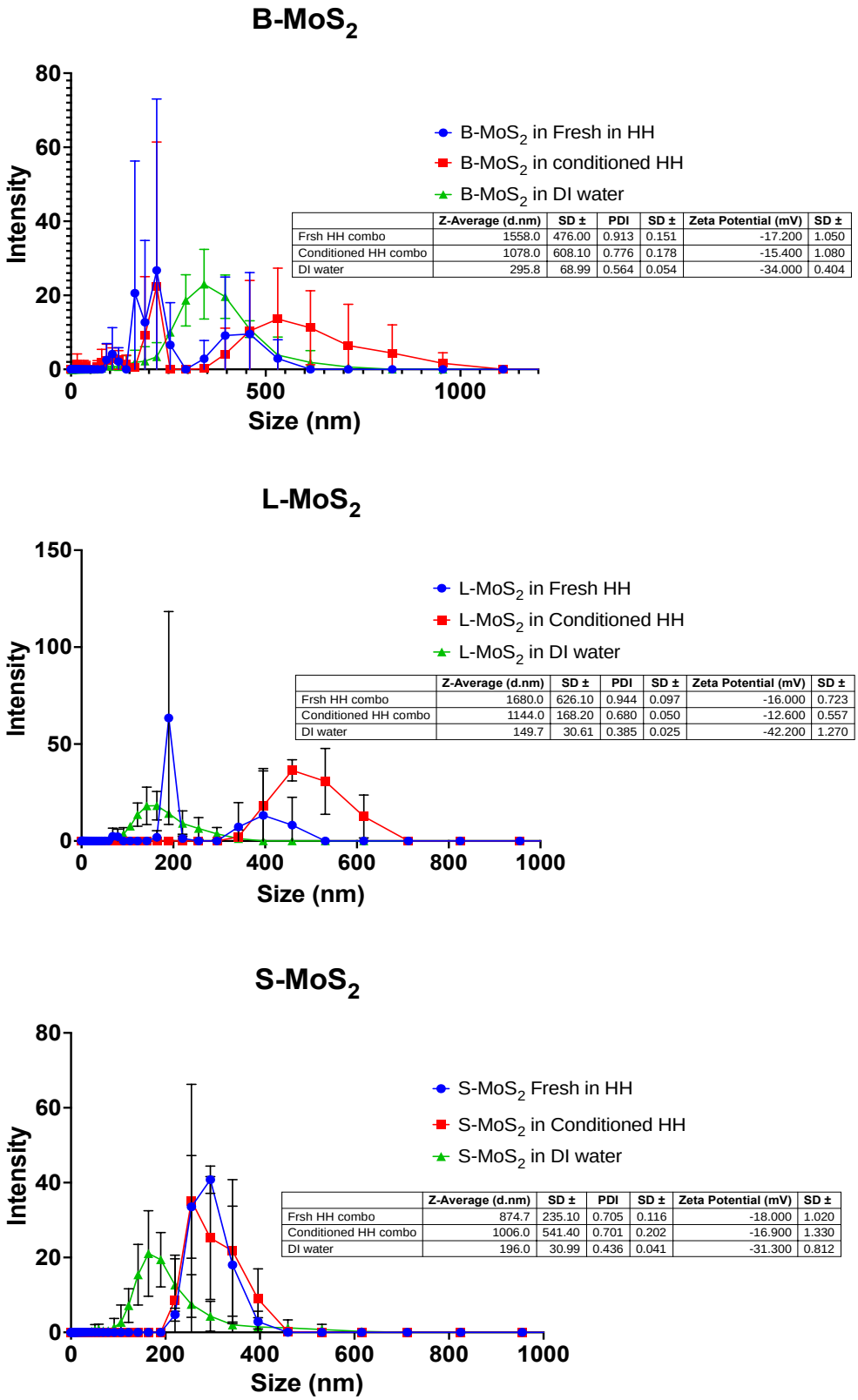

	Z-Average (d.nm)	SD ±	PDI	SD ±	Zeta Potential (mV)	SD ±
Frsh HH combo	1558.0	476.00	0.913	0.151	-17.200	1.050
Conditioned HH combo	1078.0	608.10	0.776	0.178	-15.400	1.080
DI water	295.8	68.99	0.564	0.054	-34.000	0.404

	Z-Average (d.nm)	SD ±	PDI	SD ±	Zeta Potential (mV)	SD ±
Frsh HH combo	1680.0	626.10	0.944	0.097	-16.000	0.723
Conditioned HH combo	1144.0	168.20	0.680	0.050	-12.600	0.557
DI water	149.7	30.61	0.385	0.025	-42.200	1.270

	Z-Average (d.nm)	SD ±	PDI	SD ±	Zeta Potential (mV)	SD ±
Frsh HH combo	874.7	235.10	0.705	0.116	-18.000	1.020
Conditioned HH combo	1006.0	541.40	0.701	0.202	-16.900	1.330
DI water	196.0	30.99	0.436	0.041	-31.300	0.812

Figure 5.2. The HD of the MoS_2 NMs measured by DLS in in different media (DI, HH Combo, conditioned HH Combo).

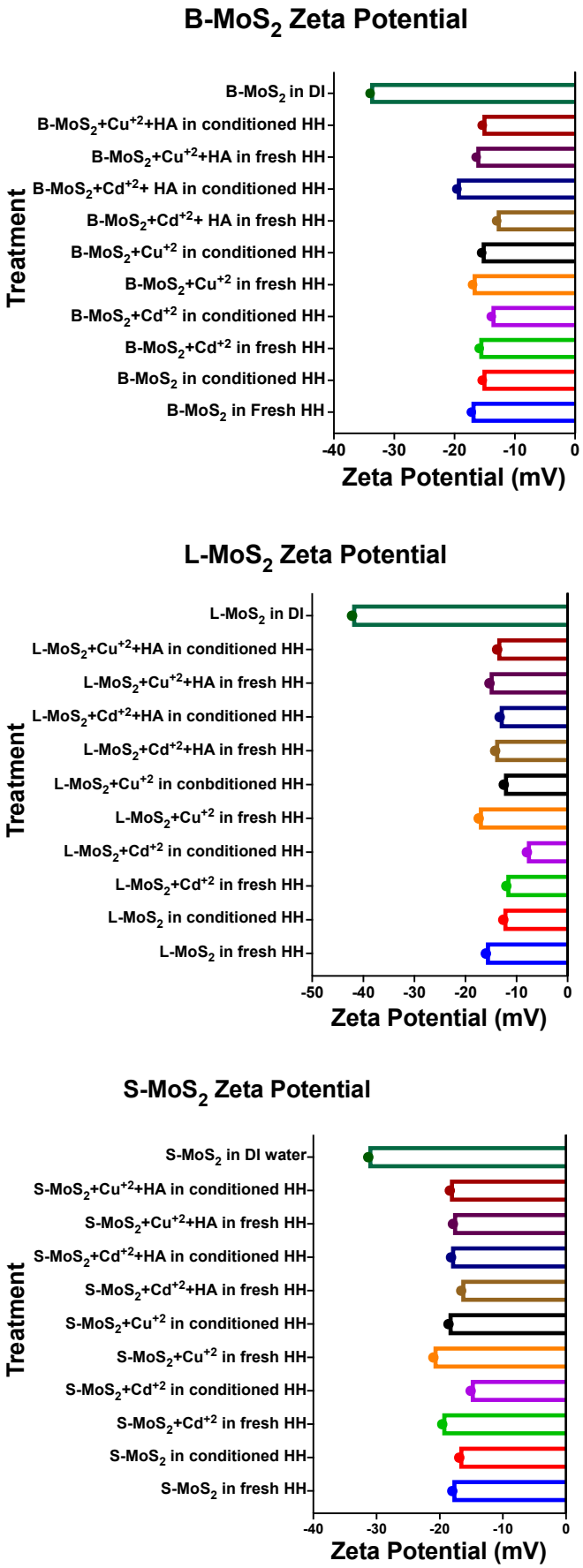

Figure 5.3. The zeta potential of MoS_2 measured by DLS in different media with HA and the HMI.

5.3 Toxicity of The MoS_2 NMs to *D. magna*

The 48h acute toxicity of the selected MoS_2 materials was assessed in fresh and conditioned HH combo medium. The results are the average of three repeated experiments and in each experiment, tested samples were performed in triplicate. The EC_{50} values were determined to be 594.9 and 598.5 mg/L (B-MoS_2), 226.9 and 230.5 mg/L (L-MoS_2), and 305.8 and 324.5 (S-MoS_2) in the fresh and conditioned medium, respectively (Figure 5.4) In all test groups, no mortality was observed up to 100 mg/L, which is the highest dose recommended by the OECD guideline for testing chemicals in ecotoxicity studies. This confirms the nontoxic nature of the studied MoS_2 particles towards *D. magna*. However, our results showed that the L-MoS_2 was the most toxic towards *D. magna* followed by the S-MoS_2 and B-MoS_2.

In chapter 3 of this thesis, we explored the medium conditioning protocol and concluded that the concentration of proteins acquired by this method is low compared to what has been reported in the literature. However, proteins do exist in the conditioned medium and it is interesting to explore the effect of these biomolecules secreted by *D. magna* on the toxicity of MoS_2, as different NMs have different abilities to adsorb proteins. In addition, MoS_2 nanosheets have high free surface energy, ultra-thin structure and a large surface area, enabling them to adsorb a large amount of proteins and easily penetrate biological membranes (Baimanov *et al.*, 2020). Their large surface area allows proteins to be adsorbed onto particles more easily than rod-like and spherical NMs, providing a flat surface for adsorbing and spreading proteins (Baimanov *et al.*, 2020). There is a small increase in EC_{50} values in the conditioned medium compared to the fresh medium in all tested groups indicating a decrease in toxicity (Figure 5.4). The EC_{50} values were increased by 0.6%, 1.5% and 5.7% for the B-MoS_2, L-MoS_2 and S-MoS_2, respectively. Interestingly, despite the low protein content in the conditioned medium, some effect was observed, and the smaller the

NM size, the more the EC_{50} was increased. This might be explained by the high surface area to volume ratio in NMs, and if a higher concentration of protein can be achieved by the conditioning method, an even greater effect could be observed.

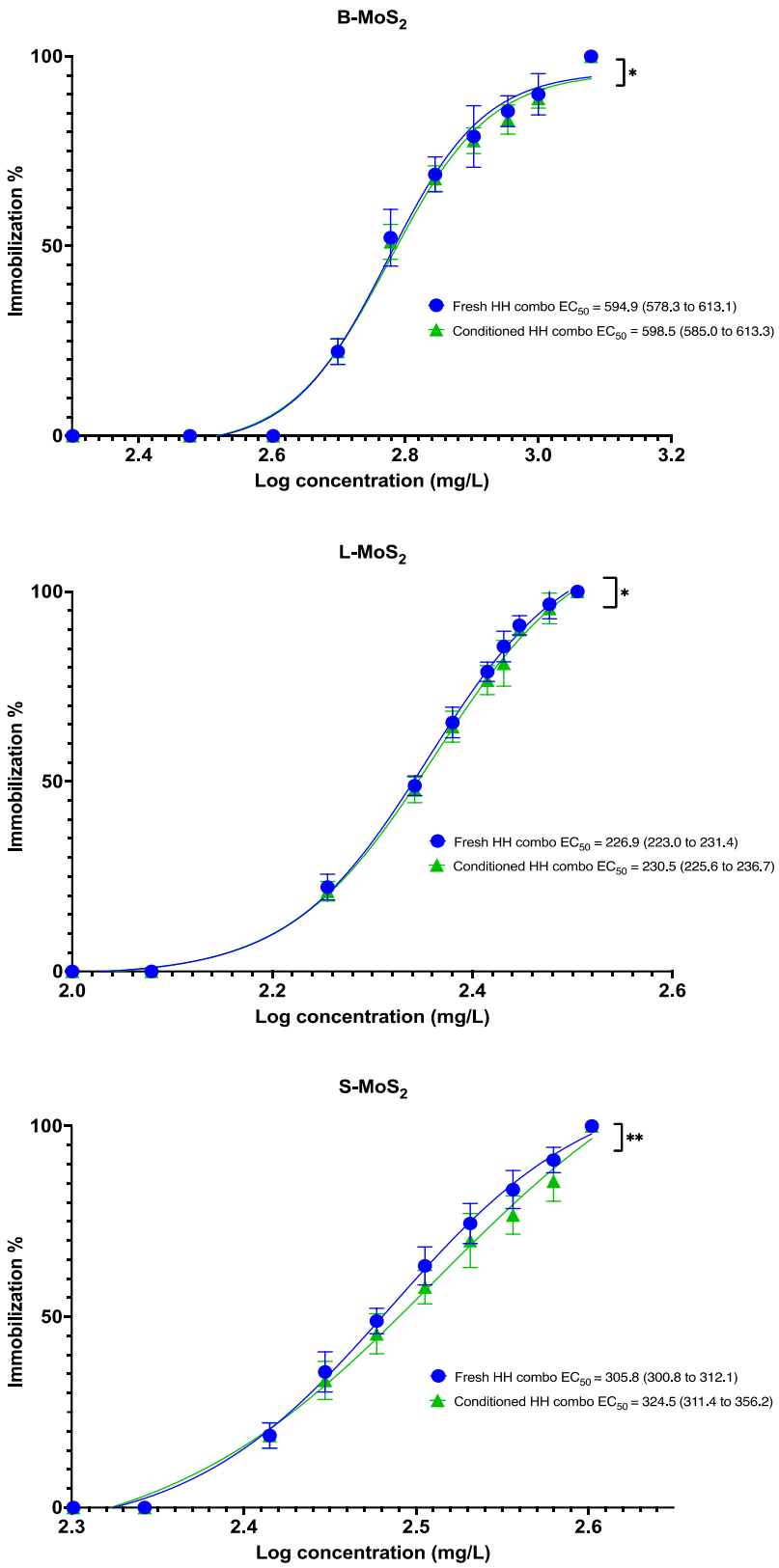

Figure 5.4. The 48h Acute toxicity of MoS_2 materials to D. magna in fresh versus conditioned HH Combo medium.

5.4 Heavy Metal Ions (HMI) Adsorption

In a batch adsorption experiment conducted on the three types of MoS_2, Cd^{+2} and Cu^{+2} were chosen as the model HMI species. The adsorption measurements were performed by varying the initial concentrations of Cd^{+2} and Cu^{+2} (0.05, 0.1, 0.5, and 1 mg/L) at two fixed MoS_2 concentrations (10 mg/L and 100 mg/L). The selected MoS_2 concentrations were based on the 48h acute toxicity results, as these concentrations caused 0% immobility in all tested groups, and as such were non-toxic. The concentrations of HMIs adsorbed onto MoS_2 materials were calculated, assuming a mass balance, by subtracting the final suspension concentration from the initial concentration. The analyses were conducted at two time points (3 h and 24 h).

In the ecosystem, salt cations and anions are present in wastewater effluents and other complex water environments, which can significantly affect the interaction and adsorption mechanism of adsorbent materials. Therefore, it is important to consider the impacts of salts and other constituents of the environment in ecotoxicity studies by applying realistic environmental conditions as much as possible. Since our toxicity tests are conducted on *D. magna* cultured in HH combo medium, all of the adsorption experiments were performed on samples suspended in freshly prepared HH combo medium (pH 7.7) to have a good correlation in the outcome of the adsorption analyses with that of the joint toxicity effects than would the case if the adsorption experiments were performed in DI water.

The adsorption amount (%) and adsorption capacity (Qe) were calculated for all analysed sample groups, as described in chapter 2 of this thesis.

B-MoS_2

At a concentration of 10 mg/L and 3h of incubating the B-MoS_2 with the HMIs, the average adsorption amounts were 19% and 32% of the exposure amount for Cd^{+2} (Table 5.2) and Cu^{+2} (Table 5.4), respectively. After 24 h of incubation, the average observed adsorption amounts were 21% and 25% for Cd^{+2} and Cu^{+2}, respectively, indicating a slight increase in Cd^{+2} adsorption and a decrease in Cu^{+2} average adsorption amount. When increasing the concentration of B-MoS_2 to 100 mg/L, the adsorption amount was 22% (Cd^{+2}) and 57% (Cu^{+2}) at 3 h (Tables 5.4 and 5.6, respectively). After 24 h, the rates remained the same for Cd^{+2} (22%) and increased to 64% for Cu^{+2}.

In all tested solutions, the adsorption amount increased when increasing the concentration of B-MoS_2 (Tables 5.3 – 5.5). Incubation time was not always a factor in increasing the adsorption amount of the HMIs onto B-MoS_2. The results also showed no direct link between increasing the concentration of HMIs and the adsorption amounts, suggesting saturation of the available binding sites. Overall, the adsorption amount was higher for Cu^{+2} than Cd^{+2}, with a maximum observed value of 90% and 28%, respectively, of the available HMIs onto the 100 mg/L B- MoS_2.

When looking at the adsorption capacity results, it was obvious that the Qe increased with increasing the concentrations of HMIs in all tested groups (Figure 5.5). This may be explained by what has been reported in the literature, for example, that the adsorption capacity increases when increasing the HMIs concentrations due to the higher gradient concentration acting as a driving force for overcoming the mass transfer resistance of ions between the solid and aqueous phases (Sevim *et al.*, 2021). The maximum Qe value observed in all B-MoS_2 mixtures was slightly higher for Cd^{+2} (6.7 mg/g) than Cu^{+2} (5.8 mg/g).

Table 5.2. The adsorption amount and adsorption capacity of 10 mg/L, B-MoS_2 for Cd^{2+} ions.

Cd + B-MoS_2 (10 mg/L)				
Concentration	**3h**		**24h**	
Cd (mg/L)	**Qe (mg/g)**	**Adsorption (%)**	**Qe (mg/g)**	**Adsorption (%)**
0.05	0.570178	**28%**	0.524483	**26%**
0.1	0.600840	**15%**	0.706650	**18%**
0.5	3.532128	**17%**	4.798797	**23%**
1.0	6.098473	**15%**	6.713597	**17%**
Average	2.700405	**19%**	3.185882	**21%**

Table 5.3. The adsorption amount and adsorption capacity of 100 mg/L, B-MoS_2 for Cd^{2+} ions.

Cd + B-MoS_2 (100 mg/L)				
Concentration	**3h**		**24h**	
Cd (mg/L)	**Qe (mg/g)**	**Adsorption (%)**	**Qe (mg/g)**	**Adsorption (%)**
0.05	0.043058	**21%**	0.056335	**28%**
0.1	0.058703	**15%**	0.072101	**18%**
0.5	0.579639	**28%**	0.524372	**26%**
1.0	0.996146	**25%**	0.739059	**18%**
Average	0.419387	**22%**	0.347967	**22%**

Table 5.4. The adsorption amount and adsorption capacity of 10 mg/L, B-MoS_2 for Cu^{2+} ions.

Cu + B-MoS_2 (10 mg/L)				
Concentration	**3h**		**24h**	
Cu (mg/L)	**Qe (mg/g)**	**Adsorption (%)**	**Qe (mg/g)**	**Adsorption (%)**
0.05	0.468035	**38%**	0.469612	**38%**
0.1	0.747725	**32%**	0.523974	**23%**
0.5	3.007515	**29%**	1.973265	**19%**
1.0	5.860586	**28%**	4.301004	**21%**
Average	2.520965	**32%**	1.816964	**25%**

Table 5.5. The adsorption amount and adsorption capacity of 100 mg/L, B-MoS_2 for Cu^{2+} ions.

Cu + B-MoS_2 (100 mg/L)				
Concentration	**3h**		**24h**	
Cu (mg/L)	**Qe (mg/g)**	**Adsorption (%)**	**Qe (mg/g)**	**Adsorption (%)**
0.05	0.094734	**77%**	0.110268	**90%**
0.1	0.141175	**61%**	0.184456	**79%**
0.5	0.442114	**42%**	0.498686	**47%**
1.0	1.003164	**48%**	0.813736	**39%**
Average	0.420297	**57%**	0.401787	**64%**

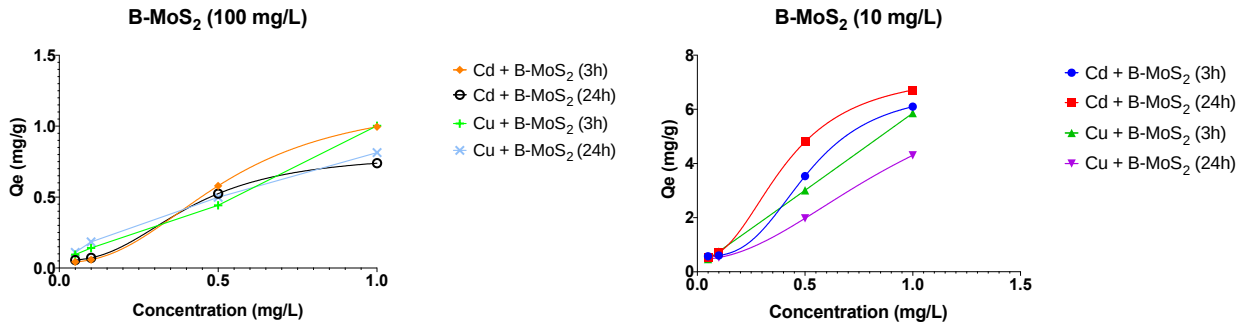

Figure 5.5. The relationship between the adsorption capacity (Qe) and the concentration of HMIs in B-MoS_2 mixture solutions.

L-MoS_2

The average adsorption amount increased with increasing incubation time in all tested groups (Tables 5.6 – 5.9). The average adsorbed amounts also increased when increasing the L-MoS_2 concentration in all tested groups, with the exception of one group where the adsorption amount remained the same (Cd^{+2} + L-MoS_2 at 24 h). A decrease in the adsorption amount was observed when increasing the concentration of both HMIs in most treatments. It was clear that the L-MoS_2 was able to remove Cu^{+2} more effectively than Cd^{+2} from the HH combo solutions with maximum observed rate of 100% and 54% respectively.

Similar to what has been observed with the Bulk MoS_2 analyses, the Qe values of the L-MoS_2 increased with increasing both HMIs concentrations in all tested groups (Figure 5.6). The average adsorption capacity was higher for Cd^{+2} than Cu^{+2}, with a maximum observed Qe value of 11.4 mg/g and 8.8 mg/g for the respective HMIs.

Table 5.6. The adsorption amount and adsorption capacity of 10 mg/L L-MoS_2 for Cd^{2+} ions.

Cd + L-MoS_2 (10 mg/L)				
Concentration	**3h**		**24h**	
Cd (mg/L)	**Qe (mg/g)**	**Adsorption (%)**	**Qe (mg/g)**	**Adsorption (%)**
0.05	0.787659	**39%**	1.096607	**54%**
0.1	1.227426	**31%**	1.507787	**38%**
0.5	6.449057	**32%**	5.982488	**29%**
1.0	11.463743	**28%**	9.639419	**24%**
Average	4.981971	**32%**	4.556575	**36%**

Table 5.7. The adsorption amount and adsorption capacity of 100 mg/L L-MoS_2 for Cd^{2+} ions.

Cd + L-MoS_2 (100 mg/L)				
Concentration	**3h**		**24h**	
Cd (mg/L)	**Qe (mg/g)**	**Adsorption (%)**	**Qe (mg/g)**	**Adsorption (%)**
0.05	0.068848	**34%**	0.077167	**38%**
0.1	Sample error	Sample error	0.143136	**36%**
0.5	0.731761	**36%**	0.684097	**34%**
1.0	Sample error	Sample error	1.453645	**36%**
Average	0.400305	**35%**	0.589511	**36%**

Table 5.8. The adsorption amount and adsorption capacity of 10 mg/L L-MoS_2 for Cu^{2+} ions.

Cu + L-MoS_2 (10 mg/L)				
Concentration	**3h**		**24h**	
Cu (mg/L)	**Qe (mg/g)**	**Adsorption (%)**	**Qe (mg/g)**	**Adsorption (%)**
0.05	1.031706	**84%**	1.257747	**100%**
0.1	1.820639	**78%**	2.126347	**91%**
0.5	5.479880	**52%**	4.500132	**43%**
1.0	8.857722	**43%**	6.800075	**33%**
Average	4.297487	**64%**	3.671075	**67%**

Table 5.9. The adsorption amount and adsorption capacity of 100 mg/L L-MoS_2 for Cu^{2+} ions.

Cu + L-MoS_2 (100 mg/L)				
Concentration	**3h**		**24h**	
Cu (mg/L)	**Qe (mg/g)**	**Adsorption (%)**	**Qe (mg/g)**	**Adsorption (%)**
0.05	0.114714	**94%**	0.129554	**100%**
0.1	0.203345	**87%**	0.235756	**100%**
0.5	0.816477	**78%**	0.938765	**89%**
1.0	2.057184	**99%**	2.086029	**100%**
Average	0.797930	**90%**	0.847526	**97%**

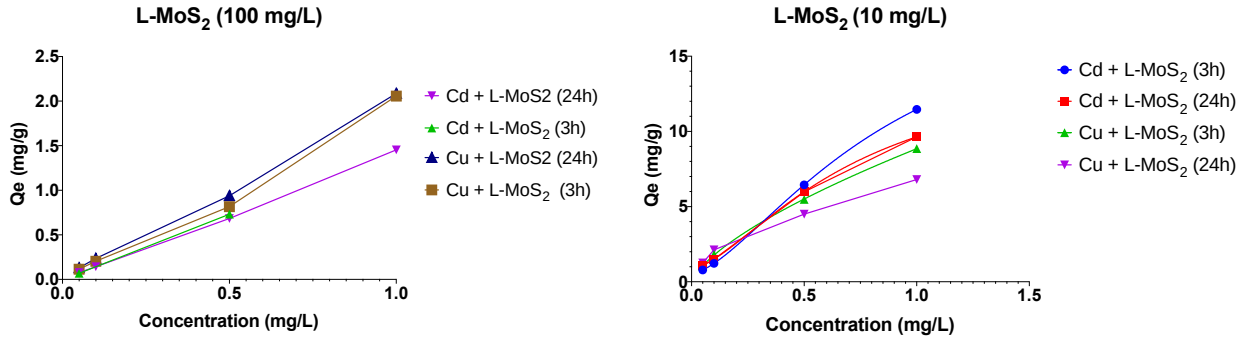

Figure 5.6. The relationship between the adsorption capacity (Qe) and the concentration of HMIs in L-MoS_2 mixture solutions.

S-MoS_2

Interestingly, the adsorption rate analyses of the S-MoS_2 showed a 100% removal of both HMIs from HH combo medium in all the tested samples, indicating a high removal efficiency of both selected metals (Tables 5.10 – 5.13). The time and concentrations of all tested chemicals had no effect on the adsorption amount.

Similar to the previously tested MoS_2 materials, the adsorption capacity of the S-MoS_2 was increased by increasing both HMIs concentrations (Figure 5.7). However, no time effect was

observed compared to the larger MoS_2 materials, as the Qe values remained almost the same when increasing the incubation time in all group treatments. The calculated Qe values were higher for Cd^{+2} than for Cu^{+2}, with the maximum adsorption capacity reaching 40.59 mg/g (Cd^{+2}) and 20.8 mg/g (Cu^{+2}).

Table 5.10. The adsorption amount and adsorption capacity (Qe) of 10 mg/L S-MoS_2 for Cd^{2+} ions.

Cd + S-MoS_2 (10 mg/L)				
Concentration	**3h**		**24h**	
Cd (mg/L)	**Qe (mg/g)**	**Adsorption (%)**	**Qe (mg/g)**	**Adsorption (%)**
0.05	2.044395	**100%**	2.099149	**100%**
0.1	3.930993	**100%**	3.986432	**100%**
0.5	20.420810	**100%**	20.476041	**100%**
1.0	40.542848	**100%**	40.597645	**100%**
Average	16.734761	**100%**	16.789817	**100%**

Table 5.11. The adsorption amount and adsorption capacity (Qe) of 100 mg/L S-MoS_2 for Cd^{2+} ions.

Cd + S-MoS_2 (100 mg/L)				
Concentration	**3h**		**24h**	
Cd (mg/L)	**Qe (mg/g)**	**Adsorption (%)**	**Qe (mg/g)**	**Adsorption (%)**
0.05	0.204442	**100%**	0.209950	**100%**
0.1	0.393136	**100%**	0.398683	**100%**
0.5	2.042122	**100%**	2.047562	**100%**
1.0	4.054277	**100%**	4.059634	**100%**
Average	1.673494	**100%**	1.678957	**100%**

Table 5.12. The adsorption amount and adsorption capacity (Qe) of 10 mg/L S-MoS_2 for Cu^{2+} ions.

Cu + S-MoS_2 (10 mg/L)				
Concentration	**3h**		**24h**	
Cu (mg/L)	**Qe (mg/g)**	**Adsorption (%)**	**Qe (mg/g)**	**Adsorption (%)**
0.05	1.242239	**100%**	1.378807	**100%**
0.1	2.348792	**100%**	2.483186	**100%**
0.5	10.536229	**100%**	10.674259	**100%**
1.0	20.727375	**100%**	20.860679	**100%**
Average	8.713659	**100%**	8.849233	**100%**

Table 5.13. The adsorption amount and adsorption capacity (Qe) of 100 mg/L S-MoS_2 for Cu^{2+} ions.

Cu + S-MoS_2 (100 mg/L)				
Concentration	**3h**		**24h**	
Cu (mg/L)	**Qe (mg/g)**	**Adsorption (%)**	**Qe (mg/g)**	**Adsorption (%)**
0.05	0.124343	**100%**	0.137845	**100%**
0.1	0.234863	**100%**	0.248494	**100%**
0.5	1.053775	**100%**	1.067369	**100%**
1.0	2.072555	**100%**	2.086226	**100%**
Average	0.871384	**100%**	0.884984	**100%**

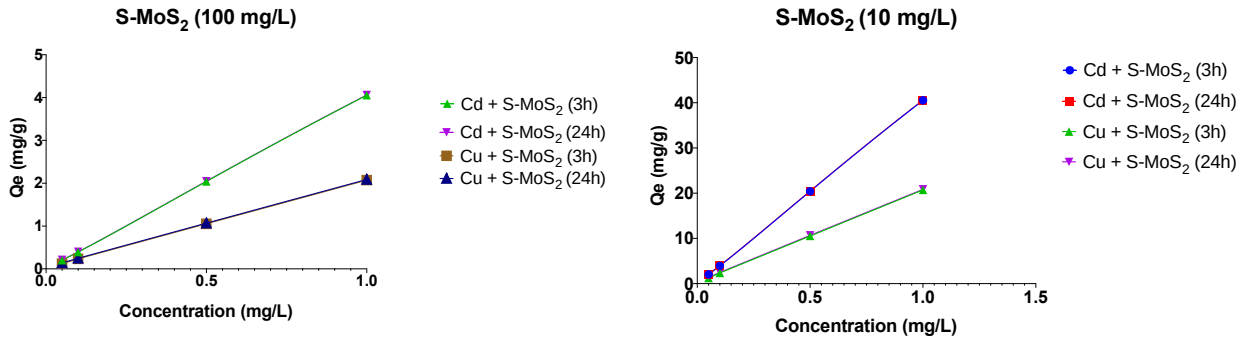

Figure 5.7. The relationship between the adsorption capacity (Qe) and concentration of HMIs in S-MoS_2 mixture solutions.

It can be concluded that MoS_2 can effectively remove HMIs from HH combo medium with the removed among depending on the size and concentration of absorbent as well as the type of metal ions. It is believed that most MoS_2 materials can remove HMIs through adsorption or redox reactions to some extent, depending on the metal's relative redox potential.

Our observations indicated that, at constant mass of particles, the smaller the MoS_2 particle size the greater the adsorption efficiency, which is consistent with the increased surface area of smaller particles relative to larger ones, leading to a high area for binding. MoS_2 in its bulk form is rarely used in adsorption applications, due to the small free spacing between its neighbouring layers (0.3-0.63 nm), limiting the access of free ions to the inner sulfur atoms (Wang *et al.*, 2018, 2020). The higher removal capacity of the two-dimensional MoS_2 nanosheets can be related to the sulfur atoms existing on both sides of a MoS_2 nanosheet which offers large accessible adsorption sites (Wang *et al.*, 2018; Baimanov *et al.*, 2020). Our study showed that the removal efficiency of MoS_2 for Cu^{+2} was better than for Cd^{+2} in most cases. This is consistent with the findings of (Wang *et al.*, 2020), who studied the adsorption affinity of MoS_2 nanosheets towards several HMIs and demonstrated that the selectivity of MoS_2 followed the order $Pb^{+2} > Cu^{+2} >> Cd^{+2} > Zn^{+2}$. They stated that 100 mg/L MoS_2 nanosheets almost completely removed Cu^{+2} and removed 90% of Cd^{+2}. The S-Mo-S monolayer MoS_2 nanosheets are stacked by weak van der Waals forces along the c-axis. The layer spacing in nanosheets is larger than the bulk materials providing a gap that can expose more S active sites and improve ion intercalation, improving the removal efficiency.

From the adsorption observations, it can be predicted that the ecotoxicity of HMIs would be affected due to the decrease of available free HMIs after being adsorbed by MoS_2.

Additionally, the concentration of MoS_2 could also impact the biotoxicity of HMIs. Therefore, in the next section, we explored the toxic behaviour of HMIs in combination with the three types of MoS_2 as well as with humic acid (HA), which is known to reduce the toxicity of HMIs by binding them and reducing their bioavailability, and thus it would be interesting to compare the HMI-toxicity reduction behaviour of HA with MoS_2 materials.

5.5 Mixture Toxicity of MoS_2 and HMIs

The acute toxicity of Cd^{+2} (0.001, 0.01, 0.05, 0.1, 0.5, 1, 1.5 mg/L) and Cu^{+2} (0.01, 0.05, 0.1, 0.5, 1 mg/L) in combination with the three types of MoS_2 materials was assessed in the presence and absence of humic acid (20 mg/L). The chosen HA concentration was based on what has been reported in the literature, of 20 mg/L representing the HA concentration found in typical surface and groundwaters (Clemente *et al.*, 2019). The immobility of daphnids was recorded after 24 h and 48 h of incubation. In a preliminary study, we identified the EC_{50} concentrations for both heavy metal ions in the presence and absence of HA.

First, the 48 h acute toxicity of HA alone (20 mg/L) mixed with both HMIs was assessed. Then the acute toxicity of HMIs in combination with two fixed concentrations (10 and 100 mg/L) of all three MoS_2 materials in the presence and absence of HA is presented. The fixed MoS_2 concentrations are the same concentrations as used in the batch adsorption experiment based on the 48h acute toxicity results. Then, the % of immobilized *D. magna* at 24 and 48 h will be correlated with the adsorption analysis.

The 48 h EC_{50} values for Cd^{+2} and Cu^{+2} towards *D. magna* were determined to be 0.08906 mg/L and 0.1003 mg/L, respectively, and once rounding the significant figures both HMIs had the same EC_{50} value (0.1 mg/L). In the presence of HA alone, the immobility of animals

recorded for Cd^{+2} treatments was largely reduced, and no mortality was observed at concentrations up to 0.5 mg/L, and with 30% immobilized neonates observed at the highest tested concentration (1.5 mg/L) as shown in (Figure 5.8). The mixture treatment of Cu^{+2} and HA showed a similar effect, with 0% mortality up to 0.5 mg/L of HMIs and 16 % immobilized animals recorded at the highest tested concentration (1 mg/L) (Figure 5.8).

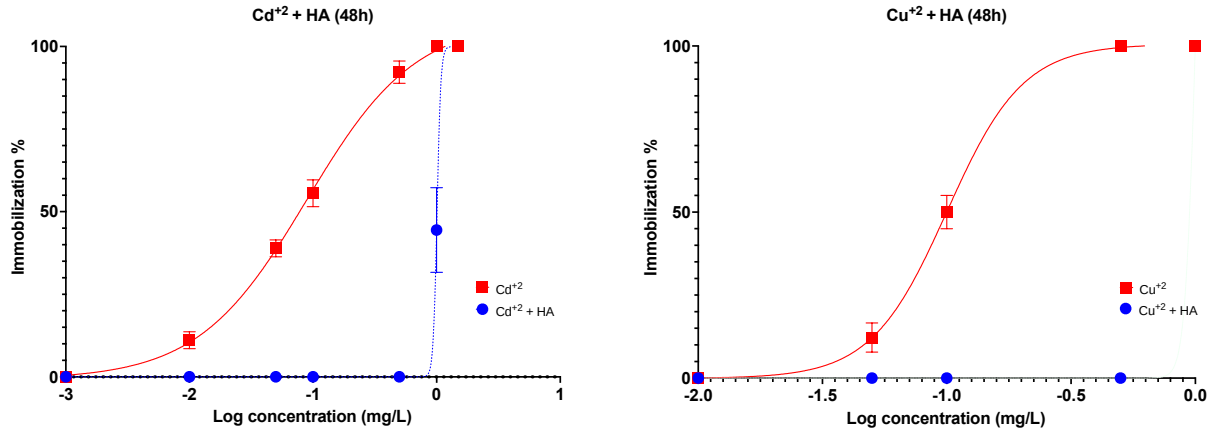

Figure 5.8. The acute toxicity of Cd^{+2} or Cu^{+2} in the presence/absence of HA (in mg/L).

B-MoS_2

In the presence of B-MoS_2 (10 mg/L), the EC_{50} value of Cd^{+2} was increased from 0.1 to 0.6 mg/L. The acute toxicity was even further decreased more when the concentration of B-MoS_2 increased to 100 mg/L (Figure 5.9). The addition of HA to the tested solutions decreased the immobilization rate of animals to 0% in all the exposure concentrations. The Cu^{+2}, in combination with 10 mg/L B-MoS_2, showed an increase in the EC_{50} of the metal ion from 0.1 to 0.2 mg/L, and the 100 mg/L B-MoS_2 also increased the EC_{50} of Cu^{+2} to 0.2 mg/L.

In the 10 mg/L B-MoS_2 mixtures, the acute toxicity of Cd^{+2} was reduced more efficiently than Cu^{+2}, and the decrease in toxicity relatively improved when increasing the B-MoS_2 concentration (Figure 5.9). The presence of HA with B-MoS_2 (10 and 100 mg/L) totally eliminated the acute toxicity of both HMIs.

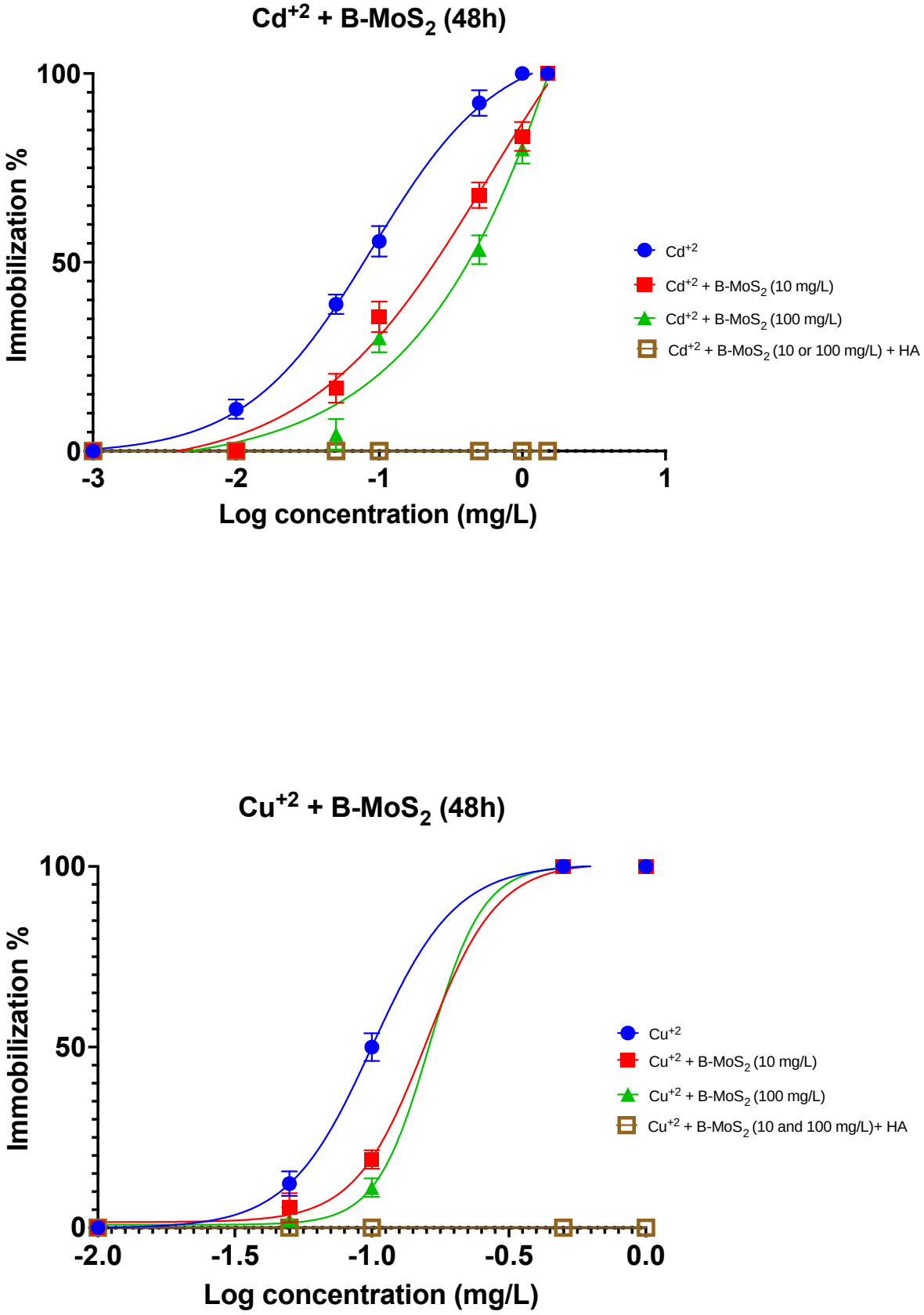

Figure 5.9. The acute toxicity of B-MoS_2 mixture solutions with Cd^{+2} or Cu^{+2} in the presence/absence of HA (in mg/L).

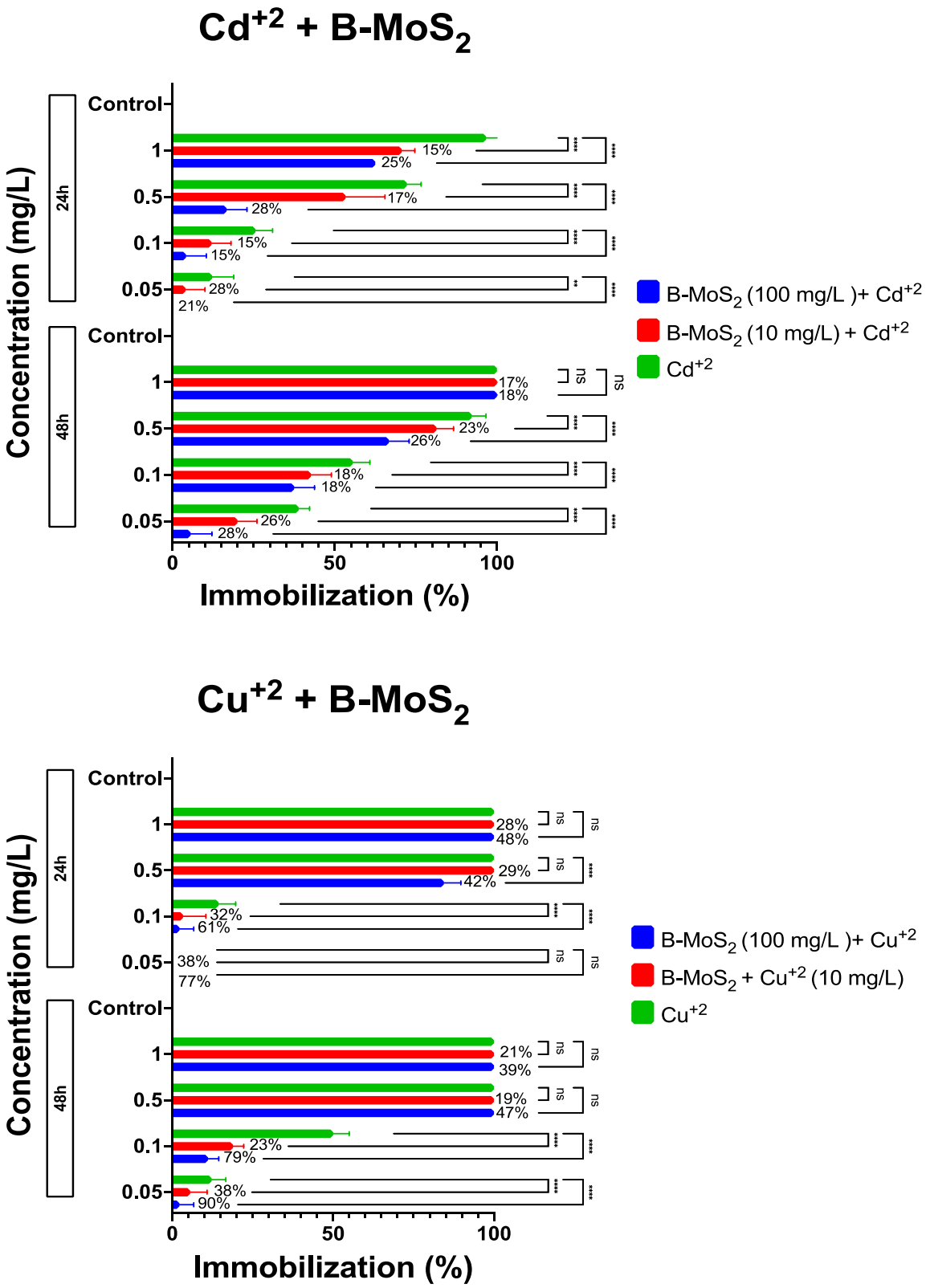

Figure 5.10. The % of immobilized D. magna in B-MoS_2 – HMI mixture solutions. The % values alongside each bar represent the adsorption amount of the same treatment. The 3h adsorption amounts are correlated with the 24 h immobility% and the 24 h adsorption amounts are correlated with the 48h immobility%. The statistical significance was calculated by a two-way ANOVA test [0.1234 (not significant, ns), 0.0332 (*), 0.0021 (**), 0.0002 (***), <0.0001 (****)], comparing the immobilization % of the HMI alone with two mixture solutions (HMI + 10 mg/L MoS_2 and HMI with 100 mg/L MoS_2).

L-MoS_2

The smaller size L-MoS_2 (10 mg/L) increased the EC_{50} of HMIs by 125% and 292% for Cd^{+2} and Cu^{+2}, respectively (Figure 5.11). While the higher concentration of L-MoS_2 increased the EC_{50} values by 511% and 370% for the metals, respectively. At 10 mg/L, the L-MoS_2 reduced the toxicity of Cu^{+2} more than Cd^{+2}, while at 100 mg/L, the acute toxicity reduction was better for Cd^{+2} than Cu^{+2}. The addition of HA to the L-MoS_2 totally eliminated the immobilization of animals (Figure 5.11). These results showed that the increase in L-MoS_2 concentration improved the toxicity reduction but changed the toxicity reduction efficiency between the two HMIs towards *D. magna*.

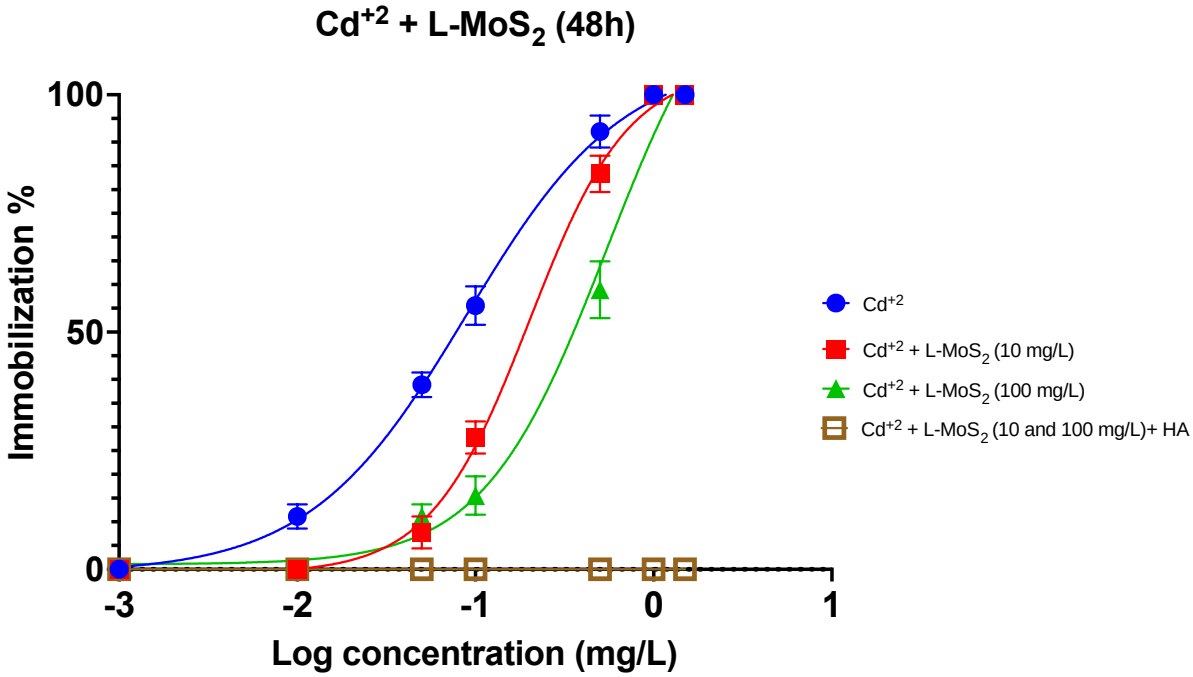

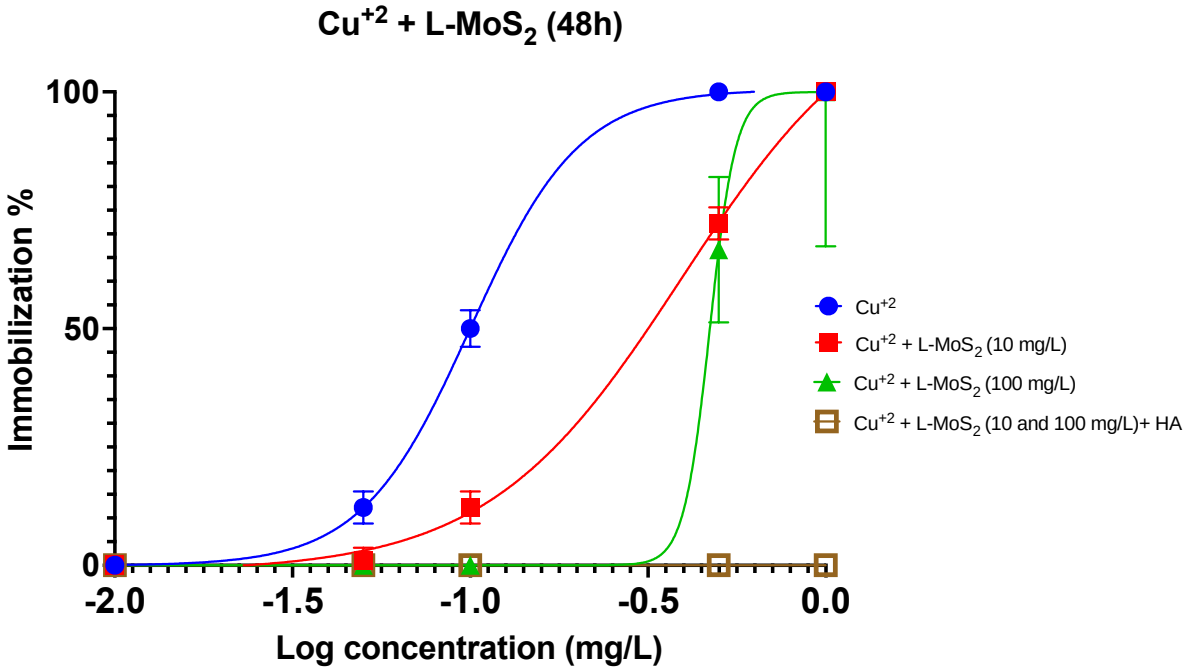

Figure 5.11. The acute toxicity of L-MoS_2 mixture solutions with Cd^{+2} or Cu^{+2} in the presence/absence of HA (in mg/L).

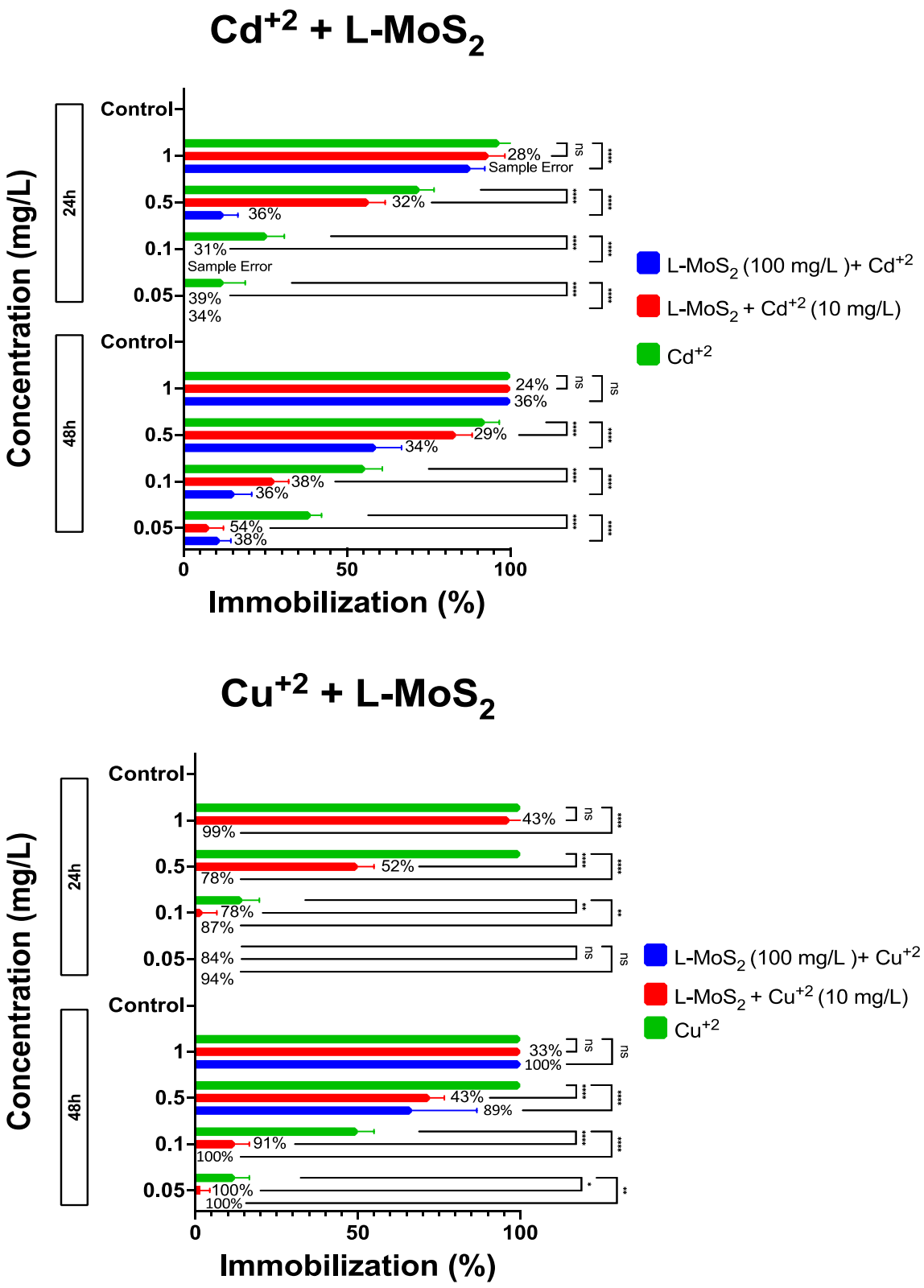

Figure 5.12. The % of immobilized D. magna in L-MoS_2 -HMI mixture solutions. The % values alongside each bar represent the amount of the HMI adsorbed to the L-MoS_2 particles of the same treatment. The 3h adsorption amounts are correlated with the 24h immobility% and the 24h adsorption amounts are correlated with the 48h immobility%. The statistical significance was calculated by a two-way ANOVA test [0.1234 (ns), 0.0332 (*), 0.0021 (**), 0.0002 (***), <0.0001 (****)], comparing the immobilization % of the HMI alone with two mixture solutions (HMI + 10 mg/L MoS_2 and HMI with 100 mg/L MoS_2).

S-MoS_2

In the S-MoS_2 (10 mg/L) nanosheets treatments, the EC_{50} of HMIs was increased by 159% (Cd^{+2}) and 1266 % (Cu^{+2}), indicating a better reduction in toxicity of Cu^{+2} compared to Cd^{+2}. At 100 mg/L, the magnitude of S-MoS_2 acute toxicity reduction was increased to 848% in Cd^{+2} solutions, whilst no toxicity was observed for the Cu^{+2} at all, with 0% immobilization in *D. magna* (Figure 5.13). In combination with the S-MoS_2 (10 and 100 mg/L), the HA totally eliminated the acute toxicity towards animals for both HMIs in all tested solutions.

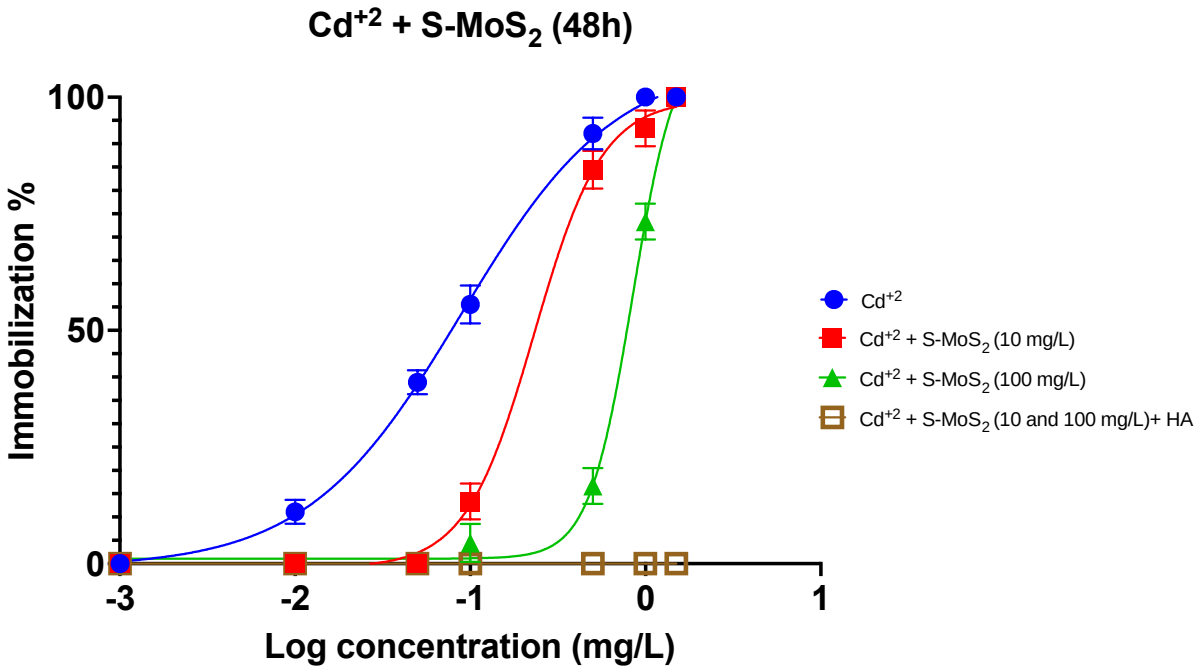

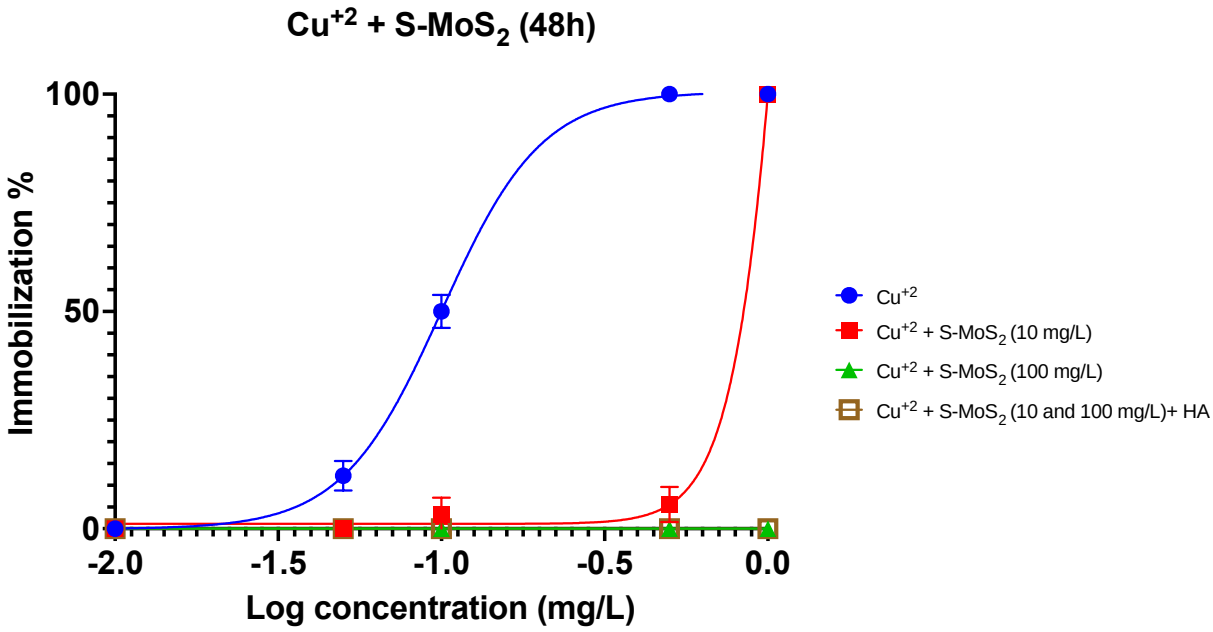

Figure 5.13. The acute toxicity of S-MoS_2 mixture solutions with Cd^{+2} or Cu^{+2} in the presence/absence of HA (in mg/L).

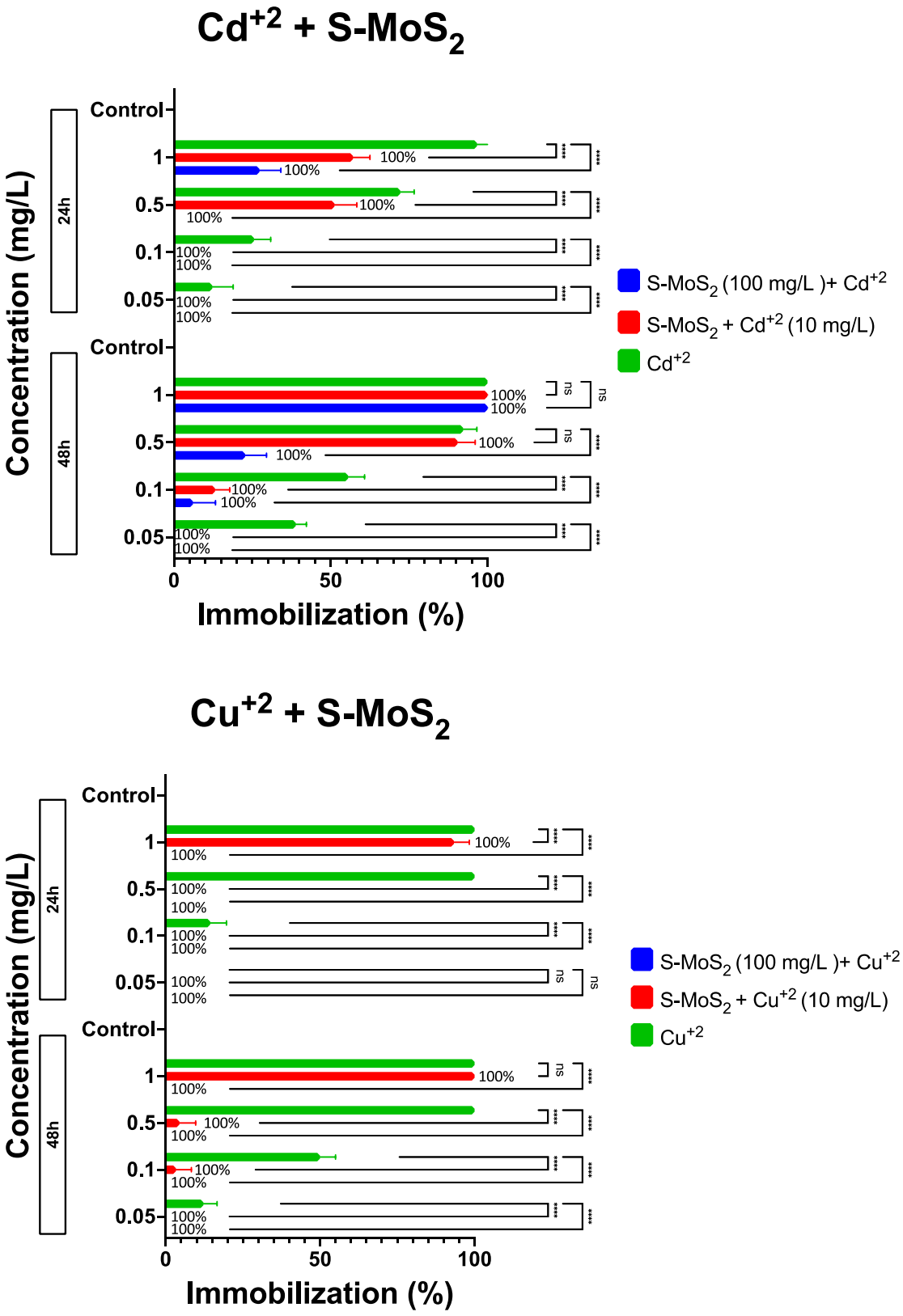

Figure 5.14. The % of immobilized D. magna in S-MoS_2 - HMI mixture solutions. The % values alongside each bar represent the adsorption amount of the same treatment. The 3h adsorption rates are correlated with the 24h immobility% and the 24h adsorption rates are correlated with the 48h immobility%. The statical significance was calculated by a two-way ANOVA test [0.1234 (ns), 0.0332 (*), 0.0021 (**), 0.0002 (***), <0.0001 (****)], comparing the immobilization % of the HMI alone with two mixture solutions (HMI + 10 mg/L MoS_2 and HMI with 100 mg/L MoS_2).

5.6 Accumulation of HMIs in *D. magna* Tissue

This was not a systematic test, as the concentrations of HMIs here are not always comparable between tested groups. This experiment was conducted to gain insight into the accumulation behaviour of the selected metals in combination with MoS_2 or HA as a preliminary study for future work. A better approach for future studies is to use the EC_{50} concentrations and increase the number of tested animals per replicate (e.g., 50 neonates for each replicate).

Only one fixed MoS_2 concentration (100 mg/L) was selected for this test. In each tested group, the concentration of HMIs after adsorption (metal ions left in HH combo after 3h and 24 of incubation with MoS_2 materials) was recorded. The same mixture solution was then freshly prepared and exposed to 10 *D. magna* neonates in triplicate following the 48 h acute toxicity protocol. A depuration step was then performed by moving the exposed daphnids into a fresh medium for 3 hours and allowing some time for their guts to empty, following which the tissue homogenate (whole-body burden) of neonates was acid digested and analysed by ICP-MS as described in chapter 2. The concentrations of metal ions were also measured for the exposure solutions (containing ions left after 48h MoS_2 adsorption + animal uptake) and the deputation solution. HMIs alone and HA combined with Cd^{+2} or Cu^{+2} were also assessed for bioaccumulation. In each tested group, the concentrations of HMIs in mg/L were presented in a part of a whole diagram to visualize the rate of present ions in each solution.

B-MoS_2

In the B-MoS_2 and Cd^{+2} mixture group, the amount of HMI present followed the order [MoS_2 + HMIs (3h)] > [MoS_2 + HMIs (24h)] > exposure solutions (at the end of the exposure period) > tissue homogenate > depuration solution (Figure 5.15). The amount adsorbed by MoS_2 at 3 h and 24 h is the results from the previous adsorption tests.

The B-MoS_2 combined with Cu^{+2} followed the same order, and the amount of uptake was larger than the amount of depuration for both metals (Figure 5.15). However, the amount of Cu^{+2} accumulated in *D. magna* after depuration was greater than that of Cd^{+2}, although in the previous adsorption analyses, the removal of Cu^{+2} by B-MoS_2 at this concentration was higher than the removal of Cd^{+2} and the reduction in HMIs toxicity by B-MoS_2 at this concentration was higher for Cu^{+2} than Cd^{+2} meaning that increased binding may have increased the uptake of HMIs.

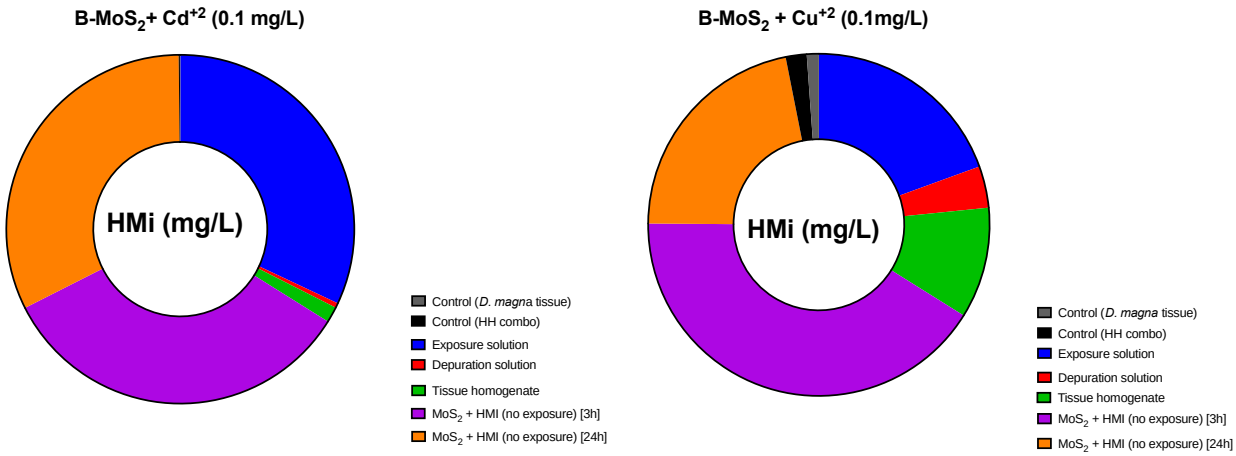

Figure 5.15. Concentrations of HMIs detected in the B-MoS_2 mixture tests – D. magna tissue, depurated solution, exposure solution at the end of the exposure experiment, and associated with (bound to) to particles.

L-MoS_2

The concentrations of Cd^{+2} found in the L-MoS_2 mixtures were in the order of; exposure solutions (at the end of the exposure period) > [MoS_2 + HMIs (3h)] > [MoS_2 + HMIs (24h)] > tissue homogenate > depuration solution (Figure 5.16). The results indicated that the presence of daphnids reduced the adsorption efficiency of L-MoS_2.

In the L-MoS_2 and Cu^{+2} mixture solutions, the order was [MoS_2 + HMIs (3h)] > tissue homogenate > [MoS_2 + HMIs (24h)] > exposure solutions (at the end of the exposure period) > depuration solution, indicating that most of Cu^{+2} ions were accumulated in the body of the daphnids in this case (Figure 5.16).

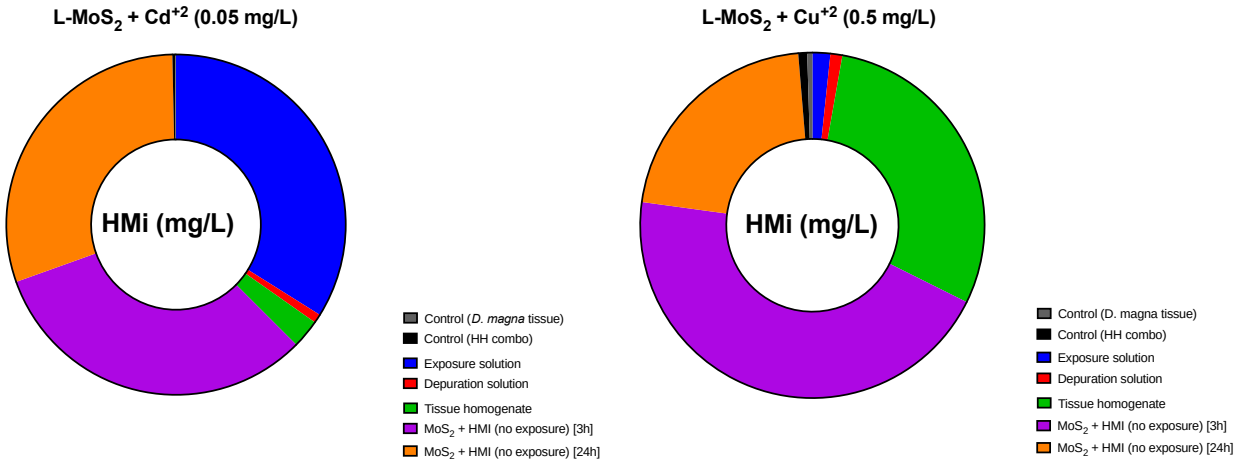

Figure 5.16. Concentrations of HMIs detected in the L-MoS_2 mixture tests - D. magna tissue, depurated solution, exposure solution at the end of the exposure experiment, and associated with (bound to) to particles.

S- MoS_2

The analyses from the S-MoS_2 and Cd^{+2} mixtures showed the following order: exposure solution (at the end of the exposure period) > tissue homogenate > depuration solution (Figure 5.17). Surprisingly, the presence of *D. magna* extremely interrupted the adsorption of Cd^{+2} onto the S-MoS_2, as in the adsorption analyses, 100 % of Cd^{+2} were removed from the solution, while here, most of the ions were found in the exposure solutions rather than being bound to the particles.

On the other hand, the order of detected metal ions when the S-MoS_2 was mixed with Cu^{+2} was; tissue homogenate > exposure solution > depuration solution. It was clear that the presence of animals interrupted the adsorption of Cu^{+2} onto the S-MoS_2, and most of the metal ions were accumulated in the body burden of daphnids. Although the immobilization rate of animals was significantly reduced in this mixture with 0% immobile daphnids.

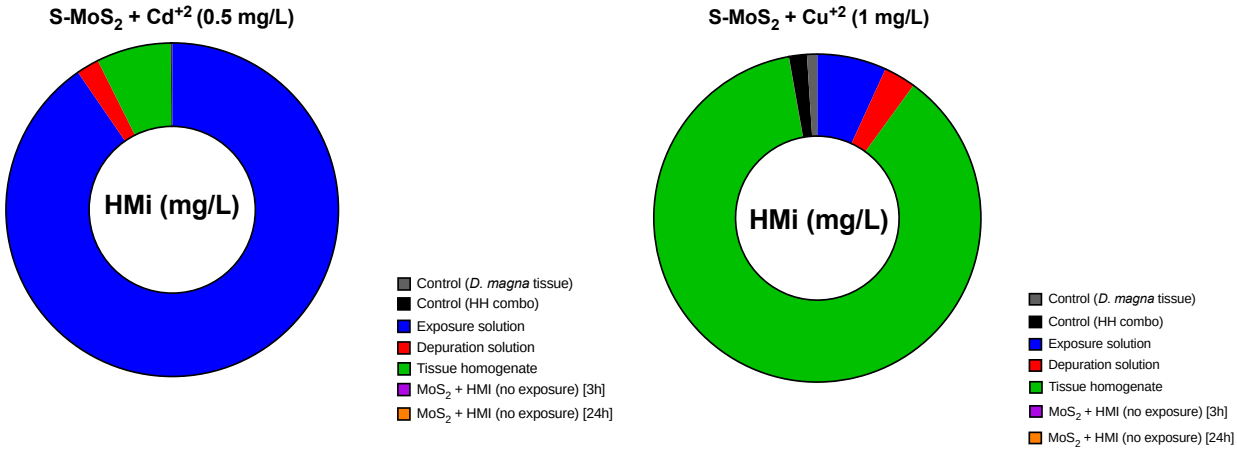

Figure 5.17. Concentrations of HMIs detected in the S-MoS_2 mixture tests - D. magna tissue, depurated solution, exposure solution at the end of the exposure experiment, and associated with (bound to) to particles.

HA

The analyses obtained from all the HA and HMIs mixtures indicated that the majority of metal ions existed in the exposure solutions at the end of the exposure period, and the concentration of HMIs depurated from the daphnids was greater than the amount of ions accumulated In the organisms (Figures 5.18 and 5.19). When comparing the acute toxicity with the accumulation analyses, the results indicate that the HA showed some HMI adsorption behaviour, which limited the bioavailability of both HMIs to *D. magna* neonates. The selected HMIs concentrations in all mixture groups were sublethal to daphnids to some degree. However, the same concentrations were 100% lethal when exposed to *D. magna* in the absence of MoS_2 or HA substances.

When neonates were exposed to concentrations of the bare metal ions (0.01 mg/L Cd^{+2} and 0.05 mg/L Cu^{+2}) which had around 10% immobilization effect, most of the detected ions were found in the exposure solutions at the end of the exposure experiments. The accumulation of Cd^{+2} in the daphnids bodies was greater than the accumulation of Cu^{+2}, and the ability of animals to depurate Cu^{+2} was greater than their ability to depurate Cd^{+2} (Figures 5.18 and 5.19) at different concentrations of HMIs keeping the HA concentration constant. Figure 5.20 shows the distribution of the HMIs in the absence of either HA or MoS_2 particles.

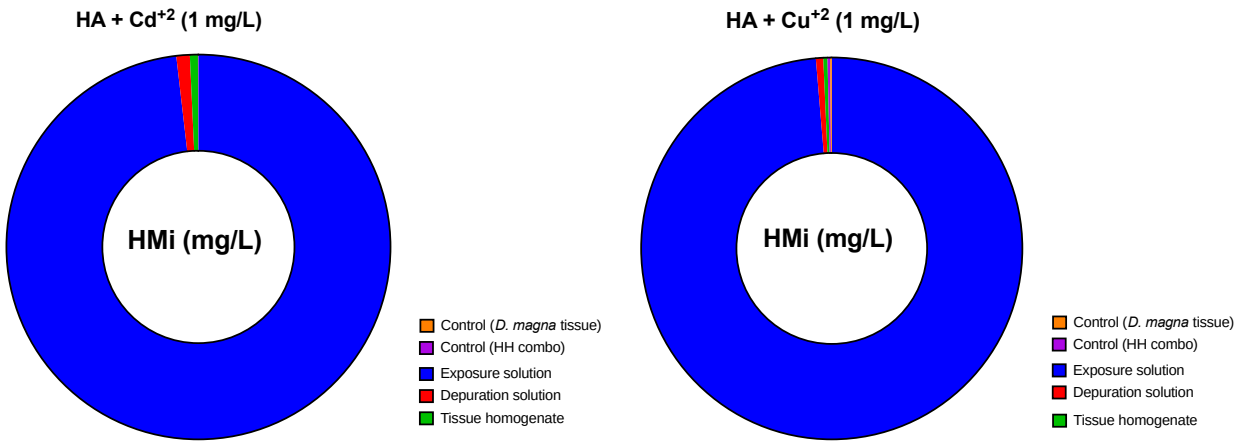

Figure 5.18. Concentrations of HMIs detected in the different compartments (daphnid body, depuration solution, exposure solution at the end of the experiment) in the case of HA mixed with 1 mg/L HMIs.

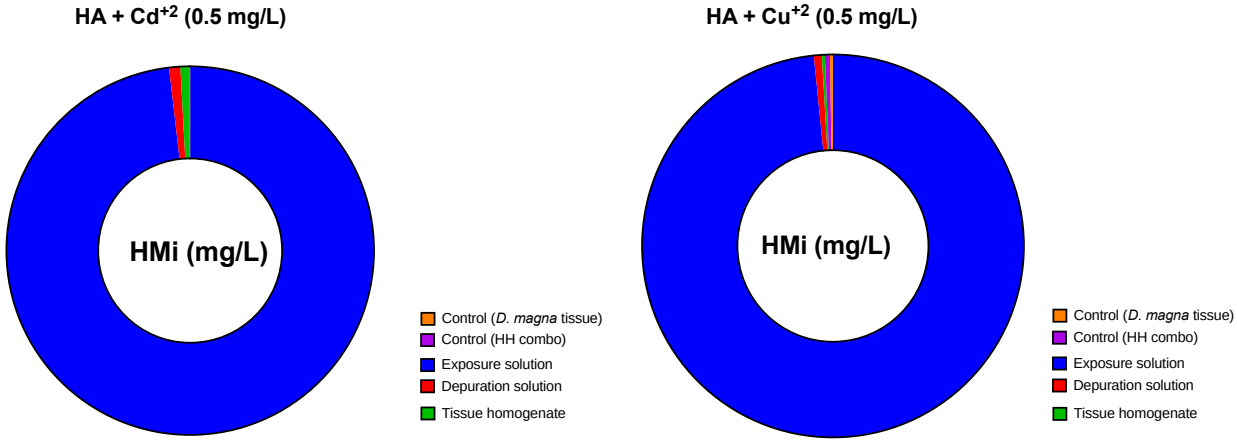

Figure 5.19. Concentrations of HMIs detected in the different compartments (daphnid body, depuration solution, exposure solution at the end of the experiment) in the case of HA mixed with 0.5 mg/L HMIs.

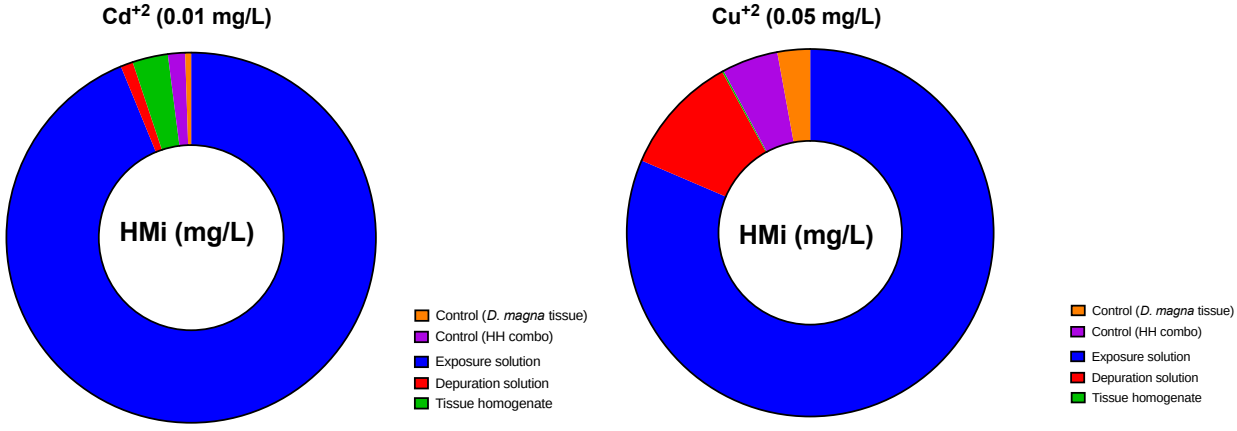

Figure 5.20. Concentrations of HMIs detected in tests performed on the HMIs alone, in the absence of either HA or MoS_2 particles; here the majority of the HMIs remained in the exposure solution at the end of the experiment, with limited uptake into the tissue and negligible depuration for Cd^{2+} and negligible uptake but considerable depuration for Cu^{2+}.

Overall, the accumulation of Cu^{+2} in *D. magna* from all tested solutions was higher than the accumulation of Cd^{+2} in *D. magna*. It can be determined that the B-MoS_2 and L-MoS_2 particles reduced the acute toxicity of HMIs by adsorption and by limiting the bioavailability to some degree. However, the smaller size (L-MoS_2) had a higher accumulation rate of both metals compared to the B-MoS_2. Whilst the smallest size (S-MoS_2) NMs highly reduced the acute toxicity of the metals but increased the accumulation of both metals in *D. magna* body (increased body burden) compared to the larger tested MoS_2 materials. The S-MoS_2 test groups also showed that the presence of daphnids dramatically reduced the adsorption rate of both metals onto the MoS_2 particles. The incubation of metals with all three MoS_2 types reduced the metal ion toxicity but did not reduce the bioavailability of HMIs compared to HA. Obviously, the toxicity reduction mechanism of MoS_2 materials is complex and requires further investigation.

In the HA mixture tests, it was clear that the humic substance alone reduced the toxicity by limiting the ability of animals to uptake the HMIs, and the rate of depuration of the HMIs was greater than the rate of accumulated ions in *D. magna* tissue homogenates.
It is known that humic acid substances can decrease the ecotoxicity of HMIs. For example, the presence of HA reduced the toxicity of solutions containing a mixture of HMIs, including Cd^{+2} and Cu^{+2}, towards freshwater shrimp by 66% (Holland *et al.,* 2013). It was suggested that the toxicity reduction was due to the precipitation and complexation of HMIs with HA, as well as the fact that HA can change the physiological behaviour of shrimps, thus an increase in survival was observed. The toxicity of HMIs can be affected by HA through their ability to bind metals at their carboxylate groups (Kungolos *et al.*, 2006). A study demonstrated that in the presence of 20 mg/L HA, the toxicity of Cu^{+2} was reduced towards

photo bacterium (Tsiridis *et al.*, 2006). The toxicity of Cu^{+2} can be reduced by 44 to 100% depending on the type of HA used (Alberts *et al.,* 2001; Tsiridis *et al.*, 2006). It has been indicated that HMIs complexation with HA mainly included metal-HA complexes while neglecting the effect of a contribution of a diffuse double layer to the binding of HMIs to humic acid (Tsiridis *et al.*, 2006). Their results concluded that the toxicity of HMIs was not always associated with the free HMIs species, and it can also be affected by other biological matter present in the test solutions. Other authors stated that the addition of chelators, including HA substances, reduced the toxicity of Cd^{+2} and Cu^{+2}, and impacted the complexation between HMIs and metal uptake into *D. magna* (Nakajima *et al.*, 2012). The study showed that the EC_{50} values of Cd^{+2} and Cu^{+2} increased with increasing the concentration of HA towards *D. magna*. They concluded that the reduction in toxicity depended on the HMIs uptake. When looking at all the metal accumulation results, it is clear that the interaction of the studied materials with *D. magna* model organism is complex and needs further systematic studies and attention.

5.7 Conclusion

The overall toxicity of MoS_2 particles confirmed the non-toxic nature of all investigated particles. However, the L-MoS_2 was the most toxic within the tested materials, followed by the S-MoS_2 and B-MoS_2, respectively. Incubating the MoS_2 particles in HH combo medium for 3 h slightly decreased the toxicity of particles, with the highest decrease observed for the S-MoS_2 NMs. Dispersing the particles in a conditioned HH combo medium decreased the HD of B-MoS_2 and L-MoS_2 but increased the HD of the S-MoS_2 particles. The PDI measurements indicated better stability in the conditioned HH combo medium compared to the non-conditioned medium for all studied particles. While the ZP measurements indicated better steric stability in the non-conditioned culture medium than in the conditioned medium. A slight decrease in the toxicity of MoS_2 materials was determined when incubating all MoS_2 particles in a conditioned HH combo medium, with the highest increase observed for S-MoS_2 particles. The 48 h acute toxicity of both HMIs was reduced when mixed with all three MoS_2 sizes, with the highest reduction achieved by the S-MoS_2 NMs, followed by the L-MoS_2 and B-MoS_2 particles, respectively. All MoS_2 particles reduced the toxicity of Cu^{+2} more than Cd^{+2}. HA alone also effectively reduced the toxicity of both heavy metal ions, and when mixed with all MoS_2, the toxicity was eliminated in all HMIs exposure concentrations. The batch adsorption analyses confirmed that all three MoS_2 particles removed both HMIs from HH combo with different removal amounts and indicated that the smaller the MoS_2 particles the more adsorption were achieved. Contact time and concentration of MoS_2 materials were not always a factor controlling the adsorption amount or capacity. While the adsorption capacity increased with increasing the concentrations of both HMIs in all tested mixtures. The B-MoS_2 and L-MoS_2 removed Cu^{+2}

more efficiently than Cd^{+2}, while the S-MoS_2 removed 100 % of both HMIs. The preliminary bioaccumulation experiment indicated complexity in the toxicity mechanism of mixture solutions but generally indicated that all MoS_2 particles reduced the toxicity but may increase the uptake/accumulation of both HMIs by *D. magna*. In contrast, HA alone reduced the toxicity as well as the uptake of HMIs.

This study provided important information about the adsorption properties of MoS_2 materials with different sizes and gave insights into their mechanisms of removing Cd^{+2} and Cu^{+2} from HH combo culture medium and these results are expected to positively contribute to addressing wastewater pollution problems. This work evaluated for the first time the role of MoS_2 materials in mitigating the toxicity of HMIs in a freshwater environment. Moreover, the overall toxicity of the emerging MoS_2 particles alone is still not evaluated enough in order to confirm their applicability, and the data generated by this study provided valuable insights into their toxicity towards an important freshwater environmental indicator, which can benefit the environmental science community in evaluating the biosafety of MoS_2 particles.

References

Alberts, J.J., Takács, M. and Pattanayek, M. (2001) 'Influence of IHSS Standard and Reference Materials on Copper and Mercury Toxicity to Vibrio fischeri', *Acta hydrochimica et hydrobiologica*, 28(7), pp. 428–435. Available at: https://doi.org/10.1002/1521-401X(20017)28:7<428::AID-AHEH428>3.0.CO;2-I.

Baimanov, D. *et al.* (2020) 'Immunological Responses Induced by Blood Protein Coronas on Two-Dimensional MoS_2 Nanosheets', *ACS Nano*, 14(5), pp. 5529–5542. Available at: https://doi.org/10.1021/acsnano.9b09744.

Clemente, Z. *et al.* (2019) 'Exploring the mechanisms of graphene oxide behavioural and morphological changes in zebrafish', *Environmental Science and Pollution Research*, 26(29), pp. 30508–30523. Available at: https://doi.org/10.1007/s11356-019-05870-z.

Gusain, R. *et al.* (2019) 'Efficient Removal of Pb(II) and Cd(II) from Industrial Mine Water by a Hierarchical MoS2/SH-MWCNT Nanocomposite', *ACS Omega*, 4(9), pp. 13922–13935. Available at: https://doi.org/10.1021/acsomega.9b01603.

Holland, A., Duivenvoorden, L.J. and Kinnear, S.H.W. (2013) 'Humic Substances Increase Survival of Freshwater Shrimp Caridina sp. D to Acid Mine Drainage', *Archives of Environmental Contamination and Toxicology*, 64(2), pp. 263–272. Available at: https://doi.org/10.1007/s00244-012-9823-y.

Klučáková, M. and Pavlíková, M. (2017) 'Lignitic Humic Acids as Environmentally-Friendly Adsorbent for Heavy Metals', *Journal of Chemistry*, 2017, p. e7169019. Available at: https://doi.org/10.1155/2017/7169019.

Kungolos, A. *et al.* (2006) 'Bioavailability and Toxicity of Heavy Metals in the Presence of Natural Organic Matter', *Journal of Environmental Science and Health, Part A*, 41(8), pp. 1509–1517. Available at: https://doi.org/10.1080/10934520600754706.

Li, W. *et al.* (2022) 'MoS2/Bentonite prepared by a facile method for efficient removal of Cd2+ from aqueous solution', *Journal of Alloys and Compounds*, 907, p. 164508. Available at: https://doi.org/10.1016/j.jallcom.2022.164508.

Martinez, D.S.T. *et al.* (2020) 'Effect of the Albumin Corona on the Toxicity of Combined Graphene Oxide and Cadmium to Daphnia magna and Integration of the Datasets into the NanoCommons Knowledge Base', *Nanomaterials*, 10(10), p. 1936. Available at: https://doi.org/10.3390/nano10101936.

Martinez, D.S.T. *et al.* (2022) 'Daphnia magna and mixture toxicity with nanomaterials – Current status and perspectives in data-driven risk prediction', *Nano Today*, 43, p. 101430. Available at: https://doi.org/10.1016/j.nantod.2022.101430.

MoS2 ACS MATERIALS (no date). Available at: https://www.acsmaterial.com/catalogsearch/result/index/?cat=&product_list_order=name&q=MoS2 (Accessed: 5 February 2023).

Nakajima, T. *et al.* (2012) 'Effect of the Addition of Chelators on the Acute Toxicity of Some Heavy Metals to Freshwater Organisms', *Journal of Water and Environment Technology*, 10(4), pp. 375–386. Available at: https://doi.org/10.2965/jwet.2012.375.

Sevim, F. *et al.* (2021) 'Adsorption capacity, isotherm, kinetic, and thermodynamic studies on adsorption behaviour of malachite green onto natural red clay', *Environmental Progress & Sustainable Energy*, 40(1), p. e13471. Available at: https://doi.org/10.1002/ep.13471.

Sinha, A., Huang, Y. and Zhao, H. (2019) 'Preparation of 3D assembly of mono layered molybdenum disulfide nanotubules for rapid screening of carbamate pesticide diethofencarb', *Talanta*, 204, pp. 455–464. Available at: https://doi.org/10.1016/j.talanta.2019.06.040.

Tsiridis, V. *et al.* (2006) 'Interactive toxic effects of heavy metals and humic acids on Vibrio fischeri', *Ecotoxicology and Environmental Safety*, 63(1), pp. 158–167. Available at: https://doi.org/10.1016/j.ecoenv.2005.04.005.

Wang, L., Wei, S. and Jiang, Z. (2020) 'Effects of humic acid on enhanced removal of lead ions by polystyrene-supported nano-Fe (0) nanocomposite', *Scientific Reports*, 10(1), p. 19663. Available at: https://doi.org/10.1038/s41598-020-76362-1.

Wang, Z. *et al.* (2018) 'Removal and Recovery of Heavy Metal Ions by Two-dimensional MoS2 Nanosheets: Performance and Mechanisms', *Environmental Science & Technology*, 52(17), pp. 9741–9748. Available at: https://doi.org/10.1021/acs.est.8b01705.

Wang, Z. *et al.* (2020) 'Superselective Removal of Lead from Water by Two-Dimensional MoS2 Nanosheets and Layer-Stacked Membranes', *Environmental Science & Technology*, 54(19), pp. 12602–12611. Available at: https://doi.org/10.1021/acs.est.0c02651.

6

Conclusions

The results achieved from this work are summarized here by pulling together the conclusions that can be drawn from the combined results obtained and demonstrating how they meet the aims and objectives of this thesis.

The first aim was to assess the role of surfactants and dispersants from the synthesis process and proteins secreted by D. magna on the toxicity of MPs/NPPs

The chemical additives used in manufacturing commercial MPs were found to be responsible for most of the toxicity effects observed from exposing *D. magna* to both cationic and anionic MPs/NNPs. Dialysis was generally a more reliable approach for washing NMs than centrifugation, although it is more time-consuming to prepare washed stock dispersions than to centrifuge the particles. The surface functionalization of PS MPs had a direct impact on the toxicity of particles, with the positively charged (NH_2-PS) being more toxic than the negatively charged (COOH-PS) particles, even after removing the chemical additives. The size of the PS NMs also played a major role in governing the toxicity of the investigated particles, as the smaller size MPs/NPPs were more toxic than the larger size particles at a constant exposure mass, which was likely due to the difference in particle numbers, as well as differences in the potential for the particles to infiltrate between the microvilli of the *Daphnia* gut following ingestion. Ageing of the as-received (unwashed) PS-NH_2 MPs/NPPs in the HH combo medium influenced the physicochemical properties and reduced the toxicity of the particles.

Assessments of protein secretion by *D. magna* indicated that a low amount of proteins was secreted by the daphnids under our tested condition compared to what has been reported in the literature. We were not able to identify the exact reason for the difference, but it could be related to problems occurring in the UoB *Daphnia* culture facility at the time of experiments. The conditioned HH combo medium had slight effect on the acute toxicity of the dialyzed NH_2-PS and COOH-PS particles and led to some agglomeration.

Extraction of proteins from *D. magna* whole tissue indicated that juveniles are easier to use for enzymatic assays than neonates, and that PBS buffer is a better option than Tris buffer for homogenizing *D. magna* tissue. The passage of NH_2-PS NMs through *D. magna* gut led to the formation of an eco-corona layer composed of secreted proteins and other biomolecules, around the surface of the particles. Higher mass concentrations of NH_2-PS MPs caused more secretion of proteins than lower mass concentrations, as expected. Due to a lack of reproducibility, fluorescence intensity measurements of the MPs/NNPs inside live daphnids using a plate reader may not be suitable for quantifying NMs uptake/accumulation.

The data obtained from this chapter provided important information to evaluate different factors that can govern the toxicity of PS NMs. Results showed that ecotoxicity studies performed using the standardized OECD 202 test guideline may significantly overestimate the impact of NMs on living organisms, or the source of the toxicity, if due consideration of additives, ageing of particles and environmentally relevant conditions are not applied, and thus a recommendation from this work is that standardized toxicity tests should be updated to consider those factors and ensure their inclusion in future studies and regulations.

The second aim was to evaluate the toxicity of graphene quantum dots (GQDs) and investigate the role of surface functionalization and particle ageing on the particle's toxicity.

Surface functionalization was found to be an essential factor in the toxic effects of GQDs towards *D. magna*. The carboxylated particles were the most toxic within the tested NMs, followed by the hydroxylated and aminated GQDs, respectively, when compared at a constant mass. Generally, cationic particles are considered to be more toxic than anionic or neutral particles, due to their electrostatic interactions with the negatively charged cell membrane. However, the results reported herein are consistent with previous results from our lab, utilizing the same GQDs to explore their toxicity to lettuce plants, which found that the hydroxylated GQDs had the highest phytotoxicity with the lowest phytotoxicity arising from the aminated GQDs (Zhang *et al.*, 2021). Particle ageing caused transformation of GQDs and altered the toxicity of the particles. Ageing of the particles in DI water led to an increase in the toxicity, while ageing them in HH combo medium decreased their toxicity and led to changes in their physicochemical properties. Incubating the particles in a (secreted protein) conditioned HH combo medium did not affect the toxicity of GQDs, but did change their physicochemical properties, indicating the possibility of an eco-corona layer formation. The toxicity of the selected NMs was found to correlate with the amount of proteins secreted by daphnids exposed to the specific GQDs, with the more toxic particles (i.e., those with the lowest EC_{50} values) resulting in more proteins being secreted by daphnids. This is consistent with earlier findings that daphnids secrete a range of proteins into the medium and that these proteins can provide mechanistic insights into the affected pathways and any potential repair mechanisms (e.g., Ellis et al., 2020). The importance of this work is that it provides significant information on the toxic effects of GQDs and the role

of surface functionalization and ageing on this, as there is a large literature gap in evaluating the toxic effects of GQDs, especially in freshwater systems and particularly towards *D. magna*. Moreover, this work provides valuable information on the importance of understanding the factors that may ameliorate the toxicity of NMs and the impact of applying environmentally relevant conditions in toxicity testing in order to avoid overestimating or underestimating results in environmental risk assessments and regulations.

The third aim was to evaluate the overall toxicity of molybdenum disulfide (MoS_2) nanosheets and to investigate the role of MoS_2 in mitigating the acute toxicity of heavy metals towards D. magna

The MoS_2 NMs were more toxic than the bulk MoS_2 materials, and the L-MoS_2 NMs were more toxic than the smaller S-MoS_2 NMs at constant mass, despite the S- MoS_2 having a higher numbers of particles due to their smaller size. The acute toxicity of MoS_2 particles incubated in a conditioned HH Combo medium was slightly decreased for all particle sizes, with the highest decrease observed in the S-MoS_2 exposures, consistent with these particles having the highest available surface area for protein binding. The acute toxicity of tested HMIs was reduced by mixing them with all three sizes of MoS_2 (10 and 100 mg/L). The smaller the MoS_2 size the more reduction in HMIs toxicity was observed, again related to the amount of surface area for binding of the HMIs. The acute toxicity of Cu^{+2} mixed with MoS_2 was reduced more than that of Cd^{+2} in most treatments, suggesting a higher binding affinity of the Cu^{2+} for the MoS_2 surface. The presence of HA also greatly reduced the toxicity of both HMIs. The batch adsorption results indicated that MoS_2 could be a prospective material for removing HMIs from wastewater. The size of MoS_2 particles had a direct impact on the removal efficiency, as the smaller the size, the greater HMIs removal was achieved,

confirming the surface-binding nature of the removal. The B-MoS_2 and L-MoS_2 showed better efficiency in removing Cu^{+2} than Cd^{+2}, while the enormous surface area of S-MoS_2 provided effectiveness at removing 100% of both HMIs in all tested conditions. The overall bioaccumulation results indicated that the presence of MoS_2 reduced the toxicity but did not prevent the animals from taking up the HMIs, and that Cu^{+2} was accumulated in *D. magna* body more than Cd^{+2} when mixed with MoS_2 materials, further confirming the binding affinity Cu^{+2}. The presence of HA reduced the HMIs uptake by *D. magna* more than the presence of MoS_2, indicating that the HA itself was less effectively ingested by the daphnids than the MoS_2 nanolayers. This work revealed for the first time the role of MoS_2 materials in alleviating the toxicity of HMIs in a freshwater environment by evaluating the toxicity and adsorption properties of MoS_2 and identifying their intrinsic mechanism/efficiency in removing Cd^{+2} and Cu^{+2} as a first step towards developing these materials to address wastewater and environmental pollution issues.

Based on the combined results of this thesis, it is clear that *D. magna* are an excellent species for exploring the toxicity of a wide range of NMs, and are sensitive to particle composition, surface charge, shape and size. The obtained data showed that *D. magna* exposure to NMs with different shapes, sources and compositions do not always behave in a similar manner and can be influenced by the physicochemical properties the NMs as well as the detailed conditions of each exposure scenario. Our data confirm that under standardized testing conditions, such as the acute OECD test for daphnia immobilization, the toxicity of NMs may be over- or under-estimated, providing further evidence for the need to revise the current regulatory guidelines for use with NMs/MPs and consolidating the need for realistic environmental conditions to be factored into the standardized testing ecotoxicity approaches.

7

Future Work

This thesis focus on understanding the toxicity of different types of NMs in an aquatic environment by applying many environmentally relevant conditions, and the obtained results can be used as a preliminary basis for future environmental studies to understand the source of toxicity of NMs in order to support the design of intrinsically safer NMs, using the so-called Safe-by-Design approach.

In the first results chapter, the impact of chemical additives on the toxicity of PS NMs was investigated and the dialysis method was found to be the most reliable in terms of removing the additives but not changing the particle concentration or causing the fluorescent dye to leach from the particles. However, it might be interesting to assess the effect of time on the removal efficiency as it could be possible for chemical additives to be removed by dialysis in a shorter time than our tests, thus reducing the time required to prepare washed stock solutions.

The mechanism of *D. magna* protein secretion was widely investigated using the Bham 2 strain. Future studies may consider testing and comparing different strains of *D. magna* to observe any significant differences in the secretion that might be correlated with differences in sensitivity to the presence of NMs. Additionally, following the medium conditioning steps, we incubated NMs in the conditioned medium for only 3 h before conducting any characterization or toxicity tests, and future work could observe more changes in the properties and toxicity behaviour if particles were incubated in the conditioned medium for longer times. Even if the secreted proteins are limited in quantity,

different NMs have different features and their ability to bind proteins may vastly differ. It would also be useful and interesting for all protein-related studies to consider their classification by mass spectrometry proteomic analyses which can then link the secreted proteins to specific repair pathways or modes of toxicity, allowing the identification of key events leading to specific adverse outcomes, such as reduced growth or reproduction. In addition, since most of the toxic effects of NMs exposed to daphnids resulted from the uptake of particles by filter feeding and accumulation in the gut, it would be interesting to assess the digestive enzyme activity of *D. magna* exposed to NMs. This was the initially intended goal for this thesis, but following the lab shut-down due to Covid-19, and the challenges with reproducibility in the daphnia facility noted earlier in the thesis, it was decided that establishing an entirely new assay and validating its performance was too risky. However, as part of confirming that particle accumulation and retention in the gut impacts feeding and/or absorption of nutrients, it remains an important unresolved question that warrants exploration.

The second results chapter of this thesis evaluated the effect of pristine particle ageing as well as ageing in a salt-based medium on the transformation and toxicity of differently charged GQD NMs. Additional ageing studies could investigate different types of media as well as different ageing approaches, such as UV exposure, to evaluate the toxicity and transformation mechanisms of NMs. Interestingly, our results found that the amine modified GQDs were least toxic, compared to the carboxyl or hydroxyl functionalized GQDs, whereas previous results on cationic gold nanorods compared to anionic gold nanorods found that the cationic particles were much more toxic to the daphnids. In that study, the shape was a key driver of the toxicity, and the charge per surface area was also found to play an important role in the toxicity (Nasser *et al.*, 2016). Thus, further characterization of

the GQDs, including charge titrations and determination of their surface area to assess the charge per surface area, might shed additional insights into the mechanism of toxicity of the particles.

The third results chapter evaluated the role of MoS_2 nanolayers in mitigating HMIs toxicity and it would be useful to perform a systematic study to assess the mechanism of uptake, release and depuration of HMIs in combination with MoS_2 to have a better understanding of the toxicity reduction mechanism. Another interesting aspect would be to investigate the role of medium composition and pH on the adsorption mechanism of MoS_2 by trying different types of environmentally relevant media and evaluating the effect of different pH values, ionic strengths and ratios of monovalent to divalent ions, and natural organic matter (Humic acid) concentrations on the adsorption efficiency of MoS_2 NMs.

Moreover, all toxicity analyses obtained in this thesis resulted from 48 h acute toxicity tests, and more toxic endpoints such as molting and chronic toxicity tests (21 days) would give a much better understanding of the long-term effects of the tested materials. For fluorescence uptake analyses, confocal microscopy would be a better alternative to quantify particles than the plate reader method. ICP-MS, ICP-OES or single-particle mass spectrometry would be great approaches to assess the accumulation amount of metal-containing NMs, but one should consider the limitation of this method in detecting hydrocarbons such as MPs and GQDs assessed here, for which additional methods are required.

References

Ellis, L.-J. and Lynch, I. (2020) 'Mechanistic insights into toxicity pathways induced by nanomaterials in Daphnia magna from analysis of the composition of the acquired protein corona', *Environmental Science: Nano*, 7(11), pp. 3343–3359. Available at: https://doi.org/10.1039/D0EN00625D.

Guo, Z. *et al.* (2020) 'Elucidating the mechanism of the surface functionalization dependent neurotoxicity of graphene family nanomaterials', *Nanoscale*, 12(36), pp. 18600–18605. Available at: https://doi.org/10.1039/D0NR04179C.

Hu, J. *et al.* (2019) 'Persistent DNA methylation changes in zebrafish following graphene quantum dots exposure in surface chemistry-dependent manner', *Ecotoxicology and Environmental Safety*, 169, pp. 370–375. Available at: https://doi.org/10.1016/j.ecoenv.2018.11.053.

Nasser, F. *et al.* (2016) 'Shape and Charge of Gold Nanomaterials Influence Survivorship, Oxidative Stress and Moulting of Daphnia magna', *Nanomaterials*, 6(12), p. 222. Available at: https://doi.org/10.3390/nano6120222.

Xie, C. *et al.* (2020) 'Elucidating the origin of the surface functionalization - dependent bacterial toxicity of graphene nanomaterials: Oxidative damage, physical disruption, and cell autolysis', *Science of The Total Environment*, 747, p. 141546. Available at: https://doi.org/10.1016/j.scitotenv.2020.141546.

Zhang, P. *et al.* (2021) 'Stress Response and Nutrient Homeostasis in Lettuce (Lactuca sativa) Exposed to Graphene Quantum Dots Are Modulated by Particle Surface Functionalization', *Advanced Biology*, 5(4), p. 2000778. Available at: https://doi.org/10.1002/adbi.202000778.